Synthesis and biological evaluation of HDAC class I/IIb and HDAC6 selective inhibitors

Inaugural dissertation

for the attainment of the title of doctor
in the Faculty of Mathematics and Natural Sciences
at the Heinrich Heine University Düsseldorf

presented by

Marc Pflieger
from Wittlich

Düsseldorf, June 2020

from the Institute of Pharmaceutical and Medicinal Chemistry

at Heinrich Heine University Düsseldorf

Published by permission of the

Faculty of Mathematics and Natural Sciences

at Heinrich Heine University Düsseldorf

Supervisor: Prof. Dr. Thomas Kurz

Co-supervisor: Prof. Dr. Matthias U. Kassack

Date of the oral examination: 14th August 2020

In memory of my grandfather Klaus-Dieter Poth

Affidavit

I declare under oath that I have produced my thesis independently and without any undue assistance by third parties under consideration of the 'Principles for the Safeguarding of Good Scientific Practice at Heinrich Heine University Düsseldorf. The presented dissertation has not been submitted to another faculty. So far, I have not attempted to earn a doctoral degree (neither successfully nor unsuccessfully).

Düsseldorf, June 2020

The presented dissertation was conducted under the supervision of Prof. Dr. Thomas Kurz from November 2016 to June 2020 at the Institute for Pharmaceutical and Medicinal Chemistry, Heinrich-Heine University Düsseldorf.

Acknowledgement

Let me take the opportunity to thank everyone who supported me in completing my PhD.

First, I would like to thank Prof Dr. Thomas Kurz without whom this research would not have been possible. Thank you for all you have done for me in the past three and a half years. It has been a valuable learning experience and one that I will always remember, and I take many lessons into my professional life in industry or academia. I appreciate the interesting and versatile projects I have had the chance to work on. In particular, I would like to thank you for giving me the opportunity to perform a research placement in Australia with Prof Andrews.

To my comrades in chemistry Alex, Beate, Leandro, Mona, Oli, Petra Tanja, Viktoria, Vitalij and Yodita, I owe you a huge debt of gratitude for creating such a nurturing environment of solidarity in the lab. I will always fondly remember our inspiring discussions about science and current affairs. They were stimulating and fun. In particular, I would like to thank Yodita Asfaha for being my lab partner and for creating an amazing lab atmosphere and our sophisticated discussions. I will always value your friendship and support. Furthermore, I would like to thank my project students Benedikt Boesen, Taner Öz and Elena Kharitonova for their dedication and their hard work they put in their research projects, which significantly contributed to the success of this work. It was a pleasure working with you.

I would like to extent my sincere gratitude to Prof. Kassack for accepting my co-supervision and our successful collaboration. Furthermore, I would like to thank him and the Kassack group, particularly Dr. Alexandra Hamacher, Christian Schrenk and Nadine Horstick-Muche for the hard work you have put into the biological evaluation of my compounds and the stimulating discussions we have had throughout our collaboration.

I am grateful for JProf. Finn Hansen as well as Dr. Sanil Bhatia and Melf Sönnichsen for the biological evaluation of my compounds and their timely and ever constructive feedback.

Adding variety and scientific exchange, I fondly remember our GRK2158 symposia such as our trip to Beijing and our numerous events. Thank you all for the memorable time.

As part of my studies I was fortunate to spend some time in Australia working with Prof. Andrews at Griffith Institute of Drug Discovery (GRIDD) in Brisbane. Thanks, must go to Prof. Andrews, her working group and especially Eva Hesping. I had the most extraordinary time with wonderful people who were welcoming, hospitable and thoroughly supportive. It was a privilege to be able to make that journey and I am a richer person for the experience.

Furthermore, I would like to thank Maria Beuer, Mohanad Aian, Dr. Schaper, Peter Behm, Dr. Peter Tommes and Gabriele Zerta from HHUCeMSA (HHU Center of Molecular and Structural Analytics) and Elemental Analysis for performing the analyses of my compounds.

I would like to extend my gratitude to the *Deutscher Akademischer Austauschdienst* (DAAD) and the *Deutsche Forschungsgemeinschaft* (DFG, 270650915/GRK2158) for financial support, which undoubtedly contributed to the completion of this work.

I would like to thank my family which supported me in every situation of my life. I could not have done this without your moral and financial support. I am, and I always will be grateful for that. Danke Oma Anita, Oma Ingrid und Opa Klaus, dass ihr immer für mich da wart, mich in all meinen Vorhaben unterstütz habt, stehts Interesse an meiner Arbeit gezeigt hattet und mich in all meiner Vorhaben bestärkt hattet. Vielen Dank!

I would like to thank my friends, especially Dr. Lars Klapal and Dr. Amy Middleton, who kept me grounded and sane through good and bad times.

Contents

Abbreviations

A2780	human ovarian cancer cell line
Ac	Acetyl
ACN	Acetonitrile
°C	Celsius
calc.	Calculated
Cal27	human oral adenosquamous carcinoma cell line
CDDP	Cisplatin
CisR	Cisplatin-resistant
conc.	Concentrated
CTCL	Cutaneous T-cell lymphoma
CU	Connecting unit
DIPEA	*N,N*-Di*iso*propylethylamine
DMF	*N,N*-Dimethylformamide
DMSO	Dimethyl sulfoxide
DNA	Deoxyribonucleic acid
e.g.	*exempli gratia*
eq.	Equivalents
ESI	Electrospray ionization
Et	Ethyl
et al.	*et alii*
FDA	Food and Drug Administration
g	Gram(s)
h	Hour(s)
HAT	Histone acetyltransferase
HATU	1-[Bis(dimethylamino)methylene]-1*H*-1,2,3-triazolo[4,5-b]pyridinium 3-oxide hexafluorophosphate
HDAC	Histone deacetylase
HDACi	Histone deacetylase inhibitor(s)
HPLC	High performance liquid chromatography

HRMS	High resolution mass spectrometry
Hz	Hertz
IC_{50}	Half maximal inhibitory concentration
in situ	Latin: in position
in vacuo	Latin: in a vacuum
J	Coupling constant (Hz)
M	Molar
Me	Methyl
mg	Milligram
min	Minute(s)
mL	Milliliter(s)
MM	Multiple myeloma
mmol	Millimole(s)
mp.	Melting point
MTT	3-(4,5-Dimethylthiazol-2-yl)-2,5-diphenyltetrazolium bromide
m/z	Mass to charge ratio
NBS	*N*-bromosuccinimide
Nm	Nanometers
NMR	Nuclear magnetic resonance
PDB	Protein Data Bank
Ph	Phenyl
ppm	Parts per million
PTCL	Peripheral T-cell lymphoma
RNA	Ribonucleic acid
RT	Room temperature
SI	Selectivity index
TFA	Trifluoroacetic acid
THF	Tetrahydrofuran
UV	Ultraviolet
ZBG	Zinc binding group

1 Introduction

1.1 Natural products

Fungi, plants and microorganisms produce a repertoire of chemical entities that are non-essential for their biological processes.[1,2] Such secondary metabolites are consolidated as natural products (Figure *1*). In contrast to the conserved primary metabolites (e.g. carbo hydrates, fatty acids, proteins, and nucleic acids) in all life forms, secondary metabolites represent a unique feature of a specific species. Natural products are derived from primary metabolites. Alkaloids[3] evolved from amino acids; malonic acid derivatives are employed in the biosynthesis of terpenes/terpenoids[4] and polyketides[5] originate from malonic acid precursors.

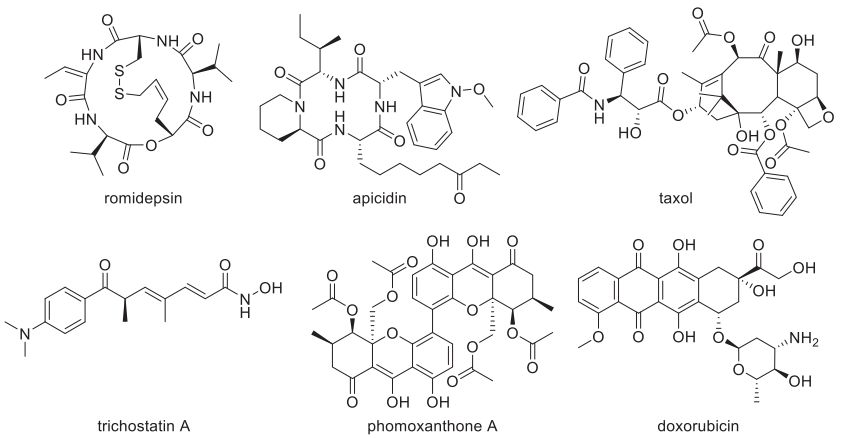

Figure 1. Selected natural products with antiproliferative properties.[6–11]

Due to the abundance and diversity of natural products as well as their frequently unknown biological activity, several hypotheses have been proposed to explain their occurrence. An approach to explain the origin of natural products is the arms race theory. According to this theory, competing organisms produce and secrete toxins to gain an evolutionary advantage. As a response to such a natural selection other species, in turn, gain an evolutionary advantage by the secretion of secondary metabolites, resulting in a constant evolutionary pressure with the survival of the most adaptable organism. For instance, life forms with restricted mobility (e.g. fungi, plant) can repel herbivores,[12,13] exhibit a resilience towards irradiation[14–16] and provide a chemistry-based method to interact with their environment (pheromones, etc.)[17] by means of natural products. Since ancient times, natural products

represent a valuable source of biologically active compounds that have been harnessed for the treatment of e.g. infections, neurodegenerative diseases and cancer.[17]

Trichostatin A (TSA) was first discovered in 1976 in an isolate of *Streptomyces hygroscopicus*.[9] TSA exhibits a polyketide linker, that connects the hydroxamic acid moiety with a *p*-amino benzoic acid (PABA) cap group. PABA, derived from the shikimic acid pathway, is submitted to a polyketide synthase, resulting in the generation of trichostatic acid.[18] Trichostatic acid is then converted by TsnB9, a hydroxylamine transferase, to the corresponding hydroxamic acid TSA (Scheme 1).

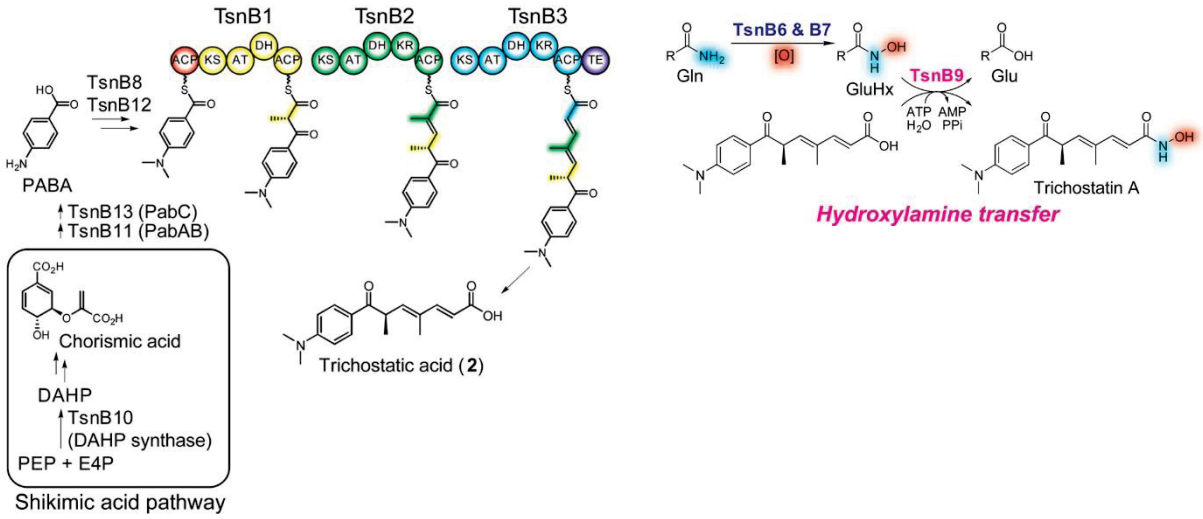

Scheme 1. Proposed biosynthesis of the natural product trichostatin A. [18]

First described as active antifungal agent,[9] TSA exhibits anti-cancer activities by the inhibition of histone deacetylases (HDAC) and represented one of the first inhibitor of those epigenetic regulators.[19]

1.2 Epigenetics and Histone deacetylases (HDACs)

The term epigenetic was coined by Conrad Waddington in 1942[20] and nowadays refers to inheritable changes of a gene function that are not the result of changes in the DNA sequence.[21] The expression of genes can be regulated or modulated by chromatin.[22] Chromatin is a tightly packed complex between DNA, histones and other proteins, which can be present in different condensation states. This condensation state is governed by regulatory enzymes and influence the transcription of coding genes. A single genome can manifest in a variety of epigenomes during the development of a cell. The

combination of the genome and the epigenome forms the phenotypic presentation of cells and direct their function and properties.[23] The biological significance of the epigenome is the imprinting of occurring gene expression events.[24] For example, the epigenome controls the X chromosomal inactivation,[25] the differentiation and development of cells[26] as well as the maintenance of the genomic integrity.[27] In this way, epigenetic alterations endow an organism with the inheritable capability to adapt to environmental changes without changing the DNA code. This process is controlled by epigenetic writers, readers and erasers.[28] Amongst the most prominent mechanisms is DNA methylation[29] and histone acetylation.[30] Over the last decades, epigenetic dysregulations, such as overexpression/mutations of HDACs, were identified as an indicator for cancer, which facilitates a cell to undergo uncontrolled proliferation and the manifestation of resistances against commonly applied anti-cancer drugs such as cisplatin. With an incidence of 80-90 %, cancer chemoresistance is the leading cause of death amongst cancer patients.[31] Whilst the monotherapy of cancer with histone deacetylase inhibitors (HDACi) prove to be limited in efficacy, the combination treatment with anti-cancer drugs (e.g. cisplatin, bortezomib, carfilzomib) has been shown to have increased efficacies in clinical trials due to occurring synergies and chemosensitising effects.[32,33] Particularly the combination of HDACi with immunotherapeutic anti-cancer drugs is a promising approach for the combat against cancer. However, the required isozyme profile of an effective chemosensitising HDACi remains to be established.

There are 11 human zinc dependant histone deacetylases that are classified according to their yeast orthologues into class I (HDAC1, HDAC2, HDAC3, HDAC8), class IIa (HDAC4, HDAC5, HDAC7, HDAC7), class IIb (HDAC6, HDAC10) and class IV (HDAC11) (Figure 2).[34]

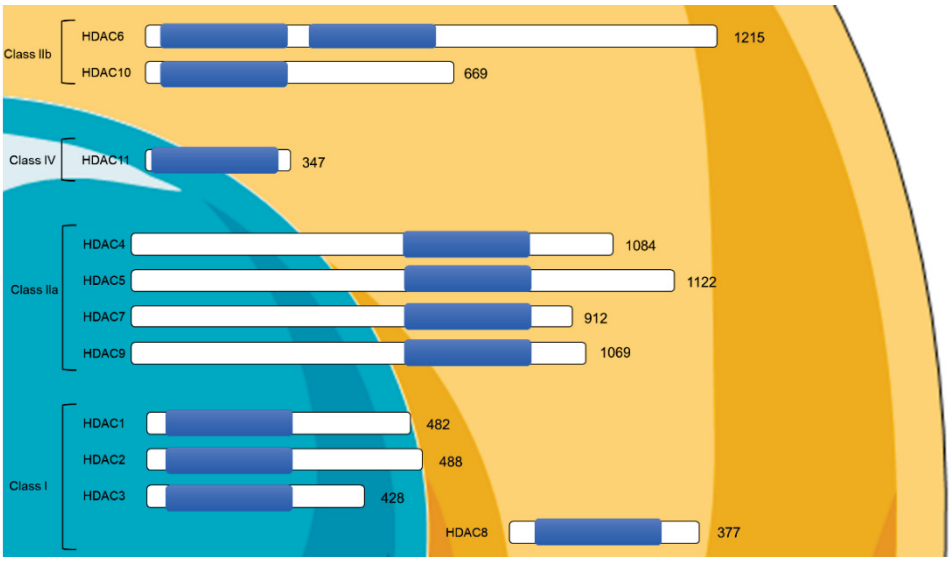

Figure 2. Cellular localization of zinc dependent-HDACs. The depicted blue bars represent the catalytic domain in the sequence (white bars). Numbers indicated the number of amino acids.[35]

In 2016, the catalytic mechanism of HDAC6 was elucidated for the CD2 of *Danio* rerio (Figure 3) and is here discussed as representative for HDACs.[36] Inside the catalytic centre of the native enzyme, a zinc ion is coordinated by one histidine (H614), two aspartate (D612, D705) and one water molecule. This water molecule forms additional hydrogen bonding with H573 and H574. Upon substrate encountering, the carbonyl of the *N*-acetylated lysine residue coordinates to Tyr745 and the zinc ion without replacing the water molecule. The resulting penta-coordinated zinc-ion activates the carbonyl residue of the amide bond and the water molecule to undergo an addition-elimination reaction. The His573-Asp610 dyad further increases the nucleophilicity of the attacking water molecule. A stabilisation of the tetrahedral transition state is realised by the coordination of Tyr745 and the zinc ion. After proton shuttling, the deacetylated lysine residue as well as the acetate is liberated and HDAC6 is accessible for another catalytic cycle.

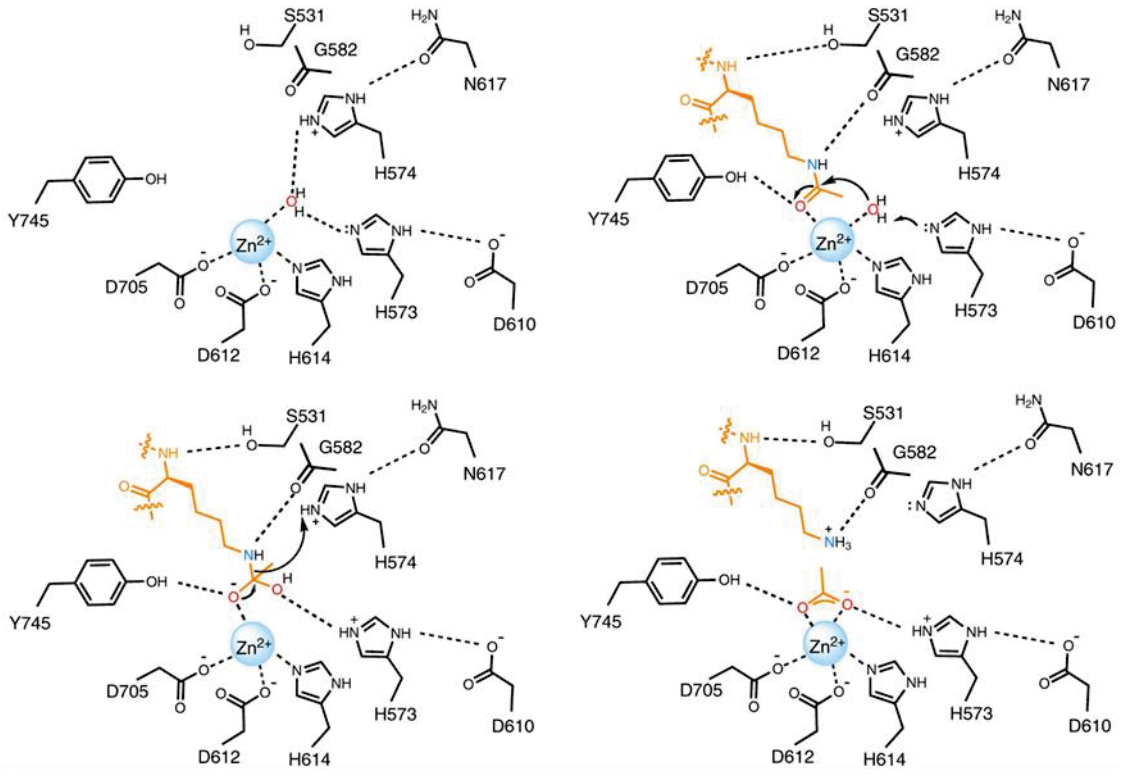

Figure 3. Mechanism of histone deacetylases.[36]

1.2.1 Class I Histone deacetylases

HDAC1, HDAC2, HDAC3 and HDAC8 are ubiquitously expressed in all human cells and are present in multi-protein complexes such CoREST (co-repressor of repressor element-1 silencing transcription factor)[37] NuRD (nucleosome remodelling and deacetylase)[38] and SIN3.[39] For instance, HDAC1 and HDAC2 are present in the CoREST complex and is responsible for the repression of neuronal genes in non-neuronal tissues.[40] Histone deacetylation cause structural changes in the chromatin structure, resulting in an altered gene expression pattern.[41] The nucleosome represents the smallest subunit of the DNA-histone protein complex.[42] A single nucleosome consists of four basic histone proteins (H2A, H2B, H3 and H4) as duplicate that interact with the negatively charged DNA backbone. Those histones form a globular structure[43] with accessible N-terminal ends, that can be chemically modified.[44] The most extensively studied modifications are histone acetylation,[45] methylation[46] and phosphorylation.[47] For instance, a condensed chromatin (heterochromatin) structure is the result of the strong interaction between lysine residues of the histone protein and the phosphate backbone of the DNA. A relaxation (euchromatin) can occur after acetylation of those lysine residues by histone acetyl transferases (HATs)[48] and thereby interrupting this ionic interaction (Scheme 2). The reverse process is catalysed by histone deacetylases (HDACs).[49] This dynamic process is essential to maintain the homeostasis of a cell and a dissonance of the abundance between HATs and HDACs can result in degeneration. Many cancer cell lines are distinguished by an overexpression of nuclear class I HDACs, resulting in a condensation of the chromatin structure in regions where tumour suppressor genes are encoded.[50] Such uncontrolled proliferating cells can circumvent apoptosis to ensure cell survival and the manifestation of resistances against commonly employed chemo therapeutics such as cisplatin. By the inhibition of class I HDACs, the expression of tumour suppressor genes can be reinstated and a chemosensitisation can be observed.[51]

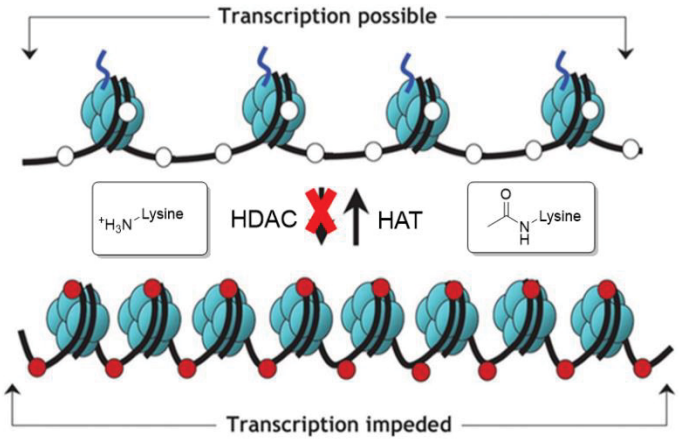

Scheme 2. Regulation of the condensation state of histones by HATs and HDACs.[52]

1.2.2 Histone deacetylase 6 (HDAC6)

With 1215 amino acids, HDAC6 is the biggest representative of the human zinc dependant HDACs.[53] Its localisation is governed by the nuclear import signal (NIS), the nuclear export signal (NES) and the SE14-domain. In differentiated cells, HDAC6 is predominantly present in the cytoplasm,[54] whereas e.g. in embryonal[55] or cancer stem cells[56] HDAC6 can also be localised inside the nucleus. In contrast to the other HDAC isozymes, HDAC6 exhibits two independent, catalytically active domains (CD1 and CD2) that are connected by the dynein motor binding domain (DMB).[57,58] Furthermore, it exhibits a *C*-terminal zinc finger ubiquitin binding domain (ZnF-UBD) (Figure 4).[34,36,58]

Figure 4. Schematic representation of the domains of HDAC6.

Due to HDAC6s localisation in the cytoplasm in differentiated cells, it predominantly targets cytoplasmic clients such as cortactin,[59] the heat shock protein 90 (HSP90),[60] peroxiredoxin[61] and α-tubulin.[62] As a result, it participates in the regulation of cell migration, cell-cell interactions and microtubular processes.

The posttranslational modification of α-tubulin,[62] such as acetylation or deacetylation, can contribute to the stability of the microtubules. Deacetylated α-tubulin is significantly less stable than its acetylated form, resulting in its depolymerisation. In this way, HDAC6 can increase microtubule dependant cell migration by the initiation of its depolymerisation. Furthermore, HDAC6 increases the cell motility by the deacetylation of cortactin, which can then interact with F-actin, resulting in an increased polymerisation and branching.

Another well evaluated client protein of HDAC6 is the chaperone heat shock protein 90 (HSP90). Deacetylated HSP90, in its active form, can recruit other client proteins such as the heat shock transcription factor 1 (HSF1) and is thereby a key modulator in several signal transduction pathways. For example,HDAC6 activity is important for glucocorticoid binding to the glucocorticoid receptor in an HSP90-p23 dependant manner. In this way, the activated glucocorticoid receptor can translocate to the nucleus and act as transcription factor.[60]

HDAC6s ZnF-UBD is particularly important for the stress response of proliferating cells. Accumulating or misfolded proteins are usually degraded by the proteasome. However, the exposure to stressors results in a degradation by the aggresome.[63] HDAC6 can recruit ubiquitinylated protein aggregates by its ZnF-UBD and transports them along the microtubular network to the microtubule organizing centre, where the formation of the aggresome occurs. Another HDAC6 mediated degradation of protein aggregates is autophagy.[64–66] In a cortactin F-actin dependant manner, HDAC6 can initiate the fusion of autophagosomes and lysosomes to remove accumulating aggregates. Furthermore, HDAC6 is a key regulator in the inactivation of reactive oxygen species (ROS) by peroxiredoxin (Prx).[61] PrxI and PrxII are responsible for the inactivation of occurring hydrogen peroxide. A deacetylation of Prx by HDAC6 causes a significantly decreased rate of the inactivation of those ROS, which can result in an increased oxidative stress of a cell.

Despite HDAC6s predominant localisation in the cytoplasm, it can translocate to the nucleus, e.g. in activated regulatory T-cells (T_{reg}), where it can deacetylate the transcription factor forkhead box P3 (FoxP3).[67] An acetylation of FoxP3 causes an abrogation of its ubiquitin mediated proteasomal degradation and the manifestation of its transcription factor purpose, resulting in an increased suppressive effect of T_{reg} cells.

An imbalance, either overexpression or downregulation, of HDAC6 has been implicated with a variety of diseases. A pharmacological intervention by the inhibition of HDAC6 for the treatment of cancer,[68] neurodegenerative[64,69] or neurological diseases[70–72] as well as immunological disorders[73–76] is currently under investigation. In oncology, the inhibition of HDAC6 is particularly interesting for its involvement in angiogenesis,[77–79] cancer metastasis[80–82] and the cellular stress response.[83–85] As immunomodulator, the inhibition of HDAC6 is of relevance due to a potential immunosuppressive effect.[86] Accumulating evidence also suggest that HDAC6 might be an attractive target for the treatment of e.g. schizophrenia,[87] anxiety[88] or Alzheimer's disease.[89]

HDACi exhibit only limited efficacies in solid tumours and the manifestation of resistances are frequently observed in clinics. However, as chemosensiters, HDACi have been shown to be capable of reverting the resistances of many cancer cell lines towards commonly applied anti-cancer drugs (e.g. cisplatin) with a synergistic induction of apoptosis.[32,33]

1.2.3 Histone deacetylase inhibitors and the rational design of isozyme selective inhibitors

Epigenetic regulators such as HDACs are promising targets for the treatment of e.g. neurological disorders and HDACi are established anti-cancer agents. The design of isozyme selective HDACi or HDAC complex specific inhibitors is an approach to overcome resistances, increase the efficacy of anti-cancer therapy, and increase patience compliance by minimising undesired side effects. Potential strategies for the design of isoform selective HDACi or HDAC complex specific inhibitors are depicted in Figure 5.[90]

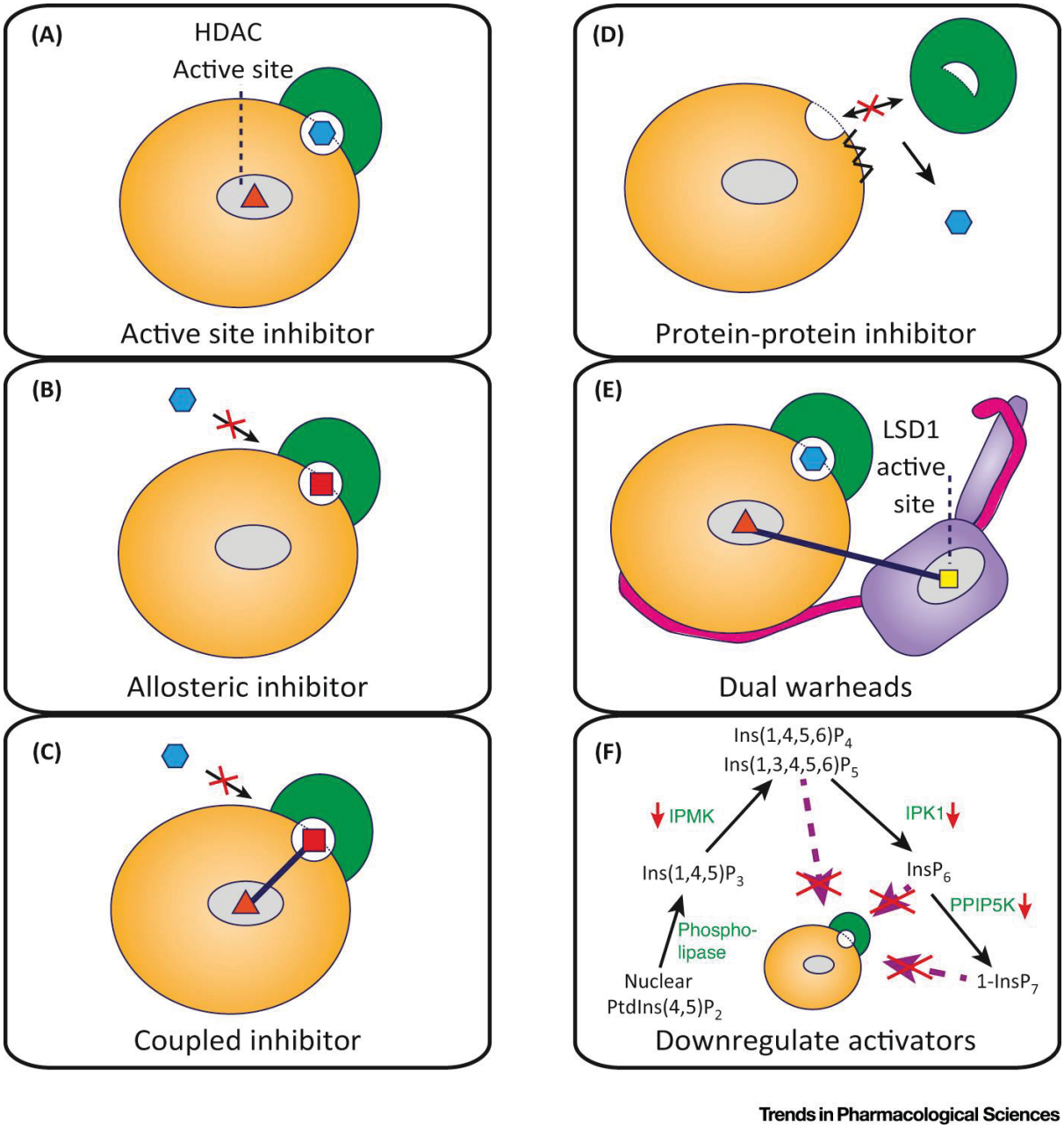

Figure 5. Strategies for the design of HDAC isoform selective/HDAC complex specific inhibition.[90]

Besides active site inhibition, the modulation of the activity of HDACs might be feasible by targeting allosteric pockets or other functional domains (e.g. ZnF-UBD of HDAC6). For instance, class I HDACs exhibit an inositol phosphate binding site at the interface between a HDAC isozyme and its co-repressor protein. Such an allosteric inhibitor could be further improved by the conjugation with an active site inhibitor (coupled inhibitor). Since many HDAC are present in multi-protein complexes (e.g. HDAC1, HDAC2, HDAC3) that form very distinct interface surfaces, the modulation of protein-protein interaction could be used for either complex stabilisation or inhibition. A similar strategy pursues the dual warhead approach which envisions the design of an inhibitor that demonstrates a HDAC active site inhibitor and an active site inhibitor for the point of interest that are connected by a flexible linker with a suitable length. This approach has been successfully demonstrated by the inhibition of a HDAC-REST corepressor 1 (CoREST) complex, which was effective against several melanoma and cutaneous squamous cell carcinoma lines.[91] Furthermore, the activity HDACs might be downregulated by inhibiting the production of activators or an allosteric substrate (e.g. inositol phosphates).

However, the design of active site inhibitors remains a valuable approach for the design of isozyme selective inhibitors. HDACs exhibit highly conserved active sites which constitute of a zinc cation, a hydrophobic tunnel, and a surface region. Based on these features, a pharmacophore model for HDACi was established consisting of a zinc-binding group (ZBG), a hydrophobic linker and a cap group (Figure *6*).[92–94]

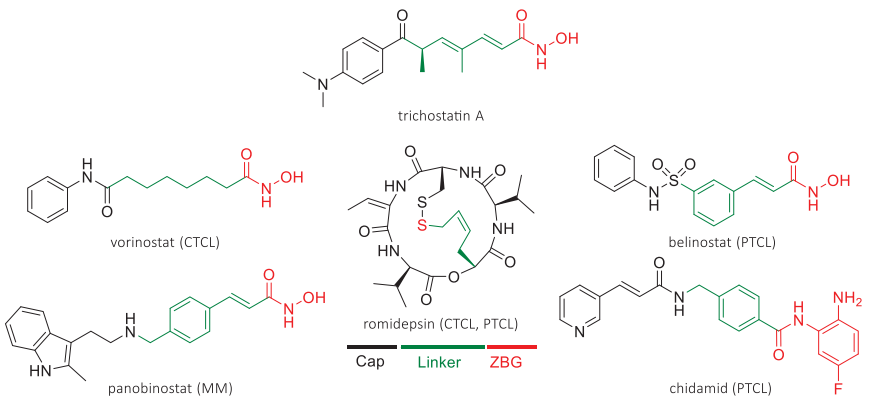

Figure 6. Pharmacophore model of selected HDAC inhibitors. HDACi are approved for the treatment of cutaneous T cell lymphoma (CTCL), peripheral T-cell lymphoma (PTCL) and multiple myeloma (MM).

Since the discovery of trichostatin A (TSA), five HDACi have been approved for the treatment of lymphoma and myeloma, which follow this pharmacophore model.[95] Vorinostat was the first EMA approved TSA derived HDACi in 2006. Further TSA derivatives followed with belinostat and

panobinostat in 2014 and 2015, respectively. However, the currently approved pan-HDAC inhibitors, particularly hydroxamic acid based inhibitors, suffer from severe side effects such as diarrhoea, neutropenia, thrombocytopenia and cardiac toxicity.[96] Furthermore, hydroxamic acids are under strong suspicion of being mutagenic by toxification via a *Losson rearrangement* (Figure 7).[97]

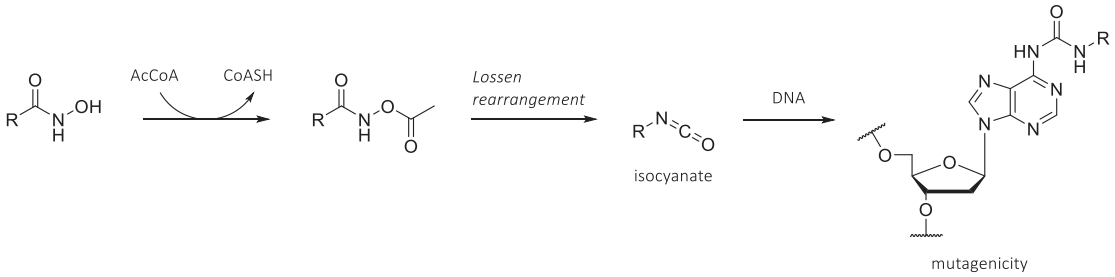

Figure 7. In vivo formation of isocyanates from hydroxamic acids by Lossen rearrangement.[97]

Whilst these HDACi display a hydroxamic acid as ZBG, chidamide[98] and romidepsin[99,100] exhibit an *o*-amino anilide and a thiol as zinc binding group, respectively. Under reducing conditions inside a cell, the disulphide bond of romidepsin is converted into its free mercapto group to interact with the active site of HDACs.

In contrast to vorinostat, belinostat and panobinostat which are HDAC pan-inhibitors, chidamide and romidepsin are class I selective HDACi. This fact signifies the importance of the ZBG and the cap group for HDAC isozyme selectivity and becomes even more apparent by considering the structural information obtained by crystallography. Each class exhibits a unique structural property that renders a differentiation between them (Figure 8). Class I HDACs are distinguished by a foot pocket that extends past the zinc ion.[101] Class IIa HDACs exhibit a lower pocket that is presented as a spacious cavity at the lower end of the entrance tunnel. In comparison to the other HDAC isozymes, HDAC6 displays a much wider and shallower entrance tunnel.[36]

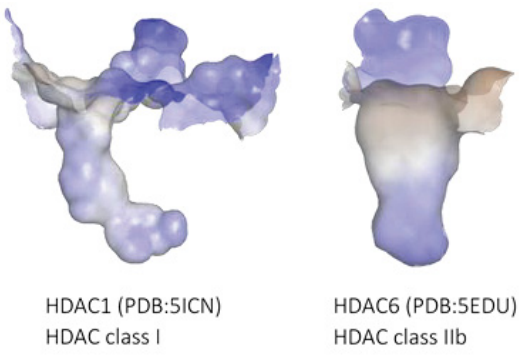

Figure 8. Surface of HDAC class I and IIb with HDAC1 and HDAC6 as representative.[101,36]

Based on these structural descriptors refined pharmacophore models were proposed for a rational design of isozyme selective inhibitors (Figure 9).[102]

Figure 9. Refined pharmacophore model for the rational design of isozyme selective HDAC inhibitors. [102]

The HDAC isozymes 1 to 3 can be selectively addressed by the employment of *o*-amino anilides such as in chidamide, entinostat and tacedinaline (Figure 10).

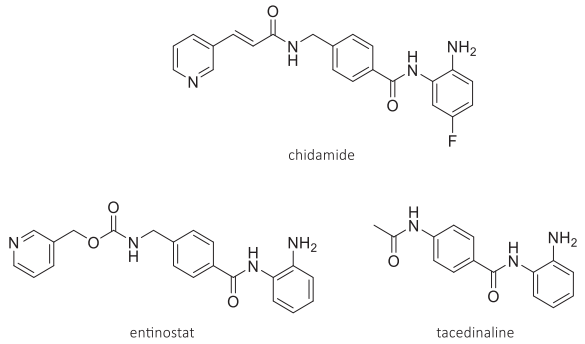

Figure 10. Selected HDAC class I inhibitors.[103–105]

Ortho-amino anilides, as bulky ZBG, exploit the foot pocket of class I HDACs which is not present in the other HDAC isozymes and only inhibit HDAC1, 2 and 3. The selectivity within this class can be obtained by different substitution patterns of the *o*-amino anilide ZBG (Figure 11).[106]

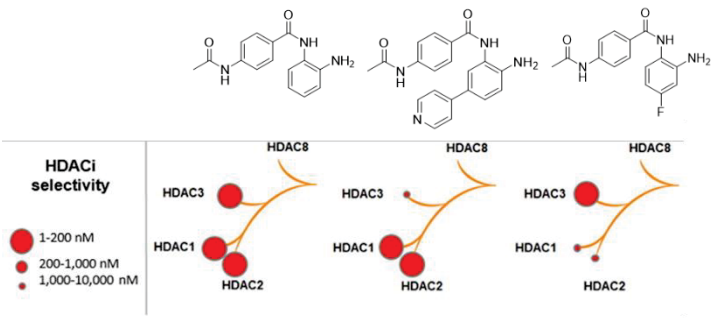

Figure 11. Isozyme selectivity profile of substituted o-amino anilides. [106]

Unsubstituted *o*-amino anilides inhibit HDAC1,2 and 3. Due to a narrower foot pocket of HDAC3, 5-aryl *o*-amino anilides predominantly inhibit HDAC1 and HDAC2. HDAC3 selectivity can be obtained by 4-fluoro substituted *o*-amino anilides. An inhibition of HDAC8 has not been observed for *o*-amino anilides.

With the absence of structural information of HDAC6, Haggarty *et. al.*, reverted to a multidimensional chemical genetic screening of more than 7,000 small molecules to discover tubacin in 2003 (Figure *12*).[107] The first discovered HDAC6 selective inhibitor tubacin demonstrates a sterically demanding cap group which distinguishes itself from pan HDACi such as vorinostat. With accumulating structural information of other HDAC isozymes, a homology model of HDAC6 was generated which resulted in the design of tubastatin A and nexturastat A.[108–110] Tubastatin A exhibited an IC_{50} of 15 nM in HDAC6 with selectivity indices of > 1000-fold over other HDAC isozymes.[108]

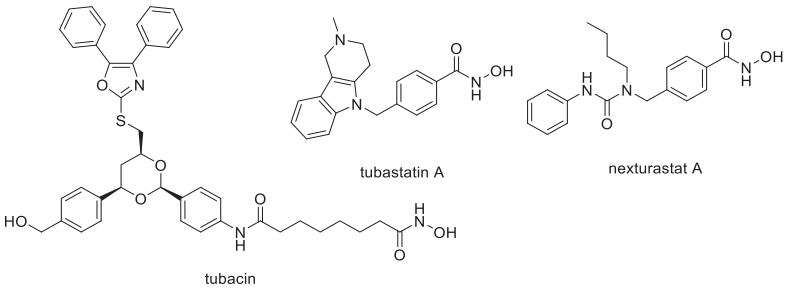

Figure 12. HDAC6 selective inhibitors.[108,109,111]

In 2016 Hai *et. al.* delivered a deeper insight into the binding modes of HDAC6 selective HDACi.[36] Based on crystallographic evaluations of *Danio rerio* HDAC6, the authors proposed that pan HDAC Inhibitors coordinate to the Zn^{2+}-Ion, inside the catalytic pocket in a bidentate manner by replacing the associated water molecule. In contrast, selective HDAC6 inhibitors exhibit a water bridged monodentate coordination to the zinc ion (Figure 13).

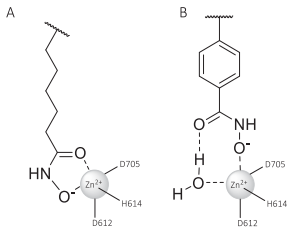

Figure 13. Representation of the bidentate (A) and monodentate (B) Zn^{2+}-binding modes observed for hydroxamate HDAC inhibitors.[36]

2 Objectives

Histone deacetylases (HDAC) are promising targets for immune modulation, the treatment of neurological disorders and are clinically validated targets for the treatment of cancer. Despite the success of HDAC inhibitors (HDACi), they suffer from severe side effects such as neutropenia, anaemia or cardio-vascular side effects[98] and their use as chemotherapeutic for the treatment of solid tumours lacks in efficacy. One approach to overcome these limitations is the development of isozyme or class selective HDACi. However, the efficacy of isozyme selective HDACi remains to be established. This work is about the development of HDAC class I/HDAC6 dual inhibitors as well as HDAC6 selective inhibitors, which could exhibit chemosensitising properties towards commonly applied anti-cancer drugs such as cisplatin.

Development of HDAC class I/HDAC6 dual inhibitors.

The first project focussed on the derivatisation of panobinostat (Scheme 3).

Scheme 3. Derivatisation of panobinostat.

By the derivatisation of the connecting unit (CU) from an amine to an alkoxyurea or alkoxyamide and the employment of different cap groups, a refined HDAC class I/HDAC6 isozyme profile was anticipated. The obtained compounds were subsequently tested on solid tumour cell lines in respect to chemosensitising properties towards cisplatin.

The second project focussed on the derivatisation of the CU of KSK64. KSK64 is a potent and selective dual HDAC class I/HDAC6 inhibitor, that shows synergistic activities with cisplatin. Furthermore, the cotreatment of KSK64 with cisplatin can revert the chemoresistance of the human squamous carcinoma cell line Cal27. In order to evaluate the structure-activity relationship of KSK64 and its alkoxyurea CU, the carba-analogue of KSK64 was synthesised and evaluated in respect to isozyme profile and chemosensitising properties (Scheme 4).

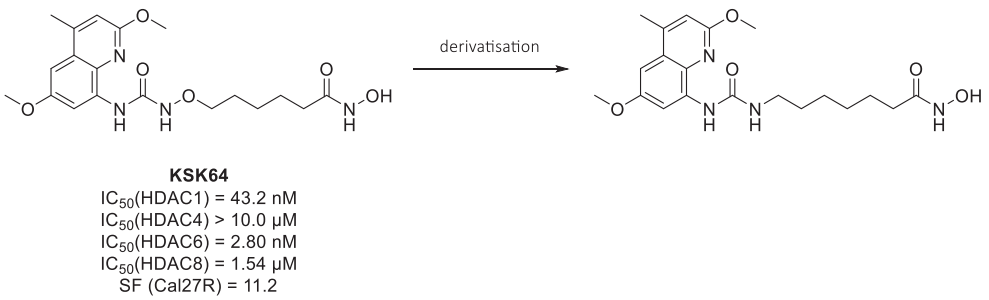

Scheme 4. Derivatisation of KSK64.

Development of HDAC6 selective inhibitors.

The design and synthesis of HDAC6 selective inhibitors was envisioned. HDAC6 selective inhibitors exhibit pharmacophore model which is comprised of a hydroxamic acid as ZBG, an aromatic linker and a sterically demanding cap group. The steric demand of such cap groups can be either satisfied by the employment of branched or bulky cap groups.

The branched cap group strategy pursued the derivatisation of nexturastat A by the introduction of a hydroxylamine subunit with various substituents in R_2 and R_3 (Scheme 5).

Scheme 5. Derivatisation of nexturastat A.

In contrast, the bulky cap group strategy for the development of HDAC6 selective inhibitors pursued the employment of chromenones as cap group (Figure 14). A particular focus was emphasised on the evaluation of different connecting units and substituents in 2 position.

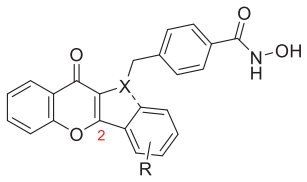

Figure 14. Chromenone based HDACi.

3 Chapter I:

Novel α,β-unsaturated hydroxamic acid derivatives overcome cisplatin resistance

Published in: Bioorganic and Medicinal Chemistry

Impact Factor: 2.802 (2018-2019)

DOI: 10.1016/j.bmc.2019.07.052

Contribution:

- Synthesis of compounds **1**, **2**, **3**, **4f**, **4g**, **5c**, **5d**, **5f**, **5h**, **5i**, **5j**, **6f**, **6g**, **7c**, **7d**, **7e**, **7f**, **7h**, **7i**, **7j**
- Manuscript and supporting information

Novel α,β-unsaturated hydroxamic acid derivatives overcome cisplatin resistance

M. Pflieger, A. Hamacher, T. Öz, N. Horstick-Muche, B. Boesen, C. Schrenk, M. U. Kassack, T. Kurz

Abstract

A series of α,β-unsaturated hydroxamic acid derivatives as novel HDAC inhibitors (HDACi) with structural modifications of the connecting unit and the CAP group was synthesized. The in vitro evaluation against the human cancer cell lines A2780 and Cal27 identified 6e and 7j as the most potent compounds regarding HDAC inhibitory activity and inhibition of proliferation. Isoform profiling against HDAC2, 4, 6 and 8 revealed a preference for HDAC2 and 6 for both compounds in contrast to the pan HDACi panobinostat. 6e and 7j enhanced significantly cisplatin-induced cytotoxicity in a combination treatment mediated by increased apoptosis induction and caspase-3/7 activation. The interaction between 6e or 7j and cisplatin was highly synergistic and more pronounced for the cisplatin resistant subline Cal27CisR. IC50 values of cisplatin were even lower in Cal27CisR pretreated with 6e or 7j than for the parental cell line Cal27. Based on our findings, the novel dual class I/HDAC6 inhibitors could serve as an option to overcome cisplatin resistance with fewer side effects in comparison to panobinostat.

1 Introduction

Cancer is, despite improved therapeutic options, after cardiovascular diseases the second most reason of fatality in industrial countries.[1] A problem of anti-cancer treatment is the occurrence of chemoresistance which can be either innate or acquired and is of multifactorial nature.[2,3] Besides the therapeutic approach to target chemoresistance mechanisms directly, addressing the aberrant gene expression machinery remains a valuable anticancer strategy[4–6]. However, as a result of the complexity of the transcriptional machinery, it has been proven to be highly challenging to design small molecules with reasonable potency and selectivity.[7] Therefore, targeting epigenetic processes in cells that underwent malignant transformation becomes increasingly important in cancer treatment.[8] Posttranslational modifications of histones such as acetylation and deacetylation of lysine residues cause a structural change of the chromatin and thereby influence gene expression.[9]

The defective silencing of tumour suppressor genes by hypoacetylation of histones is commonly observed in various cancer cells, caused by an overexpression of histone deacetylases (HDACs).[10] Such a hypoacetylation results in a more condensed heterochromatin structure impeding the accessibility of the transcriptional machinery and leading to a decreased expression of tumour suppressor genes.[11,12]

Inhibiting HDACs can thereby reinstate the expression of tumour suppressor genes, exhibit synergistic antineoplastic effects with DNA damaging agents (e.g. cisplatin) and revert chemo resistance.[13–16]

There are 11 zinc dependent human HDAC isoforms consolidated into 3 different classes according to their sequence homology.[17] Due to the high sequence homology, pan HDAC inhibitors have been designed showing no selectivity towards a single isoform. The potent pan-HDACi panobinostat was approved by the FDA in 2015 for the treatment of multiple myeloma (Figure 15). [18]

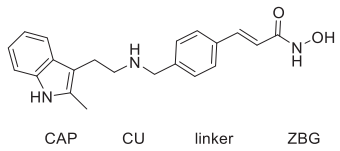

Figure 15. Chemical structure and pharmacophore model of panobinostat.

Despite the success of panobinostat, severe adverse effects such as neutropenia, anaemia or cardio-vascular side effects remain problematic.[19] Designing HDAC inhibitors with isoform selectivity might overcome this issue. However, despite the increasing endeavour to design isoform selective HDAC inhibitors, the efficacy of such compounds remains to be established. Not a single isoform selective compound has been approved by the FDA. Therefore, pan-HDAC inhibitors remain valuable entities for fundamental research and clinical applications.

Panobinostat exhibits an indole-based CAP group, an amine connecting unit (CU), a *p*-methyl cinnamyl linker and a hydroxamic acid as zinc binding group (ZBG) (Figure 1). Besides its strong zinc coordination, the reason for its potency is the unsaturated bond in the linker region, which reduces the conformational freedom and therefore decreases the net entropy of the system during ligand binding.[20] Furthermore, crystallographic evaluations identified a hydrogen bond between the amino CU and Ser531 as well as a potential pi-alkyl interaction of the indole with Pro464 in Danio rerio HDAC6 (PDB: 5EF8).[21] One potential optimisation might be the introduction of a hydroxylamine moiety as CU (Scheme 6), as it has been shown that compounds exhibiting this structural motif can overcome cisplatin chemoresistance. [7,8] By introducing other functionalised heterocycles as cap group, new binding partners might be accessed along the HDAC entrance tunnel. The objective of this work is the evaluation of the alkoxyurea and the alkoxyamide moiety as CU as well as a variety of CAP groups in respect to antiproliferative activity, HDAC isoform profiling and cisplatin resistance.

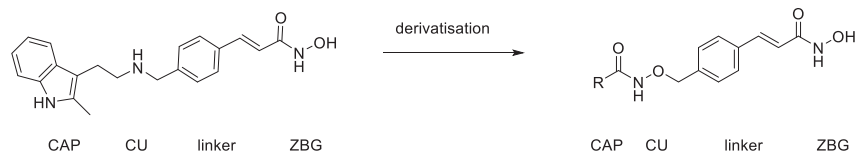

Scheme 6. Structural modification of panobinostat.

2 Results and Discussion

2.1 Chemistry

The synthesis of the alkoxyurea and alkoxyamide based hydroxamic acids required the synthesis of the hydroxylamine **3** as key intermediate (Scheme 7). The *O*-substituted hydroxylamine moiety was introduced by the conversion of **1** with *N*-hydroxyphthalimide and the following deprotection of **2** to obtain the hydroxylamine **3**

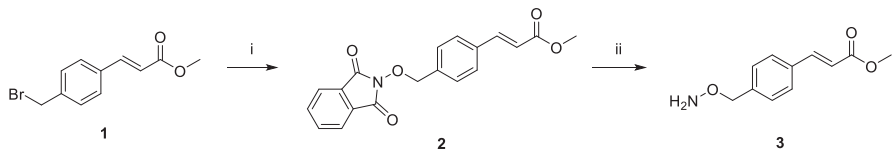

*Scheme 7. Synthesis of the hydroxylamine **3**. i) 1.50 eq H_2SO_4, MeOH, 16 h reflux, 94 %; ii) 1.17 eq NBS, 0.20 eq NBS, CCl_4, 8 h reflux, 95 %; iii) 1.20 eq* N*-hydroxyphtalimide, 2.00 eq DIPEA, ACN, 16 h reflux, 91 %; 2.00 eq hydrazine monohydrate, DCM, 16 h, RT, 95 %.*

Afterwards, **3** was transformed into an alkoxyurea derivative **4** or converted into an alkoxyamide **5** (Scheme 8). The alkoxyurea derivates **4** were obtained from the reaction of **4** with the respective isocyanate. **5** was obtained from a HATU mediated acylation of **3** with the corresponding carboxylic acid.

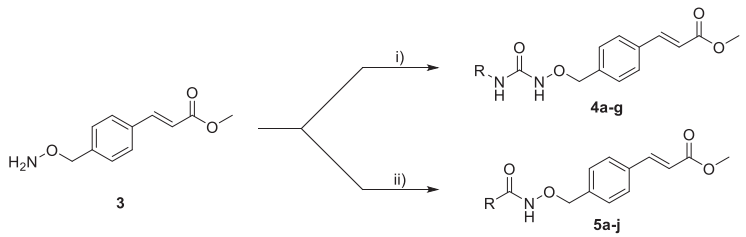

*Scheme 8. Synthesis of the alkoxyureas **4 a-g** and alkoxyamides **5 a-j**. i) 1.00 eq Isocyanate, DCM, 16 h RT, 53 – 95 %; ii) 1.00 eq carboxylic acid, 2.00 eq DIPEA, 1.00 eq HATU, DMF, 16 h RT, 40 % - 95 %.*

Subsequently, the alkoxyureas **4a-g** and alkoxyamides **5a-j** were converted into the corresponding hydroxamic acids **6a-g** and **7 a-j**, respectively. For the synthesis of the alkoxyurea based hydroxamic acids **6a-g**, the corresponding ester underwent a hydroxylaminolysis reaction under basic conditions.

However, under the same conditions the alkoxyamides hydrolysed and no hydroxamic acid was isolated. Therefore, the esters **5** were hydrolysed under basic conditions and subsequently converted into the hydroxamic acids **7** (Scheme 9).

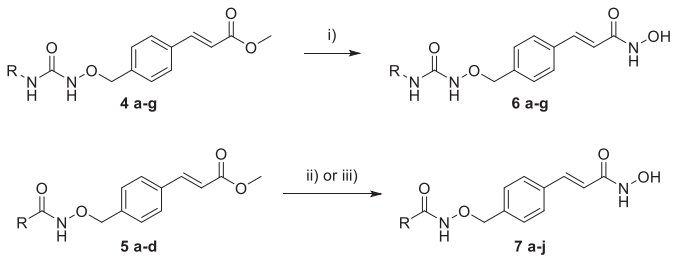

*Scheme 9. Synthesis of the hydroxamic acids **6 a-g** and **7 a-j**. i) 30.0 eq $HONH_2$ (aq), 10.0 eq NaOH, DCM/MeOH, RT 16 h, 72 - 92 %; ii) a) 5.00 eq LiOH/H2O, 16 h RT, b) 1.20 eq IBCF, 7.2 eq DIPEA, 5.0 eq $HONH_3Cl$, 16 h RT, 13-37 %; iii) 10.0 eq Hydroxylamine hydrochloride, 15.0 eq NaOMe, MeOH, MW 150 W, 70 °C, 30 mins, 34 % -37 %.*

Nevertheless, this procedure was laborious and only resulted in low yields. Hence, different methods were evaluated for the direct hydroxylaminolysis of esters exhibiting an alkoxyamide functionality. The only successful method was a microwave assisted conversion with hydroxylamine hydrochloride and sodium methanolate as base in methanol.

2.2 Biological evaluation

2.2.1 Antiproliferative activity and cellular HDAC inhibition.

The synthesised compounds were assessed for their antiproliferative activity and for their HDAC inhibitory activity in the human ovarian cancer cell line A2780 and the human tongue squamous carcinoma cell line Cal27. The results are depicted in Table 1 for the alkoxyureas **6** and in Table 2 for the alkoxyamides **7** with vorinostat and panobinostat as reference HDACi.

Initially, the influence of the connecting group was evaluated based on the example of **6b** and **7a**. The alkoxyamide **7a** featuring a phenyl cap showed an approximately two orders of magnitude higher antiproliferative activity in comparison to its corresponding alkoxyurea derivative **6b**. This difference was overcome by the introduction of methyl groups in meta position (**6c** and **7b**), indicating that the alkoxyurea **6c** adopts a different binding mode. Further derivatisation of the phenyl cap group resulted in the *p*-methoxy substituted derivative **6e** which was the most active compound amongst the alkoxyurea based hydroxamates. However, as mentioned above there is a trend that the alkoxyamides **7** are potentially more active than the corresponding alkoxyurea derivatives **6**. Therefore, the following screening focused on the alkoxyamide derivatives **7**. A variety of phenyl substituted, and heterocyclic

compounds were screened. Amongst the screened compounds, **7j** presenting a quinoline cap moiety exhibited the highest antiproliferative activity.

Overall, there is a good correlation between the antiproliferative activity and the cellular HDAC inhibition. Based on the highest antiproliferative and HDAC inhibitory activity, **6e** and **7j** were chosen for further biological evaluation.

*Table 1. Cellular HDAC inhibition and antiproliferative effect of alkoxyurea based hydroxamates **6**.*

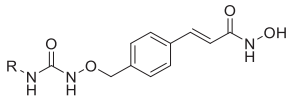

		HDAC$_i$-Assay IC$_{50}$ [µM]		MTT-Assay IC$_{50}$ [µM]	
Cpd.	R	Cal 27	A 2780	Cal 27	A 2780
6a		14.2	6.85	14.0	35.4
6b		144	190	62.0	112
6c		1.12	1.54	2.27	2.01
6d		4.21	2.29	3.49	3.39
6e	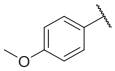	0.49	0.57	1.70	1.15
6f		40.3	43.2	34.1	38.9
6g	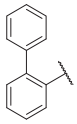	5.65	4.03	2.62	3.57
vorinostat		0.73	0.64	1.99	1.16
cisplatin		nd	nd	2.76	1.57
panobinostat		6.24 nM	7.67 nM	10.9 nM	54.8 nM

Data shown are the mean of pooled data from at least three experiments each carried out in triplicates. The standard deviations are < 10% of the mean. nd= not determined.

*Table 2. Cellular HDAC inhibition and antiproliferative effect of alkoxyamide based hydroxamates **7**.*

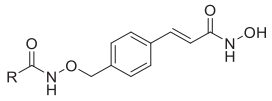

		HDAC$_i$-Assay IC$_{50}$ [µM]		MTT-Assay IC$_{50}$ [µM]	
Cpd.	R	Cal 27	A 2780	Cal 27	A 2780
7a		1.16	0.94	2.99	2.08
7b		1.09	0.90	2.24	2.33
7c	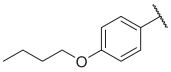	3.00	7.60	4.55	1.70
7d	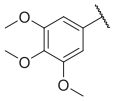	3.14	6.85	8.94	38.6
7e	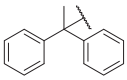	4.81	3.34	5.71	4.55
7f	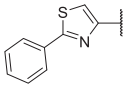	11.6	19.2	16.3	2.02
7g	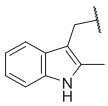	2.65	1.12	5.25	14.0
7h	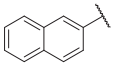	2.83	1.92	3.65	3.11
7i		4.48	1.98	4.21	3.15
7j	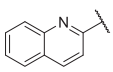	0.27	1.54	0.80	0.79
vorinostat		0.73	0.64	1.99	1.16
cisplatin		nd	nd	2.76	1.57
panobinostat		6.24 nM	7.67 nM	10.9 nM	54.8 nM

Data shown are the mean of pooled data from at least three experiments each carried out in triplicates. The standard deviations are < 10% of the mean. nd= not determined.

2.2.2 Inhibition of HDAC2, HDAC4, HDAC6 and HDAC8

6e and **7j** were first screened against human HDAC2, HDAC4, HDAC6 and HDAC8 to obtain their isoform profile. The pan HDACi vorinostat and panobinostat, the class IIa selective HDACi TMP269 and the HDAC6 selective HDACi nexturastat A were included as reference compounds (Table 3). **6e** and **7j** exhibited nanomolar activities against HDAC2 (K_i(**6e**) = 0.15 µM; K_i(**7j**) = 0.07 µM) and HDAC6 (K_i(**6e**) = 0.12 µM; K_i(**7j**) = 0.10 µM). Both compounds did not distinctively discriminate between HDAC2 and HDAC6. However, they were significantly less active against HDAC4 and HDAC8. **6e** demonstrated a selectivity index (SI) for HDAC 2 over HDAC4 or HDAC8 of 168 and 28, respectively. **7j** exhibited a 136-fold (HDAC4) and 67-fold (HDAC8) higher activity for HDAC2. Whilst panobinostat also did not discriminate between HDAC2 and HDAC6 either, it was more active against the other tested isoforms HDAC4 (SI=49) and HDAC8 (SI=57). Interestingly, the introduction of the alkoxyurea or the alkoxyamide moiety changed the isoform profile from a pan-HDACi to a class I/HDAC6 preferential inhibitor.

*Table 3. Inhibition of HDAC1, HDAC4, HDAC6, and HDAC8 by **6e** and **7j**.*

Compound	HDAC2	HDAC4	HDAC6	HDAC8
	K_i [µM]	K_i [µM]	K_i [µM]	K_i [µM]
6e	0.15	25.2	0.12	4.21
7j	0.07	9.54	0.10	4.70
vorinostat	0.10	30.1	0.04	15.7
panobinostat	0.013	0.64	0.03	0.75
nexturastat A	1.25	7.57	0.03	12.8
tubastatin A	5.77	5.38	0.01	12.3
TMP269	nd	1.77	nd	nd

Data shown are the mean of pooled data from at least three experiments each carried out in triplicates. The standard deviations are < 10% of the mean. nd = not determined.

2.2.3 Enhanced cisplatin-induced cytotoxicity

The synergistic effect of cisplatin and HDACi is well described in literature.[14] HDACi can act as chemosensitizers by reinstating the susceptibility towards DNA damaging agents. This can increase the efficacy of cisplatin. Cal27 and the cisplatin resistant subline Cal27CisR were chosen as a model system[22–25] to analyse the effects of **6e** and **7j** on cisplatin-induced cytotoxicity.[26]

After a 48 h preincubation of Cal27 or Cal27CisR with **6e** or **7j**, cisplatin was administered and incubated for a further 72 h. Subsequently, the cytotoxic effect of the tested compounds was determined by an MTT assay and shift factors were calculated by dividing the IC_{50} value of cisplatin alone by the IC_{50} value

of the drug combinations (Table 4). **6e** and **7j** caused a significant increase in cisplatin sensitivity in both cell lines. In Cal27, shift factors of 2.95 and 5.69 were obtained for **6e** and **7j**, respectively. This enhancement of cisplatin-induced cytotoxicity was even more pronounced in the cisplatin resistant cell line Cal27CisR: SF for **6e** was 4.76, SF for **7j** was 6.86. Furthermore, the combination treatment led to a complete resensitisation of Cal27CisR with IC_{50} values of cisplatin below the parental cell line Cal27. Based on these results, **6e** and **7j** were able to completely overcome cisplatin resistance of Cal27CisR as highlighted in Figure 16 for **7j**.

*Table 4. IC_{50} values of cisplatin (µM) after treatment of Cal27 and Cal27CisR with cisplatin alone or in combination with 0.5 µM of **6e** or **7j** for Cal27 or with 1.0 µM **6e** or **7j**, for Cal27CisR, respectively. SF means shift factor and was calculated as the ratio of the IC_{50} of cisplatin alone and the IC_{50} of the corresponding drug combination.*

Compound	cell line			
	Cal27		Cal27cisR	
	IC_{50}	SF	IC_{50}	SF
cisplatin	13.2	---	37.3	---
cisplatin + **6e**	4.47	2.95	7.84	4.76
cisplatin + **7j**	2.32	5.69	5.44	6.86

data shown are the mean of pooled data from at least three experiments each carried out in triplicates. the standard deviations are < 10% of the mean. all shift factors are significant (t-test, $p < 0.05$).

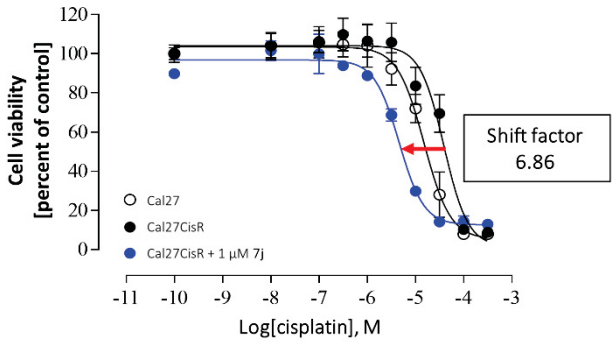

*Figure 16. **7j** restores cisplatin sensitivity of Cal27CisR. Treatment of Cal27CisR (●) with 1.00 µM of **7j** 48 h prior to cisplatin administration (blue dot) was able to reduce the IC_{50} value of cisplatin even below the IC_{50} of the parental cell line Cal27 (○).IC_{50} values were determined by MTT assay. The shift factor is defined as the ratio of the IC_{50} of cisplatin alone and the IC_{50} of the combination of **7j** with cisplatin (Table 4).*

2.2.4 Enhanced cisplatin-induced apoptosis

Next, it was evaluated if the observed enhancement of cytotoxicity affected cisplatin-induced apoptosis. Cal27 and Cal27CisR cells were treated with 0.5 µM or 1.0 µM of **6e** or **7j** for 48 h, respectively. Then, 3 µM cisplatin for Cal27 or 25 µM cisplatin for Cal27CisR was added and incubated for 24 h. Concentrations were chosen based on IC_{50} values of the respective compounds. The percentage of apoptotic nuclei with DNA content in sub-G1 was analysed by flow cytometry.

6e and **7j** alone did not induce apoptosis in neither Cal27 nor Cal27CisR (Figure 17). However, the combination in cisplatin and **6e** or **7j** caused a highly significant increase in sub-G1 population in both cell lines. In Cal27, **6e** (36.7 % ± 1.32) and **7j** (34.5 ± 1.07) caused an approximately 3-fold increase of apoptotic cells in comparison to cisplatin (11.5 ± 0.89) as single treatment. This effect was even more pronounced in Cal27CisR. A combination of **6e** and cisplatin in Cal27CisR caused a 6.0-fold (52.2 % ± 2.15) higher increase in apoptotic nuclei in comparison to the single treatment with cisplatin (8.30 % ± 1.06). **7j** and cisplatin caused an almost 4.7-fold increase (38.9 % ± 1.56) in apoptotic nuclei relatively to cisplatin alone. These data point to a synergistic effect of the HDACi and cisplatin.

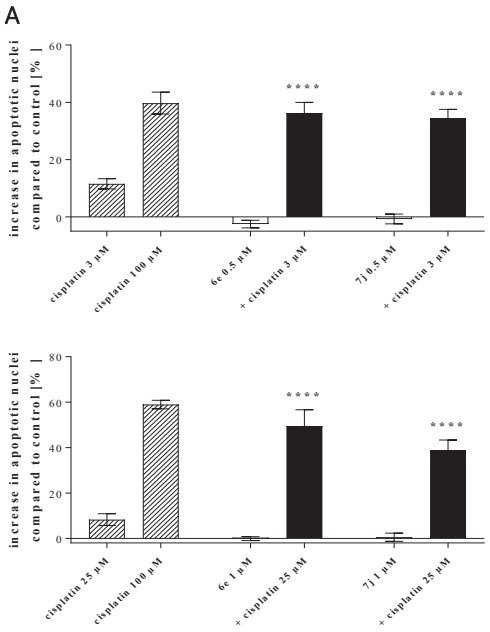

*Figure 17. **6e** and **7j** enhance cisplatin-induced apoptosis in Cal27 and Cal27 CisR cells. Cal27 (A) and Cal27 CisR (B) cells were preincubated with the indicated concentrations of **6e** or **7j**. Cisplatin was added in an IC_{50} concentration for each cell line (Cal27 3 µM (A), Cal27 CisR 25 µM (B)). Cisplatin in a concentration of 100 µM was used as a control for apoptosis induction. After a further incubation period of 24 h, apoptosis was analysed by determining the sub-G1 cell fractions by flow cytometry analysis. The number of apoptotic nuclei in the vehicle treated control (DMSO content 0.05%) was subtracted from the compound treated samples. White bars depict the incubation of cells with **6e** or **7j** only, whereas black bars show the effects of the combination of **6e** or **7j** with cisplatin, respectively. All experimental conditions were incubated for same time periods. Data are means ± SD, n = 3. Statistical analysis to compare the apoptosis induction by 3 µM cisplatin (A) or 25 µM cisplatin (B) and the combination of cisplatin and **6e** or **7j** was performed using one-way ANOVA (**** $p < 0.0001$).*

Furthermore, the combination treatment increased caspase-3/7 activity (Figure 18). **6e** and **7j** as single treatment showed no caspase-3/7 activation in Cal27 whereas in Cal27CisR a slightly higher activation in comparison to the untreated control was achieved. In combination with cisplatin however, both compounds **6e** and **7j** significantly increased the caspase-3/7 activity in a synergistic manner. In agreement to the data in Figure 3 (induction of apoptosis), the effect of caspase-3/7 activation was more pronounced in Cal27CisR. The pan-caspase inhibitor QVD completely abolished caspase-3/7 activation showing the selectivity of the compound action via caspase-3/7.

These results underpin the assumption that the main cytotoxic effect of the combination of cisplatin and **6e** or **7j** is the result of increased apoptosis.

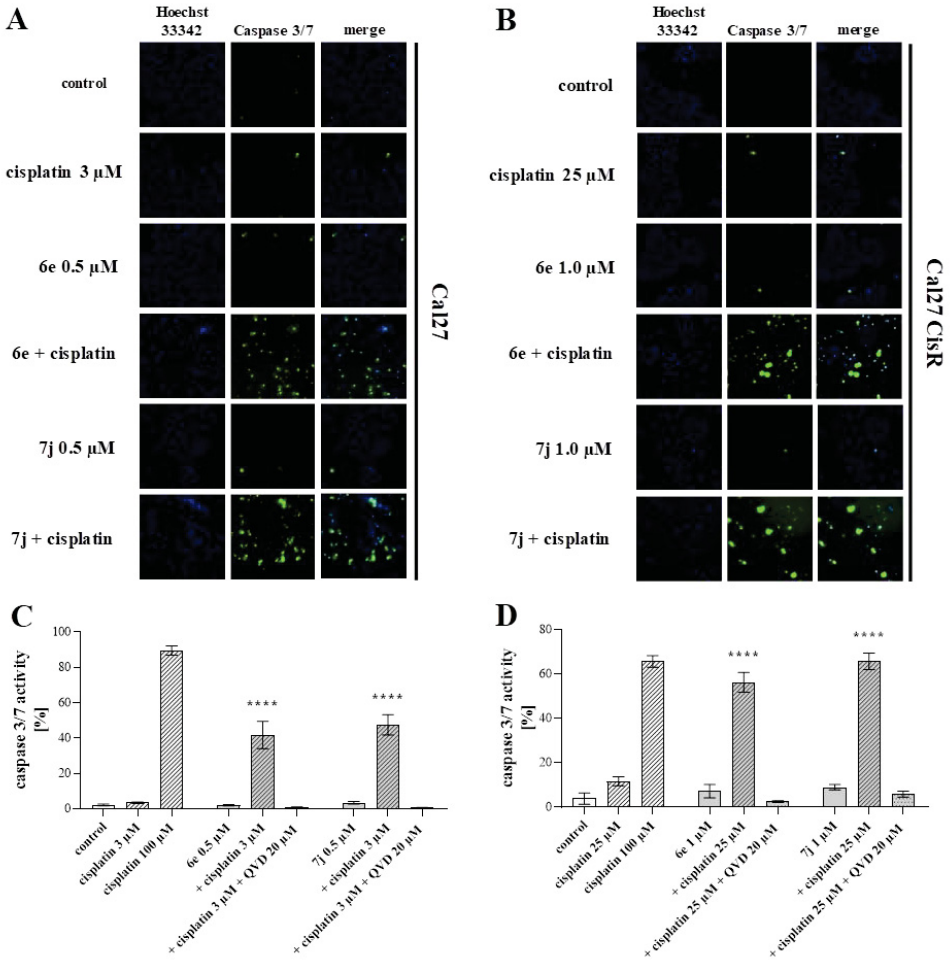

*Figure 18. **6e** and **7j** enhance cisplatin-induced apoptosis in Cal27 and Cal27 CisR cells. Cal27 (A) and Cal27 CisR (B) cells were preincubated with the indicated concentrations of **6e** or **7j**. Cisplatin was added in an IC_{50} concentration for each cell line (Cal27 3 µM (A), Cal27 CisR 25 µM (B)). Cisplatin in a concentration of 100 µM was used as a control for apoptosis induction. After a further incubation period of 24 h, apoptosis was analyzed by determining the sub-G1 cell fractions by flow cytometry analysis. The number of apoptotic nuclei in the vehicle treated control (DMSO content 0.05%) was subtracted from the compound treated samples. White bars depict the incubation of cells with **6e** or **7j** only, whereas black bars show the effects of the combination of **6e** or **7j** with cisplatin, respectively. All experimental conditions were incubated for same time periods. Data are means ± SD, n = 3. Statistical analysis to compare the apoptosis induction by 3 µM cisplatin (A) or 25 µM cisplatin (B) and the combination of cisplatin and **6e** or **7j** was performed using one-way ANOVA (**** $p < 0.0001$).*

Conclusion

A procedure for the synthesis of alkoxyamide and alkoxyurea based hydroxamic acids exhibiting a cinnamoyl linker was established. Particularly, compounds 6e and 7j displayed potent cellular HDAC inhibition and cytotoxicity in A2780 and Cal27 cells and were selected for an extensive evaluation in respect to HDAC isoform profiling and enhancement of cisplatin-induced cytotoxicity Both compounds showed a preference for HDAC2 and HDAC6 over HDAC4 and HDAC8. Particularly, 7j caused an inhibition of HDAC2 (Ki=0.07 µM) and HDAC6 (Ki=0.095 µM) at nanomolar concentrations. Interestingly, the introduction of the alkoxyurea and alkoxyamide moiety caused a significant change in the isoform profile of panobinostat from a pan-HDACi to a class I/HDAC6 preferential inhibitor. Further, 6e and 7j significantly enhanced the cytotoxic effect of cisplatin in Cal27 and even stronger in cisplatin-resistant Cal27CisR. Cisplatin sensitivity was fully restored in Cal27CisR upon pretreatment with 6e and 7j. The cytotoxic effects were mediated by a synergistic increase in cisplatin-induced apoptosis via caspase-3/7 activation. The novel reported dual class I/HDAC6 inhibitors may therefore be promising compounds to overcome cisplatin resistance and might cause fewer side effects due to a refined isoform profile in comparison to panobinostat.

Acknowledgments

This work was funded by the Deutsche Forschungsgemeinschaft (DFG, German Research Foundation) – 270650915/GRK2158. The DFG is further acknowledged for funds used to purchase the Thermo Fisher ArrayScan XTI High Content Platform used in this research (INST 208/690-1).

References

1. Siegel, R. L., Miller, K. D. & Jemal, A. Cancer statistics, 2017. *CA. Cancer J. Clin.* **67**, 7–30 (2017).

2. Zahreddine, H. & Borden, K. L. B. Mechanisms and insights into drug resistance in cancer. *Front. Pharmacol.* **4**, 28 (2013).

3. Galluzzi, L. *et al.* Molecular mechanisms of cisplatin resistance. *Oncogene* **31**, 1869–1883 (2012).

4. Isanbor, C. & O'Hagan, D. Fluorine in medicinal chemistry: A review of anti-cancer agents. *J. Fluor. Chem.* **127**, 303–319 (2006).

5. Nussbaumer, S., Bonnabry, P., Veuthey, J. L. & Fleury-Souverain, S. Analysis of anticancer drugs: A review. *Talanta* **85**, 2265–2289 (2011).

6. Eckschlager, T., Plch, J., Stiborova, M. & Hrabeta, J. Histone Deacetylase Inhibitors as Anticancer Drugs. 1–25 (2017). doi:10.3390/ijms18071414

7. Andreoli, F., Jorge Moura Barbosa, A., Daniele Parenti, M. & Del Rio, A. Modulation of Epigenetic Targets for Anticancer Therapy: Clinicopathological Relevance, Structural Data and Drug Discovery Perspectives. *Curr. Pharm. Des.* **19**, 578–613 (2013).

8. Hoelder, S., Clarke, P. A. & Workman, P. Discovery of small molecule cancer drugs: Successes,

challenges and opportunities. *Mol. Oncol.* **6**, 155–176 (2012).

9. Bannister, A. J. & Kouzarides, T. Regulation of chromatin by histone modifications. *Cell Res.* **21**, 381–395 (2011).

10. Villar-Garea, A. & Esteller, M. Histone deacetylase inhibitors: Understanding a new wave of anticancer agents. *Int. J. Cancer* **112**, 171–178 (2004).

11. Huang, L. & Pardee, A. B. Suberoylanilide hydroxamic acid as a potential therapeutic agent for human breast cancer treatment. *Mol. Med.* **6**, 849–866 (2000).

12. Marks, P. A. *et al.* Histone deacetylases and cancer: Causes and therapies. *Nat. Rev. Cancer* **1**, 194–202 (2001).

13. Roche, J. & Bertrand, P. Inside HDACs with more selective HDAC inhibitors. *Eur. J. Med. Chem.* (2016). doi:10.1016/j.ejmech.2016.05.047

14. Stenzel, K. *et al.* Alkoxyurea-Based Histone Deacetylase Inhibitors Increase Cisplatin Potency in Chemoresistant Cancer Cell Lines. *J. Med. Chem.* **60**, 5334–5348 (2017).

15. Fischer, C. *et al.* Panobinostat reduces hypoxia-induced cisplatin resistance of non-small cell lung carcinoma cells via HIF-1α destabilization. *Mol. Cancer* **14**, 4 (2015).

16. Wang, G. *et al.* Panobinostat Synergistically Enhances the Cytotoxic Effects of Cisplatin, Doxorubicin or Etoposide on High-Risk Neuroblastoma Cells. *PLoS One* **8**, e76662 (2013).

17. Haberland, M., Montgomery, R. L. & Olson, E. N. The many roles of histone deacetylases in development and physiology: Implications for disease and therapy. *Nat. Rev. Genet.* **10**, 32–42 (2009).

18. Atadja, P. & Perez, L. Discovery and Development of Farydak (NVP-LBH589, Panobinostat) as an Anticancer Drug. in *Successful Drug Discovery* 59–88 (Wiley-VCH Verlag GmbH & Co. KGaA, 2016). doi:10.1002/9783527800315.ch4

19. Tzogani, K. *et al.* EMA Review of Panobinostat (Farydak) for the Treatment of Adult Patients with Relapsed and/or Refractory Multiple Myeloma. *Oncologist* **23**, 631–636 (2018).

20. Tang, H. *et al.* Novel Inhibitors of Human Histone Deacetylase (HDAC) Identified by QSAR Modeling of Known Inhibitors, Virtual Screening, and Experimental Validation. *J. Chem. Inf. Model.* **49**, 461–476 (2009).

21. Hai, Y. & Christianson, D. W. Histone deacetylase 6 structure and molecular basis of catalysis and inhibition. *Nat. Chem. Biol.* **12**, 741–747 (2016).

22. Almeida, L. O. *et al.* NFκB mediates cisplatin resistance through histone modifications in head and neck squamous cell carcinoma (HNSCC). *FEBS Open Bio* **4**, 96–104 (2014).

23. Zhang, Y. & Li, B. E-FABP: Regulator of immune function. *Oncoscience* **1**, 398–399 (2014).

24. Giudice, F. S., Pinto, D. S., Nör, J. E., Squarize, C. H. & Castilho, R. M. Inhibition of Histone Deacetylase Impacts Cancer Stem Cells and Induces Epithelial-Mesenchyme Transition of Head and Neck Cancer. *PLoS One* **8**, e58672 (2013).

25. Enzenhofer, E. *et al.* Effect of the histone deacetylase inhibitor resminostat on head and neck squamous cell carcinoma cell lines. *Head Neck* **39**, 900–907 (2017).

26. Gosepath, E. M. *et al.* Acquired cisplatin resistance in the head-neck cancer cell line Cal27 is associated with decreased DKK1 expression and can partially be reversed by overexpression of DKK1. *Int. J. Cancer* **123**, 2013–2019 (2008).

3.1 Chapter I - Supporting information

Novel α,β-unsaturated hydroxamic acid derivatives overcome cisplatin resistance

Supporting information

Marc Pflieger[a, #], Alexandra Hamacher[a, #], Taner Öz[a], Nadine Horstick-Muche[a], Benedikt Boesen[a], Christian Schrenk[a], Matthias U. Kassack[a, #], Thomas Kurz[a, #]

[a] *Institute of Pharmaceutical and Medicinal Chemistry, Heinrich-Heine-University Düsseldorf, 40225 Düsseldorf, Germany*
[#] *MP and AH contributed equally, MUK and TK share senior and corresponding authorship*

Content

1 General Information

Reaction, monitoring and purification

Chemicals and solvents were purchased from commercial suppliers (Sigma-Aldrich, Acros Organics, TCI, Fluorochem ABCR, Alfa Aesar, J&K, Carbolution) and used without further purification. Dry solvents were obtained from Acros Organics. Ambient or room temperature correspond to 22°C. The reaction progression was monitored using Thin-Layer-Chromatography plates by Macherey Nagel (ALUGRAM Xtra SIL G/UV_{254}). Visualisation was achieved with ultraviolet irradiation (254 nm) or by staining with with a $KMnO_4$-solution (9 g $KMnO_4$, 60 g K_2CO_3, 15 mL of a 5% aqueous NaOH-solution, ad 900 mL demineralised water). Purification was either performed with prepacked Silica cartridges (Acros, RediSep® Rf Normal Phase Silica) for flash column chromatography (CombiFlashRf200, TeleDyneIsco) or by recrystallisation. Different eluent mixtures of solvents (hexane and ethyl acetate or dichloromethane and methanol) served as the mobile phase for flash column chromatography and are stated in the experimental procedure.

Analytics

An NMR-Spectrometer by Bruker (Bruker Avance III – 300, Bruker Avance DRX – 500 or Bruker Avance III - 600) were used to perform ^{1}H- and^{13}C-NMR experiments. Chemical shifts are given in parts per million (ppm), relative to residual non-deuterated solvent peak (^{1}H-NMR: DMSO-d_6 (2.50), ^{13}C-NMR: DMSOd_6 (39.52). Signal patterns are indicated as: singlet (s), doublet (d), triplet (t), quartet (q), or multiplet (m). Coupling constants, J, are quoted to the nearest 0.1 Hz and are presented as observed. ESI-MS was carried out using Bruker Daltonics UHR-QTOF maXis 4G (Bruker Daltonics) under electrospray ionization (ESI). The above-mentioned characterisations were carried out by the HHU Center of Molecular and Structural Analytics at Heinrich-Heine University Düsseldorf (http://www.chemie.hhu.de/en/analytics-center-hhucemsa.html). APCI-MS was carried out with an Advion expression^{L} CMS. Melting points were determined using a Büchi M-565 melting point apparatus. Analytical HPLC was carried out on a Knauer HPLC system comprising of an Azura P6.1L pump, an Optimas 800 autosampler, a Fast Scanning Spectro-Photometer K-2600 and a Knauer Reversed Phase column (SN: FK36). Evaluated compounds were detected at 254 nm. The solvent gradient table is shown in Table 14. The purity of all final compounds was 95% or higher.

Table 5: The solvent gradient table for analytic HPLC analysis.

Time / min	Water + 0.1% TFA	ACN + 0.1% TFA
Initial	90	10
0.50	90	10
20.0	0	100
30.0	0	100
31.0	90	10
40.0	90	10

2 Synthetic procedures

2.1 Methyl (*E*)-3-(4-(((1,3-dioxoisoindolin-2-yl)oxy)methyl)phenyl)acrylate (**2**)

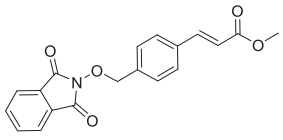

$C_{19}H_{15}NO_5$
337.33

Commercially available (*E*)-3-(4-(bromomethyl)phenyl)acrylate (1.00 g, 3.84 mmol, 1.00 eq), *N*-hydroxyphtalimide (752 mg, 4.62 mmol, 1.20 eq) and DIPEA (1.35 mL, 7.68 mmol, 2.00 eq) were dissolved in 50 mL of acetonitrile and refluxed. After 16 h, the reaction mixture was poured on 300 mL of ice water. The obtained precipitate was collected by filtration and repeatedly washed with a saturated $NaHCO_3$ solution until the filtrate became colourles. The residue was recrystallised from ethanol. 1.18 g (3.49 mmol, 91 %) of **2** was obtained as a white solid.

^{1}H NMR (600 MHz, DMSO-d_6) δ 7.86 (s, 4H), 7.78 – 7.74 (m, 2H), 7.67 (d, *J* = 16.1 Hz, 1H), 7.59 – 7.55 (m, 2H), 6.68 (d, *J* = 16.1 Hz, 1H), 5.20 (s, 2H), 3.73 (s, 3H).

^{13}C NMR (151 MHz, DMSO-d_6) δ 166.6, 163.1, 143.9, 136.5, 134.8, 134.6, 130.0, 128.5, 128.4, 123.3, 118.5, 78.7, 51.5.

M.p.: 182 °C; **HPLC:** R_t = 8.97 min, purity = 97.4 %; **ESI-MS:** 697.0 ($[2M+H]^+$).

2.2 Methyl (*E*)-3-(4-((aminooxy)methyl)phenyl)acrylate (**3**)

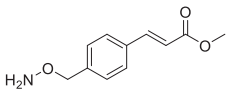

$C_{11}H_{13}NO_3$
207.23

The phthaloyl protected hydroxylamine **2** (1.00 eq, 2.00 g, 5.93mmol) was dissolved in 40.0 mL of dichloromethane- Subsequently, 2.00 eq of hydrazine monohydrate (594 mg, 11.9 mmol) were added and the reaction stirred for 16 h. The resulting precipitate was removed by filtration and the filtrate washed 3x with sat. $NaHCO_3$-solution and 1x with brine. After drying over Na_2SO_4, the product was recrystallised from hexane/ethyl acetate. In this way, 1.17 g (5.64mmol, 95%) of the hydroxylamine **3** was obtained as a white solid.

^{1}H NMR (600 MHz, DMSO-d_6) δ 7.71 – 7.67 (m, 2H), 7.66 (d, *J* = 16.1 Hz, 1H), 7.36 (d, *J* = 8.1 Hz, 2H), 6.63 (d, *J* = 16.0 Hz, 1H), 6.10 (s, 2H), 4.59 (s, 2H), 3.72 (s, 3H).

^{13}C NMR (151 MHz, DMSO-d_6) δ 166.7, 144.3, 141.1, 133.1, 128.2, 128.2, 117.5, 76.3, 51.4.

M.p.: 79°C; **HPLC:** R_t = 7.29 min, purity ≥ 99 %; **ESI-MS:** 208.3 ($[M+H]^+$).

2.3 General procedure for the synthesis of the alkoxyureas **4a-g.**

For the synthesis of the alkoxureas **4a-g**, 1.00 eq of the hydroxylamine **3** was dissolved in 15 mL of dry dichloromethane. Subsequently, 1.00 eq of the required isocyanate was added at ambient temperature. After 16 h, the product was precipitated by the addition of hexane and collected by filtration. Finally, the product was recrystallised from hexane/ethyl acetate.

2.3.1 Methyl (*E*)-3-(4-(((3-ethylureido)oxy)methyl)phenyl)acrylate (**4a**)

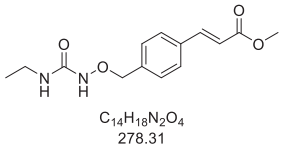

4a was synthesised from the hydroxylamine **3** (200 mg, 0.97 mmol, 1.00 eq) and ethyl isocyanate (0.08 mL, 1.45 mmol, 1.00 eq)) according to 2.3. 220 mg (0.78 mmol, 81 %) of the alkoxyurea **4a** was obtained as a white solid.

^{1}H NMR (300 MHz, DMSO-d_6) δ 9.02 (s, 1H), 7.76 – 7.61 (m, 3H), 7.45 (d, *J* = 8.2 Hz, 2H), 6.81 (t, *J* = 5.9 Hz, 1H), 6.66 (d, *J* = 16.0 Hz, 1H), 4.73 (s, 2H), 3.73 (s, 3H), 3.33 (s, 5H), 3.05 (td, *J* = 7.1, 5.8 Hz, 2H), 0.99 (t, *J* = 7.1 Hz, 3H).

^{13}C-NMR (150 MHz, DMSO-*d6*) δ (ppm) = 164.5, 156.7, 135.6, 133.4, 130.2, 128.4, 121.3, 101.6, 76.9, 50.7, 33.5, 15.5.

M.p.: 153 °C; **HPLC:** R_t = 4.71 min, purity = 99.6 %; **ESI-MS:** 279.4 ($[M+H]^+$).

2.3.2 Methyl (*E*)-3-(4-(((3-phenylureido)oxy)methyl)phenyl)acrylate (**4b**)

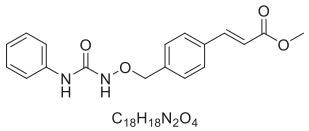

$C_{18}H_{18}N_2O_4$
326.35

4b was synthesised from the hydroxylamine **3** (200 mg, 0.97 mmol, 1.00 eq) and phenylisocyanate (0.11 mL, 0.97 mmol, 1.00 eq) according to 2.3. 210 mg (0.64 mmol, 66 %) of the alkoxyurea **4b** was obtained as a white solid.

^{1}H NMR (300 MHz, DMSO-d_6) δ 9.49 (s, 1H), 8.77 (s, 1H), 7.78 – 7.61 (m, 3H), 7.58 – 7.46 (m, 4H), 7.32 – 7.19 (m, 2H), 6.98 (ddt, *J* = 7.6, 7.0, 1.2 Hz, 1H), 6.66 (d, *J* = 16.1 Hz, 1H), 4.85 (s, 2H), 3.73 (s, 3H).

^{13}C NMR (75 MHz, DMSO-d_6) δ 166.7, 157.1, 144.2, 139.0, 139.0, 133.7, 129.2, 128.5, 128.3, 122.5, 119.5, 117.9, 77.0, 51.5.

M.p.: 148 °C; **HPLC:** R_t = 8.13 min, purity = 98.9 %; **ESI-MS:** 328.4 ($[M+H]^+$).

2.3.3 Methyl (*E*)-3-(4-(((3-(3,5-dimethylphenyl)ureido)oxy)methyl)phenyl)acrylate (**4c**)

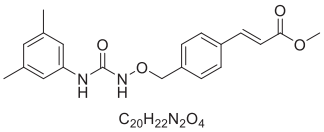

$C_{20}H_{22}N_2O_4$
354.41

4c was synthesised from the hydroxylamine **3** (210 mg, 1.00 mmol, 1.00 eq) and 3,5-dimethyl phenylisocyanate (0.14 mL, 1.00 mmol, 1.00 eq) according to 2.3. 270 mg (0.77 mmol, 77 %) of the alkoxyurea **4c** was obtained as a white solid.

^{1}H NMR (300 MHz, DMSO-d_6) δ 9.45 (s, 1H), 8.56 (s, 1H), 7.74 (d, *J* = 8.2 Hz, 2H), 7.68 (d, *J* = 16.1 Hz, 1H), 7.55 – 7.46 (m, 2H), 7.14 (dt, *J* = 1.6, 0.7 Hz, 2H), 6.67 (d, *J* = 16.1 Hz, 1H), 6.63 (dd, *J* = 1.6, 0.9 Hz, 1H), 4.85 (s, 2H), 3.73 (s, 4H), 2.22 (s, 6H).

^{13}C NMR (75 MHz, DMSO-d_6) δ 166.6, 157.0, 144.1, 139.0, 138.7, 137.3, 133.7, 129.1, 128.2, 124.0, 117.9, 117.2, 76.9, 51.4, 21.0.

M.p.: 158 °C; **HPLC:** R_t = 8.58 min, purity = 99.8 %; **ESI-MS:** 355.6 ($[M+H]^+$).

2.3.4 Methyl (*E*)-3-(4-(((3-mesitylureido)oxy)methyl)phenyl)acrylate (**4d**)

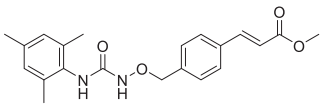

$C_{21}H_{24}N_2O_4$
368.43

4d was synthesised from the hydroxylamine **3** (300 mg, 1.45 mmol, 1.00 eq) and 2,4,6-trimethyl phenylisocyanat (240 mg, 1.45 mmol, 1.00 eq) according to 2.3. 510 mg (1.38 mmol, 95 %) of the alkoxyurea **4d** was obtained as a white solid.

^{1}H NMR (600 MHz, DMSO-d_6) δ 9.35 (s, 1H), 8.17 (s, 1H), 7.73 (d, *J* = 8.1 Hz, 2H), 7.68 (d, *J* = 16.1 Hz, 1H), 7.53 (d, *J* = 8.0 Hz, 2H), 6.86 (s, 2H), 6.67 (d, *J* = 16.1 Hz, 1H), 4.86 (s, 2H), 3.73 (s, 3H), 2.22 (s, 3H), 2.07 (s, 6H).

^{13}C NMR (151 MHz, DMSO-d_6) δ 166.7, 157.9, 144.2, 139.2, 135.8, 135.2, 133.7, 132.3, 129.3, 128.2, 128.1, 117.9, 77.0, 51.5, 20.5, 17.9.

M.p.: 179 °C; **HPLC:** R_t = 8.72 min, purity = 97.2 %; **ESI-MS:** 369.6 ($[M+H]^+$).

2.3.5 Methyl (*E*)-3-(4-(((3-(4-methoxyphenyl)ureido)oxy)methyl)phenyl)acrylate (**4e**)

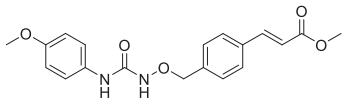

$C_{19}H_{20}N_2O_5$
356.38

4e was synthesised from the hydroxylamine **3** (300 mg, 1.45 mmol, 1.00 eq) and 4-methoxy phenylisocyanate (0.19 mL, 1.45 mmol, 1.00 eq) according to 2.3. 360 mg (1.02 mmol, 70 %) of the alkoxyurea **4e** was obtained as a white solid.

^{1}H NMR (300 MHz, DMSO-d_6) δ 9.39 (s, 1H), 8.66 (s, 1H), 7.78 – 7.69 (m, 2H), 7.67 (d, *J* = 16.1 Hz, 1H), 7.50 (d, *J* = 8.1 Hz, 2H), 7.47 – 7.34 (m, 2H), 6.96 – 6.78 (m, 2H), 6.66 (d, *J* = 16.1 Hz, 1H), 4.84 (s, 2H), 3.73 (s, 3H), 3.71 (s, 3H).

^{13}C NMR (75 MHz, DMSO-d_6) δ 166.7, 157.3, 154.9, 144.2, 139.1, 133.7, 131.9, 129.1, 128.2, 121.4, 117.9, 113.6, 76.9, 55.1, 51.5.

M.p.: 161 °C; **HPLC:** R_t= 7.09 min, purity ≥ 99 %; **ESI-MS:** 357.4 ($[M+H]^+$).

2.3.6 Methyl (*E*)-3-(4-(((3-(naphthalen-1-yl)ureido)oxy)methyl)phenyl)acrylate (**4f**)

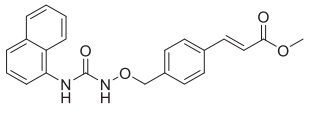

$C_{22}H_{20}N_2O_4$
376.41

4f was synthesised from the hydroxylamine **3** (300 mg, 1.45 mmol, 1.00 eq) and 1-naphtyl isocyanate (0.21 mL, 1.45 mmol, 1.00 eq) according to 2.3. 290 mg (0.77 mmol, 53 %) of the alkoxyurea **4f** was obtained as a white solid.

^{1}H NMR (300 MHz, DMSO-d_6) δ 9.63 (s, 1H), 8.86 (s, 1H), 7.98 – 7.87 (m, 1H), 7.81 – 7.66 (m, 5H), 7.63 – 7.43 (m, 6H), 6.69 (d, *J* = 16.1 Hz, 1H), 4.95 (s, 2H), 3.73 (s, 3H).

^{13}C-NMR (151 MHz, DMSO-d_6): δ (ppm) = 167.1, 158.4, 144.6, 139.5, 134.3, 134.1, 134.0, 129.8, 128.8, 128.5, 126.3, 126.1, 126.0, 125.3, 122.9, 122.0, 118.4, 77.6, 51.7.

M.p.: 156 °C; **HPLC:** R_t = 8.54 min, purity = 97.6 %; **ESI-MS:** 377.6 ($[M+H]^+$).

2.3.7 Methyl (E)-3-(4-(((3-([1,1'-biphenyl]-2-yl)ureido)oxy)methyl)phenyl)acrylate (**4g)**

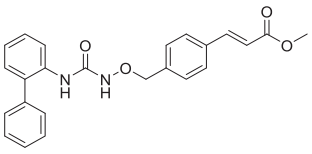

$C_{24}H_{22}N_2O_4$
402.45

4g was synthesised from the hydroxylamine **3** (300 mg, 1.45 mmol, 1.00 eq) and 1-naphtyl isocyanate (0.21 mL, 1.45 mmol, 1.00 eq) according to 2.3. 90 mg (0.77 mmol, 53 %) of the alkoxyurea **4g** was obtained as a white solid.

^{1}H NMR (600 MHz, DMSO-d_6) δ 9.66 (s, 1H), 7.98 (dd, *J* = 8.2, 1.2 Hz, 1H), 7.95 (s, 1H), 7.70 – 7.63 (m, 3H), 7.50 – 7.42 (m, 2H), 7.42 – 7.37 (m, 3H), 7.36 – 7.32 (m, 1H), 7.24 (dd, *J* = 7.6, 1.7 Hz, 1H), 7.17 (td, *J* = 7.4, 1.3 Hz, 1H), 7.13 (d, *J* = 8.1 Hz, 2H), 6.67 (d, *J* = 16.1 Hz, 1H), 4.62 (s, 2H), 3.73 (s, 3H).

^{13}C NMR (151 MHz, DMSO-d_6) δ 166.6, 156.7, 144.1, 138.1, 138.0, 134.9, 133.8, 133.0, 130.0, 129.0, 129.0, 128.9, 128.3, 128.0, 127.7, 123.7, 121.5, 118.1, 77.0, 51.5.

M.p.: 133 °C; **HPLC:** R_t =15.20 min, purity ≥ 99 %; **ESI-MS:** 403.2 ($[M+H]^+$).

2.4 General procedure for the synthesis of the alkoxyamides 5

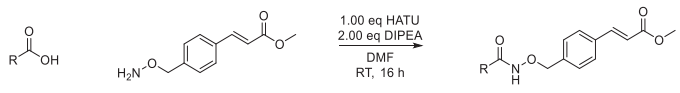

The respective carboxylic acid (1.00 eq), the coupling reagent HATU (1.00 eq) and DIPEA (2.00 eq) were dissolved in 10 mL of DMF and stirred for 10 minutes at ambient temperature. Subsequently, the hydroxylamine **3** (1.00 eq) was added and the resulting mixture stirred for 16 h at rt.

Purification method A

The solution was diluted with 50 mL of ethyl acetate and washed with a 10% (w/w)-solution (3x), sat. K_2CO_3-solution (3x) brine (1x). After drying over Na_2SO_4 the solvent removed under reduced pressure. The product was obtained after flash column chromatography (hexane/ethyl acetate).

Purification method B

The reaction mixture was diluted with 50 mL of dH_2O and the resulting precipitate collected by filtration. The product was obtained after washing with dH_2O (3x).

2.4.1 Methyl (*E*)-3-(4-((benzamidooxy)methyl)phenyl)acrylate (**5a**)

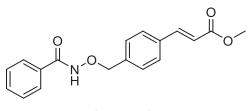

5a was synthesised from the hydroxylamine **3** (1.00 eq, 200 mg, 0.965 mmol) and benzoic acid (1.00 eq, 118 mg, 0.965 mmol) according to 2.4 and the purification method A. 286 mg (0.920mmol, 95%) of the alkoxyamide **5a** was obtained as a white solid.

^{1}H NMR (600 MHz, DMSO-d_6) δ 11.78 (s, 1H), 7.79 – 7.71 (m, 4H), 7.68 (d, *J* = 16.1 Hz, 1H), 7.58 – 7.42 (m, 5H), 6.67 (d, *J* = 16.1 Hz, 1H), 4.96 (s, 2H), 3.73 (d, *J* = 1.5 Hz, 3H).

^{13}C NMR (151 MHz, DMSO-d_6) δ 166.7, 164.5, 144.1, 138.4, 133.9, 132.3, 131.7, 129.2, 128.5, 128.4, 127.1, 118.1, 76.5, 51.5.

M.p.: = 175 °C; **HPLC:** R_t = 11.58 min, purity = 98.9 %; **ESI-MS:** 312.3 ($[M+H]^+$).

2.4.2 Methyl (*E*)-3-(4-(((3,5-dimethylbenzamido)oxy)methyl)phenyl)acrylate (**5b**)

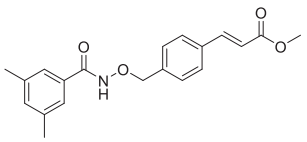

$C_{20}H_{21}NO_4$
339.39

5b was synthesised from the hydroxylamine **3** (1.00 eq, 230 mg, 1.11 mmol) and 3,4-dimethyl benzoic acid (1.00 eq, 167mg, 1.11mmol) according to 2.4 and the purification method A. 347mg (1.02mmol, 92%) of the alkoxyamide **5b** was obtained as a white solid.

^{1}H NMR (600 MHz, DMSO-d_6) δ 11.66 (s, 1H), 7.77 – 7.72 (m, 2H), 7.68 (d, *J* = 16.1 Hz, 1H), 7.50 (d, *J* = 7.9 Hz, 2H), 7.37 – 7.32 (m, 2H), 7.18 – 7.14 (m, 1H), 6.67 (d, *J* = 16.1 Hz, 1H), 5.75 (s, 0H), 4.94 (s, 2H), 3.73 (s, 3H), 2.29 (s, 6H).

^{13}C NMR (151 MHz, DMSO-d_6) δ 166.6, 144.1, 137.6, 133.9, 132.8, 129.1, 128.3, 124.8, 118.0, 76.4, 51.5, 20.8.

M.p.: = 124 °C; **HPLC:** R_t = 13.52 min, purity: ≥ 99.0 %; **APCI-MS:** 438.1 ($[M-H]^-$).

2.4.3 Methyl (*E*)-3-(4-(((4-butoxybenzamido)oxy)methyl)phenyl)acrylate (**5c**)

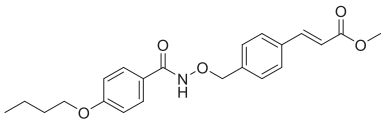

$C_{22}H_{25}NO_5$
383.44

5c was synthesised from the hydroxylamine **3** (1.00 eq, 267 mg, 1.29 mmol) and 4-butoxybenzoic acid (1.00 eq, 250 mg, 1.29 mmol) according to 2.4 and the purification method B. 438 mg (1.14 mmol, 89 %) of the alkoxyamide **5c** was obtained as a white solid.

^{1}H NMR (500 MHz, DMSO-d_6) δ 11.59 (s, 1H), 7.75 – 7.69 (m, 4H), 7.68 (d, *J* = 16.0 Hz, 1H), 7.50 (d, *J* = 7.9 Hz, 2H), 7.06 – 6.91 (m, 2H), 6.65 (d, *J* = 16.1 Hz, 1H), 4.94 (s, 2H), 4.01 (t, *J* = 6.5 Hz, 2H), 3.73 (s, 3H), 1.69 (dq, *J* = 8.6, 6.6 Hz, 2H), 1.50 – 1.32 (m, 2H), 0.93 (t, *J* = 7.4 Hz, 3H).

^{13}C NMR (126 MHz, DMSO-d_6) δ 166.5, 164.2, 161.2, 144.0, 138.5, 133.8, 129.0, 128.8, 128.2, 124.1, 117.9, 114.0, 76.4, 67.3, 51.3, 30.5, 18.6, 13.5.

M.p.: = 181 °C; **HPLC:** R_t = 10.88 min Purity: ≥ 99 %; **ESI-MS:** 384.1 ($[M+H]^+$).

2.4.4 Methyl (*E*)-3-(4-(((3,4,5-trimethoxybenzamido)oxy)methyl)phenyl)acrylate (**5d**)

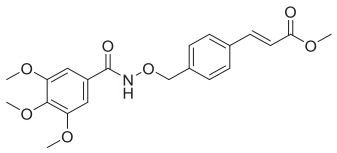

$C_{21}H_{23}NO_7$
401.42

5d was synthesised from the hydroxylamine **3** (1.00 eq, 249 mg, 1.20 mmol) and 3,4,5-trimethoxybenzoic acid (1.00 eq, 257 mg, 1.20 mmol) according to 2.4 and the purification method B. 455 mg (1.13 mmol, 95 %) of the alkoxyamide **5d** was obtained as a white solid.

^{1}H NMR (600 MHz, DMSO-d_6) δ 11.74 (s, 1H), 10.77 (s, 1H), 9.06 (s, 1H), 7.59 (d, *J* = 7.7 Hz, 2H), 7.53 – 7.42 (m, 3H), 7.09 (s, 2H), 6.49 (d, *J* = 15.8 Hz, 1H), 4.94 (s, 2H), 3.81 (s, 7H), 3.70 (s, 3H), 3.34 (s, 2H).

^{13}C NMR (151 MHz, DMSO-d_6) δ 164.3, 163.1, 153.1, 140.7, 138.4, 137.7, 135.3, 129.9, 127.9, 127.7, 119.9, 105.1, 77.1, 60.6, 56.5.

M.p.: = 164 °C; **HPLC:** R_t = 14.79, purity: ≥ 99 %; **ESI-MS: 402.1 ([M+H]$^+$)**.

2.4.5 Methyl (*E*)-3-(4-(((2,2-diphenylpropanamido)oxy)methyl)phenyl)acrylate (**5e**)

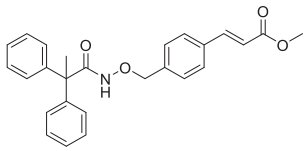

$C_{26}H_{25}NO_4$
415.49

5e was synthesised from the hydroxylamine **3** (1.00 eq, 230 mg, 1.11 mmol) and benzoic acid (1.00 eq, 251mg, 1.11mmol) according to 2.4 and the purification method A. 375mg (0.902mmol, 81%) of the alkoxyamide **5e** was obtained as a viscous colourless oil.

^{1}H NMR (600 MHz, DMSO-d_6) δ 10.94 (s, 1H), 7.76 – 7.70 (m, 2H), 7.68 (d, *J* = 16.0 Hz, 1H), 7.43 (d, *J* = 7.9 Hz, 2H), 7.29 (dd, *J* = 8.2, 6.6 Hz, 4H), 7.27 – 7.21 (m, 2H), 7.15 – 7.10 (m, 4H), 6.67 (d, *J* = 16.1 Hz, 1H), 4.84 (s, 2H), 3.73 (s, 3H), 1.81 (s, 3H).

^{13}C NMR (151 MHz, DMSO-d_6) δ 171.4, 166.6, 144.6, 144.1, 138.4, 133.8, 129.3, 128.2, 127.9, 127.9, 126.5, 118.0, 76.0, 54.7, 51.5, 26.3.

HPLC: R_t = 11.58 min, purity ≥ 99.0 %; **APCI-MS: 414.7** ([M-H]$^-$).

2.4.6 Methyl (*E*)-3-(4-(((2-phenylthiazole-4-carboxamido)oxy)methyl)phenyl)acrylate (**5f**)

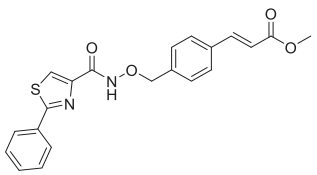

$C_{21}H_{18}N_2O_4S$
394.45

5f was synthesised from the hydroxylamine **3** (1.00 eq, 247 mg, 1.19 mmol) and 2-phenylthiazole-4-carboxylic acid (1.00 eq, 250 mg, 1.19 mmol) according to 2.4 and the purification method B. 419 mg (1.06 mmol, 89 %) of the alkoxyamide **5f** was obtained as a white solid.

^{1}H NMR (500 MHz, DMSO-d_6) δ 11.88 (s, 1H), 8.36 (s, 1H), 8.08 – 7.98 (m, 2H), 7.78 – 7.72 (m, 2H), 7.67 (d, *J* = 16.0 Hz, 1H), 7.53 (dd, *J* = 7.3, 2.5 Hz, 5H), 6.66 (d, *J* = 16.1 Hz, 1H), 5.01 (s, 2H), 3.73 (s, 3H).

^{13}C NMR (126 MHz, DMSO-d_6) δ 167.5, 166.5, 158.3, 148.4, 144.0, 138.2, 133.8, 132.3, 130.7, 129.1, 129.0, 128.2, 126.4, 124.6, 118.0, 76.7, 51.3.

M.p.: = 154 °C; **HPLC:** R_t = 14.43 min, purity: ≥ 99 %; **ESI-MS:** 395.1 ($[M+H]^+$).

2.4.7 Methyl (*E*)-3-(4-(((2-(2-methyl-1H-indol-3-yl)acetamido)oxy)methyl)phenyl)acrylate (**5g**)

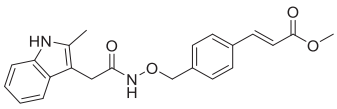

$C_{22}H_{22}N_2O_4$
378.43

5g was synthesised from the hydroxylamine **3** (1.00 eq, 230 mg, 1.11 mmol) and 2-methyl-3-indole acetic acid (1.00 eq, 230mg, 1.11mmol) according to 2.4 and the purification method A. 169mg (0.445mmol, 40%) of the alkoxyamide **5g** was obtained as a brown solid.

^{1}H NMR (600 MHz, DMSO-d_6) δ 11.17 (s, 1H), 10.78 (s, 1H), 7.70 (d, *J* = 8.0 Hz, 2H), 7.67 (d, *J* = 16.1 Hz, 1H), 7.43 (d, *J* = 7.9 Hz, 1H), 7.39 (d, *J* = 7.9 Hz, 2H), 7.22 (d, *J* = 8.0 Hz, 1H), 6.97 (t, 1H), 6.91 (t, *J* = 7.4 Hz, 1H), 6.66 (d, *J* = 16.0 Hz, 1H), 4.78 (s, 2H), 3.73 (s, 3H), 3.33 (s, 3H), 2.32 (s, 3H).

^{13}C NMR (151 MHz, DMSO-d_6) δ 167.9, 166.6, 144.1, 138.5, 135.0, 133.8, 133.2, 129.1, 128.3, 128.3, 120.0, 118.1, 118.0, 117.8, 110.2, 104.0, 76.1, 51.5, 28.6, 11.4.

M.p.: = 200 °C; **HPLC:** R_t = 11.88 min, purity: ≥ 99.0 %; **ESI-MS:** 379.5 ($[M+H]^+$).

2.4.8 Methyl (*E*)-3-(4-(((2-naphthamido)oxy)methyl)phenyl)acrylate (**5h**)

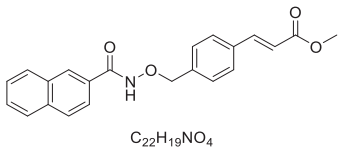

$C_{22}H_{19}NO_4$
361.40

5h was synthesised from the hydroxylamine **3** (1.00 eq, 210 mg, 1.01 mmol) and 2-Naphthoic acid (1.00 eq, 174 mg, 1.01 mmol) according to 2.4 and the purification method B. 271 mg (0.75 mmol, 74 %) of the alkoxyamide **5h** was obtained as an white solid.

^{1}H NMR (600 MHz, DMSO-d_6) δ 11.97 (s, 1H), 8.36 (d, *J* = 1.7 Hz, 1H), 8.05 – 7.94 (m, 3H), 7.83 (dd, *J* = 8.6, 1.8 Hz, 1H), 7.76 (d, *J* = 7.8 Hz, 2H), 7.68 (d, *J* = 16.0 Hz, 1H), 7.60 (dddd, *J* = 16.6, 8.2, 6.8, 1.5 Hz, 2H), 7.54 (d, *J* = 7.8 Hz, 2H), 6.67 (d, *J* = 16.0 Hz, 1H), 5.02 (s, 2H), 3.73 (s, 3H).

^{13}C NMR (151 MHz, DMSO-d_6) δ 166.7, 151.4, 144.2, 138.7, 134.2, 133.8, 133.2, 132.1, 129.1, 128.8, 128.3, 128.0, 127.6, 127.4, 126.8, 123.8, 118.0, 76.4, 51.5.

M.p.: = 207 °C; **HPLC:** R_t = 13.20 min, purity ≥ 99 %; **APCI-MS:** 360.5 ($[M-H]^-$).

2.4.9 methyl (E)-3-(4-(((isoquinoline-1-carboxamido)oxy)methyl)phenyl)acrylate (**5i**)

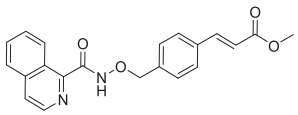

$C_{21}H_{18}N_2O_4$
362.39

5i was synthesised from the hydroxylamine **3** (1.00 eq, 250 mg, 1.21 mmol) and Isoquinoline-1-carboxylic Acid (1.21 eq, 209 mg, 1.21 mmol) according to 2.4 and the purification method B. 319 mg (0.88 mmol, 73 %) of the alkoxyamide **5i** was obtained as an white solid.

^{1}H NMR (600 MHz, DMSO-d_6) δ 12.02 (s, 1H), 8.52 (d, *J* = 5.6 Hz, 1H), 8.50 (d, *J* = 8.5 Hz, 1H), 8.04 (d, *J* = 8.2 Hz, 1H), 8.01 (d, *J* = 5.6 Hz, 1H), 7.83 (ddd, *J* = 8.2, 6.9, 1.2 Hz, 1H), 7.77 (d, *J* = 7.9 Hz, 2H), 7.73 – 7.66 (m, 1H), 7.69 (d, *J* = 16.0 Hz, 1H), 7.57 (d, *J* = 7.9 Hz, 2H), 6.68 (d, *J* = 16.0 Hz, 1H), 5.06 (s, 2H), 3.73 (s, 3H).

^{13}C NMR (151 MHz, DMSO-d_6) δ 166.6, 163.4, 150.9, 144.1, 141.0, 138.4, 136.2, 133.9, 130.8, 129.2, 128.4, 128.3, 127.2, 125.9, 125.4, 123.2, 118.1, 76.6, 51.5.

M.p.: = 121 °C; **HPLC:** R_t = 11.97 min, purity: ≥ 99 %; **APCI-MS: 361.6** ($[M-H^+]^-$).

2.4.10 Methyl (E)-3-(4-(((quinoline-2-carboxamido)oxy)methyl)phenyl)acrylate (**5j**)

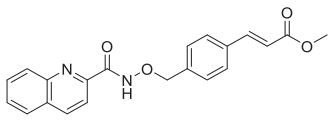

$C_{21}H_{18}N_2O_4$
362.39

5j was synthesised from the hydroxylamine **3** (1.00 eq, 353 mg, 1.73 mmol) and quinaldic acid (1.00 eq, 300 mg, 1.73 mmol) according to 2.4 and the purification method B. 583 mg (1.61 mmol, 93 %) of the alkoxyamide **5j** was obtained as an white solid.

^{1}H NMR (600 MHz, DMSO-d_6) δ 12.22 (s, 1H), 8.57 (d, *J* = 8.5 Hz, 1H), 8.15 – 8.04 (m, 3H), 7.87 (ddd, *J* = 8.4, 6.8, 1.4 Hz, 1H), 7.76 (d, *J* = 8.0 Hz, 2H), 7.72 (ddd, *J* = 8.1, 6.8, 1.2 Hz, 1H), 7.68 (d, *J* = 16.1 Hz, 1H), 7.56 (d, *J* = 8.0 Hz, 2H), 6.67 (d, *J* = 16.0 Hz, 1H), 5.04 (s, 2H), 3.73 (s, 3H).

^{13}C NMR (151 MHz, DMSO-d_6) δ 166.6, 161.8, 149.7, 146.0, 144.1, 138.4, 137.9, 133.9, 130.6, 129.2, 129.1, 128.8, 128.3, 128.2, 128.2, 118.8, 118.0, 76.6, 51.5.

M.p.: = 189 °C; **HPLC:** R_t = 13.73 min, purity: ≥ 99 %; **ESI-MS:** 363.2 ($[M+H]^+$).

2.5 General procedure for the synthesis of alkoxyurea based hydroxamic acids (6)

1.00 eq of the alkoxyurea **4** was dissolved in a mixture of dichloromethane and methanol (1:2, 15 mL/mmol). The reaction was cooled to 0°C. Afterwards, 10.0 eq of NaOH and 30.0 eq of hydroxylamine (50 % aqueous solution) were added and stirred for 16 h. The solvent was removed under reduced pressure and the remaining residue dissolved in dH_2O (10 mL/mmol). Subsequently, the resulting solution was neutralised with a 1 M HCl solution and the crude product extracted with ethyl acetate. After removing the solvent under reduced pressure, the crude product was purified by flash column chromatography (DCM/MeOH, stepwise gradient).

2.5.1 (*E*)-3-(4-(((3-ethylureido)oxy)methyl)phenyl)-*N*-hydroxyacrylamide (**6a**)

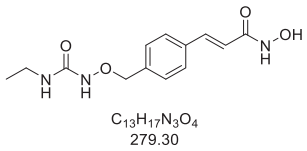

6a was synthesised from the ester **4a** (180 mg, 0.65 mmol, 1.00 eq), hydroxylamine (0.60 mL, 19.40 mmol, 30.00 eq) and NaOH (260 mg, 6.47 mmol, 10.00 eq) according to 2.5. 210 mg (0.76 mmol, 78 %) of the hydroxamic acid **6a** was obtained as an white solid.

^{1}H NMR (600 MHz, DMSO-d_6) δ 10.75 (s, 1H), 9.04 (s, 1H), 9.01 (s, 1H), 7.55 (d, *J* = 8.0 Hz, 2H), 7.48 – 7.40 (m, 3H), 6.78 (t, *J* = 5.9 Hz, 1H), 6.47 (d, *J* = 15.8 Hz, 1H), 4.71 (s, 2H), 3.06 (qd, *J* = 7.1, 5.8 Hz, 2H), 0.99 (t, *J* = 7.1 Hz, 3H).

^{13}C NMR (151 MHz, DMSO-d_6) δ 163.2, 160.1, 138.5, 134.9, 129.6, 127.8, 119.6, 100.0, 77.2, 34.1, 15.9.

M.p.: = 161 °C; **HPLC:** R_t = 5.40 min, purity = 95.1 %; **ESI-MS:** 280.4 ($[M+H]^+$).

2.5.2 (*E*)-*N*-hydroxy-3-(4-(((3-phenylureido)oxy)methyl)phenyl)acrylamide (**6b**)

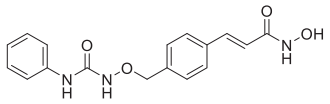

$C_{17}H_{17}N_3O_4$
327.34

6b was synthesised from the ester **4b** (250 mg, 0.61 mmol, 1.00 eq), hydroxylamine (0.56 mL, 18.40 mmol, 30.00 eq) and NaOH (250 mg, 6.13 mmol, 10.00 eq) according to 2.5. 150 mg (0.46 mmol, 75 %) of the hydroxamic acid **6b** was obtained as an white solid.

^{1}H NMR (300 MHz, DMSO-d_6) δ 9.49 (s, 1H), 8.77 (s, 1H), 7.74 (d, *J* = 8.0 Hz, 2H), 7.67 (d, *J* = 16.1 Hz, 1H), 7.57 – 7.46 (m, 4H), 7.32 – 7.19 (m, 2H), 7.05 – 6.92 (m, 1H), 6.66 (d, *J* = 16.1 Hz, 1H), 4.86 (s, 2H), 3.73 (s, 3H).

^{13}C-NMR (150 MHz, DMSO-d_6): δ 157.3, 154.9, 137.9, 138.5, 137.9, 137.8, 134.5, 129.2, 127.9, 121.7, 121.3, 119.2, 77.0.

M.p.: = 148 °C; **HPLC:** R_t = 8.13 min, purity = 98.9 %; **ESI-MS:** 328.4 ([M+H]+).

2.5.3 (*E*)-3-(4-(((3-(3,5-dimethylphenyl)ureido)oxy)methyl)phenyl)-N-hydroxyacrylamide (**6c**)

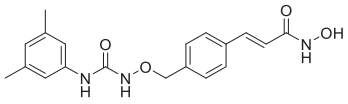

$C_{19}H_{21}N_3O_4$
355.39

6c was synthesised from the ester 4c (250 mg, 0.61 mmol, 1.00 eq), hydroxylamine (0.56 mL, 18.40 mmol, 30.00 eq) and NaOH (250 mg, 6.13 mmol, 10.00 eq) according to 2.5. 180 mg (0.50 mmol, 88 %) of the hydroxamic acid **6c** was obtained as an white solid.

^{1}H NMR (300 MHz, DMSO-d6) δ 10.28 (s, 1H), 9.45 (s, 1H), 8.78 (s, 1H), 8.55 (s, 1H), 7.57 (m, 2H), 7.48 (m, 2H), 7.44 (d, *J*=15.8, 1H), 7.13 (s, 2H), 6.62 (s, 1H), 6.54 (d, *J*= 15.8, 1H,), 4.83 (s, 2H 2.21 (s, 6H).

^{13}C NMR (151 MHz, DMSO-d_6) δ 163.2, 157.5, 139.3, 138.2, 137.9, 137.8, 135.2, 129.7, 127.8, 124.4, 120.2, 117.5, 77.6, 21.6.

M.p.: = 148 °C; **HPLC:** R_t = 9.75 min, purity ≥ 99 %; **ESI-MS:** 356.4 ($[M+H^+]^+$).

2.5.4 (*E*)-*N*-hydroxy-3-(4-(((3-mesitylureido)oxy)methyl)phenyl)acrylamide (**6d**)

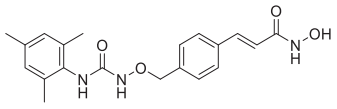

$C_{20}H_{23}N_3O_4$
369.42

6d was synthesised from the ester **4d** (370 mg, 1.00 mmol, 1.00 eq), hydroxylamine (0.92 mL, 30.00 mmol, 30.00 eq) and NaOH (400 mg, 10.00 mmol, 10.00 eq) according to 2.5. 340 mg (0.92 mmol, 92 %) of the hydroxamic acid **6d** was obtained as an white solid.

^{1}H NMR (600 MHz, DMSO-d_6) δ 10.91 (s, 1H), 10.51 (s, 0H), 9.38 (s, 1H), 9.17 – 8.33 (m, 3H), 8.18 (s, 1H), 7.55 (d, *J* = 8.0 Hz, 2H), 7.50 (d, *J* = 7.9 Hz, 2H), 7.45 (d, *J* = 15.8 Hz, 1H), 6.85 (s, 2H), 6.56 (d, *J* = 15.8 Hz, 1H), 4.83 (s, 2H), 2.21 (s, 3H), 2.06 (s, 6H).

^{13}C NMR (151 MHz, DMSO-d_6) δ 163.1, 158.4, 138.4, 138.3, 136.2, 135.6, 135.0, 132.8, 129.8, 128.6, 127.7, 119.8, 77.5, 21.0, 18.4.

M.p.: = 175 °C; **HPLC:** R_t = 10.41 min, purity ≥ 99 %; **ESI-MS:** 370.6 ($[M+H]^+$).

2.5.5 (*E*)-*N*-hydroxy-3-(4-(((3-(4-methoxyphenyl)ureido)oxy)methyl)phenyl)acrylamide (6e)

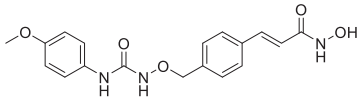

$C_{18}H_{19}N_3O_5$
357.37

6e was synthesised from the ester **4e** (300 mg, 0.84 mmol, 1.00 eq), hydroxylamine (0.77 mL, 25.30 mmol, 30.00 eq) and NaOH (340 mg, 8.42 mmol, 10.00 eq) according to 2.5. 220 mg (0.60 mmol, 72 %) of the hydroxamic acid **6e** was obtained as an white solid.

^{1}H NMR (300 MHz, DMSO-d_6) δ 9.43 (s, 1H), 8.69 (s, 1H), 7.57 (d, *J* = 7.9 Hz, 2H), 7.53 – 7.45 (m, 3H), 7.41 (dd, *J* = 9.1, 2.3 Hz, 3H), 6.90 – 6.75 (m, 2H), 6.48 (d, *J* = 15.8 Hz, 1H), 4.83 (s, 2H), 3.71 (s, 4H).

^{13}C NMR (150 MHz, DMSO-*d6*) δ 165.8, 156.4, 153.2, 143.7, 138.1, 132.8, 129.9, 128.2, 127.8, 120.0, 117.2, 112.7, 76.8, 55.0.

M.p.: = 163 °C; **HPLC:** R_t = 7.88 min, Purity = 98.9 %; **ESI-MS:** 358.5 ($[M+H]^+$).

2.5.6 (*E*)-*N*-hydroxy-3-(4-(((3-(naphthalen-1-yl)ureido)oxy)methyl)phenyl)acrylamide (**6f**)

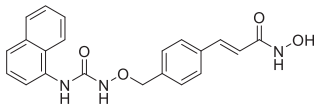

$C_{21}H_{19}N_3O_4$
377.40

6f was synthesised from the ester **4f** (250 mg, 0.66 mmol, 1.00 eq), hydroxylamine (0.62 mL, 19.90 mmol, 30.00 eq) and NaOH (270 mg, 6.64 mmol, 10.00 eq) according to 2.5. 190 mg (0.50 mmol, 76 %) of the hydroxamic acid **6f** was obtained as an white solid.

^{1}H NMR (300 MHz, DMSO-d_6) δ 12.41 (s, 1H), 9.63 (s, 1H), 8.86 (s, 1H), 8.03 – 7.87 (m, 1H), 7.85 – 7.68 (m, 4H), 7.69 – 7.36 (m, 7H), 6.57 (d, *J* = 16.0 Hz, 1H), 4.95 (s, 2H).
^{13}C NMR (151 MHz, DMSO-d_6) δ 168.0, 158.4, 144.1, 139.2, 134.5, 134.1, 134.1, 129.9, 128.8, 128.6, 128.5, 126.4, 126.2, 126.1, 125.3, 122.9, 122.1, 119.8, 77.6.
M.p.: = 163 °C; **HPLC:** R_t = 9.00 min, purity = 96.1 %; **ESI-MS:** 378.7 ($[M+H]^+$).

2.5.7 (*E*)-3-(4-(((3-([1,1'-biphenyl]-2-yl)ureido)oxy)methyl)phenyl)-*N*-hydroxyacrylamide (**6g**)

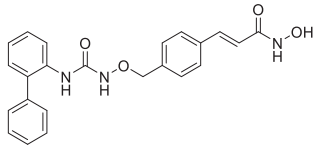

$C_{23}H_{21}N_3O_4$
403.44

6g was synthesised from the ester **4g** (300 mg, 0.75 mmol, 1.00 eq), hydroxylamine (1.37 mL, 22.4 mmol, 30.0 eq) and NaOH (298 mg, 7.45 mmol, 10.0 eq) according to 2.5. 209 mg (0.52 mmol, 70 %) of the hydroxamic acid **6g** was obtained as an white solid.
^{1}H NMR (600 MHz, DMSO-d_6) δ 10.77 (s, 1H), 9.65 (s, 1H), 9.07 (s, 1H), 7.98 (dd, *J* = 8.2, 1.2 Hz, 1H), 7.94 (s, 1H), 7.54 – 7.43 (m, 5H), 7.42 – 7.37 (m, 3H), 7.34 (ddd, *J* = 8.4, 7.4, 1.7 Hz, 1H), 7.24 (dd, *J* = 7.6, 1.7 Hz, 1H), 7.17 (td, *J* = 7.5, 1.3 Hz, 1H), 7.11 (d, *J* = 7.9 Hz, 2H), 6.48 (d, *J* = 15.8 Hz, 1H), 4.60 (s, 2H).
^{13}C NMR (151 MHz, DMSO-d_6) δ 163.1, 157.1, 138.6, 138.4, 137.3, 135.3, 135.1, 133.4, 130.5, 129.6, 129.4, 129.4, 128.5, 128.2, 127.8, 124.2, 122.0, 119.9, 77.6.
M.p.: = 385 °C; **HPLC:** Rt = 10.73 min, purity ≥ 99 %; **ESI-MS: 404.1** ($[M+H]^+$).

2.6 General procedure for the synthesis of alkoxyamide based hydroxamic acids (7)

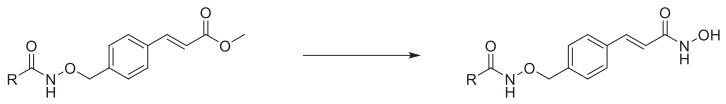

Method A

1.00 eq of the methyl ester **5** was dissolved in THF (10 mL/mmol) and 5.00 eq of a 2 M LiOH solution added. The mixture was stirred for 16 h at ambient temperature. The solution was acidified to pH 4 with a 1 M HCl solution. The resulting carboxylic acid was extracted with ethyl acetate and the combined organic phase dried over Na_2SO_4. Afterwards, the solvent was removed under reduced pressure. The obtained carboxylic acid was used without any further purification for the synthesis of the respective hydroxamic acid. Under nitrogen atmosphere, 1.00 eq of the carboxylic acid was dissolved in 10 mL DMF and cooled to 0 °C. 1.20 eq DIPEA and 1.20 eq isobutyl chloroformate was added consecutively. After 30 minutes, a solution of 5.00 eq hydroxylamine hydrochloride and 6.00 eq DIPEA in 10 mL of DIPEA was added dropwise and stirred for 16 h to room temperature. The solvent was removed under reduced pressure and resuspended in ethyl acetate. Subsequently, the organic phase was washed 3x with 1 M HCl. The solvent was removed *in vacuo* and the product purified by flash column chromatography (DCM/MeOH, step wise gradient).

Method B

1.00 eq of the alkoxyamide **5** was suspended in 2 mL of dry methanol in a microwave reaction vessel. After the addition of 10 eq of hydroxylamine hydrochloride and 15 eq of sodium methanolate (5.4 M solution in methanol). The conversion to the respective hydroxamic acid was performed under microwave irradiation (150 Watt) at 70 °C for 30 minutes. Afterwards, the reaction mixture was poured on 100 mL of ice water, acidified to pH 6 and the product extracted with ethyl acetate. The solvent of the combined organic phases was removed under reduced pressure and the product purified by flash column chromatography (DCM/MeOH).

2.6.1 (*E*)-*N*-((4-(3-(hydroxyamino)-3-oxoprop-1-en-1-yl)benzyl)oxy)benzamide (7a)

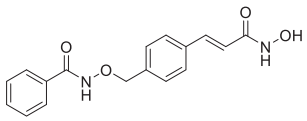

$C_{17}H_{16}N_2O_4$
312.33

7a was synthesised from the alkoxyamide **5a** (1.00 eq, 140 mg, 0.642 mmol) according to 2.6 Method A. 26.1 mg (0.083 mmol, 13 %) of the alkoxyamide **7a** was obtained as a lightly red solid over two steps.

^{1}H NMR (600 MHz, DMSO-d_6) δ 11.92 (s, 1H), 10.95 (s, 1H), 9.07 (s, 1H), 7.76 (d, *J* = 7.6 Hz, 2H), 7.57 (d, *J* = 7.8 Hz, 2H), 7.54 (t, *J* = 7.4 Hz, 1H), 7.51 – 7.42 (m, 5H), 6.57 (d, *J* = 15.7 Hz, 1H), 4.94 (s, 2H).

^{13}C NMR (151 MHz, DMSO-d_6) δ 164.4, 162.7, 137.7, 137.3, 134.8, 132.3, 131.6, 129.4, 128.4, 127.4, 127.1, 119.6, 76.5.

M.p.: = 172 °C; **HPLC:** R_t = 7.20 min, purity ≥ 99 %; **ESI-MS:** 313.3 ($[M+H]^+$).

2.6.2 (*E*)-*N*-((4-(3-(hydroxyamino)-3-oxoprop-1-en-1-yl)benzyl)oxy)-3,5-dimethylbenzamide (**7b**)

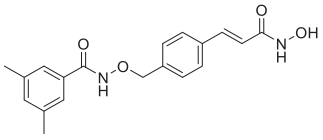

$C_{19}H_{20}N_2O_4$
340.38

7b was synthesised from the alkoxyamide **5b** (1.00 eq, 290 mg, 0.854 mmol) according to 2.6 Method A. 108 mg (0.316 mmol, 37 %) of the alkoxyamide **7b** was obtained as a lightly red solid.

^{1}H NMR (600 MHz, DMSO-d_6) δ 11.66 (s, 1H), 10.77 (s, 1H), 9.05 (s, 1H), 7.58 (d, *J* = 7.8 Hz, 2H), 7.50 – 7.44 (m, 3H), 7.34 (s, 2H), 7.17 (s, 1H), 6.48 (d, *J* = 15.8 Hz, 1H), 4.92 (s, 2H), 2.30 (s, 6H).

^{13}C NMR (151 MHz, DMSO-d_6) δ 164.7, 162.7, 137.9, 137.6, 137.3, 134.7, 132.9, 132.3, 129.3, 127.4, 124.8, 119.3, 76.5, 20.8.

M.p.: = 198 °C; **HPLC:** R_t = 9.17min, purity ≥ 99%; **ESI-MS:** 341.2 ($[M+H]^+$).

2.6.3 (*E*)-4-butoxy-*N*-((4-(3-(hydroxyamino)-3-oxoprop-1-en-1-yl)benzyl)oxy)benzamide (**7c**)

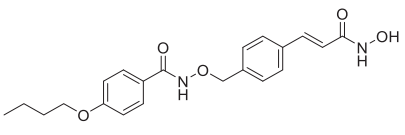

$C_{21}H_{24}N_2O_5$
384.43

7c was synthesised from the alkoxyamide **5c** (1.00 eq, 250 mg, 0.652 mmol) according to 2.6 Method B. 86.1 mg (0.224 mmol, 34 %) of the alkoxyamide **6c** was obtained as a lightly red solid.

^{1}H NMR (600 MHz, DMSO-d_6) δ 11.63 (s, 1H), 10.79 (s, 1H), 9.06 (s, 1H), 7.71 (d, *J* = 8.4 Hz, 2H), 7.59 (d, *J* = 7.7 Hz, 2H), 7.53 – 7.41 (m, 3H), 6.99 (d, *J* = 8.6 Hz, 2H), 6.50 (d, *J* = 15.8 Hz, 1H), 4.92 (s, 2H), 4.02 (t, *J* = 6.5 Hz, 2H), 1.78 – 1.65 (m, 2H), 1.43 (h, *J* = 7.4 Hz, 2H), 0.93 (t, *J* = 7.4 Hz, 3H).

^{13}C NMR (151 MHz, DMSO-d_6) δ 176.1, 175.1, 161.3, 140.2, 138.0, 137.4, 129.3, 128.9, 127.4, 124.2, 119.4, 114.1, 76.5, 67.4, 30.6, 18.7, 13.7.

M.p.: = 177 °C; **HPLC:** Rt = 10.88 min, purity ≥ 99 %; **ESI-MS**: 385. 1 ([M+H]$^+$).

2.6.4 (*E*)-*N*-((4-(3-(hydroxyamino)-3-oxoprop-1-en-1-yl)benzyl)oxy)-3,4,5-trimethoxybenzamide (**7d**).

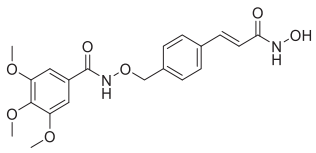

$C_{20}H_{22}N_2O_7$
402.40

7d was synthesised from the alkoxyamide **5d** (1.00 eq, 250 mg, 0.62 mmol) according to 2.6 Method B. 142 mg (0.354 mmol, 57 %) of the alkoxyamide **7d** was obtained as a lightly red solid.

^{1}H NMR (600 MHz, DMSO-d_6) δ 11.74 (s, 1H), 10.77 (s, 1H), 9.06 (s, 1H), 7.59 (d, *J* = 7.7 Hz, 2H), 7.53 – 7.42 (m, 3H), 7.09 (s, 2H), 6.49 (d, *J* = 15.8 Hz, 1H), 4.94 (s, 2H), 3.81 (s, 7H), 3.70 (s, 3H), 3.34 (s, 2H).

^{13}C NMR (151 MHz, DMSO-d_6) δ 164.3, 163.1, 153.1, 140.7, 138.4, 137.7, 135.3, 129.9, 127.9, 127.7, 119.9, 105.1, 77.1, 60.6, 56.5.

M.p.: = 98 °C; **HPLC:** R_t = 7.48, purity = 96.8 %; **ESI-MS**: 403.0 ([M+H]$^+$)

2.6.5 (*E*)-3-(4-(((2,2-diphenylpropanamido)oxy)methyl)phenyl)-*N*-hydroxyacrylamide (**7e**)

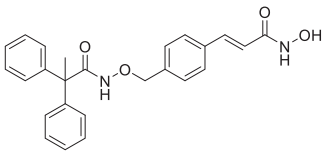

$C_{25}H_{24}N_2O_4$
416.48

7e was synthesised from the alkoxyamide **5e** (1.00 eq, 290 mg, 0.698 mmol) according to 2.6 Method B. 108 mg (0.258 mmol, 37 %) of the alkoxyamide **7e** was obtained as a lightly red solid.

^{1}H NMR (600 MHz, DMSO-d_6) δ 10.92 (s, 1H), 10.77 (s, 1H), 9.06 (s, 1H), 7.55 (d, *J* = 7.7 Hz, 2H), 7.47 (d, *J* = 15.8 Hz, 1H), 7.41 (d, *J* = 7.8 Hz, 2H), 7.29 (t, *J* = 7.3 Hz, 4H), 7.24 (t, *J* = 7.2 Hz, 2H), 7.12 (d, *J* = 7.7 Hz, 4H), 6.48 (d, *J* = 15.8 Hz, 1H), 4.82 (s, 2H), 1.81 (s, 3H).

^{13}C NMR (151 MHz, DMSO-d_6) δ 167.0, 162.7, 144.6, 137.9, 137.2, 131.6, 129.5, 127.9, 127.9, 127.3, 126.5, 119.3, 76.1, 54.7, 26.3.

M.p.: = 135 ◦C; **HPLC:** R_t = 10.80min, purity = 96.9%; **ESI-MS:** 417.3 ([M+H$^+$).

2.6.6 (*E*)-*N*-((4-(3-(hydroxyamino)-3-oxoprop-1-en-1-yl)benzyl)oxy)-2-phenylthiazole-4-carboxamide (**7f**).

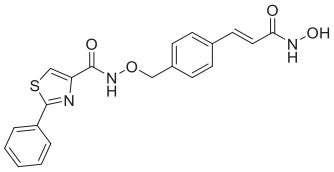

$C_{20}H_{17}N_3O_4S$
395.43

7f was synthesised from the alkoxyamide **5f** (1.00 eq, 250 mg, 0.634 mmol) according to 2.6 Method B. 160 mg (0.405 mmol, 64 %) of the alkoxyamide **7f** was obtained as a lightly red solid.

^{1}H NMR (600 MHz, DMSO-d_6) δ 11.91 (s, 1H), 10.78 (s, 1H), 9.07 (s, 1H), 8.37 (s, 1H), 8.23 – 7.95 (m, 2H), 7.59 (d, *J* = 7.9 Hz, 2H), 7.57 – 7.49 (m, 5H), 7.48 (d, *J* = 15.7 Hz, 1H), 6.49 (d, *J* = 15.9 Hz, 1H), 4.99 (s, 2H).

^{13}C NMR (151 MHz, DMSO-d_6) δ 167.6, 162.7, 158.4, 148.5, 138.0, 137.2, 134.8, 132.4, 130.8, 129.3, 129.3, 127.5, 126.5, 124.8, 119.4, 76.9.

M.p.: = 191 °C.

HPLC: R_t = 10.23 min, purity = ≥ 99 %; **ESI-MS:** 396.1 ([M+H]$^+$).

2.6.7 (E)-N-hydroxy-3-(4-(((2-(2-methyl-1H-indol-3-yl)acetamido)oxy)methyl)phenyl)acrylamide (**7g**)

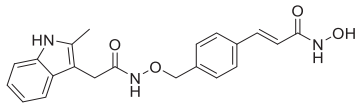

$C_{21}H_{21}N_3O_4$
379.42

7g was synthesised from the alkoxyamide **5g** (1.00 eq, 150 mg, 0.396 mmol) according to 2.6 Method A. 28.5 mg (0.08 mmol, 19%) of the alkoxyamide **7g** was obtained as a brown solid.

^{1}H NMR (600 MHz, DMSO-d_6) δ 11.16 (s, 1H), 10.78 (s, 1H), 7.54 (d, *J* = 7.8 Hz, 2H), 7.46 (d, *J* = 15.8 Hz, 1H), 7.43 (d, *J* = 7.8 Hz, 1H), 7.37 (d, *J* = 7.8 Hz, 2H), 7.22 (d, *J* = 7.9 Hz, 1H), 6.98 (t, *J* = 7.4 Hz, 1H), 6.91 (t, *J* = 7.4 Hz, 1H), 6.48 (d, *J* = 15.8 Hz, 1H), 4.76 (s, 2H), 3.33 (s, 2H), 2.32 (s, 3H).
^{13}C NMR (151 MHz, DMSO-d_6) δ 167.8, 162.6, 137.9, 137.4, 135.0, 134.7, 133.2, 129.3, 128.3, 127.4, 120.0, 119.3, 118.1, 117.8, 110.2, 104.0, 76.2, 28.6, 11.4.
M.p.: = 160 ◦C; **HPLC:** Rt = 7.95min, purity = 96.1%; **ESI-MS:** 380.3 ($[M+H]^+$).

2.6.8 (*E*)-*N*-((4-(3-(hydroxyamino)-3-oxoprop-1-en-1-yl)benzyl)oxy)-2-naphthamide (**7h**)

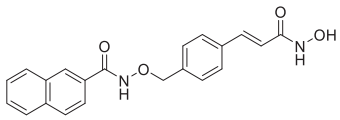

$C_{21}H_{18}N_2O_4$
362.39

7h was synthesised from the alkoxyamide **5h** (1.00 eq, 220 mg, 0.609 mmol) according to 2.6 Method B. 138 mg (0.381 mmol, 63 %) of the alkoxyamide **7h** was obtained as a lightly yellow solid.
^{1}H NMR (600 MHz, DMSO-d_6) δ 11.99 (s, 1H), 10.84 (s, 1H), 9.07 (s, 1H), 8.58 – 7.11 (m, 13H), 6.53 (d, *J* = 15.1 Hz, 1H), 5.00 (s, 2H).
^{13}C NMR (75 MHz, DMSO-d_6) δ 164.5, 162.7, 137.9, 137.3, 134.8, 134.2, 132.0, 129.6, 129.4, 128.8, 128.1, 127.8, 127.7, 127.5, 127.4, 126.9, 123.8, 119.4, 76.6.
M.p.: = 160 °C; **HPLC:** R_t = 9.50 min, purity = 96.6 %; **APCI-MS:** 414.7 ($[M-H]^-$).

2.6.9 (*E*)-*N*-((4-(3-(hydroxyamino)-3-oxoprop-1-en-1-yl)benzyl)oxy)isoquinoline-1-carboxamide (**7i**)

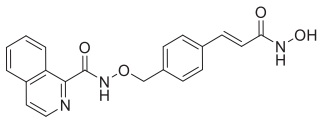

$C_{20}H_{17}N_3O_4$
363.37

7i was synthesised from the alkoxyamide **5i** (1.00 eq, 280 mg, 0.773 mmol) according to 2.6 Method B. 192 mg (0.528 mmol, 68 %) of the alkoxyamide **7i** was obtained as a purple solid.

^{1}H NMR (600 MHz, DMSO-d_6) δ 12.02 (s, 1H), 10.82 (s, 1H), 9.11 (s, 1H), 8.51 (d, *J* = 5.6 Hz, 1H), 8.49 (d, *J* = 8.6 Hz, 1H), 8.03 (d, *J* = 8.3 Hz, 1H), 8.00 (d, *J* = 5.6 Hz, 1H), 7.81 (ddd, *J* = 8.1, 6.8, 1.2 Hz, 1H), 7.73 – 7.66 (m, 1H), 7.61 (d, *J* = 7.9 Hz, 2H), 7.56 (d, *J* = 7.9 Hz, 2H), 7.51 (d, *J* = 15.8 Hz, 1H), 6.53 (d, *J* = 15.8 Hz, 1H), 5.06 (s, 2H).

^{13}C NMR (151 MHz, DMSO-d_6) δ 163.5, 162.8, 150.9, 141.1, 138.0, 137.2, 136.3, 134.9, 130.9, 129.5, 128.5, 127.5, 127.2, 125.9, 125.4, 123.2, 119.4, 76.7.

M.p.: = 176 °C; **HPLC:** R_t = 5.97 min, purity ≥ 99 %; **APCI-MS:** 362.2 ($[M-H]^-$).

2.6.10 (*E*)-*N*-((4-(3-(hydroxyamino)-3-oxoprop-1-en-1-yl)benzyl)oxy)quinoline-2-carboxamide (**7j**)

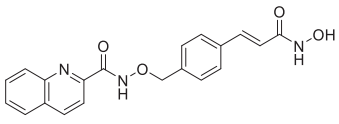

$C_{20}H_{17}N_3O_4$
363.37

7j was synthesised from the alkoxyamide **5j** (1.00 eq, 250 mg, 0.69 mmol) according to 2.6 Method B. 218 mg (0.60 mmol, 87 %) of the alkoxyamide **7j** was obtained as a lightly red solid.

^{1}H NMR (300 MHz, DMSO-d_6) δ 12.09 (s, 1H), 10.84 (s, 1H), 9.10 (s, 1H), 8.57 (d, *J* = 8.5 Hz, 1H), 8.10 (dt, *J* = 11.3, 6.0 Hz, 3H), 7.94 – 7.81 (m, 1H), 7.72 (t, *J* = 7.4 Hz, 1H), 7.57 (q, *J* = 8.0 Hz, 4H), 7.48 (d, *J* = 15.7 Hz, 1H), 6.50 (d, *J* = 15.8 Hz, 1H), 5.03 (s, 2H).

^{13}C NMR (126 MHz, DMSO-d_6) δ 162.5, 161.7, 149.7, 146.0, 137.7, 137.1, 134.7, 130.4, 129.1, 129.1, 128.8, 128.7, 128.0, 127.3, 119.4, 118.6, 76.6.

M.p.: = 155 °C; **HPLC:** R_t = 9.30 min, purity = 95.8 %; **ESI-MS:** 364.1 ($[M+H]^+$).

3 Biological evaluation

Cisplatin was purchased from Sigma (Germany) and dissolved in 0.9% sodium chloride solution, propidium iodide (PI) was purchased from PromoKine (Germany). Vorinostat was synthesized according to known procedures.[1] Stock solutions (10 mM) of the respective compounds were prepared with DMSO and diluted to the desired concentrations with the appropriate medium. All other reagents were supplied by PAN Biotech (Germany) unless otherwise stated.

3.1 Cell lines and cell culture.

The human ovarian carcinoma cell line A2780 was obtained from European Collection of Cell Cultures (ECACC, Salisbury, UK). The human tongue cell line Cal27 was obtained from the German Collection of Microorganisms and Cell Cultures (DSMZ, Germany). The corresponding cisplatin resistant CisR cell line Cal27CisR was generated by exposing the parental cell line to weekly cycles of cisplatin in an IC_{50} concentration over a period of 24 - 30 weeks as described in Gosepath *et al.* and Eckstein *et al.*. [2, 3] All cell lines were grown at 37°C under humidified air supplemented with 5% CO_2 in RPMI 1640 (A2780) or DMEM (Cal27) containing 10% fetal calf serum, 120 IU/mL penicillin, and 120 µg/mL streptomycin. The cells were grown to 80% confluency before being used in further assays.

3.2 MTT cell viability assay

The rate of cell-survival under the action of test substances was evaluated by an improved MTT assay as previously described.[4] In brief, A2780 and Cal27 cell lines were seeded at a density of 5,000 and 2,500 cells/well in 96 well plates (Corning, Germany). After 24 h, cells were exposed to increased concentrations of the test compounds. Incubation was ended after 72 h and cell survival was determined by addition of MTT solution (Serva, Germany, 5 mg/mL in phosphate buffered saline). The formazan precipitate was dissolved in DMSO (VWR, Germany). Absorbance was measured at 544 nm and 690 nm in a FLUOstar microplate-reader (BMG LabTech, Offenburg, Germany).

To investigate the effect of **6e** and **7j** on cisplatin-induced cytotoxicity, compounds were added 48 h before cisplatin administration. After 72 h, the cytotoxic effect was determined with a MTT cell viability assay and shift factors were calculated by dividing the IC_{50} value of cisplatin alone by the IC_{50} value of the drug combinations.

3.3 Whole-cell HDAC inhibition assay

The cellular HDAC assay was based on an assay published by Ciossek *et al.*[5] and Bonfils *et al.* [6] with minor modifications.

Briefly, human cancer cell lines Cal27 and A2780 were seeded in 96-well tissue culture plates (Corning, Germany) at a density of 1.5 x 10^4 cells/well in a total volume of 90 µL culture medium. After 24 h, cells were incubated for 18 h with increasing concentrations of test compounds. The reaction was started by adding 10 µL of 3 mM Boc-Lys(ε-Ac)-AMC (Bachem, Germany) to reach a final concentration of 0.3 mM.[7] The cells were incubated with Boc-Lys(ε-Ac)-AMC for 3 h under cell culture conditions. After this incubation, 100 µl/well stop solution (25 mM Tris-HCl (pH 8), 137 mM NaCl, 2.7 mM KCl, 1 mM $MgCl_2$, 1% NP40, 2.0 mg/mL trypsin, 10 µM vorinostat) was added and the reaction was developed for 3 h under cell culture conditions. Fluorescence intensity was measured at excitation of 320 nm and emission of 520 nm in a NOVOstar microplate-reader (BMG LabTech, Offenburg, Germany).

3.4 Measurement of apoptotic cells

Cal27 and Cal27CisR cells were seeded at a density of 3.2 x 10^4 cells/well in 24-well plates (Sarstedt, Germany). Cells were treated with **6e** or **7j** and cisplatin alone or in combination for the indicated time points. Supernatant was removed after a centrifugation step and the cells were lysed in 500 µL hypotonic lysis buffer (0.1% sodium citrate, 0.1% Triton X-100, 100 µg/mL PI) at 4°C in the dark overnight. The percentage of apoptotic nuclei with DNA content in sub-G1 was analyzed by flow cytometry using the CyFlow instrument (Partec, Münster, Germany).

3.5 Caspase 3/7 activation assay

Compound-induced activation of caspases 3 and 7 was analyzed by using the CellEvent Caspase 3/7 green detection reagent (Thermo Scientific Germany) according to the manufacturer´s instructions. Briefly, Cal27 and Cal27 CisR cells were seeded in 96-well-plates (Corning, Germany) at a density of 900 cells/ well. Cells were treated with **6e** or **7j** 48h prior to cisplatin. After a further incubation period of 24h medium was removed and 50 µL of CellEvent Caspase 3/7 green detection reagent (2 µM in PBS supplemented with 5% heat inactivated FBS) was added. Cells were incubated for 30 minutes at 37°C in a humidified incubator before imaging by using the Thermo Fisher ArrayScan XTI high content screening (HCS) system (Thermo Scientific). Hoechst 33342 was used for nuclei staining. The pan caspase inhibitor QVD was used in a concentration of 20 µM diluted in the appropriate medium and incubated 30 minutes prior to compound addition.

3.6 Enzyme assay

All human recombinant enzymes were purchased from Reaction Biology Corp. (Malvern, PA, USA). The HDAC activity assay of HDAC2 (catalog nr. KDA-21-277), 4 (catalog nr. KDA-21-279), 6 (catalog nr. KDA-21-213) and 8 (catalog nr. KDA-21-481) was performed in 96-well plates (Corning, Germany). Briefly 20ng of HDAC2 and HDAC8, 17.5ng of HDAC6 and 2ng of HDAC4 per reaction were used. Recombinant enzymes were diluted in assay buffer (50 mM Tris-HCL, pH 8.0, 137 mM NaCl, 2.7 mM KCl, 1 mM $MgCl_2$, and 1 mg/ml BSA). 80 µl of this dilution was incubated with 10 µl of different concentrations of inhibitors in assay buffer. After a 5 min incubation step the reaction was started with 10 µl of 300 µM (HDAC2), 150 µM (HDAC6) Boc-Lys(Ac)-AMC (Bachem, Germany) or 100 µM (HDAC4), 60 µM (HDAC8) Boc-Lys(TFa)-AMC (Bachem, Germany). The reaction was stopped after 90 min by adding 100 µl stop solution (16mg/ml trypsin, 2 µM Panobinostat for HDAC2, HDAC6 and HDAC8, 2 µM CHDI0039 (kindly provided by the CHDI Foundation Inc., New York, USA) for HDAC4 in 50 mM Tris-HCL, pH 8.0, and 100 mM NaCl. 15 min after the addition of the stop solution the fluorescence intensity was measured at excitation of 355 nm and emission of 460 nm in a NOVOstar microplate reader (BMG LabTech, Offenburg, Germany).

3.7 Data Analysis

Concentration-effect curves were constructed with Prism 7.0 (GraphPad, San Diego, CA) by fitting the pooled data of at least three experiments performed in triplicates to the four parameter logistic equation. Statistical analysis was performed using t test or one-way ANOVA.

4 References

(1) Gediya, L. K.; Chopra, P.; Purushottamachar, P.; Maheshwari, N.; Njar, V. C. O. A new simple and high-yield synthesis of suberoylanilide hydroxamic acid and its inhibitory effect alone or in combination with retinoids on proliferation of human prostate cancer cells. *J. Med. Chem.* 2005, *48*, 5047–5051.

(2) Gosepath, E. M.; Eckstein, N.; Hamacher, A.; Servan, K.; von Jonquieres, G.; Lage, H.; Györffy, B.; Royer, H. D.; Kassack, M. U. Acquired cisplatin resistance in the head-neck cancer cell line Cal27 is associated with decreased DKK1 expression and can partially be reversed by overexpression of DKK1. *Int. J. Cancer* 2008, *123*, 2013–2019.

(3) Eckstein, N.; Servan, K.; Girard, L.; Cai, D.; von Jonquieres, G.; Jaehde, U.; Kassack, M. U.; Gazdar, A. F.; Minna, J. D.; Royer H. D. Epidermal growth factor receptor pathway analysis identifies amphiregulin as a key factor for cisplatin resistance of human breast cancer cells. *J. Biol. Chem.* 2008, *283*, 739–750.

(4) Engelke L. H.; Hamacher A.; Proksch P.; Kassack M. U. Ellagic acid and resveratrol prevent the development of cisplatin resistance in the epithelial ovarian cancer cell line A2780. *J. Cancer*. 2016, *7*, 353–363.

(5) Ciossek, T.; Julius, H.; Wieland, H.; Maier, T.; Beckers, T. A homogeneous cellular histone deacetylase assay suitable for compound profiling and robotic screening. *Anal. Biochem.* 2008, *372*, 72–81.

(6) Bonfils, C.; Kalita, A.; Dubay, M.; Siu, L. L.; Carducci, M. A.; Reid, G.; Martell, R. E.; Besterman J. M.; Li, Z. Evaluation of the pharmacodynamic effects of MGCD0103 from preclinical models to human using a novel HDAC enzyme assay. *Clin. Cancer Res.* 2008, *14*, 3441–3449.

(7) Hoffmann, K; Brosch, G; Loidl, P and Jung, M. A non-isotopic assay for histone deacetylase activity. *Nucl. Acids Res.* 1999, *27, 2057–2058.*

4 Chapter II:

The carba-analogue of KSK64

Contribution:

- Synthesis of compounds **1**, **2**, **3**, **4**, **5**, **6**, **7**, **8a**, **8b**, **9a**, **9b**
- Manuscript and supporting information

The carba-analogue of KSK64

M. Pflieger, A. Hamacher, N. Horstick-Muche, M. U. Kassack, T. Kurz

Abstract

The controlled regulation of the acetylome is detrimental for the maintenance of the homeostasis of cells. An imbalance of the regulatory histone acetyl transferases (HAT) and histone deacetylase (HDAC) is associated with a variety of diseases such as cancer. The overexpression of HDACs can result in oncogenesis of cells and mediate the resistance towards commonly applied anticancer agents (e.g. cisplatin). One promising approach to target this imbalance is the employment of HDAC inhibitors, which can reinstate the homeostasis of cell and facilitate chemosensitising properties towards cisplatin. KSK64, a potent and selective HDAC class I/HDAC6 inhibitor, exhibiting an alkoxyurea connecting unit, shows promising antiproliferative properties in solid tumours and its application in combination with cisplatin reverts resistance mechanisms. Here we report the synthesis and the biological evaluation of the carba analogue of KSK64 to evaluate the influence of an alkoxyurea CU. The here reported structure activity relationship indicate that the presence of an alkoxyurea CU in HDACi can significantly increase the preference of HDACi towards HDAC6.

Introduction

Histone deacetylases (HDAC) are epigenetic erasers[1] that catalyse the hydrolytic cleavage of acetylated lysine residues.[2,3] Depending on their cellular localisation, HDACs catalyse the deacetylation of chromatin in the nucleus[4] or other non-chromatin client proteins in the cytoplasm and are numbered according to their discovery.[3] The human zinc dependant HDAC isozyme are classified according to their yeast homologues into class I (HDAC1, HDAC2, HDAC3 and HDAC8), class IIa (HDAC4, HDAC5, HDAC7, HDAC9), class IIb (HDAC6, HDAC10) and class IV with HDAC11 as the single representative. Class III, the sirtuins, are NAD^+ and consolidate a unique subclass of HDACs. As epigenetic regulators, HDACs participate in a plethora of cellular processes including cell differentiation,[5,6] cell cycle progression[7,8] and the programmed cell death.[9] Due to their diverse functions in maintaining the homeostasis of cells, their dysregulation has a tremendous impact on cell development and their dysregulation can result in the development of neurological diseases,[10,11] immunological disorders,[12] and the development of cancer.[13–16] It has been shown that in many cancer cell lines an overexpression[17,18] of HDACs (particularly class I) can circumvent apoptosis by an increased deacetylation of chromatin where tumour suppressor genes are encoded, resulting in a shift towards a condensed chromatin structure.[19] An inhibition of HDACs can re-establish homeostasis and cause the initiation of apoptosis.[2,3] With

already four FDA approved HDAC inhibitors (HDACi) on the market, HDACs are clinically validated anti-cancer targets[20] and accumulating evidence suggest a potential treatment of e.g. neurological disorders[21] and immunomodulatory properties.[22,23] Currently approved HDACi are vorinostat, belinostat, panobinostat and romidepsin for the treatment of cutaneous T-cell lymphoma (CTCL), relapsed or refractory, multiple myeloma and CTCL and peripheral T-cell lymphoma, respectively. All of the approved HDACi exhibit a mutual pharmacophore model, comprising of a zinc binding group (ZBG), a linker and a cap region. [24–26] Apart from the class I selective natural product romidepsin,[27] the first generation HDACi are pan inhibitors that show no preference towards individual isozymes. The pan-HDACi are associated with severe adverse effects such as such as neutropenia, anaemia or cardiovascular abnormalities.[15] Up until now, it is still unclear whether isozyme selective or pan HDACi as anti-cancer agents are more effective in clinics in respect to safety and efficacy.[28] It is anticipated that isozyme selective or HDACi with preferences towards selected isozyme classes might be compromise between efficacy and the occurrence of side effects. Therefore, significant research has been conducted, over the last few years, to design isozyme selective HDACi that exhibit superior pharmacological properties to first generation HDACi. Furthermore, the combination treatment of HDACi with commonly applied anti-cancer drugs (e.g., cisplatin, bortezomib, temozolomide) has been shown to have a synergist anti-cancer effect in haematological malignancies as well as in solid tumours.[29] For instance, KSK64 showed significant synergistic and chemosensitising (SF = 11.2) anti-cancer properties with cisplatin in the human ovarian cancer cell line A2780 and the adenosquamous carcinoma cell line Cal27.[30] In contrast to the first generation HDACi, KSK64 exhibits a refined HDAC isozyme profile with a preference towards class I HDACs and HDAC6. This HDAC class I/HDAC6 isozyme profile is presumably the result of the novel alkoxyurea CU which also facilitates KSK64 with its chemo-sensitising properties towards cisplatin (Figure 18)

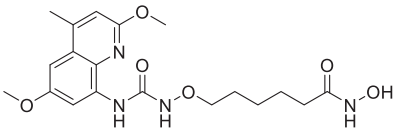

KSK64
IC_{50}(HDAC1) = 43.2 nM
IC_{50}(HDAC4) > 10.0 µM
IC_{50}(HDAC6) = 2.80 nM
IC_{50}(HDAC8) = 1.54 µM
SF (Cal27R) = 11.2

Figure 18. Structure of KSK64.[30]

The aim of this study was to determine the influence of the alkoxyurea CU in respect to the anticancer activity of KSK64 (Scheme 10). This involved the development of a synthetic strategy for the carba analogue of KSK64 exhibiting a urea CU and the anticancer property evaluation of KSK64 and its carba analogue.

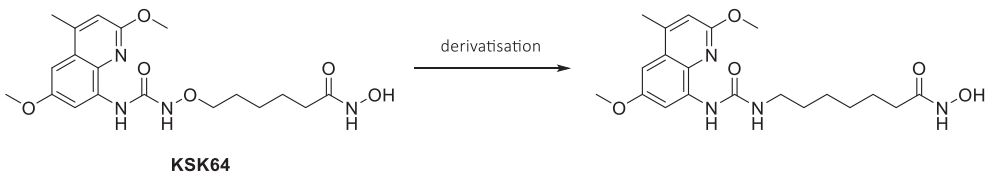

Scheme 10. Derivatisation of KSK64.

Results and Discussion

Our retrosynthetic analysis of the urea derivative is shown in Scheme 11.

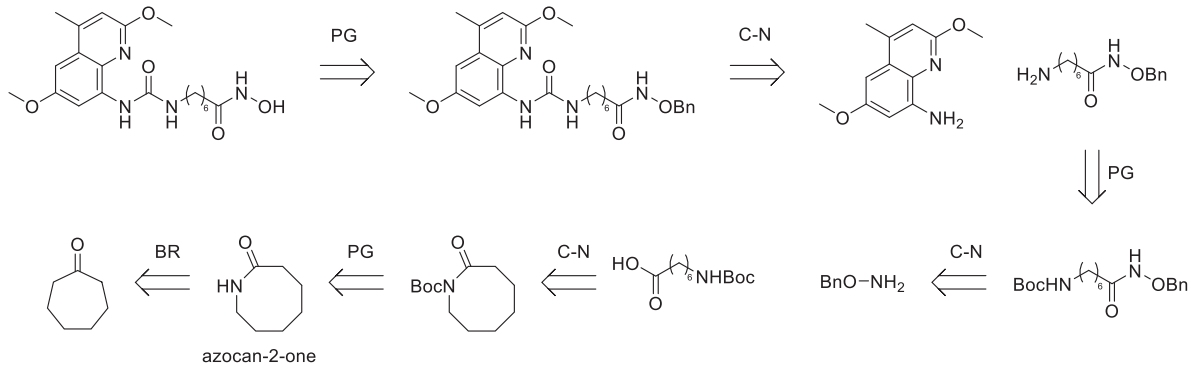

Scheme 11. Retrosynthetic analysis.

The key step of this analysis was to obtain 7-amino-*N*-(benzyloxy)heptanamide which was realised by a *Beckmann-rearrangement* (*BR*) of cycloheptanone to the corresponding azocan-2-one (**1**), followed by a Boc protection of the lactam *N*-proton. In this way, the *N*-Boc protected amine (**2**) cannot interfere with the coupling of its carboxylate with *O*-benzyl hydroxylamine.

Starting from cycloheptanone, a ring expansion was realised by a Beckmann rearrangement (Scheme 3), followed by an *N*-Boc protection of the resulting lactam **2**. The *N*-Boc protected lactam **2** was, subsequently, hydrolysed under basis conditions to obtain the carboxylic acid **3**.

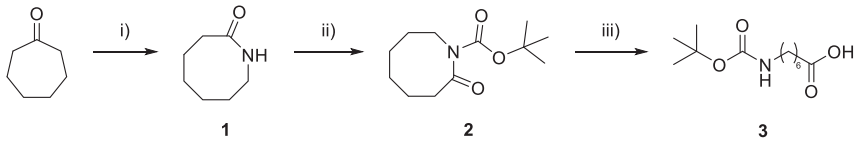

*Scheme 12. Synthesis of tert-butyl 2-oxoazocane-1-carboxylate **3**. i) 1.50 eq hydroxylamine-O-sulfonic acid, HCO_2H; ii) 1.00 eq nBuLi, 1.00 eq Boc_2O, THF; iii) 10.0 eq LiOH, THF/H_2O.*

Via a HATU mediated acylation, **3** was coupled to the *O*-benzyl hydroxylamine to obtain **4** (Scheme 4). The synthesis of the linker was completed by the boc deprotection of **4**, yielding **5** as hydrochloride.

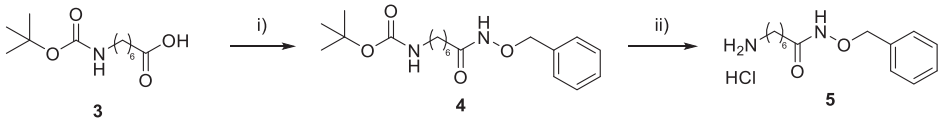

*Scheme 13. Synthesis of 7-amino-N-(benzyloxy)heptanamide hydrochloride **5**. i) 1.00 eq HATU, 2.00 eq DIPEA, 1.00 eq O-benzylhydroxylamine, DMF; iii) 20.0 eq $HCl_{(dioxane)}$, DCM*

Afterwards, **5** or its oxa-derivative **6** were used for the synthesis of the urea **8.**

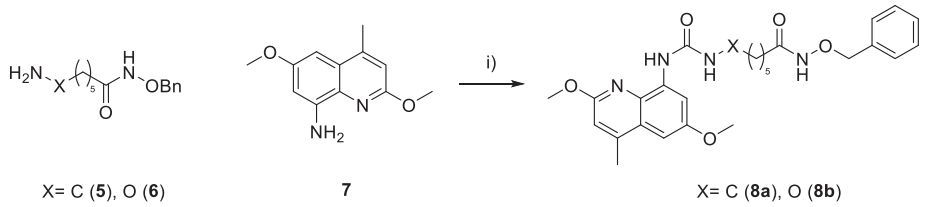

*Scheme 14. Synthesis of the urea derivatives **9**. i) 0.330 eq triphosgene, 1.00 eq DIPEA, DCM*

Finally, the *O*-benzyl protected hydroxamic acids **8** were deprotected by catalytic hydrogenation to obtain **9** (Scheme 10).

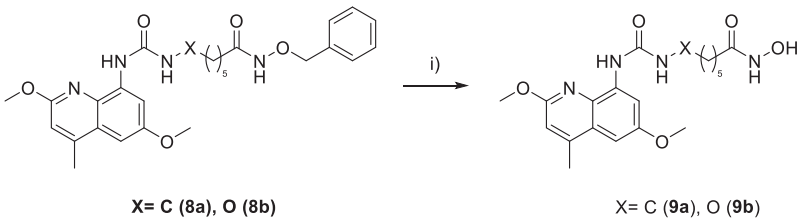

*Scheme 15. Synthesis of the hydroxamic acids **10** by deprotection of the O-benzyl hydroxamic acids **9**. i) H_2, Pd/C.*

The hydroxamic acids **9** were, subsequently, evaluated in HDAC2 and HDAC6 enzyme assays (Table 6). In the HDAC2 enzyme assay, the urea derivative **9a** exhibited an pIC_{50} value of 7.40 ± 0.06 and was approximately 19.5-fold (pIC_{50} = 6.11 ± 0.04) more active than KSK64 (**9b**). With a pIC_{50} of 7.04 ± 0.06 (**9a**) and a pIC_{50} = 7.02 ± 0.04 (**9b**), **9a** and **9b** demonstrated a SI2/6 of 0.43 and 8.1, respectively. Based on the obtained data, the urea derivative (**9a**) showed a higher inhibitory activity towards HDAC2 than the alkoxyurea derivative **9b** (**KSK64**), which indicates that the presence of an alkoxyure CU can contribute to the preference of HDACi towards HDAC6.

*Table 6. HDAC2 and HDAC6 inhibition assay of **9a** and **9b** (KSK64).*

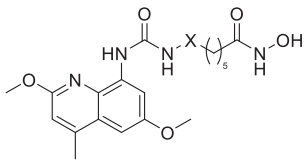

X= C (**9a**), O (**9b**)

Cmp.	X	HDAC2 pIC_{50} (IC_{50} [nM])	HDAC6 pIC_{50} (IC_{50} [nM])	SI2/6
9a	C	7.40 ± 0.06 (39.6)	7.04 ± 0.06 (96.3)	0.437
9b (KSK64)	O	6.11 ± 0.04 (790)	7.02 ± 0.04 (90.8)	8.13

Presented data are calculated from at least two experiments each performed in duplicates. Standard deviation of percent inhibition values is less than 10 %. Vehicle control was defined as 0 % inhibition. The selectivity index SI2/6 was calculated with the pIC50 values.

The cytotoxicity was evaluated by an antiproliferative assay in the human tongue squamous carcinoma cell line Cal27 and the human ovarian cancer cell line A2780 (Table 7).

9a and **9b(KSK64)** exhibited a pIC_{50} of 6.79 ± 0.09 and 6.01 ± 0.11 for Cal27, respectively. For A2780, **9a** and **9b**(KSK64) demonstrated pIC_{50} of 6.01 ± 0.02 and 5.44 ± 0.06. In both solid tumour cell lines (Cal27 and A2780), **9a** was approximately 4-fold more active than our lead compound **9b** (**KSK64**).

*Table 7: Antiproliferative effects of **9a** and **9b** (**KSK64**) in Cal27 and A2780.*

	MTT-Assay pIC_{50} (IC_{50} [µM])	
	Cal27	A2780
9a	6.79 ± 0.09 (0.164)	6.01 ± 0.02 (0.970)
9b (KSK64)	6.01 ± 0.11 (0.980)	5.44 ± 0.06 (3.66)

Presented data are calculated from at least two experiments each performed in duplicates. Standard deviation of percent inhibition values is less than 10 %. Vehicle control was defined as 0 % inhibition.

Conclusion

Here we report the synthesis of the carba analogue (**9a**) of KSK64 (**9b**) and their preliminary biological evaluation. This synthesis involved the *Beckmann-rearrangement* of cycloheptanone to obtain the corresponding lactam **1**. Subsequently, the *N*-acidic proton was Boc protected (**2**) to circumvent the interference with the following reactions after lactam hydrolysis (**3**). The resulting carboxylic acid **3** was coupled with *O*-benzyl hydroxylamine (**4**) and the amine deprotected (**5**). **5** was, subsequently, coupled with the amine **7** to obtain the benzyl protected hydroxamic acid **8a**. After catalytic hydrogenation, the carba analogue of **KSK64** was obtained (**9a**). The HDAC enzyme inhibition assays of the **9a** and **9b** indicate that the derivatisation of HDACi, exhibiting a urea CU, with an alkoxyurea CU can result in an increased preference towards HDAC6.

References

1. Arrowsmith, C. H., Bountra, C., Fish, P. V., Lee, K. & Schapira, M. Epigenetic protein families: A new frontier for drug discovery. *Nat. Rev. Drug Discov.* **11**, 384–400 (2012).
2. Bertrand, P. Inside HDAC with HDAC inhibitors. *European Journal of Medicinal Chemistry* vol. 45 2095–2116 (2010).
3. Roche, J. & Bertrand, P. Inside HDACs with more selective HDAC inhibitors. *Eur. J. Med. Chem.* **121**, 451–483 (2016).
4. Rodriquez, M. *et al.* Chemistry and Biology of Chromatin Remodeling Agents: State of Art and Future Perspectives of HDAC Inhibitors. *Curr. Med. Chem.* **13**, 1119–1139 (2006).
5. Göttlicher, M. *et al.* Valproic acid defines a novel class of HDAC inhibitors inducing differentiation of transformed cells. *EMBO J.* **20**, 6969–6978 (2001).
6. Nencioni, A. *et al.* Histone deacetylase inhibitors affect dendritic cell differentiation and immunogenicity. *Clin. Cancer Res.* **13**, 3933–3941 (2007).
7. Vallo, S. *et al.* HDAC inhibition delays cell cycle progression of human bladder cancer cells in vitro. *Anticancer. Drugs* **22**, 1002–1009 (2011).
8. Noh, E. J., Lim, D. S., Jeong, G. & Lee, J. S. An HDAC inhibitor, trichostatin A, induces a delay at G2/M transition, slippage of spindle checkpoint, and cell death in a transcription-dependent manner. *Biochem. Biophys. Res. Commun.* **378**, 326–331 (2009).
9. Marks, P. A. & Jiang, X. Histone deacetylase inhibitors in programmed cell death and cancer therapy. *Cell Cycle* **4**, 549–551 (2005).
10. Fischer, A., Sananbenesi, F., Mungenast, A. & Tsai, L. H. Targeting the correct HDAC(s) to treat cognitive disorders. *Trends Pharmacol. Sci.* **31**, 605–617 (2010).
11. Alam, M. S., Getz, M. & Haldar, K. Chronic administration of an HDAC inhibitor treats both neurological and systemic Niemann-Pick type C disease in a mouse model. *Sci. Transl. Med.* **8**, 326ra23-326ra23 (2016).
12. Fairlie, D. P. & Sweet, M. J. HDACs and their inhibitors in immunology: Teaching anticancer drugs

new tricks. *Immunol. Cell Biol.* **90**, 3–5 (2012).

13. Li, Y. & Seto, E. HDACs and HDAC inhibitors in cancer development and therapy. *Cold Spring Harb. Perspect. Med.* **6**, a026831 (2016).

14. Zhao, C., Dong, H., Xu, Q. & Zhang, Y. Histone deacetylase (HDAC) inhibitors in cancer: a patent review (2017-present). *Expert Opin. Ther. Pat.* **30**, 263–274 (2020).

15. Witt, O., Deubzer, H. E., Milde, T. & Oehme, I. HDAC family: What are the cancer relevant targets? *Cancer Lett.* **277**, 8–21 (2009).

16. Khan, O. & La Thangue, N. B. HDAC inhibitors in cancer biology: Emerging mechanisms and clinical applications. *Immunol. Cell Biol.* **90**, 85–94 (2012).

17. Shao, Y., Gao, Z., Marks, P. A. & Jiang, X. Apoptotic and autophagic cell death induced by histone deacetylase inhibitors. *Proc. Natl. Acad. Sci.* **101**, 18030–18035 (2004).

18. Bandyopadhyay, D., Mishra, A. & Medrano, E. E. Overexpression of histone deacetylase 1 confers resistance to sodium butyrate-mediated apoptosis in melanoma cells through a p53-mediated pathway. *Cancer Res.* **64**, 7706–7710 (2004).

19. Arts, J., Schepper, S. & Emelen, K. Histone Deacetylase Inhibitors: From Chromatin Remodeling to Experimental Cancer Therapeutics. *Curr. Med. Chem.* **10**, 2343–2350 (2003).

20. Dell'Aversana, C., Lepore, I. & Altucci, L. HDAC modulation and cell death in the clinic. *Exp. Cell Res.* **318**, 1229–1244 (2012).

21. Chuang, D.-M., Leng, Y., Marinova, Z., Kim, H.-J. & Chiu, C.-T. Multiple roles of HDAC inhibition in neurodegenerative conditions. *Trends Neurosci.* **32**, 591–601 (2009).

22. Wang, L., de Zoeten, E. F., Greene, M. I. & Hancock, W. W. Immunomodulatory effects of deacetylase inhibitors: therapeutic targeting of FOXP3+ regulatory T cells. *Nat. Rev. Drug Discov.* **8**, 969–981 (2009).

23. Licciardi, P. V., Ververis, K., Tang, M. L., El-Osta, A. & Karagiannis, T. C. Immunomodulatory Effects of Histone Deacetylase Inhibitors.

24. Jung, M. *et al.* Amide analogues of trichostatin A as inhibitors of histone deacetylase and inducers of terminal cell differentiation. *J. Med. Chem.* **42**, 4669–4679 (1999).

25. Finnin, M. S. *et al.* Structures of a histone deacetylase homologue bound to the TSA and SAHA inhibitors. *Nature* **401**, 188–193 (1999).

26. Jung, M. Inhibitors of Histone Deacetylase as New Anticancer Agents. *Curr. Med. Chem.* **8**, 1505–1511 (2012).

27. Bertino, E. M. & Otterson, G. A. Romidepsin: a novel histone deacetylase inhibitor for cancer. *Expert Opin. Investig. Drugs* **20**, 1151–1158 (2011).

28. Depetter, Y. *et al.* Selective pharmacological inhibitors of HDAC6 reveal biochemical activity but functional tolerance in cancer models. *Int. J. Cancer* **145**, 735–747 (2019).

29. Suraweera, A., O'Byrne, K. J. & Richard, D. J. Combination therapy with histone deacetylase inhibitors (HDACi) for the treatment of cancer: Achieving the full therapeutic potential of HDACi. *Front. Oncol.* **8**, 1–15 (2018).

30. Stenzel, K. *et al.* Alkoxyurea-Based Histone Deacetylase Inhibitors Increase Cisplatin Potency in Chemoresistant Cancer Cell Lines. *J. Med. Chem.* **60**, 5334–5348 (2017).

4.1 Chapter II – Supporting information

The carba-analogue of KSK64

Supporting information

M. Pflieger, A. Hamacher, N. Horstick-Muche, M. U. Kassack, T. Kurz,

Contents

1 General Information

Reaction, monitoring and purification

Chemicals and solvents were purchased from commercial suppliers (Sigma-Aldrich, Acros Organics, TCI, Fluorochem ABCR, Alfa Aesar, J&K, Carbolution) and used without further purification. Dry solvents were obtained from Acros Organics. Ambient or room temperature correspond to 22°C. The reaction progression was monitored using Thin-Layer-Chromatography plates by Macherey Nagel (ALUGRAM Xtra SIL G/UV_{254}). Visualisation was achieved with ultraviolet irradiation (254 nm) or by staining with a $KmnO_4$-solution (9 g $KmnO_4$, 60 g K_2CO_3, 15 mL of a 5% aqueous NaOH-solution, ad 900 mL demineralised water). Purification was either performed with prepacked Silica cartridges (RediSep® Rf Normal Phase Silica, RediSep® Rf RP C18) for flash column chromatography (CombiFlashRf200, TeleDyneIsco) or by recrystallisation. Different eluent mixtures of solvents (hexane and ethyl acetate or dichloromethane and methanol) served as the mobile phase for flash column chromatography and are stated in the experimental procedure.

Analytics

An NMR-Spectrometer by Bruker (Bruker Avance III – 300, Bruker Avance DRX – 500 or Bruker Avance III – 600) were used to perform ^{1}H- and^{13}C-NMR experiments. Chemical shifts are given in parts per million (ppm), relative to residual non-deuterated solvent peak (^{1}H-NMR: DMSO-d_6 (2.50), ^{13}C-NMR: DMSOd_6 (39.52). Signal patterns are indicated as: singlet (s), doublet (d), triplet (t), quartet (q), or multiplet (m). Coupling constants, J, are quoted to the nearest 0.1 Hz and are presented as observed. ESI-MS was carried out using Bruker Daltonics UHR-QTOF maXis 4G (Bruker Daltonics) under electrospray ionization (ESI). The above-mentioned characterisations were carried out by the HHU Center of Molecular and Structural Analytics at Heinrich-Heine University Düsseldorf (http://www.chemie.hhu.de/en/analytics-center-hhucemsa.html). APCI-MS was carried out with an Advion expression^{L} CMS. Melting points were determined using a Büchi M-565 melting point apparatus (uncorrected). Analytical HPLC was carried out on a Knauer HPLC system comprising of an Azura P6.1L pump, an Optimas 800 autosampler, a Fast Scanning Spectro-Photometer K-2600 and a Knauer Reversed Phase column (SN: FK36). Evaluated compounds were detected at 254 nm. The solvent gradient table is shown in Table 14. The purity of all final compounds was 95% or higher.

Table 8: The solvent gradient table for analytic HPLC analysis.

Time / min	Water + 0.1% TFA	ACN + 0.1% TFA
Initial	90	10
0.50	90	10
20.0	0	100
30.0	0	100
31.0	90	10
40.0	90	10

2 Synthetic procedures

2.1 Synthesis of azocan-2-one (**1**)

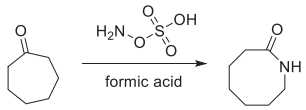

1 was accessed via a Beckmann rearrangement. [1]

All spectroscopic data were in agreement with literature. [1]

2.2 Synthesis of tert-butyl 2-oxoazocane-1-carboxylate (**2**)

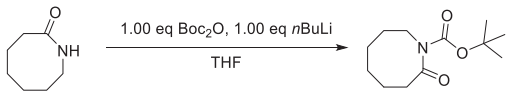

2 was synthesised according to Giovannini *et. Al.*. [2]

All spectroscopic data were in agreement with literature. [2]

2.3 Synthesis of 7-((tert-butoxycarbonyl)amino)heptanoic acid (**3**)

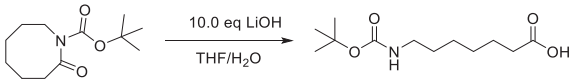

1.00 eq (4.40 mmol, 1.0 g) of **2** was dissolved in 22 mL of THF. 10.0 eq (44.0 mmol, 1.05 g) of LiOH was dissolved in 4 mL of dH_2O and added to the reaction. After 16 h at ambient temperature, the reaction solution was poured on 100 mL of H_2O, acidified with 1 M $HCl_{(aq)}$ and the product extracted with EtOAc. The combined organic layers were dried over Na_2SO_4 and the solvent removed under reduced pressure. 0.97 g (3.95 mmol, 90 %) of **3** was obtained as a white solid.

^{1}H NMR (600 MHz, DMSO-d_6) δ 11.96 (s, 1H), 6.74 (t, *J* = 5.8 Hz, 1H), 2.94 – 2.82 (m, 2H), 2.18 (t, *J* = 7.4 Hz, 2H), 1.46 (td, *J* = 14.6, 7.3 Hz, 2H), 1.36 (s, 10H), 1.23 (tq, *J* = 8.7, 5.2, 3.8 Hz, 4H).

^{13}C NMR (151 MHz, DMSO-d_6) δ 174.5, 155.6, 77.3, 40.1, 33.6, 29.4, 28.3, 28.3, 26.0, 24.5.

M.p.: 47.5 °C; **MS** (+APCI): 190 $[M-^tBU+2H]^+$.

2.4 Synthesis of tert-butyl (7-((benzyloxy)amino)-7-oxoheptyl)carbamate (**4**)

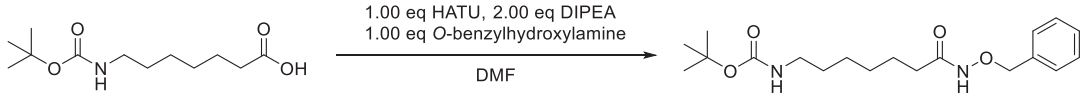

1.00 eq (3.39 mmol, 831 mg) of **6**, 1.00 eq (3.39 mmol, 1.29 g) of HATU and 2.00 eq (6.77 mmol, 880 mg, 1.19 mL) of DIPEA were combined in 10 mL of DMF. After 10 minutes at RT, 1.00 eq (3.39 mmol, 417 mg) of *O*-benzyl hydroxalamine were added to the reaction mixture and stirred for 16 h at ambient temperature. Subsequently, the solvent was removed *in vacuo* and the residue resuspended in 50 mL of EtOAc. The organic layer was washed with 10 % aq. Citric acid (x3), aq. Sat. $NaHCO_3$ (x3), brine (x1) and dried over Na_2SO_4. 1.12 g (3.20 mmol, 94 %) of **7** was obtained as a white solid after flash chromatography (*n*-hexane/EtOAc).

^{1}H NMR (600 MHz, DMSO-d_6) δ 10.9 (s, 1H), 7.7 – 7.2 (m, 5H), 6.8 (t, *J* = 5.8 Hz, 1H), 4.8 (s, 2H), 2.9 (q, *J* = 6.7 Hz, 2H), 1.9 (t, *J* = 7.3 Hz, 2H), 1.5 – 1.4 (m, 2H), 1.4 (s, 12H), 1.2 (p, *J* = 3.9, 3.4 Hz, 4H).

^{13}C NMR (75 MHz, DMSO-d_6) δ 169.3, 155.5, 136.0, 128.6, 128.1, 128.1, 77.2, 76.7, 39.7, 32.1, 29.3, 28.2, 28.1, 25.9, 24.8.

M.p.: 56.1 °C; **MS** (+APCI): 295 [M-^{t}BU+2H]$^+$.

2.5 Synthesis of 7-amino-N-(benzyloxy)heptanamide hydrochloride (**5**)

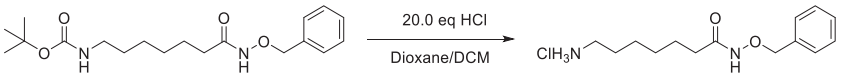

1.00 eq (2.74 mmol, 960 mg) of **4** was dissolved in 27.4 mL of DCM and cooled on ice. Subsequently, 20 eq (54.8 mmol, 13,7 mL) of a 4 M HCl in dioxane solution were added and stirred for 4 h on ice. The product was precipitated by the addition of 1 volume of hexane and the product collected by filtration. 760 mg (2.65 mmol, 97 %) of **5** was obtained as a white solid.

^{1}H NMR (600 MHz, DMSO-d_6) δ 11.12 (s, 1H), 8.10 (s, 3H), 7.44 – 7.28 (m, 5H), 4.78 (s, 2H), 2.71 (qt, *J* = 9.4, 4.6 Hz, 2H), 1.96 (t, *J* = 7.3 Hz, 2H), 1.54 (p, *J* = 7.6 Hz, 2H), 1.48 (p, *J* = 7.4 Hz, 2H), 1.33 – 1.25 (m, 2H), 1.25 – 1.12 (m, 2H).

^{13}C NMR (75 MHz, DMSO-d_6) δ 169.2, 136.0, 128.6, 128.2, 128.1, 76.7, 38.6, 32.0, 27.8, 26.6, 25.4, 24.6.

M.p.: 110.3°C; **MS** (+APCI): 287 [M+H]$^+$.

2.6 Synthesis of 6-(aminooxy)-N-(benzyloxy)hexanamide (**6**)

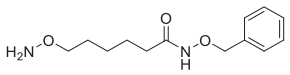

6 was synthesised according to Stenzel *et. Al.*.[3]

All spectroscopic data were in agreement with literature. [3]

2.7 Synthesis of 2,6-dimethoxy-4-methylquinolin-8-amine (**7**)

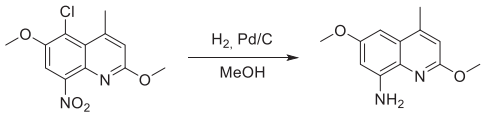

1.00 eq (3.54 mmol, 1 g) of 5-chloro-2,6-dimethoxy-4-methyl-8-nitroquinoline[4] was dissolved in 70 mL of Methanol. After the addition of 5 mol% of 10 % Pd/C (0.177, 0.188 g) the catalytic hydrogenation was performed for 5 h. Subsequently, 10.0 eq of TEA (35.4 mmol, 3.58 g, 2.6 mL) were added to the reaction mixture. The solution was filtered over celite®, the solvent removed under reduced pressure and the product purified by flash column chromatography (Hex/DCM + 0.1 % TEA). 461 mg (2.11 mmol, 60 %) was obtained as a white solid.

^{1}H NMR (600 MHz, DMSO-d_6) δ 6.79 (t, *J* = 1.2 Hz, 1H), 6.50 (dd, *J* = 2.6, 1.0 Hz, 1H), 6.45 (dd, *J* = 2.6, 1.0 Hz, 1H), 5.69 (s, 2H), 3.93 (d, *J* = 1.0 Hz, 3H), 3.79 (d, *J* = 1.1 Hz, 3H), 2.49 (t, *J* = 1.1 Hz, 3H).

^{13}C NMR (151 MHz, DMSO-d_6) δ 158.3, 156.5, 146.3, 145.0, 130.6, 125.6, 112.3, 99.9, 90.8, 54.9, 52.5, 18.7.

M.p.: 135.7 °C; **HPLC**: R_t= min, purity %, **MS** (+APCI): 219 $[M+H]^+$.

2.8 General procedure of the synthesis of urea derivatives (**8**)

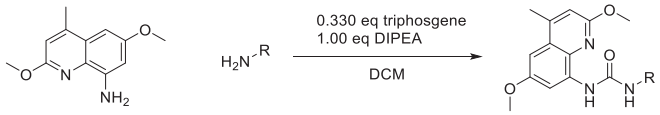

0.330 eq (0.660 mmol, 196 mg) of triphosgene was dissolved in 30 mL of dry DCM and cooled in ice. 1.00 eq of 2 was dissolved in 10 mL of dry DCM and added dropwise to the triphosgene solution over a period of 30 minutes. 1.0 eq of DIPEA was mixed with 10 mL of dry DCM and added dropwise to the reaction solution over a period of 30 minutes and stirred for an addition 30 minutes at RT. Subsequently, 1.00 eq of the respective amine derivative was dissolved in 10 mL of dry DCM and added over a period of 30 minutes. The reaction was stirred for 16 h at ambient temoerature, the solvent was removed *in vacuo* and the residue resuspended in EtOAc. Afterwards, the organic phease was washed with dH_2O (x3), brine (x1) and dried over Na_2SO_4. Finally, the product was purified by flash column chromatography (Hexane/DCM).

2.8.1 Synthesis of *N*-(benzyloxy)-7-(3-(2,6-dimethoxy-4-methylquinolin-8-yl)ureido)heptanamide (**8a**)

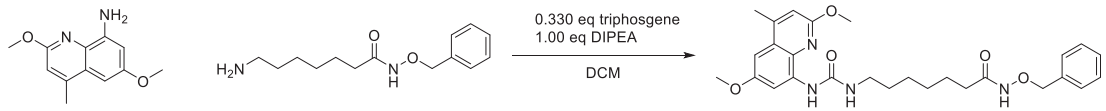

8a was synthesised according to general procedure 2.9 on a 1.83 mmol scale with a yield of 35 % (315 mg, 0.634 mmol) and obtained as a white solid.

^{1}H NMR (300 MHz, DMSO-d_6) δ 8.67 (s, 1H), 7.50 (t, J = 5.5 Hz, 1H), 7.43 – 7.28 (m, 5H), 6.89 (d, J = 1.1 Hz, 1H), 6.79 (d, J = 2.7 Hz, 1H), 4.78 (s, 2H), 4.05 (s, 3H), 3.84 (s, 3H), 3.13 (q, J = 6.6 Hz, 2H), 2.55 (d, J = 1.0 Hz, 3H), 1.96 (t, J = 7.2 Hz, 2H), 1.49 (dp, J = 13.7, 7.3 Hz, 5H), 1.29 (h, J = 5.3 Hz, 5H).

^{13}C NMR (75 MHz, DMSO- d_6) δ 169.3, 159.0, 155.8, 154.8, 146.7, 136.1, 130.6, 128.6, 128.1, 128.0, 124.8, 112.6, 105.8, 95.2, 76.7, 55.1, 53.1, 32.1, 29.5, 28.2, 26.1, 24.8, 18.4.

M.p.: 171.2°C; **MS** (+APCI): 496 $[M+H]^+$.

2.8.2 Synthesis of *N*-(benzyloxy)-6-((3-(2,6-dimethoxy-4-methylquinolin-8-yl)ureido)oxy)hexanamide (8b)

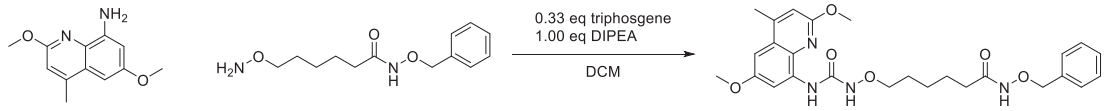

8a was synthesised according to general procedure 2.9 on a 1.83 mmol scale with a yield of 35 % (315 mg, 0.634 mmol) and obtained as a white solid.

^{1}H NMR (300 MHz, DMSO-d_6) δ 10.94 (s, 1H), 9.94 (s, 1H), 9.58 (s, 1H), 8.13 (d, *J* = 2.7 Hz, 1H), 7.45 – 7.24 (m, 5H), 6.92 (d, *J* = 1.2 Hz, 1H), 6.89 (d, *J* = 2.7 Hz, 1H), 4.77 (s, 2H), 3.97 (s, 3H), 3.87 (d, *J* = 6.1 Hz, 5H), 2.56 (d, *J* = 1.0 Hz, 3H), 1.96 (t, *J* = 7.2 Hz, 2H), 1.64 (p, *J* = 7.0 Hz, 2H), 1.52 (p, *J* = 7.2 Hz, 2H), 1.39 – 1.22 (m, 2H).

^{13}C NMR (75 MHz, DMSO-d_6) δ 169.2, 159.3, 156.3, 155.8, 147.2, 136.1, 134.2, 130.8, 128.7, 128.2, 128.1, 125.0, 113.0, 106.3, 96.7, 76.7, 75.9, 55.3, 52.6, 32.1, 27.5, 24.8, 24.7, 18.4.

M.p.: 176.2°C; **MS** (+APCI): 497 $[M+H]^+$.

2.9 General procedure for the synthesis of hydroxamic acids (9)

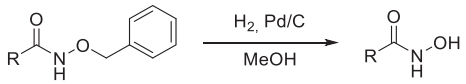

8 was dissolved in 50 mL of MeOH and 5 mol% of 10 % Pd/C was added to the reaction solution. The catalytic hydrogenation was performed for 5 h and reaction solution filtered through celite®. Afte the solvent was removed under reduced pressure, the product was purified by flash column chromatography (DCM/MeOH).

2.9.1 Synthesis of 7-(3-(2,6-dimethoxy-4-methylquinolin-8-yl)ureido)-N-hydroxyheptanamide (**9a**)

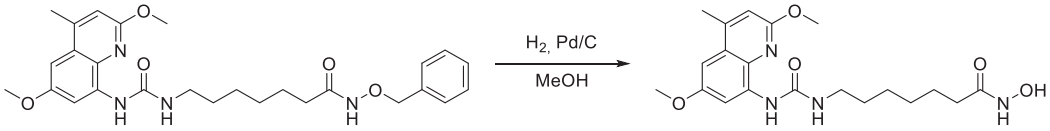

9a was synthesised according to general procedure 2.9 on a 0.503 mmol scale with a yield of 64% (130 mg, 0.32 mmol) and obtained as a pink solid.

^{1}H NMR (300 MHz, DMSO-d_6) δ 10.34 (s, 1H), 9.94 (s, 1H), 9.59 (s, 1H), 8.66 (s, 1H), 8.13 (d, *J* = 2.7 Hz, 1H), 6.96 (d, *J* = 1.2 Hz, 1H), 6.92 (d, *J* = 2.7 Hz, 1H), 3.98 (s, 3H), 3.88 (d, *J* = 4.9 Hz, 5H), 2.71 – 2.55 (m, 3H), 1.94 (t, *J* = 7.3 Hz, 2H), 1.65 (p, *J* = 6.8 Hz, 2H), 1.58 – 1.42 (m, 2H), 1.34 (dq, *J* = 9.1, 4.6, 3.4 Hz, 2H).

^{13}C NMR (75 MHz, DMSO-d_6) δ 168.9, 159.3, 156.2, 155.7, 147.2, 134.1, 130.8, 125.0, 113.0, 106.2, 96.6, 75.8, 55.3, 52.6, 32.1, 27.5, 24.8, 18.4.

M.p.: 151.0°C; HPLC: R_t= 11.10 min, purity 95.3 %, **MS** (+APCI): 407 $[M+H]^+$.

2.9.2 Synthesis of 6-((3-(2,6-dimethoxy-4-methylquinolin-8-yl)ureido)oxy)-N-hydroxyhexanamide (**9b**)

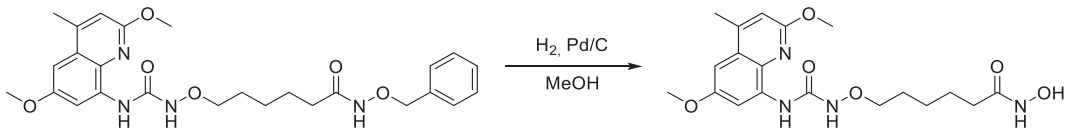

10b was synthesised according to general procedure 2.9 on a 1.00 mmol scale with a yield of 64% (260 mg, 0.643 mmol) and obtained as a white solid.

^{1}H NMR (300 MHz, DMSO-d_6) δ 8.67 (s, 1H), 7.50 (t, *J* = 5.5 Hz, 1H), 7.43 – 7.28 (m, 5H), 6.89 (d, *J* = 1.1 Hz, 1H), 6.79 (d, *J* = 2.7 Hz, 1H), 4.78 (s, 2H), 4.05 (s, 3H), 3.84 (s, 3H), 3.13 (q, *J* = 6.6 Hz, 2H), 2.55 (d, *J* = 1.0 Hz, 3H), 1.96 (t, *J* = 7.2 Hz, 2H), 1.49 (dp, *J* = 13.7, 7.3 Hz, 5H), 1.29 (h, *J* = 5.3 Hz, 5H).

^{13}C NMR (75 MHz, DMSO-d_6) δ 169.3, 159.0, 155.8, 154.8, 146.7, 136.1, 130.6, 128.6, 128.1, 128.0, 124.8, 112.6, 105.8, 95.2, 76.7, 55.1, 53.1, 32.1, 29.5, 28.2, 26.1, 24.8, 18.4.

M.p.: 202.2°C; **HPLC**: R_t= 10.05 min, purity 96.5 %, **MS** (+APCI): 405 $[M+H]^+$.

3 References

1. Hexahydro-2-(1*H*)-Azocinone. Org. Synth. 63, 188 (1985).

2. Giovannini, A., Savoia, D. & Umani-Ronchi, A. Organometallic Ring-Opening Reactions of N-Acyl and N-Alkoxycarbonyl Lactams. Synthesis of Cyclic Imines. J. Org. Chem. 54, 228–234 (1989).

3. Stenzel, K. et al. Alkoxyurea-Based Histone Deacetylase Inhibitors Increase Cisplatin Potency in Chemoresistant Cancer Cell Lines. J. Med. Chem. 60, 5334–5348 (2017).

4. Ugwuegbulam, C. O.; Foy, J. E. US6479660 (B1) – Process for the preparation of anti-malarial drugs. 2002.

5 Chapter III:

The next generation of histone deacetylase 6 inhibitors

Contribution:

- Synthesis of compounds **1a-c**, **2a-c**, **3a-d**, **4a-d**, **5**, **6**, **7**, **8a-g**, **9a-j**, **10**, **11**
- Manuscript and supporting information

The Next generation of histone deacetylase 6 inhibitors.

M. Pflieger, F. Hansen, T. Kurz

Abstract

The Acetylome of cells is important to maintain the homeostasis of an individual cell. Abnormal changes can result in the pathogenesis of immunological or neurological diseases and degeneration might promote the manifestation of cancer. Particularly, the pharmacological intervention of the acetylome with pan-histone deacetylase (HDAC) inhibitors is clinically validated. However, these drugs exhibit a poor patient compliance due to severe side effects. HDAC selective inhibitors might promote patient compliance and represent a valuable opportunity in personalised medicine. Therefore, we envisioned the development of HDAC6 selective inhibitors. In the course of our lead structure identification, we demonstrated that a hydroxylamine subunit proves to be beneficial for HDAC6 selectivity and established the synthesis of *N*-alkoxycarbamate based hydroxamic acids **9**. Here we report *N*-alkoxycarbamate based hydroxamic acids that showed an up to 4.4-fold higher selectivity towards HDAC6 than nexturastat A. With the discovery of the HDAC6 selective *N*-alkoxycarbamate based hydroxamic acids **9**, a CRBN-E3 ligase targeting proteolysis targeting chimera (PROTAC) **11** was developed to address non-active site associated activities.

Introduction

Histone deacetylases (HDACs) are proteases that catalyse the cleavage of acetylated lysine residues (isopeptide bonds).[1] Human zinc dependant histone deacetylases (HDACs) are classified into class I (HDAC1, HDAC2, HDAC3, HDAC8), class IIa (HDAC4, HDAC5, HDAC7, HDAC9), class IIb (HDAC6, HDAC10) and class IV (HDAC11). Depending on their cellular localisation, they influence the condensation state of histones,[2] participate in the post-translational modifications of cytosolic proteins[3] or even might act as an epigenetic reader in the case of class IIa.[4] Amongst humans, their diverse array of functions renders them a valuable target for the pharmacological intervention of immunological[5–8] or neurodegenerative diseases[9,10] and are clinically validated targets for the treatment of cancer.[11]

HDAC6 is unique amongst the HDACs as it features two catalytically active domains (Figure 19).[12] Whilst CD1 has a high specificity in the substrate recognition of acetylated *C*-terminal lysine residues, CD2 exhibits a promiscuity towards a wide range of client proteins.[13,14] In addition to those domains, HDAC6 displays an inherent zinc-finger ubiquitin binding domain (ZnF-UBP),[14–16] which enables it to recognise ubiquitinylated proteins. The rigidly controlled localisation of HDAC6 in the cytoplasm is the result of

the interplay between the nuclear export signal (NES), the nuclear localisation signal (NLS) and the Ser-Glu-containing tetrapeptide (SE14).[17]

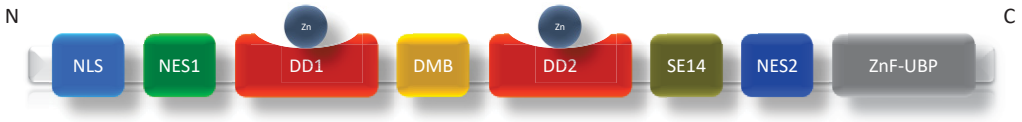

Figure 19. Schematic representation of HDAC6 domains.

HDAC6 catalyses the deacetylation of e.g. α-Tubulin,[18] Cortactin[19] and HSP90[20] and is of relevance for the pathogenesis of cancer[21] as well as in immunological[22] and neurological diseases.[23–25] Its participation in pathogenesis or disease progression is tissue dependant and of multifactorial nature. Despite intensive research, the clinical significance of HDAC6 selective inhibitors, as single agent, remains controversial.[26] Increasing evidence suggest, that the anti-cancer effect of those biologically active compounds is the result of concentrations at which other HDAC isozymes, particularly class I HDACs, are also inhibited. Nevertheless, the pharmacological intervention of cancer by addressing HDAC6, remains a promising target due to its participation in the invasiveness of cancer cells and its immunomodulatory properties.

Currently approved HDAC inhibitors (HDACi) are vorinostat, belinostat, panobinostat, romidepsine and chidamide for the treatment of haematological malignancies. All approved HDACi exhibit a mutual pharmacophore model: a zinc binding group (ZBG), a linker, and a cap group. [27–29] Whilst romidepsin[30,31] and chidamide[32] are HDAC class I selective, the remaining are regarded as pan inhibitors as they do not differentiate between individual isozymes. Since the elucidation of structural information of HDACs,[16] the design of selective inhibitors was significantly accelerated. Despite their high sequence identity inside the catalytic pocket, HDACs exhibit distinct features that allows a rational design for isozyme selective inhibitors.

Particularly in comparison to HDAC1, [33] HDAC6[16] exhibits a much wider and shallower entrance tunnel (Figure 20). In the course of the accumulation of structural information of HDACs, the traditional HDACi pharmacophore model (ZBG, linker, cap) was insufficient for the design of selective inhibitor and a revised pharmacophore model was developed. The pharmacophore model for HDAC6 inhibitors comprises of a ZBG, an aromatic linker and a sterically demanding surface cap group (S-CAP) (Figure 21).[34]

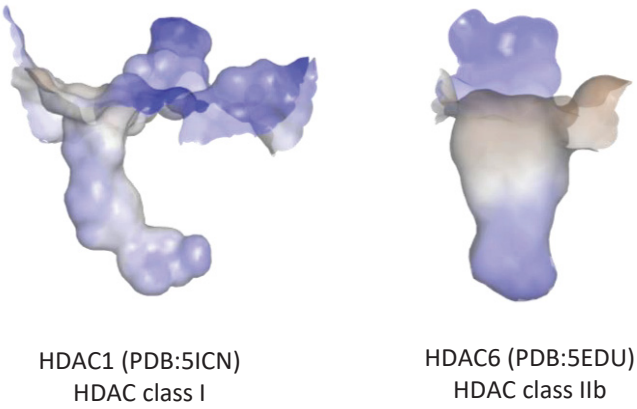

Figure 20. Surface comparison of HDAC1 and HDAC6.[16,33]

Based on these structural features and the revised pharmacophore model, the selectivity towards HDAC6 can be governed by a sterically demanding cap group (Figure 21). Two of the most prominent HDAC6 selective inhibitors are nexturastat A and tubastatin A, of which both exhibit a sterically demanding cap group . Whilst tubstastin A realises this steric demand by a bulky cap group, nexturastat A facilitates its selectivity by the exhibition of a branched cap group.

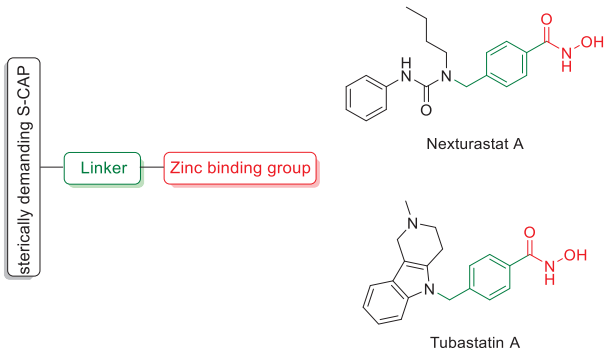

Figure 21. Revised pharmacophore model for the design of selective HDAC6 inhibitors. [34–36]

Here we report a rational derivatisation of Nexturastat A to improve HDAC6 selectivity (Figure 22).

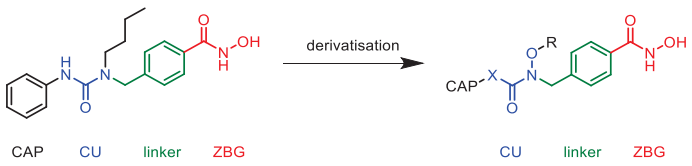

Figure 22. Structural modification of Nexturastat A.

Results and Discussion

Nexturastat A is a selective HDAC6 inhibitor with a low nanomolar activity and a reported 600-fold selectivity for HDAC6 over HDAC1.[37] Despite its high selectivity reported[37] by Bergman *et al.*, Nexturastat A exhibited only a selectivity index of 24 in our HDAC enzyme assays (Table 9). Therefore, we envisioned structural modifications of Nexturastat A by the introduction of a hydroxylamine-based connecting unit (CU) to increase the selectivity towards HDAC6, whilst maintaining the potency of nexturastat A.

Synthesis of branched alkoxyurea based hydroxamic acids.

In order to evaluate the influence of the hydroxylamine CU in respect to HDAC isozyme profile, the direct alkoxyurea derivative of Nexturastat A was synthesised (**4a**). Based on a retrosynthetic analysis (Scheme 16), *N*-Boc-*O*-alkylhydroxylamines were synthesised either by the *N*-Boc protection of *O*-substituted hydroxylamines or by the *O*-alkylation of *N*-Boc-hydroxylamines.

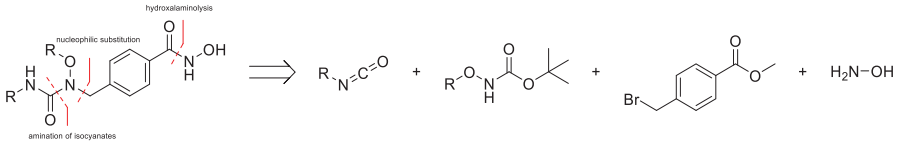

Scheme 16. Retrosynthetic analysis of N-oxyalkyl urea based hydroxamic acids.

The *O*-substituted hydroxylamine moiety was introduced to the benzyl linker by the *N*-alkylation of **1** with methyl 4-(bromomethyl)benzoate (Scheme 17). As the purification of this intermediate was laborious, **2** was accessed after Boc-deprotection over two steps.

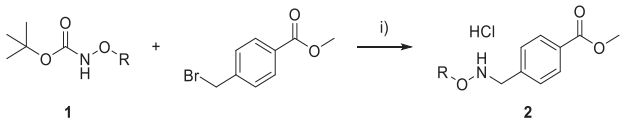

*Scheme 17. Synthesis of the substituted hydroxylamines **2**. I) 1.10 eq methyl 4-(bromomethyl)benzoate 1.20 eq NaH; ii) 5.00 eq $HCl_{(dioxane)}$, DCM.*

Subsequently, the branched alkoxyurea derivatives **3** were synthesised by the conversion of **2** with the respective isocyanate (Scheme 18).

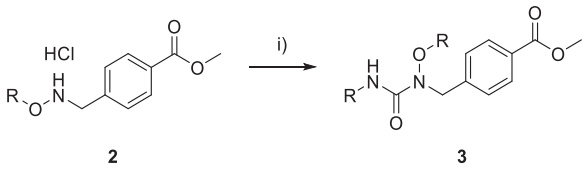

*Scheme 18. Synthesis of the branched alkoxyurea derivatives **3**. I) 1.00 eq RCNO, 1.00 eq DIPEA, DCM.*

Finally, the esters were converted into the corresponding hydroxamic acids **4** by hydroxylaminolysis (Scheme 19).

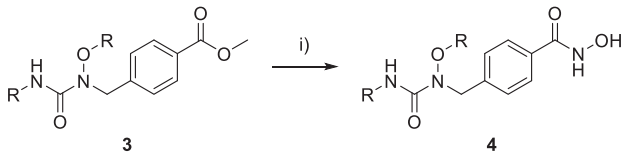

*Scheme 19. Synthesis of branched alkoxyurea based hydroxamic acids **4**. I) 30.0 eq $H_2NOH_{(aq)}$, 10.0 eq NaOH, DCM/MeOH.*

Inhibition of HDAC1 and HDAC6 by branched alkoxyurea based hydroxamic acids.

The branched alkoxyurea based hydroxamic acids **4** were subjected to HDAC1/6 isozyme profiling in order to evaluate their HDAC6 selectivity and their inhibitory potential. Table 9 depicts the isozyme profiling of compounds **4**.

Table 9. HDAC1/6 isozyme profiling of compounds 4. The presented data are the result of N=3.

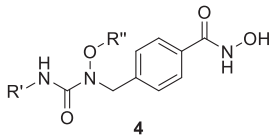

4

	R‘	R’’	HDAC1 IC_{50} [µM]	HDAC2 IC_{50} [µM]	HDAC3 IC_{50} [µM]	HDAC6 IC_{50} [µM]	SI 1/6	SI 2/6	SI 3/6
4a	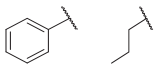		0.742 ± 0.039	1.42 ± 0.082	0.902 ± 0.008	0.020 ± 0.003	37.1	71.2	45.1
4b	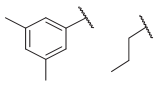		0.299 ± 0.057	0.515 ± 0.043	0.375 ± 0.084	0.014 ± 0.002	21.4	36.8	26.8
4c	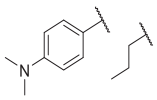		0.715 ± 0.010	1.14 ± 0.074	0.972 ± 0.064	0.022 ± 0.002	32.5	51.8	44.2
4d	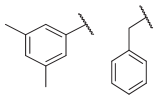		2.89 ± 0.125	3.59 ± 0.410	3.12 ± 0.578	0.341 ± 0.021	8.49	10.5	9.15
Nexturastat A			0.504 ± 0.033	0.861 ± 0.008	0.730 ± 0.033	0.021 ± 0.001	24	41.0	34.8

Values are the mean of three experiments.

In contrast to the reported 600-fold selectivity of Nexturastat A for HDAC6 over HDAC1, it showed a moderate selectivity index of 24 in our enzyme assay. The hydroxylamine derivative **4a** showed a 1.5-fold increase in selectivity, whilst maintaining the inhibitory activity (0.020 ± 0.003 µM) of HDAC6. A higher selectivity towards HDAC6 was anticipated by sterically demanding substituents such as 3,5-dimethylphenyl (**4b**) or by a 4-(*N,N*-dimethyl amino)-phenyl (**4c**). However, these substituent patterns had either no significant impact on the selectivity (**4c**) or was even disadvantageous in the case of **4b**. Furthermore, the introduction of a benzyl group to R'' (**4d**) resulted in a significant decreased inhibition of HDAC6 (0.341 ± 0.021 µM) with a concomitant decrease in selectivity as evidenced by the comparison with **4b**. Since the gain in selectivity, due to the hydroxylamine subunit was only marginal, we intended to increase the chemical space and transitioned to *N*-alkoxy ^{t}butyl-carbamate based hydroxamic acids.

Synthesis of branched *N*-alkoxycarbamate based hydroxamic acids and lead structure identification.

The desired *O*-substituted ^{t}butyl-(*N*-oxy) carbamate based hydroxamic acid (**6**) was synthesised by the conversion of **2** (free hydroxylamine) with di-*tert*-butyl dicarbonate (**5**) and their subsequent transformation by hydroxylaminolysis to **6** (Scheme 20).

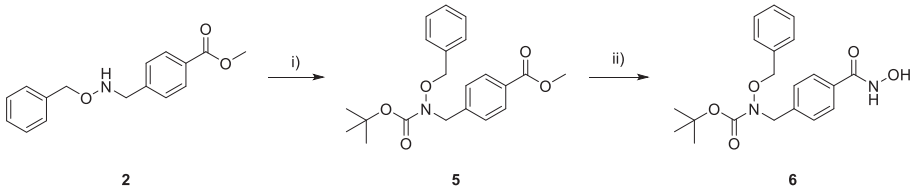

*Scheme 20. Synthesis of O-benzyl-^{t}butyl-(N-oxy) carbamate based hydroxamic acids **6**. I) 1.20 eq Boc_2O, 3.00 eq TEA, DCM; ii) a) 10.0 eq LiOH, THF/MeOH; b) 1.00 eq HATU, 1.20 eq H2NOH • HCl, 3.20 eq DIPEA, DMF.*

Compound **6** was then tested in an HDAC1 and HDAC6 inhibition assay (Table 10).

*Table 10. HDAC1/6 inhibitory activity of compound **6** and **4d**. The presented data are the result of N=3.*

	HDAC1 IC_{50} [μM]	HDAC6 IC_{50} [μM]	SI 1/6
6	0.745 ± 0.032	0.017 ± 0.001	44
4d	2.89 ± 0.125	0.341 ± 0.021	8.5
Nexturastat A	0.504 ± 0.033	0.021 ± 0.001	24

Values are the mean of three experiments.

By the comparison of **4d** with **6** it became apparent that the ^{t}butyl-carbamate resulted in an increased HDAC6 inhibition with a coherent increase in selectivity. Based on these initial finding, we identified **6** as a lead structure and modified **6** at the *N*-hydroxy substituent. For this purpose, a synthetic strategy for a late stage *O*-alkylation of *N*-alkoxy ^{t}butyl carbamates was developed to efficiently increase the structural diversity of our compound set (Scheme 21).

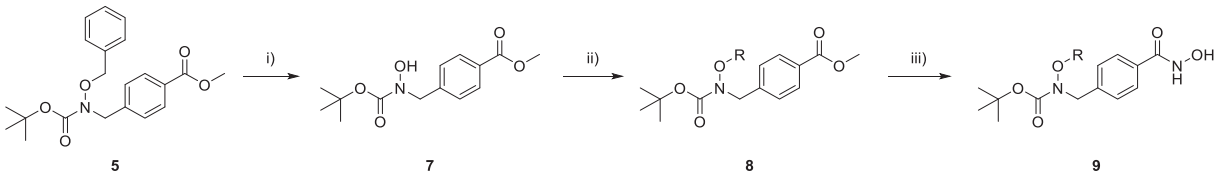

*Scheme 21. Synthesis of O-substituted-(N-alkoxy) carbamate based hydroxamic acids (**9**). I) H_2, Pd/C, MeOH; ii) 1.20 eq NaH (60 %, mineral oil), 2.00 eq RX, DMF; iii) a) 10.0 eq LiOH, THF/MeOH; b) 1.00 eq HATU, 1.20 eq H2NOH • HCl, 3.20 eq DIPEA, DMF.*

5 underwent catalytic hydrogenation to access the unsubstituted *N*-alkoxy carbamate **7**, which was alkylated (**8**) and converted into the respected hydroxamic acid **9**. Since the aliphatic propyl substituents resulted in an increased HDAC6 selectivity index for **4**, **7** was solely alkylated with aliphatic substituents. Table 11 depicts the isozyme profiling of the synthesised branched *N*-alkoxycarbamate based hydroxamic acids **6** and **9**.

*Table 11. HDAC1/6 isozyme profiling of compounds **6** and **9**. The presented data are the result of N=3.*

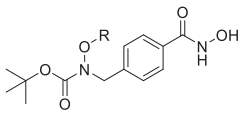

Cmp	R	HDAC1 IC_{50} [μM]	HDAC6 IC_{50} [μM]	SI 1/6
6		0.745 ± 0.032	0.017 ± 0.0001	43.8
9a		1.05 ± 0.101	0.016 ± 0.004	65.6
9b		1.59 ± 0.085	0.015 ± 0.002	106
9c		4.46 ± 1.004	0.048 ± 0.004	92.9
9d		3.97± 1.101	0.049 ± 0.001	81.0
9e		3.81 ± 0.485	0.055 ± 0.003	69.3
9f		8.48 ± 2.136	0.099 ± 0.002	85.7
9g		4.26 ± 0.446	0.054 ± 0.006	78.9
9h		2.72 ± 0.236	0.041 ± 0.002	66.3
9i		3.57 ± 0.719	0.079 ± 0.002	45.2
Vorinostat		0.096 ± 0.011	0.056 ± 0.009	1.71
Nexturastat A		0.504 ± 0.033	0.021 ± 0.0001	24.0

Values are the mean of three experiments.

By the removal of the benzyl group of **6**, the free *N*-hydroxy carbamate (**9a**) exhibited a significantly increased HDAC6 selectivity (SI(1/6)=65.8) whilst maintaining the inhibitory activity (0.016 µM) thereof. The *N*-methoxy carbamate derivative **9b** resulted in a SI of 106 for HDAC6 over HDAC1. With increasing chain length, the HDAC6 selectivity decreased with a concomitant decrease in inhibitory activity. Branched substituents were neither beneficial for HDAC6 inhibition, nor their selectivity index.

Subsequently, the compounds which exhibited at least a 3-fold higher selectivity (SI ≥ 72) towards HDAC6 than nexturastat A (**9b**, **9c**, **9d**, **9f**, **9g**) were further subjected to HDAC2 and HDAC3 isozyme profiling (Table 12).

*Table 12. HDAC1, HDCA2, HDAC3 and HDAC6 isozyme profiling of **9**.*

Cmp	HDAC1 IC_{50} [µM]	HDAC2 IC_{50} [µM]	HDAC3 IC_{50} [µM]	HDAC6 IC_{50} [µM]	SI 1/6	SI 2/6	SI 3/6
9b	1.59 ± 0.085	2.53 ± 0.051	1.79 ± 0.282	0.015 ± 0.002	106	169	119
9c	4.46 ± 1.00	8.19 ± 1.49	5.77 ± 0.299	0.048 ± 0.004	92.9	171	120
9d	3.97± 1.10	7.46 ± 0.759	5.30 ± 0.896	0.049 ± 0.001	81.0	152	108
9f	8.48 ± 2.14	13.5 ± 0.615	11.5 ± 0.700	0.099 ± 0.002	85.7	136	116
9g	4.26 ± 0.446	7.23 ± 0.278	5.75 ± 1.13	0.054 ± 0.006	78.9	134	106
Vorinostat	0.096 ± 0.011	0.156 ± 0.015	0.088 ± 0.007	0.056 ± 0.009	1.71	2.79	1.57
Nexturastat A	0.504 ± 0.033	0.861 ± 0.008	0.730 ± 0.033	0.021 ± 0.001	24.0	41.0	34.8

Values are the mean of three experiments.

In summary, the derivatisation of nexturast A with a hydroxylamine subunit (**4a**) in the cap region resulted in an increased HDAC6 selectivity, which might be the result of a more favourable conformation in the catalytic pocket. Based on these findings, we further modified the urea connecting unit with a carabamate CU, resulting in the identification of a lead structure (**6**) exhibiting an approximately 2-fold increased selectivity compared to nexturastat A. With **6** in hand and our initial structure-activity relationship, we developed an HDAC6 inhibitor (SI=106, **MPK169**), which exhibited a 4.4-fold higher selectivity than nexturastat A.

Proteolysis targeting chimera (PROTAC).

Pharmacological intervention by active site inhibition has several drawbacks which a cell can counter regulate or circumvent by e.g. overexpression of the target enzyme, increased supply of the native ligand or by mutations to decrease binding affinity. Furthermore, the occupational driven inhibition of target proteins usually does not interfere with scaffold interactions such as protein-protein interactions or the zinc-finger ubiquitin binding domain. Considering that HDAC6 has two active domains, the statistical probability of two inhibitors binding to the same enzyme is rather low and scaffold associated activities are not addressed by active site inhibition, we envisioned to transition to an event driven PROTAC mediated protein degradation. Such an approach can avoid a cellular inhibition response and address secondary scaffold associated HDAC6 activities. A PROTAC is a heterobifunctional entity that exhibits a ligand for the point of interest (POI), here HDAC6, and an E3 recruiting element which is connected by a linker. Based on our HDAC6 selective branched *N*-alkoxycarbamate motif, we designed the PROTAC **11** with pomalidomide as E3 recruiting element (Scheme 22).

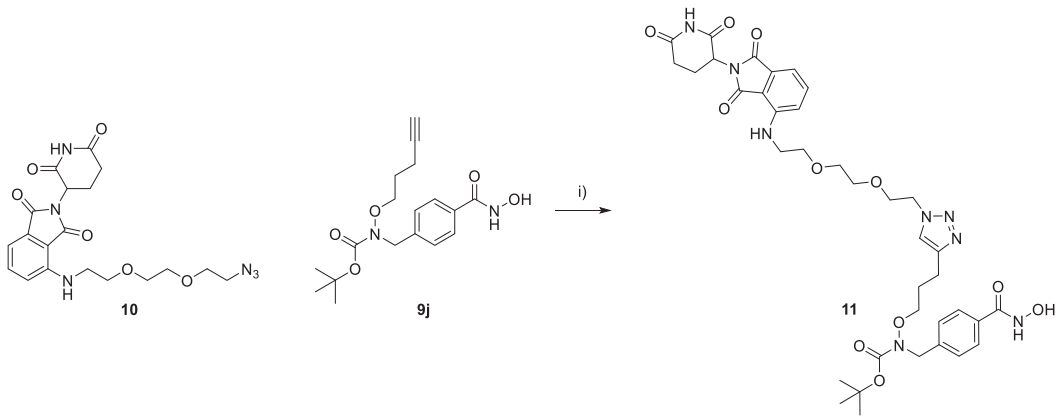

*Scheme 22. Synthesis of PROTAC **11** by a 1,3-dipolar cycloaddition. I) 1.10 eq. $CuSO_4$, 6.00 eq sodium L-ascorbate, H_2O/t-BuOH.*

The pomalidomide derivative **10**[38], exhibiting an azide linker, was connected to the alkyne functionalised branched *N*-alkoxycarbamate based hydroxamic acid **9j** via an 1,3-dipolar cycloaddition with stoichiometric amounts of $CuSO_4$, resulting in the PROTAC **11**. Initial attempts with catalytic amounts of $CuSO_4$ did not yield the respective product, presumably due to the chelation of copper by the hydroxamate moiety.[39] Subsequently, the PROTAC **11** was subjected to isozyme profiling (Table 13). Under the tested conditions, **11** inhibited HDAC6 with an IC_{50} = 0.043 ± 0.004 µM and HDAC class I

enzymes in the micromolar range, resulting in selectivity indices of up to 74.4 with an approximately 3.1-fold higher selectivity towards HDAC6 than nexturastat A.

*Table 13. HDAC isozyme profiling of PROTAC **11**.*

Cmp	HDAC1 IC_{50} [μM]	HDAC2 IC_{50} [μM]	HDAC3 IC_{50} [μM]	HDAC6 IC_{50} [μM]	SI 1/6	SI 2/6	SI 3/6
11	3.20 ± 0.763	3.18 ± 0.417	2.32 ± 0.028	0.043 ± 0.004	74.4	74.0	54.0
Vorinostat	0.096 ± 0.011	0.156 ± 0.015	0.088 ± 0.007	0.056 ± 0.009	1.71	2.79	1.57
Nexturastat A	0.504 ± 0.033	0.861 ± 0.008	0.730 ± 0.033	0.021 ± 0.001	24.0	41.0	34.8

Values are the mean of three experiments.

Conclusion.

HDAC6 is a major effector in the non-histone mediated regulation of cellular processes and represents a valuable target in the pharmacological intervention of immunological as well as neurological diseases. In addition, HDAC6 selective inhibitors remain valuable tools to explore the potential participation of HDAC6 in tumorigenesis. In this study, we developed a synthetic strategy for the synthesis of *N*-alkoxycarbamate based hydroxamic acids that exhibited an up to 4.4-fold higher SI1/6 than the established HDAC6 selective inhibitor nexturastat A, whilst maintaining its potency. Based on the discovery of these selective inhibitors, a PROTAC with a pomalidomide E3 recruiting element was designed that might be employed in the selective HDAC6 degradation.

References

1. Bertrand, P. Inside HDAC with HDAC inhibitors. *European Journal of Medicinal Chemistry* vol. 45 2095–2116 (2010).
2. Marks, P. A. *et al.* Histone deacetylases and cancer: Causes and therapies. *Nat. Rev. Cancer* **1**, 194–202 (2001).
3. Gallinari, P., Di Marco, S., Jones, P., Pallaoro, M. & Steinkühler, C. HDACs, histone deacetylation and gene transcription: From molecular biology to cancer therapeutics. *Cell Res.* **17**, 195–211 (2007).
4. Mathias, R. A., Guise, A. J. & Cristea, I. M. Post-translational modifications regulate class IIa histone deacetylase (HDAC) function in health and disease. *Mol. Cell. Proteomics* **14**, 456–470 (2015).
5. Hull, E. E., Montgomery, M. R. & Leyva, K. J. HDAC Inhibitors as Epigenetic Regulators of the Immune System: Impacts on Cancer Therapy and Inflammatory Diseases. *Biomed Res. Int.* **2016**, 1–15 (2016).
6. Licciardi, P. V. & Karagiannis, T. C. Regulation of Immune Responses by Histone Deacetylase Inhibitors. *ISRN Hematol.* **2012**, 1–10 (2012).
7. Moreno-Gonzalo, O. *et al. HDAC6 controls innate immune and autophagy responses to TLR-mediated signalling by the intracellular bacteria Listeria monocytogenes*. *PLoS Pathogens* vol. 13 (2017).
8. Knox, T. *et al.* Selective HDAC6 inhibitors improve anti-PD-1 immune checkpoint blockade therapy by decreasing the anti-inflammatory phenotype of macrophages and down-regulation of immunosuppressive proteins in tumor cells. *Sci. Rep.* **9**, 6136 (2019).
9. Pandey, U. B. *et al.* HDAC6 rescues neurodegeneration and provides an essential link between autophagy and the UPS. *Nature* **447**, 859–863 (2007).
10. Simões-Pires, C. *et al.* HDAC6 as a target for neurodegenerative diseases: What makes it different from the other HDACs? *Mol. Neurodegener.* **8**, 7 (2013).
11. Richardson, P. G. *et al.* PANORAMA 2: Panobinostat in combination with bortezomib and dexamethasone in patients with relapsed and bortezomib-refractory myeloma. *Blood* **122**, 2331–2337 (2013).
12. Seidel, C., Schnekenburger, M., Dicato, M. & Diederich, M. Histone deacetylase 6 in health and disease. *Epigenomics* **7**, 103–118 (2015).
13. Hai, Y. & Christianson, D. W. Histone deacetylase 6 structure and molecular basis of catalysis and inhibition. *Nat. Chem. Biol.* **12**, 741–747 (2016).
14. Miyake, Y. *et al.* Structural insights into HDAC6 tubulin deacetylation and its selective inhibition. *Nat. Chem. Biol.* **12**, 748–754 (2016).
15. Haberland, M., Montgomery, R. L. & Olson, E. N. The many roles of histone deacetylases in development and physiology: Implications for disease and therapy. *Nat. Rev. Genet.* **10**, 32–42 (2009).
16. Hai, Y. & Christianson, D. W. Histone deacetylase 6 structure and molecular basis of catalysis and inhibition. *Nat. Chem. Biol.* **12**, 741–747 (2016).
17. Liu, Y., Peng, L., Seto, E., Huang, S. & Qiu, Y. Modulation of histone deacetylase 6 (HDAC6)

nuclear import and tubulin deacetylase activity through acetylation. *J. Biol. Chem.* **287**, 29168–29174 (2012).

18. Hubbert, C. *et al.* HDAC6 is a microtubule-associated deacetylase. *Nature* **417**, 455–458 (2002).

19. Zhang, X. *et al.* HDAC6 Modulates Cell Motility by Altering the Acetylation Level of Cortactin. *Mol. Cell* **27**, 197–213 (2007).

20. Kovacs, J. J. *et al.* HDAC6 regulates Hsp90 acetylation and chaperone-dependent activation of glucocorticoid receptor. *Mol. Cell* **18**, 601–607 (2005).

21. Li, T. *et al.* Histone deacetylase 6 in cancer. *J. Hematol. Oncol.* **11**, 1–10 (2018).

22. Li, A., Chen, P., Leng, Y. & Kang, J. Histone deacetylase 6 regulates the immunosuppressive properties of cancer-associated fibroblasts in breast cancer through the STAT3–COX2-dependent pathway. *Oncogene* **37**, 5952–5966 (2018).

23. Fukada, M., Nakayama, A., Mamiya, T., Yao, T. P. & Kawaguchi, Y. Dopaminergic abnormalities in Hdac6-deficient mice. *Neuropharmacology* **110**, 470–479 (2016).

24. Jochems, J. *et al.* Antidepressant-like properties of novel HDAC6-selective inhibitors with improved brain bioavailability. *Neuropsychopharmacology* **39**, 389–400 (2014).

25. Govindarajan, N. *et al.* Reducing HDAC6 ameliorates cognitive deficits in a mouse model for Alzheimer's disease. *EMBO Mol. Med.* **5**, 52–63 (2013).

26. Depetter, Y. *et al.* Selective pharmacological inhibitors of HDAC6 reveal biochemical activity but functional tolerance in cancer models. *Int. J. Cancer* **145**, 735–747 (2019).

27. Jung, M. *et al.* Amide analogues of trichostatin A as inhibitors of histone deacetylase and inducers of terminal cell differentiation. *J. Med. Chem.* **42**, 4669–4679 (1999).

28. Finnin, M. S. *et al.* Structures of a histone deacetylase homologue bound to the TSA and SAHA inhibitors. *Nature* **401**, 188–193 (1999).

29. Jung, M. Inhibitors of Histone Deacetylase as New Anticancer Agents. *Curr. Med. Chem.* **8**, 1505–1511 (2012).

30. Vandermolen, K. M., McCulloch, W., Pearce, C. J. & Oberlies, N. H. Romidepsin (Istodax, NSC 630176, FR901228, FK228, depsipeptide): A natural product recently approved for cutaneous T-cell lymphoma. *J. Antibiot. (Tokyo).* **64**, 525–531 (2011).

31. Iyer, S. P. & Foss, F. F. Romidepsin for the Treatment of Peripheral T-Cell Lymphoma. *Oncologist* **20**, 1084–1091 (2015).

32. Shi, Y. K. *et al.* Results from a multicenter, open-label, pivotal phase II study of chidamide in relapsed or refractory peripheral T-cell lymphoma. *Ann. Oncol.* **26**, 1766–1771 (2015).

33. Watson, P. J. *et al.* Insights into the activation mechanism of class i HDAC complexes by inositol phosphates. *Nat. Commun.* **7**, 11262 (2016).

34. Melesina, J., Praetorius, L., Simoben, C. V., Robaa, D. & Sippl, W. Design of selective histone deacetylase inhibitors: Rethinking classical pharmacophore. *Future Med. Chem.* **10**, 1537–1540 (2018).

35. Butler, K. V. *et al.* Rational design and simple chemistry yield a superior, neuroprotective HDAC6 inhibitor, tubastatin A. *J. Am. Chem. Soc.* **132**, 10842–10846 (2010).

36. Tavares, M. T. *et al.* Synthesis and Pharmacological Evaluation of Selective Histone Deacetylase

6 Inhibitors in Melanoma Models. *ACS Med. Chem. Lett.* **8**, 1031–1036 (2017).

37. Bergman, J. A. *et al.* Selective histone deacetylase 6 inhibitors bearing substituted urea linkers inhibit melanoma cell growth. *J. Med. Chem.* **55**, 9891–9899 (2012).

38. An, Z., Lv, W., Su, S., Wu, W. & Rao, Y. Developing potent PROTACs tools for selective degradation of HDAC6 protein. *Protein Cell* **10**, 606–609 (2019).

39. Farkas, E., Enyedy, É. A., Micera, G. & Garribba, E. Coordination modes of hydroxamic acids in copper(II), nickel(II) and zinc(II) mixed-ligand complexes in aqueous solution. *Polyhedron* **19**, 1727–1736 (2000).

5.1 Chapter III – Supporting information

The Next generation of histone deacetylase 6 inhibitors.

Supporting information

M. Pflieger, F. Hansen, T. Kurz

Contents

1 General Information

Reaction, monitoring and purification

Chemicals and solvents were purchased from commercial suppliers (Sigma-Aldrich, Acros Organics, TCI, Fluorochem ABCR, Alfa Aesar, J&K, Carbolution) and used without further purification. Dry solvents were obtained from Acros Organics. Ambient or room temperature correspond to 22°C. The reaction progression was monitored using Thin-Layer-Chromatography plates by Macherey Nagel (ALUGRAM Xtra SIL G/UV_{254}). Visualisation was achieved with ultraviolet irradiation (254 nm) or by staining with a $KmnO_4$-solution (9 g $KmnO_4$, 60 g K_2CO_3, 15 mL of a 5% aqueous NaOH-solution, ad 900 mL demineralised water). Purification was either performed with prepacked Silica cartridges (RediSep® Rf Normal Phase Silica, RediSep® Rf RP C18) for flash column chromatography (CombiFlashRf200, TeleDyneIsco) or by recrystallisation. Different eluent mixtures of solvents (*n*-hexane and ethyl acetate or dichloromethane and methanol) served as the mobile phase for flash column chromatography and are stated in the experimental procedure.

Analytics

An NMR-Spectrometer by Bruker (Bruker Avance III – 300, Bruker Avance DRX – 500 or Bruker Avance III – 600) were used to perform ^{1}H- and^{13}C-NMR experiments. Chemical shifts are given in parts per million (ppm), relative to residual non-deuterated solvent peak (^{1}H-NMR: DMSO-d_6 (2.50), ^{13}C-NMR: DMSOd_6 (39.52). Signal patterns are indicated as: singlet (s), doublet (d), triplet (t), quartet (q), or multiplet (m). Coupling constants, J, are quoted to the nearest 0.1 Hz and are presented as observed. ESI-MS was carried out using Bruker Daltonics UHR-QTOF maXis 4G (Bruker Daltonics) under electrospray ionization (ESI). The above-mentioned characterisations were carried out by the HHU Center of Molecular and Structural Analytics at Heinrich-Heine University Düsseldorf (http://www.chemie.hhu.de/en/analytics-center-hhucemsa.html). APCI-MS was carried out with an Advion expression^{L} CMS. Melting points were determined using a Büchi M-565 melting point apparatus (uncorrected). Analytical HPLC was carried out on a Knauer HPLC system comprising of an Azura P6.1L pump, an Optimas 800 autosampler, a Fast Scanning Spectro-Photometer K-2600 and a Knauer Reversed Phase column (SN: FK36). Evaluated compounds were detected at 254 nm. The solvent gradient table is shown in Table 14. The purity of all final compounds was 95% or higher.

Table 14: The solvent gradient table for analytic HPLC analysis.

Time / min	Water + 0.1% TFA	ACN + 0.1% TFA
Initial	90	10
0.50	90	10
20.0	0	100
30.0	0	100
31.0	90	10
40.0	90	10

2 Synthetic procedures

2.1 Synthesis of *tert*-butyl (benzyloxy)carbamate (**1a**)[1]

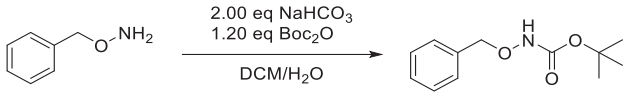

1.00 eq (70.0 mmol, 11.2 g) *O*-benzylhydroxylamine was dissolved in 80 mL of a mixture of DCM and dH_2O (1:1). After the reaction was cooled on ice, 2.00 eq (140 mmol, 11.8 g) of $NaHCO_3$ and 1.20 eq (84.0 mmol, 18.3 g) of Boc_2O was added and stirred for 3 h at ambient temperature. The reaction mixture was diluted with 40 mL of sat. aq. $NaHCO_3$ solution and the product extracted with DCM. The combined org. layers were dried over Na_2SO_4 and the solvent removed under reduced pressure. After crystallisation from *n*-hexane, 5.83 g (26.1 mmol, 37 %) of **1a** was obtained as colourless crystals.

All spectroscopic data agreed with literature.[1]

2.2 Synthesis of *tert*-butyl methoxycarbamate (**1b**)

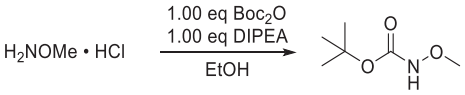

1.00 eq (25.0 mmol, 2.06 g) of *O*-methylhydroxylamine hydrochloride was combined with 1.00 eq (25.0 mmol, 3.25 g, 4.38 mL) of DIPEA and 1.00 eq (25 mmol, 5.74 g) of Boc_2O in 50 mL of EtOH. After 16 h whilst stirring at RT, the solvent was removed, and the product purified by flash column chromatography (*n*-hexane/EtOAc). 3.07 g (20.9 mmol, 84 %) of **1b** was obtained as colourless oil.

^{1}H NMR (600 MHz, DMSO-d_6) δ 9.98 (s, 1H), 3.51 (s, 3H), 1.40 (s, 9H).

^{13}C NMR (151 MHz, DMSO-d_6) δ 156.0, 79.5, 63.1, 40.1, 28.1.

2.3 Synthesis of *tert*-butyl propoxycarbamate (**1c**)

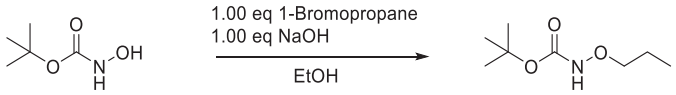

1.00 eq (75.1 mmol, 10 g) of *tert*-butyl *N*-Hydroxycarbamate was combined with 1.00 eq (75.1 mmol, 3 g) of NaOH and 1.00 eq (75.1 eq, 9.24 g, 6.82 mL) of 1-bromopropane in 250 mL of Ethanol. After 6 h at 70 °C whilst stirring, the solvent was removed *in vacuo* and the product purified by flash column chromatography (*n*-hexane/EtOAc). 7.42 g (42.3 mmol, 56 %) of **1c** was obtained as colourless oil.

^{1}H NMR (300 MHz, DMSO-d_6) δ 9.89 (s, 1H), 3.63 (t, J = 6.5 Hz, 2H), 1.64 – 1.43 (m, 2H), 1.40 (s, 8H), 0.87 (t, J = 7.4 Hz, 3H).

^{13}C NMR (75 MHz, DMSO-d_6) δ 156.1, 79.4, 76.8, 28.1, 20.9, 10.4.

2.4 General procedure for the synthesis of methyl 4-((alkoxyamino)methyl)benzoate hydrochloride (**2**)

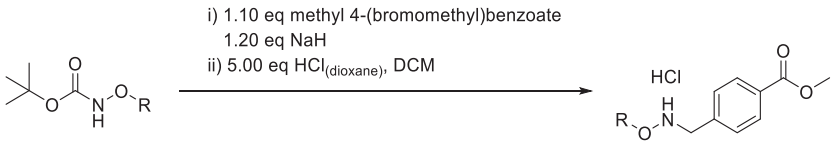

1.00 eq of *tert*-butyl alkoxycarbamate was dissolved in 4 mL/mmol of THF and cooled to 0°C. After 30°C whilst stirring, 1.10 eq of methyl 4-(bromomethyl)benzoate was added and stirred for 16 h to RT. The solvent was removed under reduced pressure and the precipitate resuspended in 50 mL of EtOAc. Subsequently, the organic layer was washed with dH_2O (3x), brine (1x) and dried over Na_2SO_4. After the solvent was removed *in vacuo*, the product was dissolved in 10 mL/mmol DCM and 5.00 eq of 5 M HCl in dioxane added. The product was collected by filtration, washed with DCM (3x).

2.4.1 Synthesis of methyl 4-(((benzyloxy)amino)methyl)benzoate hydrochloride (**2a**)

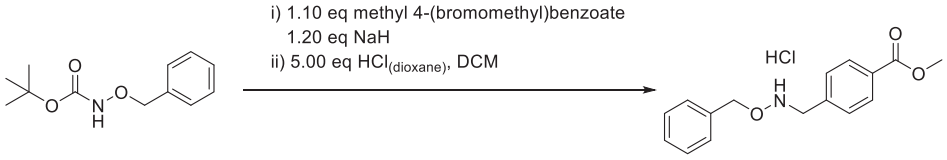

2a was synthesised from 7.50 g (51.0 mmol) of **1a**, 8.46 g (37.0 mmol) of methyl 4-(bromomethyl)benzoate and 1.61 g (40.3 mmol) of NaH (60%, mineral oil) in 134 mL of THF according to general procedure 2.4. 9.46 g (30.7 mmol, 91 %) of **2a** was obtained as a colourless solid over two steps.

^{1}H NMR (300 MHz, DMSO-d_6) δ 8.05 – 7.89 (m, 2H), 7.79 – 7.60 (m, 2H), 7.37 (h, J = 1.2 Hz, 5H), 5.13 (s, 2H), 4.51 (s, 2H), 3.86 (s, 3H).

^{13}C NMR (75 MHz, DMSO-d_6) δ 166.2, 144.7, 138.2, 128.9, 128.8, 128.1, 128.1, 128.1, 127.4, 75.0, 54.9, 52.0.

M.p.: 194.2 °C, **HPLC**: R_t=11.3, purity = 95.0 %, **MS** (+APCI): 272 $[M+H]^+$

2.4.2 Synthesis of methyl 4-((methoxyamino)methyl)benzoate hydrochloride (**2b**)

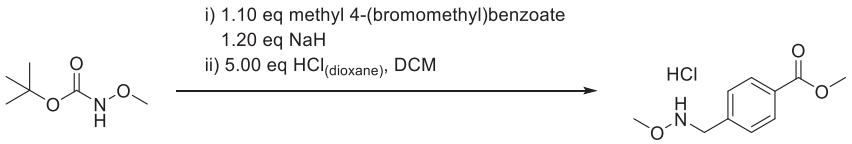

2b was synthesised from 7.50 g (51.0 mmol) of **1b**, 12.8 g (56.1 mmol) of methyl 4-(bromomethyl)benzoate and 2.45 g (61.2 mmol) of NaH (60% mineral oil) in 204 mL of THF according to general procedure 2.4. 17.4 g (46.5 mmol, 91 %) of **2b** was obtained as a colourless solid over two steps.

^{1}H NMR (300 MHz, DMSO-d_6) δ 8.06 – 7.90 (m, 2H), 7.76 – 7.64 (m, 2H), 4.46 (s, 2H), 3.86 (s, 3H), 3.84 (s, 3H).

^{13}C NMR (75 MHz, DMSO-d_6) δ 166.2, 144.8, 128.9, 128.7, 128.1, 60.8, 54.5, 52.0.

M.p.: 181.8 °C, **HPLC**: R_t=5.92, purity = 98.2 %, **MS** (+APCI): 1961 $[M+H]^+$

2.4.3 Synthesis of methyl 4-((propoxyamino)methyl)benzoate hydrochloride (**2c**)

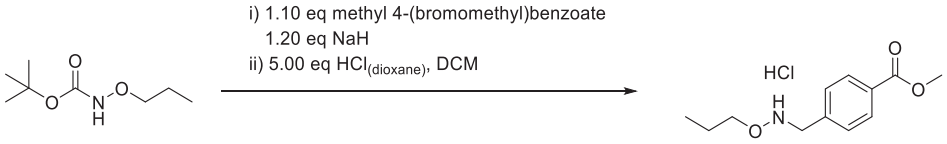

2c was synthesised from 7.00 g (39.9 mmol) of **1c**, 10.1 g (43.9 mmol) of methyl 4-(bromomethyl)benzoate and 1.92 g (47.9 mmol) of NaH (60% mineral oil) in 160 mL of THF according to general procedure 2.4. 9.49 g (36.6 mmol, 92 %) of **2c** was obtained as a colourless solid over two steps.

^{1}H NMR (300 MHz, DMSO-d_6) δ 8.03 – 7.92 (m, 2H), 7.78 – 7.66 (m, 2H), 4.46 (s, 2H), 4.05 (t, *J* = 6.5 Hz, 2H), 3.86 (s, 3H), 1.55 (dtd, *J* = 13.8, 7.3, 6.4 Hz, 2H), 0.82 (t, *J* = 7.4 Hz, 3H).

^{13}C NMR (75 MHz, DMSO-d_6) δ 165.8, 135.9, 130.8, 129.9, 129.0, 74.3, 52.2, 51.2, 20.7, 10.0.

M.p.: 227.8 °C, **HPLC**: R_t=7.95, purity ≥ 99 %, **MS** (+APCI): 224 $[M+H]^+$

2.5. General procedure for the synthesis of *O* substituted *N*-oxyurea derivatives (**3**)

1.00 eq of methyl 4-((alkoxyamino)methyl)benzoate hydrochloride was suspended in 25 mL/mmol of DCM. Subsequently, 1.00 eq of DIPEA and 1.00 eq of the respective isocyante were added and stirred for 16 h at ambient temperature. The solvent was removed under reduced pressure, the residue resuspended in EtOAc and washed with dH2O (3x) and brine (1x). After drying over Na_2SO_4, the curde product was purified by flash column chromatography (*n*-hexane/EtOAc).

2.5.1 Synthesis of methyl 4-((1-(benzyloxy)-3-(3,5-dimethylphenyl)ureido)methyl)benzoate (**3a**)

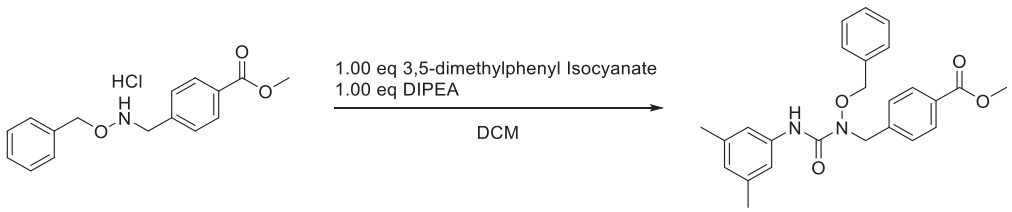

3a was synthesised from 158 mg (0.583 mmol) of **3a**, 85.5 mg (0.583 mmol) of 3,5-dimethylphenyl Isocyanate in 15 mL of DCM. The product was obtained as a colourless solid with a yield of 85 % (0.495 mmol, 207 mg).

^{1}H NMR (300 MHz, DMSO-d_6) δ 8.69 (s, 1H), 7.98 – 7.86 (m, 2H), 7.52 – 7.27 (m, 7H), 7.13 (dd, *J* = 1.6, 0.9 Hz, 2H), 6.65 (tt, *J* = 1.6, 0.8 Hz, 1H), 4.90 (s, 2H), 4.72 (s, 2H), 3.83 (s, 3H), 2.25 – 2.17 (m, 6H).

^{13}C NMR (75 MHz, DMSO-d_6) δ 166.0, 156.4, 142.8, 138.5, 137.3, 135.5, 129.6, 129.2, 128.7, 128.6, 128.5, 128.3, 124.4, 117.7, 76.0, 52.1, 50.9, 21.0.

M.p.: 116.9 °C; HPLC: R_t=17.68 , purity = 95.8 %, **MS** (+APCI): 419 $[M+H]^+$

2.5.2 Synthesis of methyl 4-((3-(3,5-dimethylphenyl)-1-propoxyureido)methyl)benzoate (**3b**)

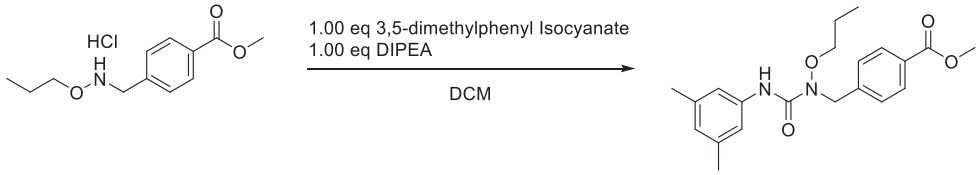

3b was synthesised from 200 mg (0.776 mmol) of **2c**, 114 mg (0.776 mmol) of 3,5-dimethylphenyl Isocyanate in 19.0 mL of DCM. The product was obtained as a colourless solid with a yield of 73 % (0.565 mmol, 209 mg).

^{1}H NMR (300 MHz, DMSO-d_6) δ 8.70 (s, 1H), 8.02 – 7.84 (m, 2H), 7.55 – 7.40 (m, 2H), 7.29 – 7.14 (m, 2H), 6.66 (tt, *J* = 1.6, 0.8 Hz, 1H), 4.75 (s, 2H), 3.84 (s, 3H), 3.80 (t, *J* = 6.8 Hz, 2H), 2.29 – 2.17 (m, 6H), 1.63 (h, *J* = 7.2 Hz, 2H), 0.85 (t, *J* = 7.4 Hz, 3H).

^{13}C NMR (75 MHz, DMSO-d_6) δ 166.0, 156.5, 143.0, 138.6, 137.3, 129.2, 128.7, 128.6, 124.4, 117.8, 75.8, 52.1, 50.8, 21.0, 20.7, 10.2.

M.p.: 99.3 °C; **HPLC**: R_t=17.37 min, purity ≥ 99 %, **MS** (+APCI): 371 $[M+H]^+$

2.5.3 Synthesis of methyl 4-((3-phenyl-1-propoxyureido)methyl)benzoate (**3c**)

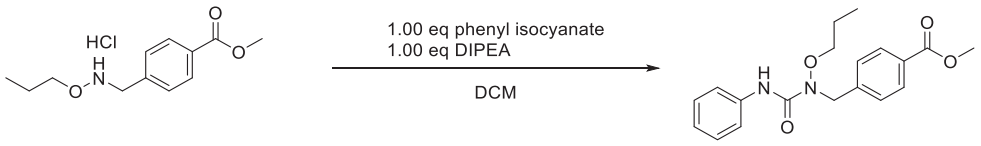

3c was synthesised from 200 mg (0.779 mmol) of **2c**, 92.8 mg (0.779 mmol) of phenyl isocyanate in 19.4 mL of DCM. The product was obtained as a colourless solid with a yield of 73 % (0.570 mmol, 195 mg).

^{1}H NMR (600 MHz, DMSO-d_6) δ 8.88 (s, 1H), 8.00 – 7.87 (m, 2H), 7.63 – 7.53 (m, 2H), 7.52 – 7.42 (m, 2H), 7.33 – 7.20 (m, 2H), 7.02 (tt, *J* = 7.4, 1.2 Hz, 1H), 4.77 (s, 2H), 3.84 (s, 3H), 3.82 (t, *J* = 6.8 Hz, 2H), 1.63 (h, *J* = 7.3 Hz, 2H), 0.86 (t, *J* = 7.4 Hz, 3H).

^{13}C NMR (151 MHz, DMSO-d_6) δ 166.5, 157.0, 143.4, 139.3, 129.7, 129.1, 129.1, 128.9, 123.4, 120.6, 76.3, 52.6, 51.2, 21.2, 10.7.m.p.: °C; HPLC: R_t=17.37 min, purity ≥ 99 %, ESI-MS: .

M.p.: 55.8°C; **HPLC**: R_t=15.53 min, purity = 95.2 %, **MS** (+APCI): 343 $[M+H]^+$

2.6 Synthesis of methyl 4-((3-(4-(dimethylamino)phenyl)-1-propoxyureido)methyl)benzoate (**3d**)

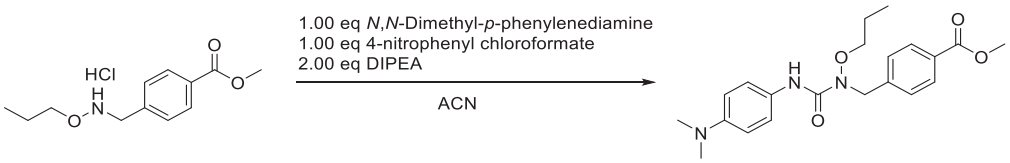

1.00 eq (0.963 mmol, 250 mg) of **2c** was combined with, 1.00 eq of (0.963 mmol, 131 mg) *N*,*N*-Dimethyl-*p*-phenylenediamine, 1.00 eq (0.963, 200 mg) of 4-nitrophenyl chloroformate and 2.00 eq (1.93 mmol, 250 mg, 0.337 mL) of DIPEA in 20 mL of I. After the reaction was refluxed for 16 h, the solvent was removed and the precipitate resuspended in EtOAc. The resulting solution was washed with dH_2O (3x) and brine (1x) and dried over Na_2SO_4. **3d** was obtained as yellow solid after recrystallisation from *n*-hexane/EtOAc with a yield of 75 % (0.718 mmol, 277 mg).

^{1}H NMR (600 MHz, DMSO-d_6) δ 8.63 (s, 1H), 8.07 – 7.89 (m, 2H), 7.58 – 7.42 (m, 2H), 7.42 – 7.30 (m, 2H), 6.82 – 6.47 (m, 2H), 4.74 (s, 2H), 3.85 (s, 3H), 3.79 (t, *J* = 6.8 Hz, 2H), 2.84 (s, 6H), 1.62 (p, *J* = 7.2 Hz, 2H), 0.85 (t, *J* = 7.4 Hz, 3H).

^{13}C NMR (151 MHz, DMSO-d_6) δ 166.5, 157.5, 147.6, 143.6, 129.6, 129.2, 129.0, 128.8, 122.6, 113.0, 76.3, 52.5, 51.6, 41.0, 21.2, 10.7.

M.p.: 86.7 °C, **HPLC**: R_t=10.08 min, purity ≥ 99 %, **MS** (+APCI): 386 $[M+H]^+$

2.7 General procedure for the synthesis of *N* alkoxy substituted urea based hydroxamic acids (**4**)

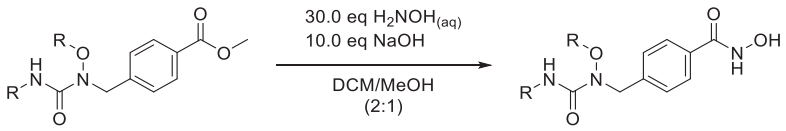

1.00 eq of **3** was dissolved in 30 mL of DCM/MeOH (2:1) and cooled on ice. Afterwards, 30.0 eq of $H_2NOH_{(aq)}$ and 10.0 eq of freshly grinded NaOH was added to the reaction solution and stirred for 16 h to ambient temperature. The reaction was neutralised with a 1 M HCl solution and the product extracted with EtOAc. After the combined organic layers were dried over Na_2SO_4, the product was purified by flash column chromatography (DCM/30 % MeOH in DCM).

2.7.1 Synthesis of *N*-hydroxy-4-((3-phenyl-1-propoxyureido)methyl)benzamide (**4a**)

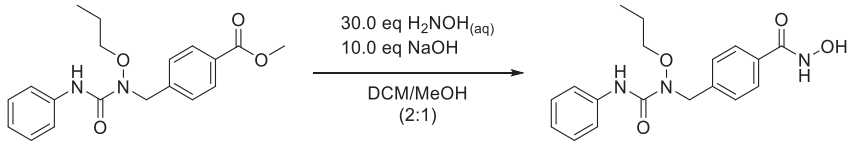

4a was synthesised according to general procedure 2.7 on a 0.538 mmol scale and obtained as a white solid with a yield of 67 % (0.390 mmol, 145 mg).

^{1}H NMR (300 MHz, DMSO-d_6) δ 11.16 (s, 1H), 9.00 (s, 1H), 8.86 (s, 1H), 7.77 – 7.66 (m, 2H), 7.61 – 7.52 (m, 2H), 7.42 – 7.34 (m, 2H), 7.32 – 7.23 (m, 2H), 7.02 (ddt, *J* = 7.7, 6.9, 1.2 Hz, 1H), 4.73 (s, 2H), 3.82 (t, *J* = 6.8 Hz, 2H), 1.64 (h, *J* = 7.2 Hz, 2H), 0.87 (t, *J* = 7.4 Hz, 3H).

^{13}C NMR (151 MHz, DMSO-d_6) δ 164.5, 157.0, 140.9, 139.3, 132.3, 128.9, 128.8, 127.3, 123.3, 120.5, 76.2, 51.1, 21.2, 10.7.

M.p.: 151.4 °C; **HPLC**: R_t=14.48 min, purity ≥ 99 %. **HRMS** (+ESI): calc. for $C_{18}H_{22}N_3O_4$ 344.1605 $[M+H]^+$, found 344.1605. **EA** calc. for $C_{18}H_{22}N_3O_4$ C 62.96, H 6.16, N 12.24, found C 63.18, H 6.13, N 12.19.

2.7.2 Synthesis of *N*-hydroxy-4-((3-(3,5-dimethylphenyl)-1-propoxyureido)methyl)benzamide (**4b**)

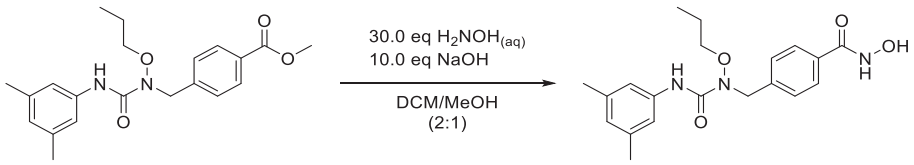

4b was synthesised according to general procedure 2.7 on a 0.776 mmol scale and obtained as a white solid with a yield of 76 % (0.587 mmol, 218 mg).

^{1}H NMR (300 MHz, DMSO-d_6) δ 11.16 (s, 1H), 9.01 (s, 1H), 8.67 (s, 1H), 7.77 – 7.62 (m, 2H), 7.44 – 7.29 (m, 2H), 7.20 (dt, *J* = 1.5, 0.7 Hz, 2H), 6.66 (td, *J* = 1.6, 0.9 Hz, 1H), 4.71 (s, 2H), 3.80 (t, *J* = 6.8 Hz, 2H), 2.29 – 2.15 (m, 6H), 1.63 (h, *J* = 7.2 Hz, 2H), 0.86 (t, *J* = 7.4 Hz, 3H).

^{13}C NMR (151 MHz, DMSO-d_6) δ 164.1, 156.5, 140.5, 138.6, 137.4, 131.8, 128.4, 126.9, 124.4, 117.8, 75.8, 50.7, 21.1, 20.7, 10.2.

M.p.: 164.5°C; **HPLC**: R_t=12.37 min, purity ≥ 99 %, **MS** (+APCI): 372 $[M+H]^+$.

2.7.3 Synthesis of *N*-hydroxy-4-((3-(4-(dimethylamino)phenyl)-1-propoxyureido)methyl)benzamide (**4c**)

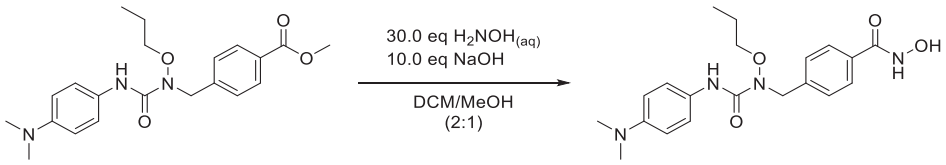

4c was synthesised according to general procedure 2.7 on a 0.623 mmol scale and obtained as a white solid with a yield of 34 % (0.215 mmol, 83 mg).

^{1}H NMR (300 MHz, DMSO-d_6) δ 11.17 (s, 1H), 9.00 (s, 1H), 8.59 (s, 1H), 7.70 (d, *J* = 7.9 Hz, 2H), 7.38 (d, *J* = 8.0 Hz, 2H), 7.32 (d, *J* = 8.7 Hz, 2H), 6.67 (d, *J* = 8.7 Hz, 2H), 4.69 (s, 2H), 3.78 (t, *J* = 6.7 Hz, 2H), 2.83 (s, 6H), 1.62 (q, *J* = 7.1 Hz, 2H), 0.86 (t, *J* = 7.4 Hz, 3H).

^{13}C NMR (151 MHz, DMSO-d_6) δ 164.1, 157.1, 147.1, 140.7, 131.8, 128.4 (d, *J* = 8.7 Hz), 126.8, 122.0, 112.6, 75.7, 51.1, 40.6, 20.8, 10.3.

M.p.: 71.4°C; **HPLC**: R_t=12.68 min, purity ≥ 99 %, **MS** (+APCI): 387 $[M+H]^+$.

2.7.4 Synthesis of *N*-hydroxy-4-((3-(3,5-dimethylphenyl)-1- benzyloxyureido)methyl)benzamide (**4d**)

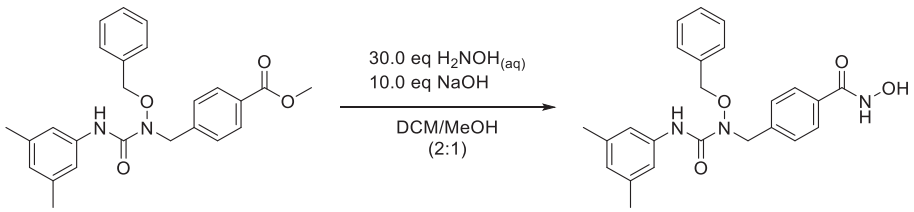

4d was synthesised according to general procedure 2.7 on a 0.776 mmol scale and obtained as a white solid with a yield of 76 % (0.587 mmol, 218 mg).

^{1}H NMR (300 MHz, DMSO-d_6) δ 11.18 (s, 1H), 9.03 (s, 1H), 8.67 (s, 1H), 7.81 – 7.65 (m, 2H), 7.47 (dq, *J* = 4.4, 2.4 Hz, 2H), 7.38 (td, *J* = 8.4, 4.0 Hz, 5H), 7.14 (d, *J* = 1.5 Hz, 2H), 6.65 (s, 1H), 4.91 (s, 2H), 4.68 (s, 2H), 2.21 (s, 6H).

^{13}C NMR (75 MHz, DMSO-d_6) δ 164.1, 156.5, 140.4, 138.5, 137.4, 135.6, 131.9, 129.7, 128.5, 128.4, 128.3, 126.9, 124.5, 117.7, 76.0, 50.8, 21.1.

M.p.: 254.1°C; **HPLC**: R_t=12.68 min, purity = 95.5 %, **MS** (+APCI): 420 $[M+H]^+$.

2.8 Synthesis of methyl 4-(((benzyloxy)(*tert*-butoxycarbonyl)amino)methyl)benzoate (**5**)

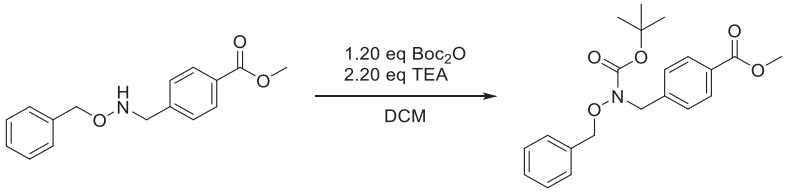

1.00 eq (15.0 mmol, 4.07 g) of **2a** was combined with 1.20 eq (18 mmol, 3.93 g) of Boc_2O and 3.00 eq (45.0 mmol, 4.55 g, 6.27 mL) of TEA in 15 mL of DCM and stirred for 16 h at ambient temperature. The solvent was removed under reduced pressure, the residue resuspended in EtOAc and the resulting solution washed with dH_2O (x3), brine (x1). The organic layer was dried over Na_2CO_3 and the product purified by flash column chromatography (*n*-hexane/EtOAc). 3.80 g (10.2 mmol, 68 %) of **5** was obtained as a colourless oil.

^{1}H NMR (600 MHz, DMSO-d_6) δ 11.21 (s, 1H), 9.05 (s, 1H), 7.75 – 7.70 (m, 2H), 7.40 – 7.32 (m, 7H), 4.78 (s, 2H), 4.64 (s, 2H), 1.42 (s, 9H).

^{13}C NMR (126 MHz, DMSO-d_6) δ 166.4, 155.5, 143.1, 129.6, 129.0, 128.4, 81.3, 62.0, 52.4, 52.0, 28.2.

HPLC: R_t=17.50 min, purity ≥ 99 %, **MS** (+APCI): 316 $[M-^tBu+2H]^+$.

2.9 Synthesis of methyl 4-(((*tert*-butoxycarbonyl)(hydroxy)amino)methyl)benzoate (**7**)

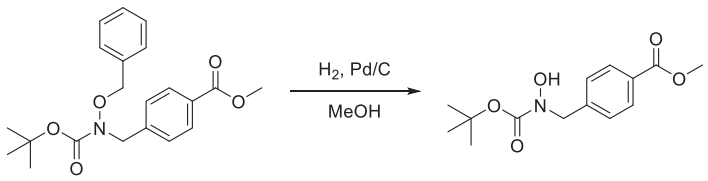

1.00 eq (10 mmol, 3.71 g) of **5** was combined with 0.05 eq of 10 % Pd/C (0.500 mmol, 0.532 g) in 40 mL of MeOH (4 mL/mmol). The benzyl deprotection occurred within 5 h at ambient temperature under an atmosphere of hydrogen. Subsequently, the reaction was filtered over celite. After the solvent was removed under reduced pressure, the residue was dissolved in EtOAc and filtered over a silica plug and the silica plug thoroughly washed with EtOAc. The solvent of the filtrate was removed under reduced pressure and the residue recrystallised in *n*-hexane/EtOAc. 2.20 g of **7** (7.81 mmol, 78 %) was obtained as colourless crystals.

^{1}H NMR (300 MHz, DMSO-d_6) δ 9.48 (s, 1H), 8.00 – 7.89 (m, 2H), 7.45 – 7.36 (m, 2H), 4.62 (s, 2H), 3.85 (s, 3H), 1.41 (s, 9H).

^{13}C NMR (75 MHz, DMSO-d_6) δ 166.0, 155.9, 143.2, 129.1, 128.4, 127.8, 80.0, 54.1, 51.9, 27.9.

M.p.: 98.1°C; **HPLC**: R_t=11.15 min, purity ≥ 99 %, **MS** (+APCI): 267 $[M-^{t}Bu+I+2H]^{+}$.

2.10 General procedure for the *O*-alkylation of **7** (**8**)

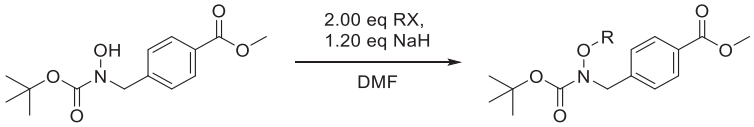

1.00 eq of **8** (1 mmol, 281 mg) was dissolved in 10 mL of dry DMF and cooled to -20°C. 1.2 eq of NaH (1.2 mmol, 48 mg, 60% oil dispersion) was added and stirred for 30 minutes. Afterwards, the reaction was stirred for another 30 minutes at ambient temperature after which 2.0 eq of the respective alkylation reagent RX (2 mmol) was added and stirred for 16 h at ambient temperature. The solvent was removed under reduced pressure, the residue resuspended in EtOAc, the organic layer washed with dH_2O (x3) and brine (x1) and dried over Na_2SO_4. After the solvent was removed *in vacuo*, the product was purified by flash column chromatography (*n*-hexane/EtOAc).

2.10.1 Synthesis of methyl 4-(((*tert*-butoxycarbonyl)(ethoxy)amino)methyl)benzoate (**8a**)

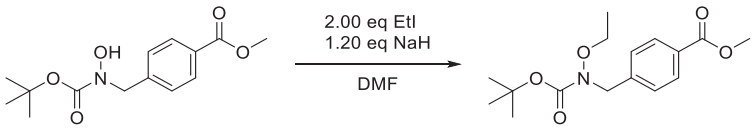

The synthesis of **8a** was performed according to general procedure 2.10 with 2.0 eq (2.0 mmol, 0.318 g, 0.164 mL) of iodoethane. 280 mg (0.904 mmol, 90 %) of **8a** was obtained as a clear oil.

^{1}H NMR (300 MHz, DMSO-d_6) δ 7.99 – 7.91 (m, 2H), 7.45 – 7.39 (m, 2H), 4.65 (s, 2H), 3.85 (s, 3H), 3.80 (t, *J* = 7.1 Hz, 2H), 1.40 (s, 9H), 1.08 (t, *J* = 7.0 Hz, 3H).

^{13}C NMR (75 MHz, DMSO-d_6) δ 165.9, 155.3, 142.7, 129.0, 128.6, 128.0, 80.6, 69.4, 52.3, 51.9, 27.7, 13.3.

HPLC: R_t=14.80 min, purity =94.3 %, **MS** (+APCI): 254 [M-^{t}Bu+2H]$^+$.

2.10.2 Synthesis of methyl 4-((butoxy(*tert*-butoxycarbonyl)amino)methyl)benzoate (**8b**).

The synthesis of **8b** was performed according to general procedure 2.10 with 2.0 eq (2.0 mmol, 0.368 g, 0.228 mL) of 1-iodobutane. 278 mg (0.824 mmol, 82 %) of **8b** was obtained as a clear oil.

^{1}H NMR (300 MHz, DMSO-d_6) δ 8.00 – 7.89 (m, 2H), 7.42 (d, J = 8.1 Hz, 2H), 4.65 (s, 2H), 3.85 (s, 3H), 3.76 (t, J = 6.3 Hz, 2H), 1.41 (s, 11H), 1.37 – 1.16 (m, 2H), 0.83 (t, J = 7.3 Hz, 3H).

^{13}C NMR (75 MHz, DMSO- d_6) δ 165.9, 155.3, 142.7, 129.0, 128.6, 128.0, 80.6, 73.5, 52.0, 51.9, 29.5, 27.7, 18.5, 13.4.

HPLC: R_t=17.13 min, purity ≥ 99 %, **MS** (+APCI): 283 [M-^{t}Bu+2H]$^+$.

2.10.3 Synthesis of methyl 4-(((*tert*-butoxycarbonyl)(isopropoxy)amino)methyl)benzoate (**8c**)

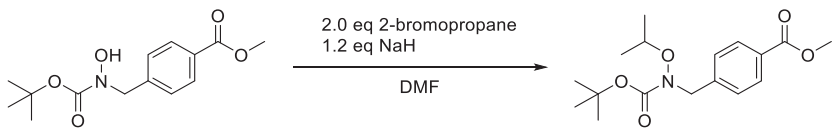

The synthesis of **8c** was performed according to general procedure 2.10 with 2.0 eq (2.0 mmol, 0.135 g, 0.103 mL) of 2-bromopropane. 136 mg (0.421 mmol, 42 %) of **8c** was obtained as a clear oil.

^{1}H NMR (300 MHz, DMSO-d_6) δ 7.96 – 7.89 (m, 2H), 7.46 – 7.34 (m, 2H), 4.63 (s, 2H), 4.11 – 3.92 (m, 1H), 3.83 (s, 3H), 1.37 (s, 9H), 1.09 (d, *J* = 6.2 Hz, 6H).

^{13}C NMR (75 MHz, DMSO-d_6) δ 166.0, 156.2, 142.9, 129.1, 128.6, 128.1, 80.7, 75.8, 53.5, 52.0, 27.8, 20.7.

HPLC: R_t=15.33 min, purity ≥ 99 %, **MS** (+APCI): 267 [M-^{t}Bu+2H]$^+$.

2.10.4 Synthesis of methyl 4-(((*tert*-butoxycarbonyl)(isobutoxy)amino)methyl)benzoate (**8d**)

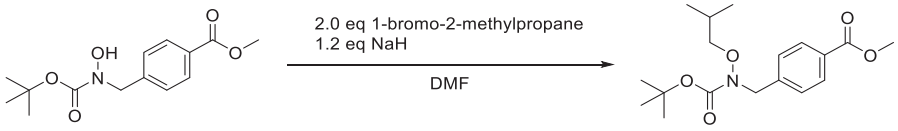

The synthesis of **8d** was performed according to general procedure 2.10 with 2.0 eq (2.0 mmol, 0. 274 g, 0. 217 mL) of 1-bromo-2-methylpropane. 230 mg (0. 682 mmol, 68 %) of **8d** was obtained as a clear oil.

^{1}H NMR (300 MHz, DMSO-d_6) δ 7.99 – 7.88 (m, 2H), 7.50 – 7.36 (m, 2H), 4.65 (s, 2H), 3.85 (s, 3H), 3.55 (d, *J* = 6.4 Hz, 2H), 1.73 (dh, *J* = 13.4, 6.7 Hz, 1H), 1.41 (s, 9H), 0.83 (d, *J* = 6.7 Hz, 6H).

^{13}C NMR (75 MHz, DMSO-d_6) δ 167.6 – 164.4 (m), 155.3, 142.7, 129.1, 128.6 (d, *J* = 1.7 Hz), 128.1, 80.7, 80.2, 52.0, 51.9 (d, *J* = 2.6 Hz), 27.8, 27.7 (d, *J* = 5.8 Hz), 26.7, 19.0.

HPLC: R_t=17.17 min, purity ≥ 99 %, **MS** (+APCI): 282 [M-^{t}Bu+2H]$^+$.

2.10.5 Synthesis of methyl 4-(((*tert*-butoxycarbonyl)(isopentyloxy)amino)methyl)benzoate (**8e**)

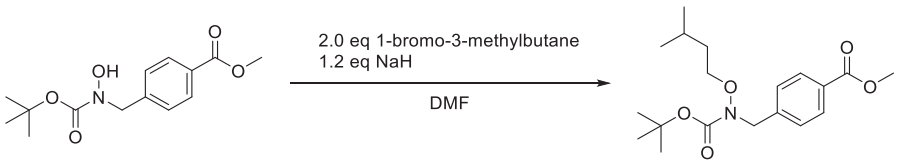

The synthesis of **8e** was performed according to general procedure 2.10 with 2.0 eq (2.0 mmol, 0.302 g, 0.252 mL) of 1-bromo-3-methylbutane. 311 mg (0.885 mmol, 89 %) of **8e** was obtained as a clear oil.

^{1}H NMR (300 MHz, DMSO-d_6) δ 7.98 – 7.90 (m, 2H), 7.46 – 7.37 (m, 2H), 4.65 (s, 2H), 3.84 (s, 3H), 3.78 (t, *J* = 6.5 Hz, 2H), 1.59 (dq, *J* = 13.3, 6.7 Hz, 1H), 1.40 (s, 9H), 1.34 (q, *J* = 6.6 Hz, 2H), 0.81 (d, *J* = 6.6 Hz, 6H).

^{13}C NMR (75 MHz, DMSO-d_6) δ 165.9, 155.3, 142.7, 129.1, 128.6, 128.0, 80.7, 72.3, 52.1, 51.9, 36.4, 27.8, 24.3, 22.2.

HPLC: R_t=17.93 min, purity ≥ 99 %, **MS** (+APCI): 296 [M-^{t}Bu+2H]$^+$.

2.10.6 Synthesis of methyl 4-(((*tert*-butoxycarbonyl)(cyclohexylmethoxy)amino)methyl)benzoate (**8f**)

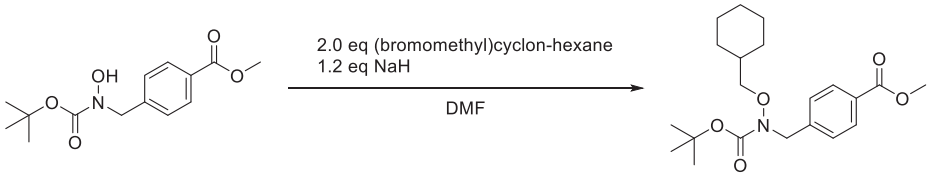

The synthesis of **8f** was performed according to general procedure 2.10 with 2.0 eq (2.0 mmol, 0.354 g, 0.279 mL) of (bromomethyl)cyclon-hexane. 296 mg (0. 784 mmol, 78 %) of **8f** was obtained as a clear oil.

^{1}H NMR (300 MHz, DMSO-d_6) δ 7.98 – 7.89 (m, 2H), 7.49 – 7.34 (m, 2H), 4.63 (s, 2H), 3.84 (s, 3H), 3.57 (d, *J* = 6.2 Hz, 2H), 1.73 – 1.50 (m, 5H), 1.40 (s, 10H), 1.27 – 0.99 (m, 3H), 0.99 – 0.71 (m, 2H).

^{13}C NMR (75 MHz, DMSO-d_6) δ 166.0, 155.4, 142.7, 129.1, 128.6, 128.1, 80.7, 79.2, 51.9 (d, *J* = 3.4 Hz), 36.2, 29.3, 27.8, 25.9, 25.2.

HPLC: R_t=19.32 min, purity ≥ 99 %, **MS** (+APCI): 322 [M-^{t}Bu+2H]$^+$.

2.10.7 Synthesis of methyl 4-(((*tert*-butoxycarbonyl)(pent-4-yn-1-yloxy)amino)methyl)benzoate (**8g**)

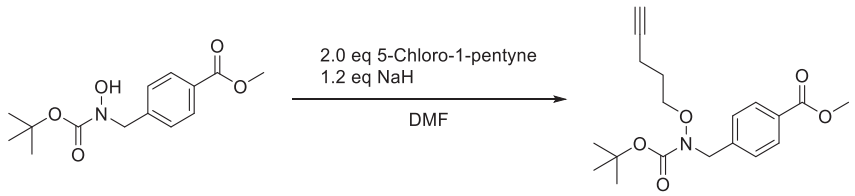

The synthesis of **8f** was performed according to general procedure 2.10 with 2.0 eq (2.0 mmol, 0.214 g, 0.220 mL) of 5-Chloro-1-pentyne. 205 mg (0. 590 mmol, 59 %) of **8f** was obtained as a clear oil.

^{1}H NMR (300 MHz, Chloroform-*d*) δ 8.04 – 7.96 (m, 2H), 7.44 – 7.36 (m, 2H), 4.65 (s, 2H), 3.91 (s, 3H), 3.86 (t, *J* = 6.1 Hz, 2H), 2.23 (td, *J* = 7.0, 2.7 Hz, 2H), 1.92 (t, *J* = 2.7 Hz, 1H), 1.79 – 1.67 (m, 2H), 1.48 (s, 9H).

^{13}C NMR (75 MHz, Chloroform-*d*) δ 167.0, 156.5, 142.4, 129.9, 129.5, 128.4, 83.6, 82.0, 73.3, 68.9, 53.4, 52.2, 28.4, 27.2, 15.3.

HPLC: R_t=16.70 min, purity ≥ 99 %, **MS** (+APCI): 292 $[M\text{-}^{t}Bu+2H]^{+}$.

2.11 General procedure for the synthesis of *N*-oxy-carbamate based hydroxamic acids **6** and **9**

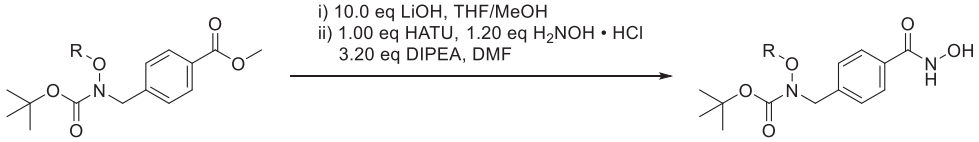

1.00 eq of the respective ester was dissolved in a mixture of THF/MeOH (1:1, 10 mL/mmol), 10 eq of 5 M $LiOH_{(aq)}$ was added and stirred for 3 h at ambiet temperature. The reaction was acidified with a 1 M HCl solution to pH=4 and the product extracted with EtOAc, after which the combined layers were dried over Na_2SO_4 and concentrated. Subsequently, the obtained carboxylic acid was dissolved in dry DMF (10 mL/mmol), 1.0 eq HATU and 3.2 eq DIPEA werde added and the solution stirred at RT. After 10 minutes, 1.2 eq H_2NOH • HCl was added to the solution. The reaction was stirred for 16 h at RT, the solvent removed under reduced pressure and the product purified by reverse flash column chromatography (H_2O/I).

2.11.1 Synthesis of *tert*-butyl (benzyloxy)(4-(hydroxycarbamoyl)benzyl)carbamate (**6**)

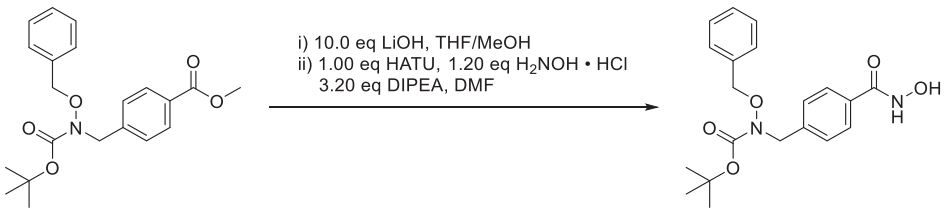

6 was synthesised according to general procedure 2.11 on a 0.538 mmol scale and obtained as a white solid with a yield of 67 % (0.390 mmol, 145 mg).

^{1}H NMR (600 MHz, DMSO-d_6) δ = 11.20 (s, 1H), 9.04 (s, 1H), 7.74 – 7.69 (m, 2H), 7.39 – 7.31 (m, 7H), 4.77 (s, 2H), 4.63 (s, 2H), 1.41 (s, 9H).

^{13}C NMR (151 MHz, DMSO- d_6) δ 164.0, 155.5, 140.3, 135.4, 131.9, 129.4, 128.3, 128.0, 127.9, 127.0, 80.9, 75.9, 51.9, 27.9.

M.p.: 130.6°C; **HPLC**: R_t=11.89 min, purity ≥ 99 %. **MS** (+APCI): 317 [M-^{t}Bu+2H]$^+$.

2.11.2 Synthesis of *tert*-butyl (cyclohexylmethoxy)(4-(hydroxycarbamoyl)benzyl)carbamate (**9a**)

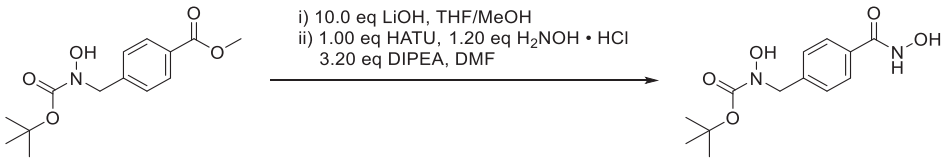

9a was synthesised according to general procedure 2.11 on a 1.00 mmol scale and obtained as a white solid with a yield of 17 % (0.174 mmol, 49 mg).

^{1}H NMR (300 MHz, DMSO-d_6) δ 11.18 (s, 1H), 9.42 (s, 1H), 9.00 (d, J = 1.9 Hz, 1H), 7.79 – 7.64 (m, 2H), 7.37 – 7.29 (m, 2H), 4.57 (s, 2H), 1.41 (s, 9H).

^{13}C NMR (75 MHz, DMSO-d_6) δ 164.1, 156.0, 140.9, 131.6, 127.6, 126.9, 80.0, 54.0, 28.0.

M.p.: 158.1°C; **HPLC**: R_t=14.12 min, purity =95.4 %, **MS** (+APCI): 227 [M-^{t}Bu+2H]$^+$.

2.11.3 Synthesis of *tert*-butyl (benzyloxy)(4-(hydroxycarbamoyl)benzyl)carbamate (**9b**)

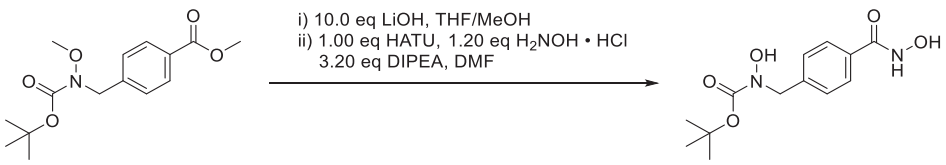

9b was synthesised according to general procedure 2.11 on a 0.508 mmol scale and obtained as a white solid with a yield of 65 % (0.330 mmol, 97.8 mg).

^{1}H NMR (600 MHz, DMSO-d_6) δ 11.19 (s, 1H), 9.01 (s, 1H), 7.72 (d, *J* = 7.9 Hz, 2H), 7.33 (d, *J* = 7.9 Hz, 2H), 4.62 (s, 2H), 3.56 (s, 3H), 1.41 (s, 9H).

^{13}C NMR (151 MHz, DMSO-d_6) δ 164.0, 155.2, 140.3, 131.8, 127.8, 127.0, 80.9, 61.6, 51.5, 40.1, 27.9.

M.p.: 140.4 °C; **HPLC**: R_t=8.68 min, purity ≥ 99 %, **MS** (+APCI): 241 [M-^{t}Bu+2H]$^+$, **EA** calc. for $C_{14}H_{20}N_2O_5$ C 56.75, H 6.80, N 9.45, found C 56.86, H 6.78, N 9.35.

2.11.4 Synthesis of *tert*-butyl ethoxy(4-(hydroxycarbamoyl)benzyl)carbamate (**9c**)

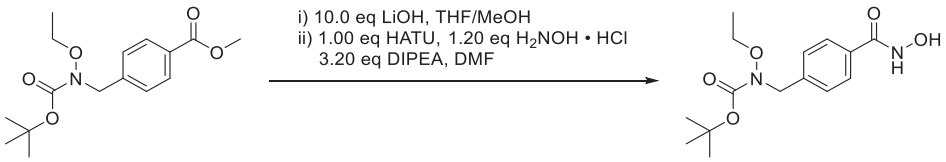

9c was synthesised according to general procedure 2.11 on a 0.965 mmol scale and obtained as a white solid with a yield of 54 % (0.517 mmol, 160 mg).

^{1}H NMR (300 MHz, DMSO-d_6) δ 11.19 (s, 1H), 9.02 (s, 1H), 7.82 – 7.65 (m, 2H), 7.40 – 7.26 (m, 2H), 4.61 (s, 2H), 3.80 (q, *J* = 7.0 Hz, 2H), 1.40 (s, 9H), 1.07 (t, *J* = 7.0 Hz, 3H).

^{13}C NMR (75 MHz, DMSO-d_6) δ 164.0, 155.4, 140.3, 131.8, 127.7, 126.8, 80.6, 69.4, 52.2, 27.8, 13.3.

M.p.: 136.1 °C, **HPLC**: R_t=9.51 min, purity ≥ 99 %, **MS** (+APCI): 255 [M-^{t}Bu+2H]$^+$

2.11.5 Synthesis of *tert*-butyl (4-(hydroxycarbamoyl)benzyl)(propoxy)carbamate (**9d**)

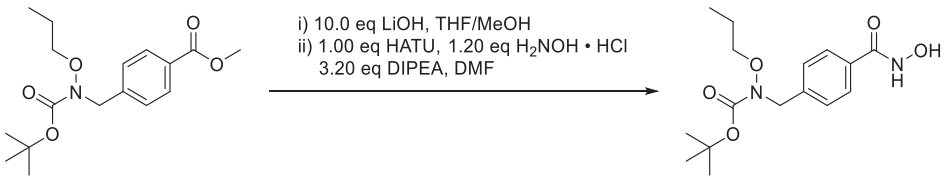

9d was synthesised according to general procedure 2.11 on a 1.00 mmol scale and obtained as a white solid with a yield of 60 % (0.604 mmol, 196 mg).

^{1}H NMR (300 MHz, DMSO-d_6) δ 11.25 – 11.13 (m, 1H), 9.10 – 8.96 (m, 1H), 7.80 – 7.64 (m, 2H), 7.34 (d, *J* = 8.2 Hz, 2H), 4.61 (s, 2H), 3.72 (t, *J* = 6.4 Hz, 2H), 1.54 – 1.43 (m, 2H), 1.41 (s, 9H), 0.85 (t, *J* = 7.4 Hz, 3H).

^{13}C NMR (75 MHz, DMSO-d_6) δ 164.0, 155.4, 140.3, 131.8, 127.8, 126.8, 80.6, 75.4, 51.9, 27.8, 20.9, 10.4.

M.p.: 107.8°C; **HPLC**: R_t=10.69 min, purity ≥ 99 %, **MS** (+APCI) 269 [M-^{t}Bu+2H]$^+$

2.11.6 Synthesis of *tert*-butyl (4-(hydroxycarbamoyl)benzyl)(propoxy)carbamate (**9e**)

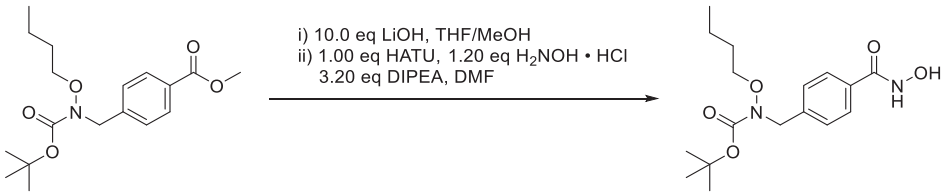

9e was synthesised according to general procedure 2.11 on a 0.69 mmol scale and obtained as a white solid with a yield of 57 % (0.39 mmol, 132 mg).

^{1}H NMR (300 MHz, DMSO-d_6) δ 11.22 (s, 1H), 9.05 (s, 1H), 8.09 (d, *J* = 7.9 Hz, 0H), 7.74 (d, *J* = 7.9 Hz, 2H), 7.36 (d, *J* = 7.9 Hz, 2H), 4.63 (s, 2H), 3.77 (t, *J* = 6.3 Hz, 2H), 1.57 – 1.19 (m, 12H), 0.85 (t, *J* = 7.3 Hz, 3H).

^{13}C NMR (75 MHz, DMSO-d_6) δ 164.1, 155.5, 140.5, 131.8, 127.9, 127.0, 80.8, 73.6, 51.9, 29.7, 27.9, 18.8, 13.7.

M.p.: 101.0 °C, **HPLC**: R_t=11.80 min, purity = 95.4 %, **MS** (+APCI) 283 [M-^{t}Bu+2H]$^+$

2.11.7 Synthesis of *tert*-butyl (4-(hydroxycarbamoyl)benzyl)(isopropoxy)carbamate (**9f**)

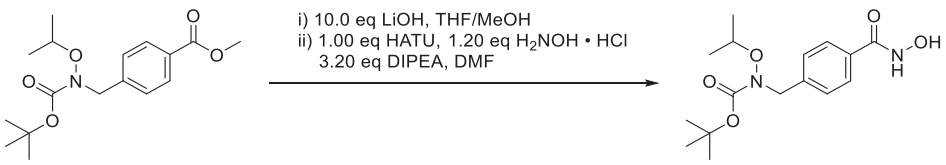

9f was synthesised according to general procedure 2.11 on a 0.588 mmol scale and obtained as a white solid with a yield of 63 % (0.37 mmol, 120 mg).

^{1}H NMR (300 MHz, DMSO-d_6) δ 11.18 (s, 1H), 9.02 (s, 1H), 7.74 – 7.67 (m, 2H), 7.35 – 7.28 (m, 2H), 4.59 (s, 2H), 4.13 – 3.94 (m, 1H), 1.39 (s, 9H), 1.10 (d, *J* = 6.2 Hz, 6H).^

^{13}C NMR (75 MHz, DMSO-d_6) δ 164.1, 156.3, 140.5, 131.8, 127.9, 126.9, 80.7, 75.8, 53.4, 27.9, 20.8.

M.p.: 109.3 °C, **HPLC**: R_t=10.44 min, purity ≥ 99 %, **MS** (+APCI) 269 [M-^{t}Bu+2H]$^+$.

2.11.8 Synthesis of *tert*-butyl (4-(hydroxycarbamoyl)benzyl)(isobutoxy)carbamate (**9g**)

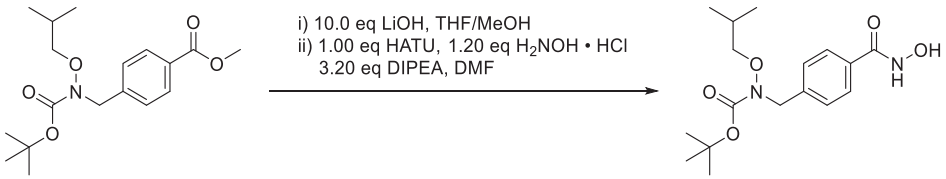

9g was synthesised according to general procedure 2.11 on a 0.643 mmol scale and obtained as a white solid with a yield of 61 % (0.39 mmol, 132 mg).

^{1}H NMR (300 MHz, DMSO-d_6) δ 11.19 (s, 1H), 9.02 (s, 1H), 7.78 – 7.62 (m, 2H), 7.34 (d, J = 8.1 Hz, 2H), 4.60 (s, 2H), 3.54 (d, J = 6.4 Hz, 2H), 1.73 (hept, J = 6.6 Hz, 1H), 1.41 (s, 9H), 0.84 (d, J = 6.7 Hz, 6H).

^{13}C NMR (75 MHz, DMSO- d_6) δ 164.1, 155.5, 140.4, 131.9, 128.0, 127.0, 80.8, 80.2, 51.8, 27.9, 26.9, 19.2.

M.p.: 125.7 °C, **HPLC**: R_t=11.86 min, purity = 97.5 %, **MS** (+APCI) 283 [M-^{t}Bu+2H]$^+$.

2.11.9 Synthesis of *tert*-butyl (4-(hydroxycarbamoyl)benzyl)(isopentyloxy)carbamate (**9h**)

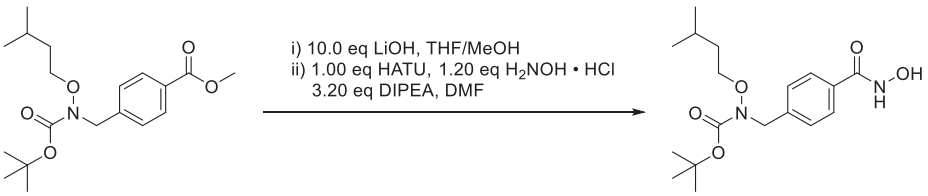

9h was synthesised according to general procedure 2.11 on a 0.590 mmol scale and obtained as a white solid with a yield of 61 % (0.360 mmol, 127 mg).

^{1}H NMR (300 MHz, DMSO-d_6) δ 11.19 (s, 1H), 9.02 (s, 1H), 7.72 (d, *J* = 7.8 Hz, 2H), 7.33 (d, *J* = 7.9 Hz, 2H), 4.60 (s, 2H), 3.77 (t, *J* = 6.5 Hz, 2H), 1.60 (dq, *J* = 13.5, 6.8 Hz, 1H), 1.41 (s, 11H), 0.82 (d, *J* = 6.6 Hz, 6H).

^{13}C NMR (75 MHz, DMSO-d_6) δ 164.0, 155.5, 140.4, 131.8, 127.9, 127.0, 80.7, 72.3, 51.9, 36.5, 27.9, 24.4, 22.4.

M.p.: 105.4 °C, **HPLC**: R_t=12.69 min, purity ≥ 99 %, **MS** (+APCI) 283 [M-^{t}Bu+2H]$^+$.

2.11.10 Synthesis of *tert*-butyl (cyclohexylmethoxy)(4-(hydroxycarbamoyl)benzyl)carbamate (**9i**)

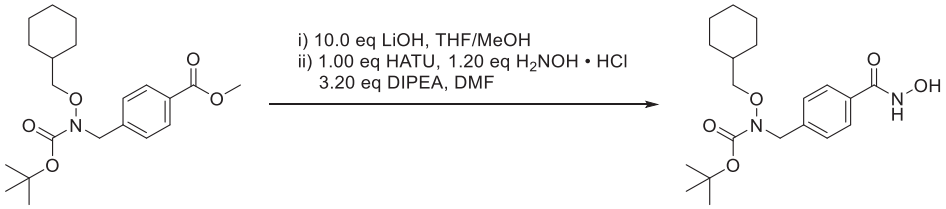

9i was synthesised according to general procedure 2.11 on a 0.614 mmol scale and obtained as a white solid with a yield of 54 % (0.333 mmol, 126 mg).

^{1}H NMR (300 MHz, DMSO-d_6) δ 11.18 (s, 1H), 9.02 (s, 1H), 7.77 – 7.64 (m, 2H), 7.32 (d, *J* = 8.2 Hz, 2H), 4.59 (s, 2H), 3.56 (d, *J* = 6.3 Hz, 2H), 1.72 – 1.50 (m, 5H), 1.40 (s, 10H), 1.14 (dq, *J* = 18.9, 13.7, 12.7 Hz, 5H), 0.89 (qd, *J* = 14.3, 13.2, 3.4 Hz, 2H).

^{13}C NMR (75 MHz, DMSO-d_6) δ 164.1, 155.5, 140.4, 131.8, 128.0, 127.0, 80.7, 79.2, 51.7, 36.2, 29.4, 27.9, 26.0, 25.3.

M.p.: 110.5 °C, **HPLC**: R_t=14.12 min, purity =95.4 %, **MS** (+APCI) 323 [M-^{t}Bu+2H]$^+$.

2.11.11 Synthesis of *tert*-butyl (cyclohexylmethoxy)(4-(hydroxycarbamoyl)benzyl)carbamate (**9j**)

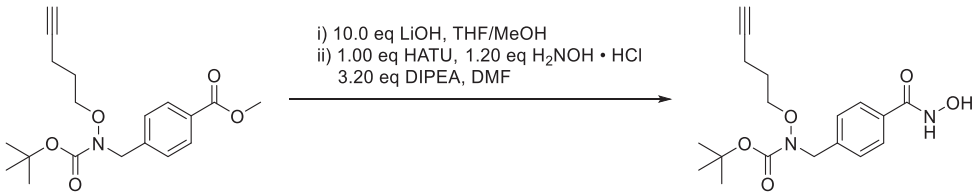

9j was synthesised according to general procedure 2.11 on a 0.837 mmol scale and obtained as a colourless oil with a yield of 24 % (0.201 mmol, 70 mg).

^{1}H NMR (300 MHz, DMSO-d_6) δ 11.20 (s, 1H), 9.03 (s, 1H), 7.80 – 7.65 (m, 2H), 7.42 – 7.22 (m, 2H), 4.61 (s, 2H), 3.83 (t, *J* = 6.1 Hz, 2H), 2.76 (t, *J* = 2.6 Hz, 1H), 2.21 (td, *J* = 7.1, 2.7 Hz, 2H), 1.72 – 1.58 (m, 2H), 1.42 (s, 9H).

^{13}C NMR (75 MHz, DMSO-d_6) δ 164.1, 155.5, 140.3, 131.9, 127.9, 127.0, 83.8, 80.9, 72.5, 71.5, 51.9, 27.9, 26.8, 14.6.

HPLC: R_t=14.12 min, purity =95.4 %, **MS** (+APCI) 293 $[M-^tBu+2H]^+$.

2.12 Synthesis of 4-((2-(2-(2-azidoethoxy)ethoxy)ethyl)amino)-2-(2,6-dioxopiperidin-3-yl)isoindoline-1,3-dione (**10**)

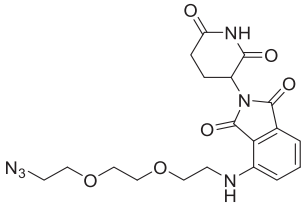

10 was synthesised according to Wu *et.*al.[2]

All spectroscopic data agreed with literature.[2]

2.13 Synthesis of *tert*-butyl (3-(1-(2-(2-(2-((2-(2,6-dioxopiperidin-3-yl)-1,3-dioxoisoindolin-4-yl)amino)ethoxy)ethoxy)ethyl)-1H-1,2,3-triazol-4-yl)propoxy)(4-(hydroxycarbamoyl)benzyl)carbamate (**11**)

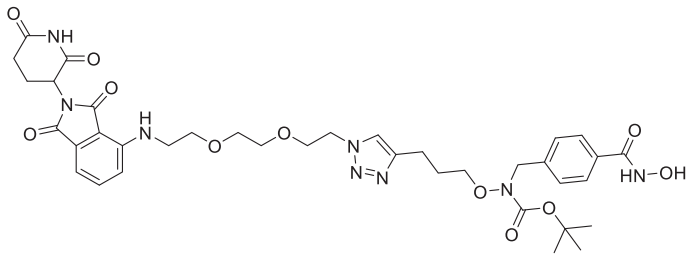

11 was synthesis from 1.00 eq (0.207 mmol, 37 mg) of **10k** and 1.00 eq (0.207 mmol, 89 mg) of **11** according to Wu *et.*al.[2] and obtained as a yellow solid with a yield of 22 % (0.046 mmol, 36 mg).

^{1}H NMR (300 MHz, DMSO-d_6) δ 11.18 (s, 1H), 11.09 (s, 1H), 9.01 (s, 1H), 7.77 (s, 1H), 7.72 (d, *J* = 8.2 Hz, 2H), 7.57 (dd, *J* = 8.6, 7.1 Hz, 1H), 7.34 (d, *J* = 8.2 Hz, 2H), 7.12 (d, *J* = 8.6 Hz, 1H), 7.04 (d, *J* = 7.0 Hz, 1H), 6.59 (t, *J* = 5.6 Hz, 1H), 5.05 (dd, *J* = 12.8, 5.4 Hz, 1H), 4.61 (s, 2H), 4.44 (t, *J* = 5.2 Hz, 2H), 3.79 (td, *J* = 5.8, 5.3, 2.7 Hz, 4H), 3.58 (t, *J* = 5.3 Hz, 2H), 3.53 (s, 4H), 3.49 – 3.36 (m, 2H), 3.01 – 2.78 (m, 1H), 2.68 – 2.51 (m, 3H), 1.99 (s, 2H), 1.77 (s, 1H), 1.39 (s, 9H).

^{13}C NMR (75 MHz, DMSO-d_6) δ 172.75, 170.03, 169.06 – 168.77 (m), 167.23, 155.40, 146.33, 146.01, 140.33, 136.19, 132.04, 131.80, 127.84, 126.91, 122.13, 110.66, 109.21, 99.48, 81.32 – 80.26 (m), 73.26, 69.57, 68.78, 48.52, 41.63, 27.80, 21.63.

HPLC: R_t=11.23 min, purity =96.2 %, **MS** (+APCI) 723 $[M-^tBu+2H]^+$.

3 References

1. Bongini, A., Cardillo, G., Gentilucci, L. & Tomasini, C. Synthesis of Enantiomerically Pure Aziridine-2-imides by Cyclization of Chiral 3′-Benzyloxyamino Imide Enolates. *J. Org. Chem.* **62**, 9148–9153 (1997).

2. Wu, H. *et al.* Development of Multifunctional Histone Deacetylase 6 Degraders with Potent Antimyeloma Activity. *J. Med. Chem.* **62**, 7042–7057 (2019).

6 Chapter IV:

Chromenones: A suitable CAP group to govern HDAC6 selectivity?

Contribution:

- Synthesis of compounds **1a-i**, **2a-i**, **3a-i**, **4**, **5**, **6**, **7a-c**, **8a-c**, **9**, **10**, **11**, **12**, **13**, **14**
- Manuscript and supporting information

Chromenones: A suitable CAP group to govern HDAC6 selectivity?

M. Pflieger, A. Hamacher, N. Horstick-Muche, E. Kharitonova, M. U. Kassack, T. Kurz

Abstract

Currently approved pan-histone deacetylase inhibitors (HDACi) exhibit limited efficacy in solid tumours and cause severe side effects. Novel isozyme selective inhibitors might overcome these limitations and present valuable biologically active compounds for the treatment of non-cancer diseases such as autoimmune diseases, depression, schizophrenia or Alzheimer's disease. In recent years, HDAC6 has been attracting significant attention as potential target in neurology, immunology, and oncology. Here we report HDACi, exhibiting a chromenone scaffold as HDAC6 selectivity directing CAP group and developed **3h** which showed an 1.6-fold higher HDAC6 selectivity index than the HDAC6 selective inhibitor tubastatin A. Due to their low antiproliferative properties ($pIC_{50} \leq 5.16$), the here reported HDAC6 selective inhibitors represent valuable tools for exploring the pharmaceutical potential of HDAC6 in neurology, immunology and the suppression of metastasis.

Introduction

Histone deacetylases (HDAC) are zinc dependant metalloproteases that catalyse the hydrolytic cleavage of acetylated lysine residues.[1] As epigenetic regulators, they participate in variety of biological processes such as cell differentiation[2] and cell cycle progression.[3] Furthermore, they are essential key enzymes in the posttranslational modification of client proteins[4] and control e.g. the activity of chaperones[5] and the degradation of misfolded proteins.[6] According to their yeast homologues, zinc dependant HDACs are categorised into class I (HDAC1, HDAC2, HDAC8), class IIa (HDAC4, HDAC5, HDAC7, HDAC9), class IIb (HDAC6, HDAC10) and class IV (HDAC11).[7] Whilst nuclear class I HDACs participate in the control of the condensation state of histones,[8] cytoplasmic HDACs controls the activity of client proteins by posttranslational modification.[9] Currently, approved HDAC inhibitors (HDACi) are not selective for a specific HDAC isozyme (pan inhibitors). Despite their clinical efficacy and chemosensitising properties towards cisplatin,[10] the application of HDACi suffers from severe side effects such as neutropenia, anaemia or cardiovascular side effects.[11] Therefore, accumulating research has been focused on the design of selective HDACi over the last few years. Nevertheless, the efficacy of isozyme selective HDACi remains to be established, especially for their employment as anti-cancer agent.[12] In addition, their evaluation and significance as immunomodulator[13] or as neurological active compounds[14–16] becomes increasingly apparent. In this respect, HADC6 has been attracting significant

attention as target for the pharmacological intervention of e.g. neurodegenerative diseases, as immunomodulatory target and cancer.

Despite the high sequence homology of HDAC isozymes, the design of selective HDACi is possible due to structural differences in their tertiary structure which has been revealed by crystallographic analyses.[17–20] For example, HDAC6 exhibits a much wider and shallowed entrance tunnel than nuclear HDAC class I isozymes. Based on these findings, the traditional pharmacophore model, [21–23] comprising of a zinc binding group (ZBG), a linker and a cap group, was refined and formulated for each class of HDACs. [24] The selective inhibition of HDAC6 is possible by the employment of a sterically demanding cap groups, a linker and a ZBG. The most commonly applied HDAC6 selective inhibitors in research are nexturastat A and tubastatin A which follow this refined pharmacophore model (Figure 23).[25–27]

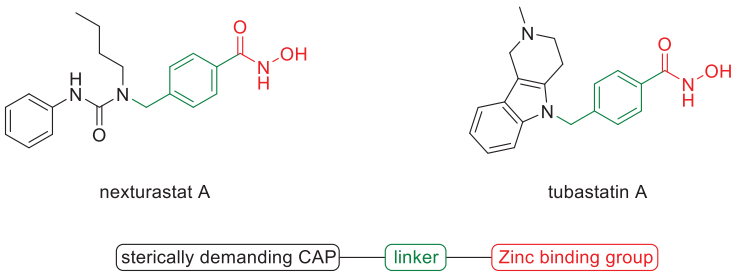

Figure 23. The refined pharmacophore model of HDAC6 selective inhibitors with nexturastat A and tubastatin A as representative.[25,27]

Whilst nexturastat A exerts its selectivity by a branched cap group, tubastatin A exhibits a bulky cap. Other bulky cap groups, such as γ-pyrones, might be employed to obtain HDAC6 selectivity.

The benzoannelated γ-pyrones, or more often referred to as chromones, comprise of a class of secondary metabolites that are abundant in nature, particularly in plants.[28] Their scaffold has been used in the development of active pharmaceutical ingredients for the treatment of e.g. urinary bladder spasms,[29] rheumatoid arthritis,[30] asthma[31] or cancer (Figure 24).[32] Due to their synthetic accessibility, their potential for diversification as drug template and their proven effectiveness in the development of novel medicines as well as their drug-like properties, the chromone core motif is considered a privileged structure in medicinal chemistry.[33–35]

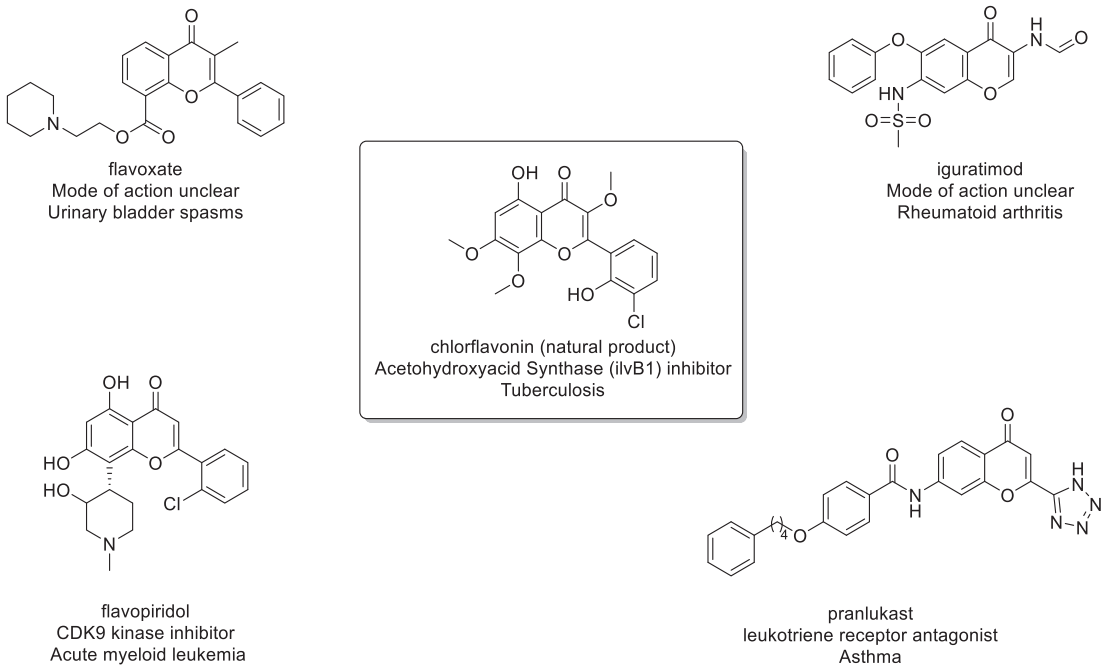

Figure 24. Natural product derived drugs exhibiting a chromone core structure. [29–32,36]

Commonly used reactions for the synthesis of chromones are the *Baker-Venkataraman* flavone synthesis,[37] the *Kostanecki-Robinson* reaction[38,39] or the *Algar-Flynn-Oyamada* (AFO) reaction[40] for the synthesis of flavonols (Scheme 23). In a *Baker-Venkataraman* flovone synthesis, an *o*-acylated phenol ester rearranges into an *o*-hydroxy-1,3-diketone, followed by a cyclisation under acidic conditions. In contrast, the *Kostanecki-Robinson* reaction follows a condensation of *o*-hydroxyaryl ketones with anhydrides. The *Algar-Flynn-Oyamada* reaction pursues an oxidative cyclysation of chalcones into the corresponding flavonol.

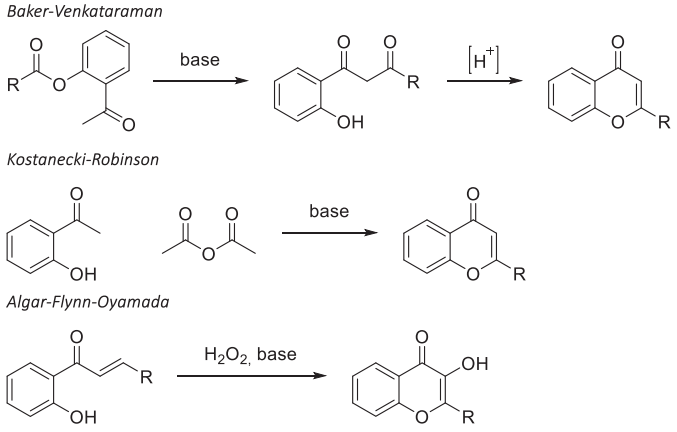

Scheme 23. Commonly used methods for the synthesis of chromones.

The aim of this work was to develop HDAC6 selective inhibitors, that exhibit a sterically demanding chromone based cap group.

Results and Discussion

In our endeavour to design HDAC6 selective inhibitors, we performed a retrosynthetic analysis of chromenone based hydroxamic acids **3** (Scheme 24). Based on our analysis, 3-hydroxy functionalised chromenones **1** were connected to the linker by a nucleophilic substitution. Subsequently, the hydroxamic acid moiety is introduced by the transformation of an ester into the respective hydroxamic acid (**3**).

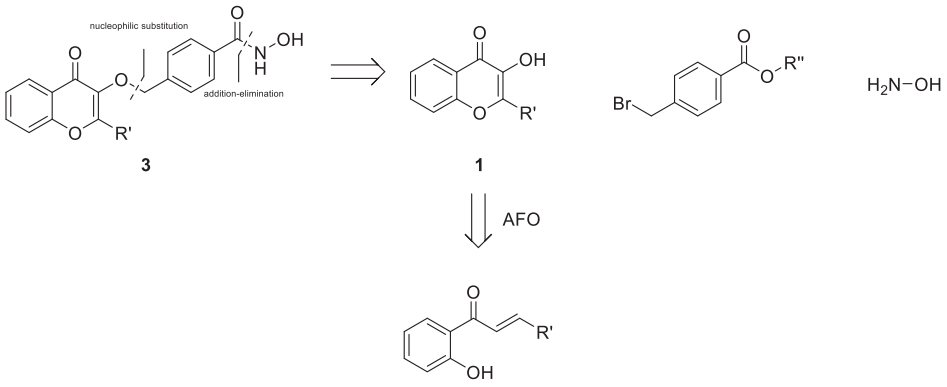

Scheme 24. Retrosynthetic analysis of chromenone based hydroxamic acids.

In the AFO reaction, a chalcone is converted into the respective 3-hydroxy-4*H*-chromen-4-one (**1b**). Initial attempts to convert 1-(2-hydroxyphenyl)ethan-1-one and benzaldehyde into their chalcone resulted in taring with 0.50 eq. of DBU or NaOH in ethanol. Even 4.00 eq. of KOH in THF or 2.20 eq. of $Ba(OH)_2$ did not yield the respective chalcone. However, the employment of 4.00 eq. of NaOH in ethanol prove to be a suitable condition for the conversion of 1-(2-hydroxyphenyl)ethan-1-one with benzaldehyde to the desired chalcone with a yield of 81 % after recrystallisation in ethanol. The AFO reaction was performed with 2.20 eq of NaOH and 2.00 of H_2O_2 in ethanol and resulted in the respective 3-hydroxy-2-phenyl-4*H*-chromen-4-one (25 % after recrystallisation). Over two steps, a yield of approximately 20 % was obtained. In order to improve the yield and to minimise the employment of resources, a one pot *Claisen-Schmidt* condensation, AFO sequence was established (Scheme 25).

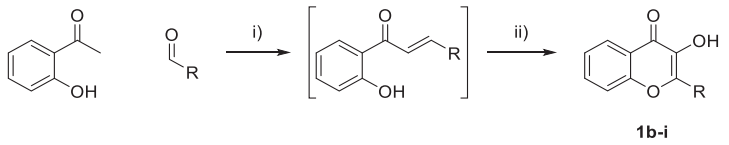

Scheme 25. One pot Claisen-Schmidt condensation AFO sequence for the synthesis of 3-hydroxy chromenones. I) 4.00 eq $NaOH_{(aq)}$, EtOH; ii) 2.20 eq H_2O_2.

With the same starting material, this sequence resulted in a yield of 31 % which corresponded to an increase of 10 % in isolated product. Due to the significant increase in yield, this sequence was employed for the synthesis of 3-hydroxy-4*H*-chromen-4-ones, exhibiting different aromatic substituents in 2-position (**1b-i**). However, a modified procedure had to be applied when a heterocyclic aldehyde was used in the reaction sequence, as it resulted in taring. For nicotinaldehyde, the reaction was refluxed for 3 h after the addition of hydrogen peroxide.

Subsequently, the obtained 3-hydroxy-4H-chromen-4-ones were alkylated with tert-butyl 4-(bromomethyl)benzoate (Scheme 26), resulting in the ethers **2**.

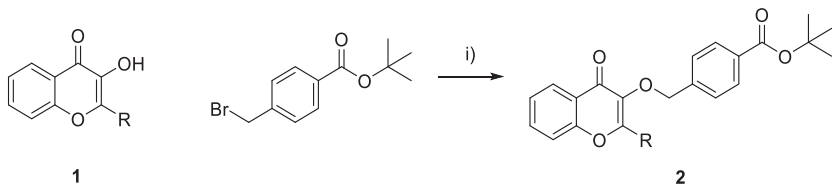

*Scheme 26. O-alkylation of 3-hydroxy-4H-chromen-4-ones **1**. I) 5.00 eq K_2CO_3, DMF.*

The acid labile ^{t}butyl ester was deprotected with TFA and converted with hydroxylamine to the corresponding hydroxamic acids **3** in a HATU mediated acylation reaction (Scheme 27).

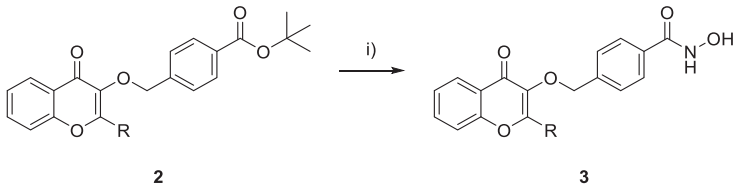

*Scheme 27. Synthesis of the hydroxamic acids **3**. I) a) TFA/DCM, b) 1.00 eq HATU, 1.20 eq H_2NOH • HCl, 3.20 eq DIPEA, DMF.*

However, one drawback of the HATU mediated *N*-acylation of hydroxylamine was that a complete separation of the product from HOAt was laborious on normal phase silica. Therefore, C-18 functionalised silica (RP-flash chromatography) had to be employed to obtain the desired hydroxamic acids **3**.

Subsequently, the HDAC inhibitory potential of **3** was assessed by HDAC2 and HDAC6 enzyme assays (Table 15).

*Table 15. HDAC2 and HDAC6 inhibition of **3**.*

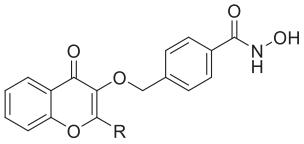

	R	HDAC2 pIC_{50} (IC_{50} [µM])	HDAC6 pIC_{50} (IC_{50} [µM])	SI 2/6
3a		6.17 ± 0.04 (0.670)	7.47 ± 0.04 (0.034)	20.0
3b		4.98 ± 0.02 (10.6)	6.48 ± 0.10 (0.329)	31.6
3c		5.16 ± 0.03 (6.87)	6.53 ± 0.07 (0.294)	23.4
3d		5.05 ± 0.02 (8.84)	6.55 ± 0.10 (0.283)	31.6
3e		5.03 ± 0.02 (9.37)	6.26 ± 0.11 (0.533)	17.0
3f		5.08 ± 0.03 (8.31)	6.31 ± 0.06 (0.494)	17.0
3g		5.00 ± 0.02 (10.0)	6.71 ± 0.10 (0.194)	51.3
3h	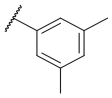	3.55 ± 0.11 (285)	5.98 ± 0.08 (1.04)	269
3i		5.32 ± 0.07 (4.76)	7.04 ± 0.15 (0.092)	52.5
Tubastatin A		5.04 ± 0.03 (9.19)	7.26 ± 0.08 (0.017)	166
Nexturastat A		5.70 ± 0.050 (1.99)	7.31 ± 0.082 (0.048)	40.7

Presented data are calculated from at least two experiments each performed in duplicates. Standard deviation of percent inhibition values is less than 10 %. Vehicle control was defined as 0 % inhibition.

In the HDAC inhibition assay, the HDAC6 selective inhibitors tubastatin A and nexturastat A were employed as reference compounds and exhibited a SI2/6 of 166 (pIC_{50} = 7.26 ± 0.08) and 40.7 (pIC_{50} = 7.31 ± 0.082), respectively. **3a**, exhibiting the 4*H*-chromen-4-one cap group resulted in a pIC_{50} (HDAC2) = 6.17 ± 0.04 and a pIC_{50} (HDAC6) = 7.47 ± 0.04 with a SI2/6 of 20.0 and thereby defined the lead structure of the here reported chromenone based hydroxamic acids **3**. The 2-phenyl substituted derivative of **3a** (**3b**) showed a pIC_{50} of 4.98 ± 0.02 for HDAC2 and a pIC_{50} of 6.48 ± 0.10 for HDAC6 with an SI2/6 of 31.6. **3b** demonstrated an approximately 1.6-fold higher selectivity towards HDAC6 with a coherent decrease in activity of one order of magnitude, compared to **3a**. In order to further increase the selectivity towards HDAC6, 2-aryl substituted 4*H*-chromen-4-one based hydroxamic acids **3** were evaluated. The tested *o*-substituted derivatives (**3c**-**3g**) exhibited a similar HDAC2 inhibition to **3b** with pIC_{50} values of around 5.00. However, the fluoro- (**3c**), chloro- (**3d**) and bromo- (**3e**) functionalised derivatives demonstrated a pIC_{50} of 6.53 ± 0.07 (SI2/6 = 31.6), 6.55 ± 0.10 (SI2/6 = 23.4) and 6.26 ± 0.11 (SI2/6 = 17.0) in HDAC6, respectively. The difluoro- (**3f**) and the dimethyl (**3g**) derivatives resulted in an inhibition of HDAC6 with pIC_{50} values of 6.31 ± 0.06 (SI2/6 =17.0) and 6.71 ± 0.10 (SI2/6 =51.3). **3h**, the 3,5-dimethyl derivative exhibited a decreased inhibition of HDAC2 (pIC_{50} = 3.55 ± 0.11) with a concomitant decreased inhibition of HDAC6 (pIC_{50} = 3.55 ± 0.11), resulting in an overall SI2/6 of 269. The 3-pyridinyl derivative **3i** demonstrated a pIC_{50} of 5.32 ± 0.07 in HDAC2 and a pIC50 of 7.04 ± 0.15 in HDAC6. In respect to the isozyme selectivity of the tested HDAC inhibitors, **3h** was the most selective compound with a HDAC2/6 selectivity index (SI) of 269, which correlates to an approximately 1.6-fold higher selectivity towards HDAC6 over HDAC2 with a 19-fold lower inhibition, compared to tubastatin A. In comparison to nexturastat A, **3g** and **3i** exhibited an approximately 1.3-fold higher selectivity towards HDAC6.

It has been shown that the connecting unit (CU) has a significant impact on the isozyme profile of HDAC inhibitors as well as on their biological activity. Therefore, we focussed on the derivatisation of the ether CU to a nitrogen-based CU as well as the evaluation of the linker length (Scheme 5).

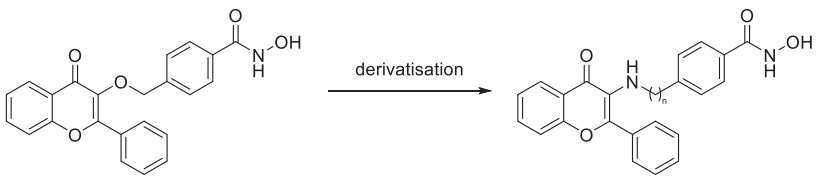

*Scheme 28. Connecting unit derivatisation of compound **3a**.*

For the synthesis of nitrogen based CU, we envisioned to modify the 3-hydroxy substituent with an amine functionalised linker (Scheme 29).

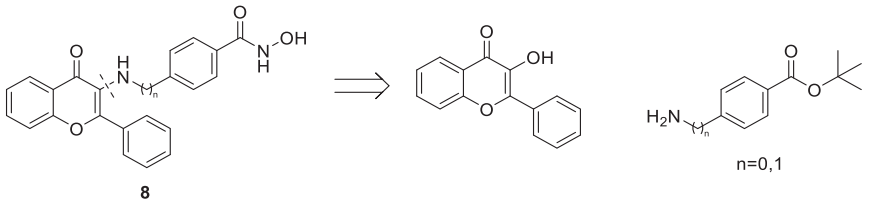

*Scheme 29. Retrosynthetic analysis of 3-amino substituted chromenones **8**.*

A similar transformation with aliphatic amines has been reported by Takechi et. Al..[41] Their procedure involved the tosylation of the 3-hydroxy substituent and the subsequent conversion with amines resulting in the 3-amino substituted products. However, under the same reaction conditions a conversion with *tert*-butyl 4-aminobenzoate was not observed. Therefore, we developed a palladium catalysed amination of 4*H*-chromen-4-ones. For this purpose, **1b** or **1i** was triflated (**4**) and converted with an amine to the respective 3-amino substituted 4*H*-chromen 4 ones (**7a-c**, Scheme 30).

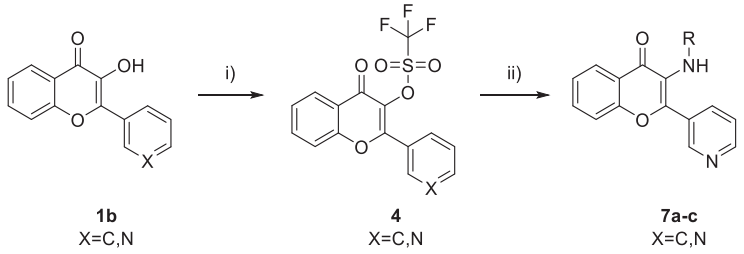

*Scheme 30. Synthesis of 3-amino functionalised chromenones **7a-c**. i) 2.00 eq Tf_2O, 2.10 eq DIPEA, DCM, ii) 1.10 eq RNH_2, 0.100 eq $Pd_2(dba)_3$ 0.150 eq Xantphos 5.00 eq Cs_2CO_3, PhMe.*

Subsequently, the 3-amino functionalised chromenones **7** were converted into their corresponding hydroxamic acid (**8a-c**, Scheme 31).

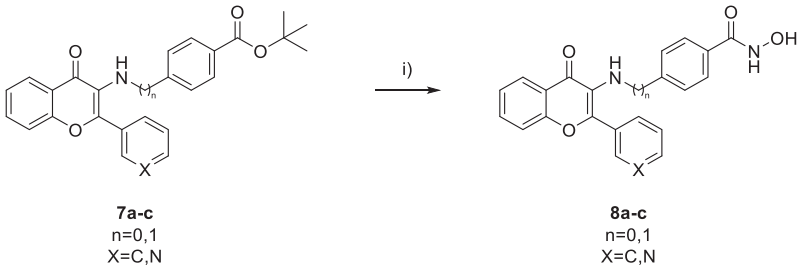

*Scheme 31. Synthesis of 3-amine chromenone based hydroxamic acids **8a-c**. i) a) TFA/DCM, b) 1.00 eq HATU, 1.20 eq $H_2NOH \cdot HCl$, 3.20 eq DIPEA, DMF.*

To further improve our biological activity profile, we proposed a cyclisation of the amine in 3 position with the 2' carbon at the 2-phenyl substituent (Scheme 32), resulting in the chromeno[3,2-*b*]indol-11(10*H*)-one based hydroxamic acid **14**.

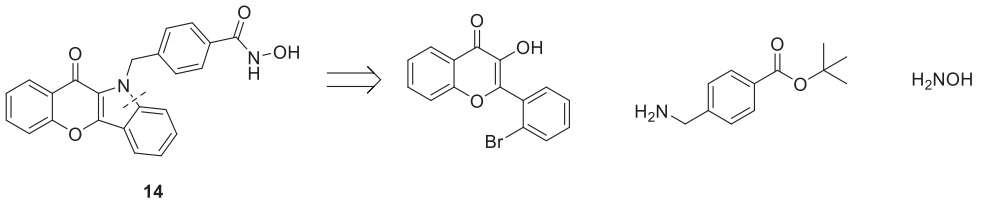

14

*Scheme 32. Retrosynthetic analysis of **14** by a palladium catalysed, intramolecular cyclisation.*

Despite intensive efforts, we could not perform the desired transformation with a variety of bases, different palladium species in various solvent. Therefore, we pursued the construction of the chromeno[3,2-*b*]indol-11(10*H*)-one heterocycle by an oxidative cyclisation (Scheme 33)

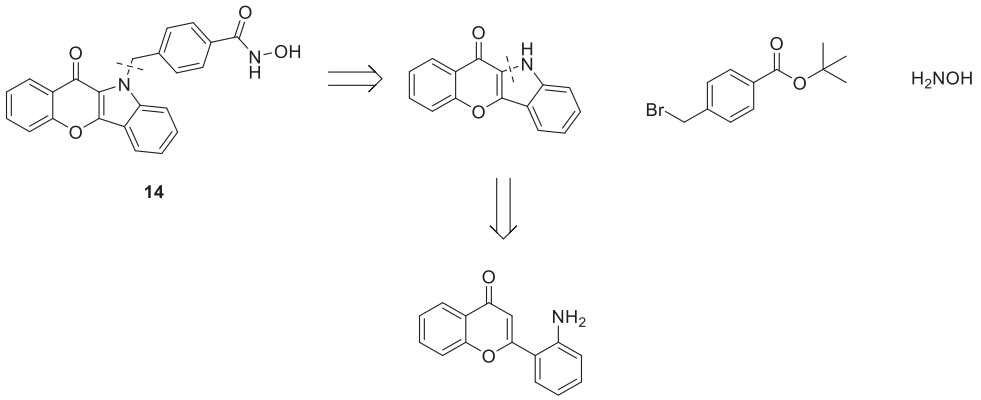

14

*Scheme 33. Retrosynthetic analysis of **14** by an oxidative cyclisation.*

The 2-(2-aminophenyl)-4*H*-chromen-4-one was accessed by a *Baker-Venkataraman* flavone synthesis (Scheme 34).

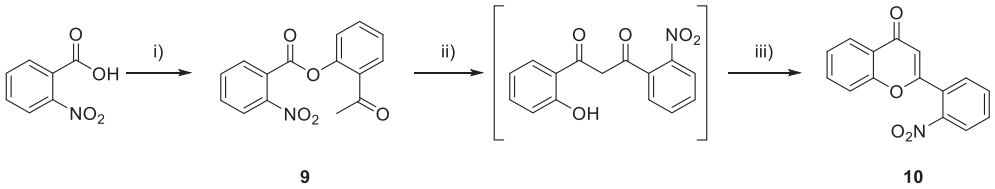

9 **10**

*Scheme 34. Synthesis of **10** by a Baker-Venkataraman flavone synthesis. I) a) 1.30 eq oxalyl chloride, 0.100 eq DMF, DCM; b) 1.00 eq 1-(2-hydroxyphenyl)ethan-1-one, 1.20 eq DIPEA, DCM; ii) 2.50 eq NaH, THF; iii) H_2SO_4.*

The nitro derivative **9** was reduced (**11**) with tin(II) chloride under acidic conditions (Scheme 11) and the oxidative cyclisation performed according to Moon *et al.* (Scheme 35).[42]

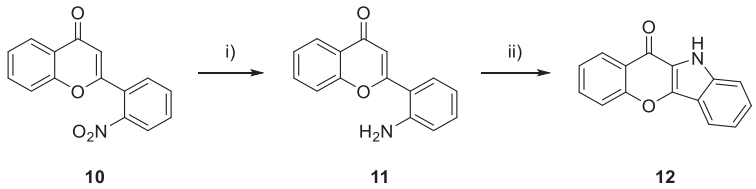

*Scheme 35. Synthesis of **12** by an oxidative cyclisation. I) 4.00 eq $SnCl_2$ • 2 H_2O, conc. $HCl_{(aq)}$/AcOH; ii) 1.20 eq. $Cu(Oac)_2$, 0.200 eq. $Zn(Otf)_2$ toluene, DMSO.*

However, after the oxidative cyclization **12** was obtained with a yield of 12 %, on a 1 mmol scale. To obtain **12** in a higher yield, we performed a *Cadogan-Sundberg* reaction[43] from **10** in triethyl phosphite. With this procedure, **12** was obtained with a yield of 38 % (Scheme 36).

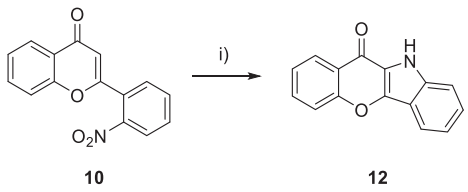

*Scheme 36. Synthesis of **12** by a* Cadogan-Sundberg reaction. I) *P(Ome)$_3$.*

Subsequently, **12** was alkylated with the benzyl linker (**13**) and transformed into the corresponding hydroxamic acid **14** (Scheme 37).

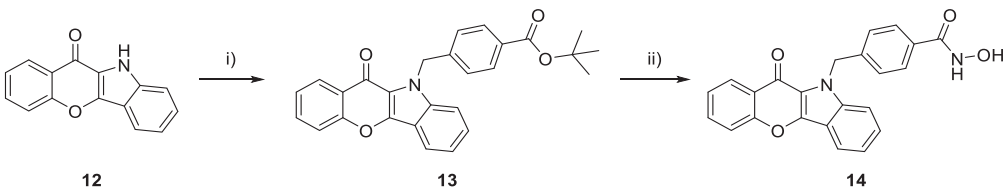

*Scheme 37. Synthesis of **14**. I) 1.20 eq NaH (60 %), 1.10 eq tert-butyl 4-(bromomethyl)benzoate, DMF; ii) a) TFA/DCM b)1.00 eq HATU, 1.20 eq H_2NOH • HCl, 3.20 eq DIPEA, DMF.*

The 3-amino chromenone based (**8a-c**) and chromeno[3,2-*b*]indol-11(10*H*)-one based (**14**) hydroxamic acids were subsequently subjected to HDAC2 and HDAC6 enzyme assays to assess their selectivity towards HDAC6 (Table 16).

*Table 16. HDAC2 and HDAC6 inhibition of **6** and **12**.*

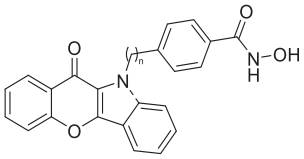

	n	R	HDAC2 pIC_{50} (IC_{50} [µM])	HDAC6 pIC_{50} (IC_{50} [µM])	SI2/6
8a	0		5.09 ± 0.03 (8.05)	6.36 ± 0.16 (0.435)	18.6
8b	0		5.47 ± 0.05 (3.41)	6.46 ± 0.05 (0.347)	9.77
8c	1		5.36 ± 0.22 (4.38)	6.79 ± 0.11 (0.162)	26.9
14	1		5.28 ± 0.08 (5.21)	6.64 ± 0.16 (0.231)	24.5
Tubastatin A			5.04 ± 0.03	7.26 ± 0.08	166
Nexturastat A			5.70 ± 0.050	7.31 ± 0.082	40.7

Presented data are calculated from at least two experiments each performed in duplicates. Standard deviation of percent inhibition values is less than 10 %. Vehicle control was defined as 0 % inhibition.

Compound **8a** exhibited a pIC_{50} of 5.09 ± 0.03 (SI2/6 = 18.6) and 6.36 ± 0.16 (SI2/6 = 9.77) for HDAC2 and HDAC6, respectively. The 3-pyridyl derivative **8b** demonstrated an increased inhibition of HDAC2 (pIC_{50} = 5.47 ± 0.05) and HDAC6 (pIC_{50} = 6.46 ± 0.05), resulting in a SI2/6 of 9.77. The linker length had a significant impact on HDAC6 inhibition and selectivity. A methylene group in the linker region (**8c**) caused an increased HDAC6 inhibition (pIC_{50} = 6.79 ± 0.11) whilst maintaining a similar inhibition of HDAC2, resulting in a SI2/6 of 26.9. Compound **12**, the annulated derivative of **8c** exhibited a pIC_{50} value of 5.28 ± 0.08 (HDAC2) and 6.64 ± 0.16 (HDAC6) with a SI of 24.5 for HDAC2 and HDAC6, respectively.

To assess the antiproliferative potential of the synthesised chromenone based hydroxamic acids, they were tested in the human ovarian cancer cell line A2780 and the human tongue squamous carcinoma cell line Cal27 (Table 17).

Table 17. Antiproliferative activity of chromenone based hydroxamic acids in Cal27 and A2780.

	MTT-Assay pIC_{50} (IC_{50} [µM])	
	Cal27	A2780
3a	5.38 ± 0.04 (4.19)	5.04 ± 0.03 (9.12)
3b	4.58 ± 0.08 (26.1)	4.55 ± 0.13 (28.1)
3c	4.62 ± 0.05 (24.0)	4.58 ± 0.05 (26.2)
3d	4.58 ± 0.07 (26.4)	4.47 ± 0.07 (34.0)
3e	4.55 ± 0.07 (28.2)	4.45 ± 0.11 (35.2)
3f	4.69 ± 0.08 (20.2)	4.41 ± 0.04 (38.6)
3g	4.61 ± 0.07 (24.5)	4.51 ± 0.10 (30.9)
3h	5.10 ± 0.04 (7.89)	5.16 ± 0.06 (6.89)
3i	4.69 ± 0.08 (20.2)	4.42 ± 0.08 (38.3)
8a	4.52 ± 0.11 (30.4)	4.46 ± 0.06 (34.6)
8b	5.05 ± 0.05 (8.87)	4.41 ± 0.09 (38.6)
8c	4.60 ± 0.08 (25.2)	4.50 ± 0.13 (31.9)
14	4.59 ± 0.05 (26.0)	4.54 ± 0.04 (29.0)

Presented data are calculated from at least two experiments each performed in duplicates. Standard deviation of percent inhibition values is less than 10 %. Vehicle control was defined as 0 % inhibition.

All tested compounds showed limited antiproliferative effects in Cal27 and A2780 with pIC_{50} ranging from 4.52 to 5.10 and 4.41 to 5.16, respectively. There is a good correlation between the pIC_{50} values obtained from Cal27 as well as A2780 and the pIC_{50} values from the HDAC2 enzyme assays, which indicate that the antiproliferative effect is likely to be the result of class I HDAC inhibition rather than HDAC6 inhibition in the tested cancer cell lines.

Conclusion

HDAC6 is an epigenetic eraser and a major player in the posttranslational modification of client proteins. Its inhibition represents a valuable pharmaceutical target for immunomodulation, the pharmacological intervention in neurodegenerative diseases and a potential application in oncology. Here, we report the synthesis of chromenone based hydroxamic acids, that exhibit either an ether or a nitrogen-based CU and successfully established a palladium catalysed approach for the synthesis of 3-amino substituted chromenones with unprecedented yields and reaction times.

Our explorative approach to utilise chromones as bulky and HDAC6 selectivity directing CAP group resulted in the discovery of Compound **3g** (MPK781), **3h** (MPK805) and **3i** (MPK509). **3h** exhibited an approximately 1.6-fold higher SI2/6 than tubastatin A, but a 19-fold lower inhibitory activity. The Compounds **3g** and **3i** exhibited an almost 1.3-fold higher selectivity towards HDAC6, in comparison to nexturastat A. All tested compounds showed low antiproliferative activities with pIC_{50} values ranging from 4.41 to 5.16 in Cal27 and A2780, which correlates with HDAC2 inhibition. Presumably, the observed antiproliferative properties of the tested cell lines is caused by HDAC2 inhibition.

Due to the low cytotoxicity of the here reported compounds, we propose that chromone based hydroxamic acid are valuable tools as HDAC6 selective inhibitors to explore their pharmaceutical potential in neurology, immunology or might suppress metastasis.

References

1. Bertrand, P. Inside HDAC with HDAC inhibitors. *European Journal of Medicinal Chemistry* vol. 45 2095–2116 (2010).

2. Göttlicher, M. *et al.* Valproic acid defines a novel class of HDAC inhibitors inducing differentiation of transformed cells. *EMBO J.* **20**, 6969–6978 (2001).

3. Vallo, S. *et al.* HDAC inhibition delays cell cycle progression of human bladder cancer cells in vitro. *Anticancer. Drugs* **22**, 1002–1009 (2011).

4. Brandl, A., Heinzel, T. & Krämer, O. H. Histone deacetylases: salesmen and customers in the post-translational modification market. *Biol. Cell* **101**, 193–205 (2009).

5. Rao, R., Fiskus, W., Ganguly, S., Kambhampati, S. & Bhalla, K. N. HDAC Inhibitors and Chaperone Function. in *Advances in Cancer Research* vol. 116 239–262 (Academic Press, 2012).

6. Rodriguez-Gonzalez, A. *et al.* Role of the aggresome pathway in cancer: Targeting histone deacetylase 6-dependent protein degradation. *Cancer Res.* **68**, 2557–2560 (2008).

7. De Ruijter, A. J. M., Van Gennip, A. H., Caron, H. N., Kemp, S. & Van Kuilenburg, A. B. P. Histone deacetylases (HDACs): Characterization of the classical HDAC family. *Biochemical Journal* vol. 370 737–749 (2003).

8. Davie, J. R. Histone modifications, chromatin structure, and the nuclear matrix. *J. Cell. Biochem.* **62**, 149–157 (1996).

9. Gallinari, P., Di Marco, S., Jones, P., Pallaoro, M. & Steinkühler, C. HDACs, histone deacetylation and gene transcription: From molecular biology to cancer therapeutics. *Cell Res.* **17**, 195–211 (2007).

10. Stenzel, K. *et al.* Alkoxyurea-Based Histone Deacetylase Inhibitors Increase Cisplatin Potency in Chemoresistant Cancer Cell Lines. *J. Med. Chem.* **60**, 5334–5348 (2017).

11. Tzogani, K. *et al.* EMA Review of Panobinostat (Farydak) for the Treatment of Adult Patients with Relapsed and/or Refractory Multiple Myeloma. *Oncologist* **23**, 631–636 (2018).

12. Depetter, Y. *et al.* Selective pharmacological inhibitors of HDAC6 reveal biochemical activity but functional tolerance in cancer models. *Int. J. Cancer* **145**, 735–747 (2019).

13. Li, A., Chen, P., Leng, Y. & Kang, J. Histone deacetylase 6 regulates the immunosuppressive properties of cancer-associated fibroblasts in breast cancer through the STAT3–COX2-dependent pathway. *Oncogene* **37**, 5952–5966 (2018).

14. Fukada, M., Nakayama, A., Mamiya, T., Yao, T. P. & Kawaguchi, Y. Dopaminergic abnormalities in Hdac6-deficient mice. *Neuropharmacology* **110**, 470–479 (2016).

15. Jochems, J. *et al.* Antidepressant-like properties of novel HDAC6-selective inhibitors with improved brain bioavailability. *Neuropsychopharmacology* **39**, 389–400 (2014).

16. Govindarajan, N. *et al.* Reducing HDAC6 ameliorates cognitive deficits in a mouse model for Alzheimer's disease. *EMBO Mol. Med.* **5**, 52–63 (2013).

17. Watson, P. J. *et al.* Insights into the activation mechanism of class i HDAC complexes by inositol phosphates. *Nat. Commun.* **7**, 11262 (2016).

18. Bürli, R. W. *et al.* Design, synthesis, and biological evaluation of potent and selective class IIa histone deacetylase (HDAC) inhibitors as a potential therapy for huntington's disease. *J. Med. Chem.* **56**, 9934–9954 (2013).

19. Hai, Y. & Christianson, D. W. Histone deacetylase 6 structure and molecular basis of catalysis and inhibition. *Nat. Chem. Biol.* **12**, 741–747 (2016).

20. Tabackman, A. A., Frankson, R., Marsan, E. S., Perry, K. & Cole, K. E. Structure of 'linkerless' hydroxamic acid inhibitor-HDAC8 complex confirms the formation of an isoform-specific subpocket. *J. Struct. Biol.* **195**, 373–378 (2016).

21. Jung, M. *et al.* Amide analogues of trichostatin A as inhibitors of histone deacetylase and inducers of terminal cell differentiation. *J. Med. Chem.* **42**, 4669–4679 (1999).

22. Finnin, M. S. *et al.* Structures of a histone deacetylase homologue bound to the TSA and SAHA inhibitors. *Nature* **401**, 188–193 (1999).

23. Jung, M. Inhibitors of Histone Deacetylase as New Anticancer Agents. *Curr. Med. Chem.* **8**, 1505–1511 (2012).

24. Melesina, J., Praetorius, L., Simoben, C. V., Robaa, D. & Sippl, W. Design of selective histone deacetylase inhibitors: Rethinking classical pharmacophore. *Future Med. Chem.* **10**, 1537–1540 (2018).

25. Butler, K. V. *et al.* Rational design and simple chemistry yield a superior, neuroprotective HDAC6 inhibitor, tubastatin A. *J. Am. Chem. Soc.* **132**, 10842–10846 (2010).

26. Bergman, J. A. *et al.* Selective histone deacetylase 6 inhibitors bearing substituted urea linkers inhibit melanoma cell growth. *J. Med. Chem.* **55**, 9891–9899 (2012).

27. Tavares, M. T. *et al.* Synthesis and Pharmacological Evaluation of Selective Histone Deacetylase

6 Inhibitors in Melanoma Models. *ACS Med. Chem. Lett.* **8**, 1031–1036 (2017).

28. Khadem, S. & Marles, R. J. Chromone and flavonoid alkaloids: Occurrence and bioactivity. *Molecules* vol. 17 191–206 (2012).

29. BRADLEY, D. V. & CAZORT, R. J. Relief of Bladder Spasm by Flavoxate. A Comparative Study. *J. Clin. Pharmacol. J. New Drugs* **10**, 65–68 (1970).

30. Li, J. *et al.* Efficacy and safety of iguratimod for the treatment of rheumatoid arthritis. *Clin. Dev. Immunol.* **2013**, 1–16 (2013).

31. Enna, S. J. & Bylund, D. B. Pranlukast. in *xPharm: The Comprehensive Pharmacology Reference* vol. 63 1–1 (Elsevier, 2011).

32. Deep, A. *et al.* Flavopiridol as cyclin dependent kinase (CDK) inhibitor: a review. *New J. Chem.* **42**, 18500–18507 (2018).

33. Reis, J., Gaspar, A., Milhazes, N. & Borges, F. Chromone as a Privileged Scaffold in Drug Discovery: Recent Advances. *J. Med. Chem.* **60**, 7941–7957 (2017).

34. Silva, C. F. M., Batista, V. F., Pinto, D. C. G. A. & Silva, A. M. S. Challenges with chromone as a privileged scaffold in drug discovery. *Expert Opin. Drug Discov.* **13**, 795–798 (2018).

35. Gaspar, A., Matos, M. J., Garrido, J., Uriarte, E. & Borges, F. Chromone: A valid scaffold in medicinal chemistry. *Chem. Rev.* **114**, 4960–4992 (2014).

36. Rehberg, N. *et al.* Chlorflavonin Targets Acetohydroxyacid Synthase Catalytic Subunit IlvB1 for Synergistic Killing of Mycobacterium tuberculosis. *ACS Infect. Dis.* **4**, 123–134 (2018).

37. Ameen, D. & Snape, T. J. Mechanism and application of baker-venkataraman o→c acyl migration reactions. *Synth.* **47**, 141–158 (2015).

38. v. Kostanecki, S. & Różycki, A. Ueber eine Bildungsweise von Chromonderivaten. *Berichte der Dtsch. Chem. Gesellschaft* **34**, 102–109 (1901).

39. Allan, J. & Robinson, R. CCXC. - An accessible derivative of chromonol. *J. Chem. Soc. Trans.* **125**, 2192–2195 (1924).

40. Wang, Z. Algar-Flynn-Oyamada (AFO) Reaction. in *Comprehensive Organic Name Reactions and Reagents* 52–56 (John Wiley & Sons, Inc., 2010). doi:10.1002/9780470638859.conrr013.

41. Takechi, A., Takikawa, H., Miyake, H. & Sasaki, M. Synthesis of 3-aminoflavones from 3-hydroxyflavones via 3-tosyloxy- or 3-mesyloxyflavones. *Chem. Lett.* **35**, 128–129 (2006).

42. Moon, Y., Kim, Y., Hong, H. & Hong, S. Synthesis of heterocyclic-fused benzofurans via C–H functionalization of flavones and coumarins. *Chem. Commun.* **49**, 8323–8325 (2013).

43. Kaur, M. & Kumar, R. C-N and N-N bond formation via reductive cyclization: Progress in cadogan/cadogan-sundberg reaction. *ChemistrySelect* **3**, 5330–5340 (2018).

6.1 Chapter IV – Supporting information

Chromenones: A suitable CAP group to govern HDAC6 selectivity?

Supporting information

M. Pflieger, A. Hamacher, N. Horstick-Muche, E. Kharitonova, M. U. Kassack, T. Kurz

Contents

1 General Information

Reaction, monitoring and purification

Chemicals and solvents were purchased from commercial suppliers (Sigma-Aldrich, Acros Organics, TCI, Fluorochem ABCR, Alfa Aesar, J&K, Carbolution) and used without further purification. Dry solvents were obtained from Acros Organics. Ambient or room temperature correspond to 22°C. The reaction progression was monitored using Thin-Layer-Chromatography plates by Macherey Nagel (ALUGRAM Xtra SIL G/UV_{254}). Visualisation was achieved with ultraviolet irradiation (254 nm) or by staining with a $KmnO_4$-solution (9 g $KmnO_4$, 60 g K_2CO_3, 15 mL of a 5% aqueous NaOH-solution, ad 900 mL demineralised water). Purification was either performed with prepacked Silica cartridges (RediSep® Rf Normal Phase Silica, RediSep® Rf RP C18) for flash column chromatography (CombiFlashRf200, TeleDyneIsco) or by recrystallisation. Different eluent mixtures of solvents (hexane and ethyl acetate or dichloromethane and methanol) served as the mobile phase for flash column chromatography and are stated in the experimental procedure.

Analytics

An NMR-Spectrometer by Bruker (Bruker Avance III – 300, Bruker Avance DRX – 500 or Bruker Avance III – 600) were used to perform ^{1}H- and^{13}C-NMR experiments. Chemical shifts are given in parts per million (ppm), relative to residual non-deuterated solvent peak (^{1}H-NMR: DMSO-d_6 (2.50), ^{13}C-NMR: DMSOd_6 (39.52). Signal patterns are indicated as: singlet (s), doublet (d), triplet (t), quartet (q), or multiplet (m). Coupling constants, J, are quoted to the nearest 0.1 Hz and are presented as observed. ESI-MS was carried out using Bruker Daltonics UHR-QTOF maXis 4G (Bruker Daltonics) under electrospray ionization (ESI). The above-mentioned characterisations were carried out by the HHU Center of Molecular and Structural Analytics at Heinrich-Heine University Düsseldorf (http://www.chemie.hhu.de/en/analytics-center-hhucemsa.html). APCI-MS was carried out with an Advion expression^{L} CMS. Melting points were determined using a Büchi M-565 melting point apparatus (uncorrected). Analytical HPLC was carried out on a Knauer HPLC system comprising of an Azura P6.1L pump, an Optimas 800 autosampler, a Fast Scanning Spectro-Photometer K-2600 and a Knauer Reversed Phase column (SN: FK36). Evaluated compounds were detected at 254 nm. The solvent gradient table is shown in Table 14. The purity of all final compounds was 95% or higher.

Table 18: The solvent gradient table for analytic HPLC analysis.

Time / min	Water + 0.1% TFA	ACN + 0.1% TFA
Initial	90	10
0.50	90	10
20.0	0	100
30.0	0	100
31.0	90	10
40.0	90	10

2 Synthetic procedures

2.1 Synthesis of 3-hydroxy-4*H*-chromen-4-one (**1a**)

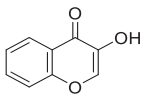

1a was synthesised according to Spadafora et. Al.. [1]

^{1}H NMR (300 MHz, DMSO-d_6) δ 9.15 (s, 1H), 8.23 (s, 1H), 8.11 (dd, *J* = 8.1, 1.6 Hz, 1H), 7.75 (ddd, *J* = 8.7, 7.0, 1.7 Hz, 1H), 7.61 (dd, *J* = 8.5, 1.0 Hz, 1H), 7.44 (ddd, *J* = 8.1, 7.0, 1.1 Hz, 1H).

^{13}C NMR (75 MHz, DMSO-d_6) δ 172.7, 155.3, 141.9, 140.8, 133.4, 125.0, 124.5, 122.7, 118.4.

M.p.: 178.3 °C, **Lit.**: 178 – 180 °C[2]; **HPLC**: R_t=7.53 min, purity ≥ 96.3 %, **MS** (+APCI): 163 $[M+H]^+$.

2.2 General procedure for the synthesis of 2-substituted 3-hydroxy-4*H*-chromen-4-ones (**1b-1i**)

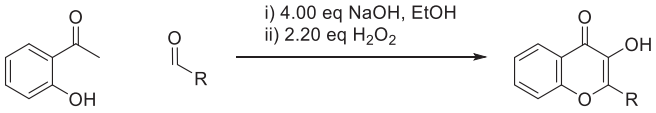

1.00 eq of 1-(2-hydroxyphenyl)ethan-1-one and 1.00 eq of the respective aldehyde was mixed with Ethanol (3 mL/mmol) and 4.00 eq of a 5M aq. NaOH solution were added to the reaction solution. After 16 h at ambient temperature, whilst stirring, 2.20 eq of H_2O_2 (30 % aq. Solution) were added and stirred for another 16 h. The reaction mixture was poured on 600 mL of ice water, neutralised with 1 M aq. HCl solution and the precipitate collected by filtration. Subsequently, the precipitate was washed thoroughly with dH_2O and the product recrystallised from EtOH.

2.2.1 Synthesis of 3-hydroxy-2-phenyl-4H-chromen-4-one (**1b**)

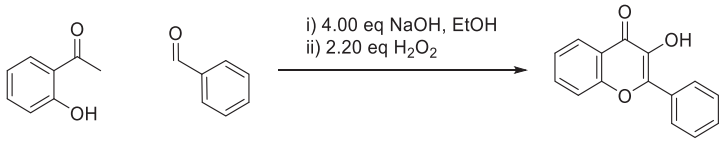

1b was synthesised according to general procedure 2.3.1 on a 40 mmol scale and obtained as a yellow solid with a yield of 31 % (12.3 mmol, 3.28 g).

^{1}H NMR (600 MHz, DMSO-d_6) δ 9.62 (s, 1H), 8.29 – 8.18 (m, 2H), 8.12 (dd, *J* = 8.0, 1.6 Hz, 1H), 7.80 (ddd, *J* = 8.6, 6.9, 1.7 Hz, 1H), 7.76 (dd, *J* = 8.5, 1.1 Hz, 1H), 7.57 (dd, *J* = 8.4, 6.9 Hz, 2H), 7.53 – 7.48 (m, 1H), 7.51 – 7.44 (m, 1H).

^{13}C NMR (151 MHz, DMSO-d_6) δ 173.0, 154.6, 145.2, 139.1, 133.7, 131.3, 129.9, 128.5, 127.7, 124.8, 124.6, 121.3, 118.4.

M.p.: 173.6°C; **HPLC**: R_t=14.30 min, purity ≥ 99 %, **MS** (+APCI): 239 $[M+H]^+$.

2.2.2 Synthesis of 2-(2-fluorophenyl)-3-hydroxy-4H-chromen-4-one (**1c**)

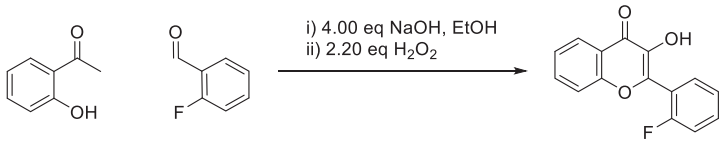

1c was synthesised according to general procedure 2.3.1 on a 20 mmol scale and obtained as a yellow solid with a yield of 24 % (4.8 mmol, 1.23 g).

^{1}H NMR (300 MHz, DMSO-d_6) δ 9.42 (s, 1H), 8.15 (ddd, *J* = 8.0, 1.7, 0.5 Hz, 1H), 7.83 – 7.72 (m, 2H), 7.68 – 7.55 (m, 2H), 7.48 (ddd, *J* = 8.1, 7.0, 1.1 Hz, 1H), 7.43 – 7.33 (m, 2H).

^{13}C NMR (151 MHz, DMSO-d_6) δ 173.2, 159.6 (d, *J* = 251.9 Hz), 155.5, 143.9, 140.0, 134.3, 133.0 (d, *J* = 8.4 Hz), 131.7 (d, *J* = 2.6 Hz), 125.4, 125.2, 124.9 (d, *J* = 3.5 Hz), 122.3, 119.5 (d, *J* = 13.9 Hz), 118.9, 116.6 (d, *J* = 21.3 Hz).

M.p.: 184.1°C; **HPLC**: R_t=13.37 min, purity = 98.8 %, **MS** (+APCI): 257 $[M+H]^+$.

2.2.3 Synthesis of 2-(2-chlorophenyl)-3-hydroxy-4*H*-chromen-4-one (**1d**)

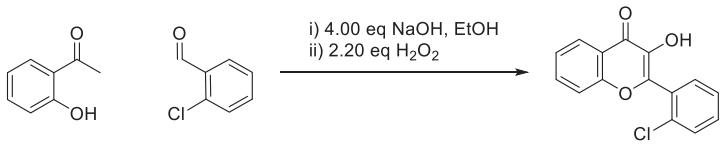

1d was synthesised according to general procedure 2.3.1 on a 43.6 mmol scale and obtained as a yellow solid with a yield of 21 % (9.17 mmol, 2.5 g).

^{1}H NMR (600 MHz, DMSO-d_6) δ 9.35 (s, 1H), 8.17 (dd, *J* = 8.1, 1.7 Hz, 1H), 7.81 (ddd, *J* = 8.7, 7.0, 1.7 Hz, 1H), 7.71 (dd, *J* = 7.6, 1.8 Hz, 1H), 7.66 (ddd, *J* = 8.6, 3.8, 1.1 Hz, 2H), 7.58 (td, *J* = 7.8, 1.8 Hz, 1H), 7.55 – 7.47 (m, 2H).

^{13}C NMR (151 MHz, DMSO-d_6) δ 173.4, 155.4, 146.6, 139.8, 134.3, 133.2, 132.5, 132.3, 130.5, 130.2, 127.7, 125.4, 125.2, 122.5, 118.9.

m.p.: 183.8 °C; **HPLC**: R_t=13.53 min, purity ≥ 99 %, **MS** (+APCI): 273 $[M+H]^+$.

2.2.4 Synthesis of 2-(2-bromophenyl)-3-hydroxy-4H-chromen-4-one (**1e**)

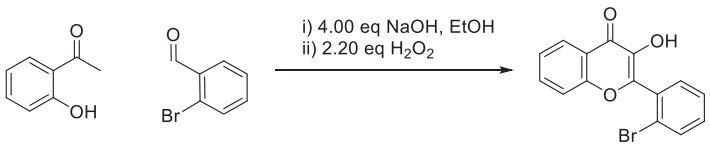

1e was synthesised according to general procedure 2.3.1 on a 40 mmol scale and obtained as a yellow solid with a yield of 32 % (12.6 mmol, 4.0 g).

^{1}H NMR (300 MHz, DMSO-d_6) δ 9.32 (s, 1H), 8.16 (ddd, *J* = 8.0, 1.7, 0.5 Hz, 1H), 7.86 – 7.74 (m, 2H), 7.72 – 7.60 (m, 2H), 7.60 – 7.42 (m, 3H).

^{13}C NMR (75 MHz, DMSO-d_6) δ 173.0, 154.9, 147.4, 139.1, 133.9, 132.9, 132.1, 132.1, 132.0, 127.7, 125.0, 124.8, 122.6, 122.1, 118.4.

M.p.: 182.8 °C; **HPLC**: R_t=14.17 min, purity ≥ 99 %, **MS** (+APCI): 317 $[M+H]^+$.

2.2.5 Synthesis of 2-(2,6-difluorophenyl)-3-hydroxy-4*H*-chromen-4-one (**1f**)

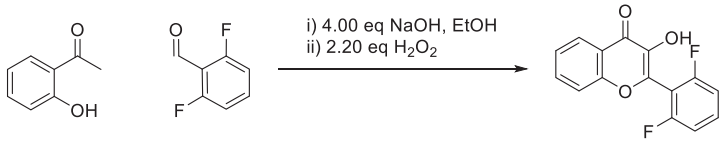

1f was synthesised according to general procedure 2.3.1 on a 40 mmol scale and obtained as a yellow solid with a yield of 34 % (13.7 mmol, 3.75 g).

^{1}H NMR (300 MHz, DMSO-d_6) δ 9.71 (s, 1H), 8.17 (dd, *J* = 8.0, 1.6 Hz, 1H), 7.82 (ddd, *J* = 8.7, 7.1, 1.7 Hz, 1H), 7.77 – 7.62 (m, 2H), 7.51 (ddd, *J* = 8.1, 7.0, 1.1 Hz, 1H), 7.39 – 7.26 (m, 2H).

^{13}C NMR (75 MHz, DMSO-d_6) δ 172.5, 159.6 (dd, *J* = 251.8, 6.6 Hz), 155.1, 140.8, 138.1, 133.9, 133.4 (t, *J* = 10.5 Hz), 125.0, 124.8, 121.9, 118.2, 112.4 – 111.6 (m), 108.4 (t, *J* = 19.8 Hz).

M.p.: 224.2 °C; **HPLC**: R_t=13.31 min, purity = 97.2 %, **MS** (+APCI): 275 $[M+H]^+$.

2.2.6 Synthesis of 2-(2,6-dimethylphenyl)-3-hydroxy-4*H*-chromen-4-one (**1g**)

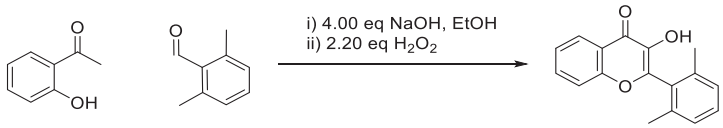

1g was synthesised according to general procedure 2.3.1 on a 40 mmol scale and obtained as a yellow solid with a yield of 34 % (13.7 mmol, 3.75 g).

^{1}H NMR (300 MHz, DMSO-d_6) δ 9.11 (s, 1H), 8.18 (dd, *J* = 8.0, 1.6 Hz, 1H), 7.79 (ddd, *J* = 8.6, 7.0, 1.7 Hz, 1H), 7.65 (dd, *J* = 8.6, 1.0 Hz, 1H), 7.49 (ddd, *J* = 8.0, 7.0, 1.1 Hz, 1H), 7.32 (dd, *J* = 8.3, 6.8 Hz, 1H), 7.23 – 7.13 (m, 2H), 2.18 (s, 6H).

^{13}C NMR (75 MHz, DMSO-d_6) δ 172.7, 155.2, 148.1, 139.1, 137.0, 133.5, 130.3, 129.7, 127.3, 124.9, 124.5, 122.1, 118.4, 19.2.

M.p.: 178.1 °C; **HPLC**: Rt=14.69 min, purity ≥ 99 %, **MS** (+APCI): 267 $[M+H]^+$.

2.2.7 Synthesis of 2-(3,5-dimethylphenyl)-3-hydroxy-4H-chromen-4-one (**1h**)

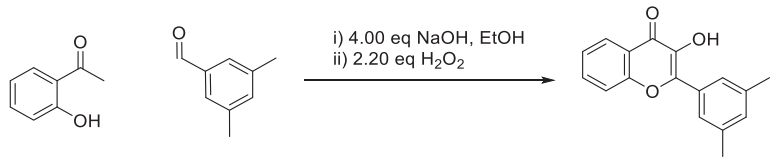

1h was synthesised according to general procedure 2.3.1 on a 40 mmol scale and obtained as a yellow solid with a yield of 34 % (13.7 mmol, 3.75 g).

^{1}H NMR (300 MHz, DMSO-d_6) δ 8.15 – 8.05 (m, 1H), 7.97 (d, *J* = 1.6 Hz, 2H), 7.81 – 7.67 (m, 2H), 7.41 (ddd, *J* = 8.1, 5.0, 3.1 Hz, 1H), 7.05 (d, *J* = 2.0 Hz, 1H), 2.41 – 2.32 (m, 6H).

^{13}C NMR (126 MHz, DMSO-d_6) δ 174.8, 154.3 (d, *J* = 6.8 Hz), 137.1 (d, *J* = 8.2 Hz), 130.3 (d, *J* = 25.8 Hz), 121.2, 118.2 (d, *J* = 2.8 Hz), 21.1.

M.p.: 157.5°C; HPLC: Rt=17.19 min, purity = 96.3 %, **MS** (+APCI): 267 $[M+H]^+$.

2.2.8 Synthesis of 3-hydroxy-2-(pyridine-3-yl)-4H-chromen-4-one (**1i**)

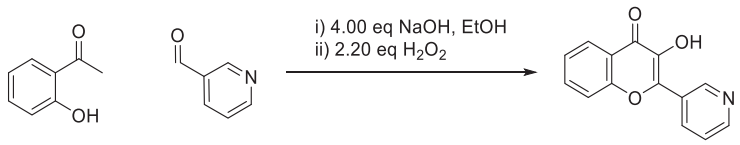

1i was synthesised according to a modified procedure of general procedure 2.3.1 on a 43.6 mmol scale. After the addition of hydrogen peroxide, the solution was refluxed for 3 h. 3b was obtained as a purple solid with a yield of 34 % (14.6 mmol, 3.49 g).

^{1}H NMR (600 MHz, DMSO-d_6) δ 10.0 (s, 1H), 9.5 – 9.3 (m, 1H), 8.7 (dd, *J* = 4.8, 1.6 Hz, 1H), 8.5 (dt, *J* = 8.1, 1.9 Hz, 1H), 8.1 (dd, *J* = 8.0, 1.6 Hz, 1H), 7.9 – 7.7 (m, 2H), 7.6 (ddd, *J* = 8.1, 4.8, 0.9 Hz, 1H), 7.5 (ddd, *J* = 8.0, 6.7, 1.3 Hz, 1H).

^{13}C NMR (151 MHz, DMSO-d_6) δ 173.0, 154.7, 150.2, 148.3, 143.1, 139.8, 134.8, 133.9, 127.6, 124.8, 124.7, 123.6, 121.4, 118.5.

M.p.: °C; **HPLC**: R_t=6.07 min, purity ≥ 99 %, **MS** (+APCI): 240 $[M+H]^+$.

2.3 General procedure for the *O* alkylation of 3-hydroxy-4*H*-chromen-4-ones (**2**)

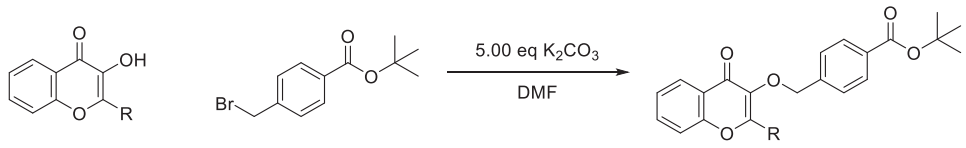

1.00 eq of **1** was combined with 1.10 eq of *tert*-butyl 4-(bromomethyl)benzoate and 5.00 eq. of anhydrous K_2CO_3 in dry DMF (20 mL/mmol). The reaction was stirred for 6 h at ambient temperature and the solvent removed under reduced pressure. Subsequently, the obtained residue was resuspended in EtOAc, the organic layer washed with dH_2O (x3), brine (x1) and dried over Na_2SO_4. Finally, the product was purified by flash column chromatography (*n*-hexane/EtOAc).

2.3.1 Synthesis of tert-butyl 4-(((2-(3,5-dimethylphenyl)-4-oxo-4H-chromen-3-yl)oxy)methyl)benzoate (**2a**)

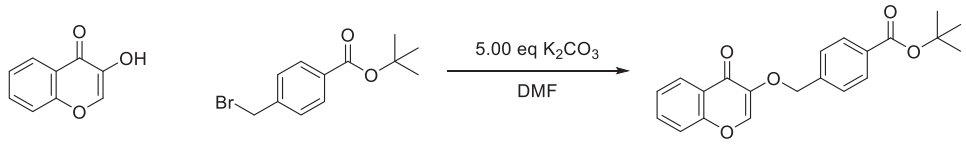

2a was synthesised according to general procedure 2.5 on a 2 mmol scale and obtained as a colourless solid with a yield of 55 % (1.1 mmol, 386 mg).

^{1}H NMR (300 MHz, DMSO-d_6) δ 8.40 (s, 1H), 8.12 (ddd, *J* = 8.0, 1.7, 0.5 Hz, 1H), 7.95 – 7.88 (m, 2H), 7.79 (ddd, *J* = 8.7, 7.0, 1.7 Hz, 1H), 7.64 (ddd, *J* = 8.6, 1.1, 0.5 Hz, 1H), 7.60 – 7.54 (m, 2H), 7.47 (ddd, *J* = 8.1, 7.1, 1.1 Hz, 1H), 5.14 (s, 2H), 1.54 (s, 9H).

^{13}C NMR (126 MHz, DMSO-d_6) δ 162.7, 153.2, 142.5, 140.7, 139.4, 131.9, 129.0, 127.1, 125.8, 123.1, 122.9, 116.4, 78.8, 69.1, 25.8.

M.p.: 122.0 °C; **HPLC**: R_t = 13.83, purity ≥ 99 %, **MS** (+APCI): 353 $[M+H]^+$.

2.3.2 Synthesis of tert-butyl 4-(((4-oxo-2-phenyl-4H-chromen-3-yl)oxy)methyl)benzoate (**2b**)

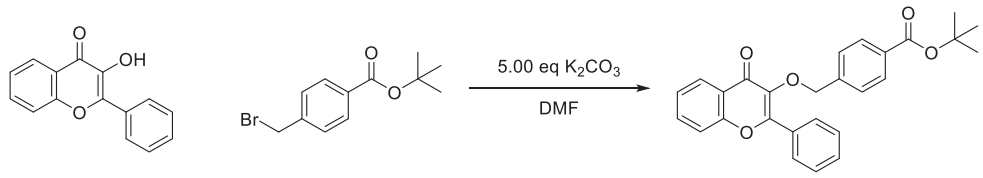

2b was synthesised according to general procedure 2.5 on a 1 mmol scale and obtained as a colourless solid with a yield of 75 % (0.747 mmol, 320 mg).

^{1}H NMR (600 MHz, DMSO-d_6) δ 8.14 (dd, *J* = 8.0, 1.6 Hz, 1H), 7.98 (dt, *J* = 6.7, 1.7 Hz, 2H), 7.88 – 7.78 (m, 3H), 7.74 (d, *J* = 8.4 Hz, 1H), 7.53 (dtd, *J* = 16.6, 8.0, 7.4, 3.0 Hz, 4H), 7.43 (d, *J* = 8.1 Hz, 2H), 5.16 (s, 2H), 1.53 (s, 9H).

^{13}C NMR (151 MHz, DMSO-d_6) δ 174.0, 164.7, 155.9, 154.8, 141.6, 139.2, 134.2, 130.9, 130.8, 130.4, 128.9, 128.6, 128.5, 127.9, 125.2, 125.0, 123.5, 118.5, 80.7, 72.6, 27.8.

M.p.: 133.3 °C; **HPLC**: R_t=20.48 min, purity ≥ 99 %, **MS** (+APCI): 429 $[M+H]^+$.

2.3.3 Synthesis of *tert*-butyl 4-(((2-(2-fluorophenyl)-4-oxo-4*H*-chromen-3-yl)oxy)methyl)benzoate (**2c**)

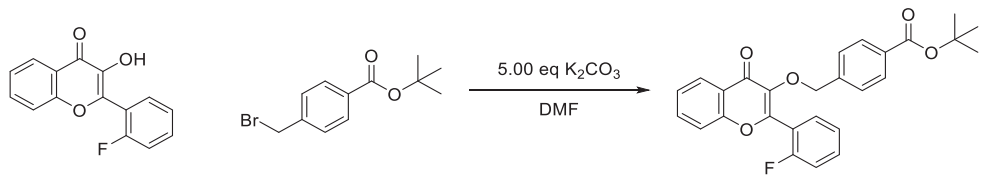

2c was synthesised according to general procedure 2.5 on a 2 mmol scale and obtained as a colourless solid with a yield of 87 % (1.75 mmol, 777 mg).

^{1}H NMR (600 MHz, DMSO-d_6) δ 8.18 (dd, *J* = 8.0, 1.7 Hz, 1H), 7.85 (ddd, *J* = 8.7, 7.1, 1.7 Hz, 1H), 7.78 – 7.72 (m, 2H), 7.69 (dd, *J* = 8.6, 0.9 Hz, 1H), 7.68 – 7.60 (m, 2H), 7.55 (ddd, *J* = 8.1, 7.1, 1.0 Hz, 1H), 7.39 – 7.32 (m, 2H), 7.26 – 7.20 (m, 2H), 5.15 (s, 2H), 1.53 (s, 9H).

^{13}C NMR (75 MHz, DMSO-d_6) δ 173.6, 164.6, 159.2 (d, *J* = 250.9 Hz), 155.1, 153.0, 141.5, 139.9, 134.4, 133.1 (d, *J* = 8.5 Hz), 131.3 (d, *J* = 2.1 Hz), 130.7, 128.8, 127.7, 125.4, 125.1, 124.5 (d, *J* = 3.5 Hz), 123.7, 118.4 (d, *J* = 13.7 Hz), 116.0 (d, *J* = 21.2 Hz), 80.7, 72.7, 27.8.

M.p.: 114.9°C; **HPLC**: R_t=19.75 min, purity ≥ 99 %, **MS** (+APCI): 447 $[M+H]^+$.

2.3.4 Synthesis of tert-butyl 4-(((2-(2-chlorophenyl)-4-oxo-4H-chromen-3-yl)oxy)methyl)benzoate (**2d**)

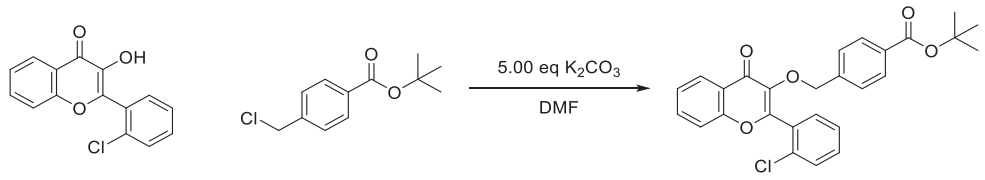

2d was synthesised according to general procedure 2.5 on a 1.47 mmol scale and obtained as a colourless solid with a yield of 93 % (1.36 mmol, 630 mg).

^{1}H NMR (300 MHz, DMSO-d_6) δ 8.19 (ddd, *J* = 8.0, 1.7, 0.5 Hz, 1H), 7.85 (ddd, *J* = 8.7, 7.1, 1.7 Hz, 1H), 7.77 – 7.71 (m, 2H), 7.71 – 7.44 (m, 6H), 7.21 – 7.13 (m, 2H), 5.11 (s, 2H), 1.52 (s, 9H).

^{13}C NMR (75 MHz, DMSO-d_6) δ 173.8, 164.6, 155.5, 155.0, 141.5, 139.8, 134.4, 132.5, 132.3, 131.7, 130.7, 129.6, 129.5, 128.8, 127.6, 127.2, 125.4, 125.1, 123.8, 118.5, 80.7, 72.8, 27.7.
M.p.: 96.9 °C; **HPLC**: R_t=20.37 min, purity ≥ 99 %, **MS** (+APCI): 463 $[M+H]^+$

2.3.5 Synthesis of *tert*-butyl 4-(((2-(2-bromophenyl)-4-oxo-4H-chromen-3-yl)oxy)methyl)benzoate (**2e**)

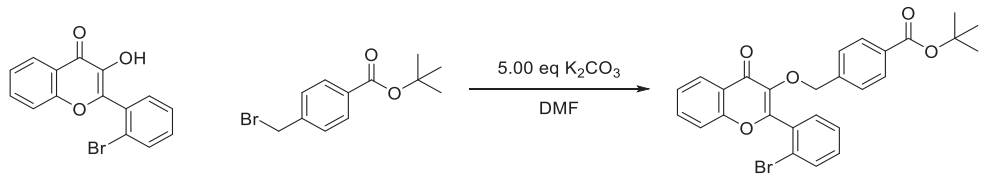

2e was synthesised according to general procedure 2.5 on a 2 mmol scale and obtained as a colourless solid with a yield of 87 % (1.75 mmol, 777 mg).

^{1}H NMR (300 MHz, DMSO-d_6) δ 8.19 (ddd, *J* = 8.0, 1.7, 0.5 Hz, 1H), 7.91 – 7.45 (m, 9H), 7.23 – 7.12 (m, 2H), 5.11 (s, 2H), 1.52 (s, 9H).

^{13}C NMR (126 MHz, DMSO-d_6) δ 174.2, 165.0, 157.2, 155.4, 141.9, 140.0, 134.8, 133.1, 132.7, 132.1, 132.0, 131.2, 129.2, 128.0, 127.9, 125.8, 125.5, 124.3, 122.6, 118.9, 81.0, 73.3, 28.2.

M.p.: 59.4 °C; **HPLC**: R_t=20.51 min, purity ≥ 99 %, **MS** (+APCI): 509 $[M+H]^+$

2.3.6 Synthesis of *tert*-butyl 4-(((2-(2,6-difluorophenyl)-4-oxo-4*H*-chromen-3-yl)oxy)methyl)benzoate (**2f**)

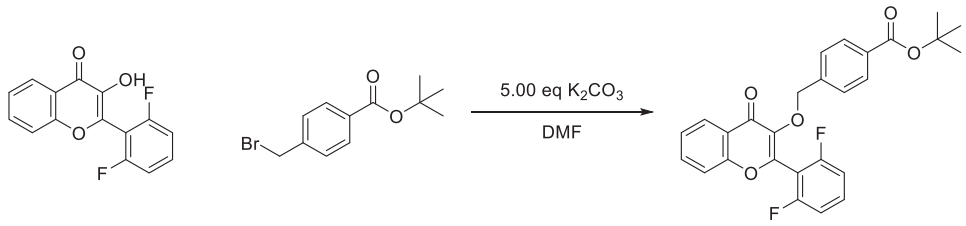

2f was synthesised according to general procedure 2.5 on a 2 mmol scale and obtained as a colourless solid with a yield of 84 % (1.68 mmol, 780 mg).

^{1}H NMR (300 MHz, DMSO-d_6) δ 8.19 (ddd, *J* = 8.0, 1.7, 0.5 Hz, 1H), 7.86 (ddd, *J* = 8.7, 7.1, 1.7 Hz, 1H), 7.79 – 7.63 (m, 4H), 7.56 (ddd, *J* = 8.1, 7.1, 1.1 Hz, 1H), 7.31 – 7.21 (m, 2H), 7.21 – 7.12 (m, 2H), 5.17 (s, 2H), 1.53 (s, 9H).

^{13}C NMR (75 MHz, DMSO-d_6) δ 173.3, 164.6, 159.5 (dd, *J* = 252.1, 6.1 Hz), 155.2, 147.5, 141.2, 140.9, 134.7, 134.1 (t, *J* = 10.5 Hz), 131.0 – 125.5 (m), 125.3, 123.7, 118.5, 112.1 (d, *J* = 24.2 Hz), 108.4 – 107.4 (m), 80.7, 72.7, 27.7.

M.p.: 90.8 °C; **HPLC**: R_t=19.78 min, purity ≥ 99 %, **MS** (+APCI): 465 $[M+H]^+$

2.3.7 Synthesis of tert-butyl 4-(((2-(2,6-dimethylphenyl)-4-oxo-4H-chromen-3-yl)oxy)methyl)benzoate (**2g**)

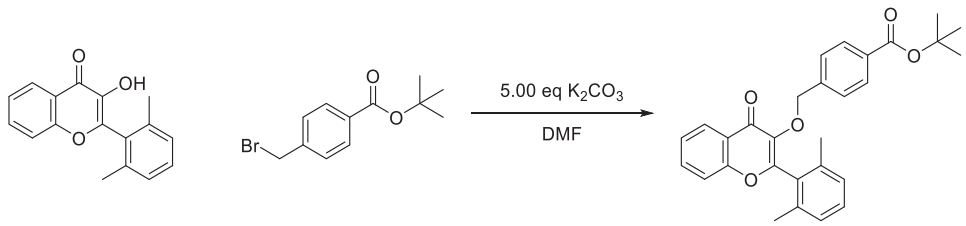

2g was synthesised according to general procedure 2.5 on a 2 mmol scale and obtained as a colourless solid with a yield of 96 % (1.93 mmol, 879 mg).

^{1}H NMR (300 MHz, DMSO-d_6) δ 8.21 (ddd, *J* = 8.0, 1.7, 0.5 Hz, 1H), 7.84 (ddd, *J* = 8.6, 7.0, 1.7 Hz, 1H), 7.75 – 7.64 (m, 3H), 7.55 (ddd, *J* = 8.1, 7.0, 1.1 Hz, 1H), 7.37 (dd, *J* = 8.1, 7.1 Hz, 1H), 7.23 – 7.13 (m, 2H), 7.12 – 7.01 (m, 2H), 5.05 (s, 2H), 2.12 (s, 6H), 1.53 (s, 9H).

^{13}C NMR (75 MHz, DMSO-d_6) δ 173.6, 164.6, 157.3, 155.3, 141.9, 139.9, 136.9, 134.2, 130.7, 130.1, 129.9, 128.8, 127.4, 125.3, 125.1, 123.9, 118.5, 80.7, 72.6, 27.7, 19.2.

M.p.: 54.5 °C; **HPLC**: R_t=21.00 min, purity ≥ 99 %, **MS** (+APCI): 457 $[M+H]^+$.

2.3.8 Synthesis of tert-butyl 4-(((2-(3,5-dimethylphenyl)-4-oxo-4H-chromen-3-yl)oxy)methyl)benzoate (2h)

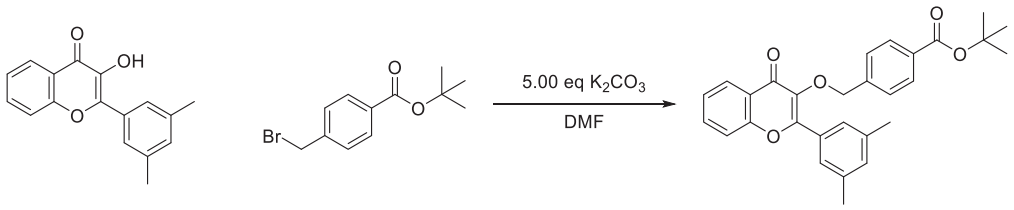

2h was synthesised according to general procedure 2.5 on a 2 mmol scale and obtained as a colourless solid with a yield of 77 % (1.53 mmol, 700 mg).

^{1}H NMR (300 MHz, Chloroform-*d*) δ 8.29 (ddd, *J* = 8.0, 1.7, 0.5 Hz, 1H), 7.91 – 7.82 (m, 2H), 7.68 (ddd, *J* = 8.6, 7.1, 1.7 Hz, 1H), 7.59 – 7.49 (m, 3H), 7.42 (ddd, *J* = 8.1, 7.0, 1.1 Hz, 1H), 7.39 – 7.29 (m, 2H), 7.12 (tt, *J* = 1.7, 0.8 Hz, 1H), 5.17 (s, 2H), 2.35 (q, *J* = 0.7 Hz, 6H), 1.59 (s, 9H).

^{13}C NMR (126 MHz, Chloroform-*d*) δ 175.2, 165.7, 157.3, 155.5, 141.5, 139.9, 138.0, 133.5, 132.5, 131.7, 130.9, 129.4, 128.3, 126.7, 126.0, 124.8, 124.4, 118.2, 81.1, 73.7, 28.4, 21.4.

M.p.: 150.5 °C; **HPLC**: R_t=21.95 min, purity ≥ 99 %, **MS** (+APCI): 457 $[M+H]^+$.

2.3.9 Synthesis of tert-butyl 4-(((4-oxo-2-(pyridine-3-yl)-4H-chromen-3-yl)oxy)methyl)benzoate (2i)

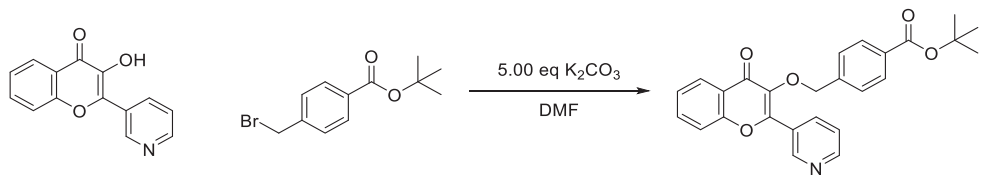

2i was synthesised according to general procedure 2.5 on a 1 mmol scale and obtained as a colourless solid with a yield of 89 % (0.887 mmol, 381 mg).

^{1}H NMR (600 MHz, Chloroform-*d*) δ 9.19 (d, *J* = 2.1 Hz, 1H), 8.64 (dd, *J* = 4.9, 1.6 Hz, 1H), 8.23 (dd, *J* = 8.0, 1.6 Hz, 1H), 8.21 (dt, *J* = 8.0, 2.0 Hz, 1H), 7.84 – 7.79 (m, 2H), 7.66 (ddd, *J* = 8.6, 7.0, 1.7 Hz, 1H), 7.49 (d, *J* = 8.4 Hz, 1H), 7.44 – 7.35 (m, 1H), 7.37 – 7.31 (m, 1H), 7.29 (d, *J* = 8.1 Hz, 2H), 5.22 (s, 2H), 1.54 (s, 9H).

^{13}C NMR (75 MHz, DMSO-d_6) δ 173.8, 163.8, 154.9, 153.7, 151.2, 149.0, 139.6, 139.5, 135.9, 134.3, 132.4, 128.1, 126.8, 126.7, 125.3, 125.0, 123.5, 123.5, 118.6, 72.8.

M.p.: 96:9 °C; **HPLC**: R_t=min, purity ≥ %, **MS** (+APCI): 430 $[M+H]^+$.

2.4 General procedure for the synthesis of Hydroxamic acids (**3**).

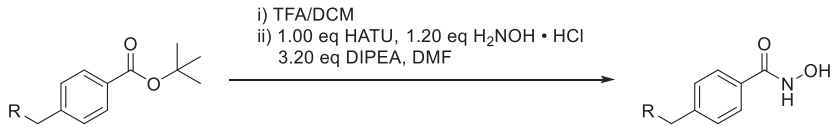

1.00 eq of the respective *tert*-butyl ester was dissolved in a mixture of TFA/DCM (1:1, 10 mL/mmol) and stirred for 3 h at ambient temperature. The reaction was acidified with a 1 M HCl solution to pH=4 and the product extracted with EtOAc, after which the combined layers were dried over Na_2SO_4 and the product dried *in vacuo*. Subsequently, the obtained carboxylic acid was dissolved in dry DMF (10 mL/mmol), 1.00 eq HATU and 3.20 eq DIPEA were added and the solution stirred for 10 minutes. Afterwards, 1.00 eq of 1.20 eq H_2NOH • HCl was added to the solution. After 16 h at RT. The solvent was removed under reduced pressure and the product purified by reverse flash column chromatography (H_2O/I).

2.4.1 Synthesis of *N*-hydroxy-4-(((4-oxo-4*H*-chromen-3-yl)oxy)methyl)benzamide (**3a**)

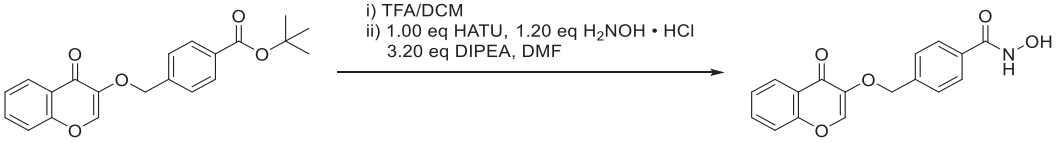

3a was synthesised according to general procedure 2.14 on a 1.00 mmol scale and the product was obtained as a white solid with a yield of 68 % (0.678 mmol, 211 mg).

^{1}H NMR (300 MHz, DMSO-d_6) δ 11.25 (s, 1H), 9.06 (s, 1H), 8.42 (s, 1H), 8.12 (dd, *J* = 8.0, 1.6 Hz, 1H), 7.89 – 7.72 (m, 3H), 7.65 (dd, *J* = 8.7, 1.0 Hz, 1H), 7.57 – 7.50 (m, 2H), 7.47 (ddd, *J* = 8.1, 7.0, 1.1 Hz, 1H), 5.10 (s, 2H).

^{13}C NMR (75 MHz, DMSO-d_6) δ 172.28, 163.92, 155.17, 144.03, 142.79, 139.54, 133.95, 132.50, 127.85, 127.05, 125.16, 124.93, 123.50, 118.45, 71.01.

M.p.: 187.1 °C; **HPLC**: R_t=7.99 min, purity ≥ 99 %, **MS** (+APCI): 312 $[M+H]^+$.

2.4.2 Synthesis of *N*-hydroxy-4-(((4-oxo-2-phenyl-4*H*-chromen-3-yl)oxy)methyl)benzamide (**3b**)

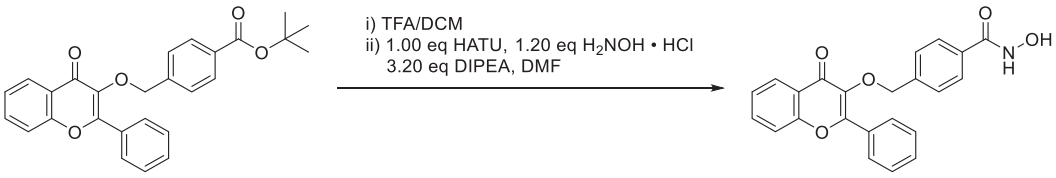

3b was synthesised according to general procedure 2.14 on a 0.467 mmol scale and the product was obtained as a white solid with a yield of 41 % (0.192 mmol, 74.4 mg).

^{1}H NMR (300 MHz, DMSO-d_6) δ 11.20 (s, 1H), 9.03 (s, 1H), 8.15 (dd, *J* = 8.0, 1.6 Hz, 1H), 8.06 – 7.94 (m, 2H), 7.85 (ddd, *J* = 8.6, 6.9, 1.7 Hz, 1H), 7.76 (dd, *J* = 8.5, 1.1 Hz, 1H), 7.72 – 7.64 (m, 2H), 7.62 – 7.47 (m, 4H), 7.44 – 7.35 (m, 2H), 5.14 (s, 2H).

^{13}C NMR (75 MHz, DMSO-d_6) δ 173.9, 163.8, 155.8, 154.7, 139.7, 139.2, 134.0, 132.3, 130.8, 130.3, 128.4, 128.4, 127.8, 126.7, 125.1, 124.9, 123.5, 118.4, 72.7.

M.p.: 183.4 °C; **HPLC**: R_t=11.48 min, purity = 97.5 %, **MS** (+APCI): 388 $[M+H]^+$.

2.4.3 Synthesis of 4-(((2-(2-fluorophenyl)-4-oxo-4*H*-chromen-3-yl)oxy)methyl)-*N*-hydroxybenzamide (**3c**)

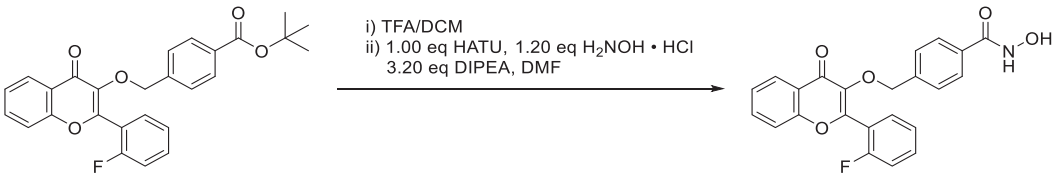

3c was synthesised according to general procedure 2.14 on a 1.0 mmol scale and the product was obtained as a white solid with a yield of 55 % (0.548 mmol, 222 mg).

^{1}H NMR (300 MHz, DMSO-d_6) δ 11.18 (s, 1H), 9.09 – 8.96 (m, 1H), 8.19 (dd, *J* = 8.1, 1.6 Hz, 1H), 7.86 (ddd, *J* = 8.7, 7.1, 1.7 Hz, 1H), 7.70 (dd, *J* = 8.7, 1.0 Hz, 1H), 7.67 – 7.50 (m, 5H), 7.44 – 7.29 (m, 2H), 7.23 – 7.09 (m, 2H), 5.11 (s, 2H).

^{13}C NMR (75 MHz, DMSO-d_6) δ 173.6, 163.8, 159.2 (d, *J* = 250.7 Hz), 155.1, 153.0, 139.9, 139.7, 134.4, 133.2 (d, *J* = 8.7 Hz), 132.2, 131.3 (d, *J* = 2.1 Hz), 127.7, 126.7, 125.4, 125.2, 124.5 (d, *J* = 3.5 Hz), 123.8, 118.5, 118.5 (d, *J* = 14.5 Hz), 116.0 (d, *J* = 21.1 Hz), 72.8.

M.p.: 181.4 °C; **HPLC**: R_t=11.30 min, purity ≥ 99 %, **MS** (+APCI): 406 $[M+H]^+$.

2.4.4 Synthesis of 4-(((2-(2-chlorophenyl)-4-oxo-4*H*-chromen-3-yl)oxy)methyl)-*N*-hydroxybenzamide (3d)

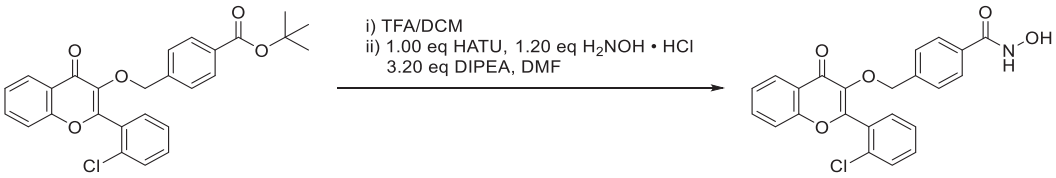

3d was synthesised according to general procedure 2.14 on a 1.0 mmol scale and the product was obtained as a white solid with a yield of 56 % (0.559 mmol, 236 mg).

^{1}H NMR (300 MHz, DMSO-d_6) δ 11.17 (s, 1H), 9.01 (s, 1H), 8.20 (dd, *J* = 8.0, 1.6 Hz, 1H), 7.85 (ddd, *J* = 8.6, 7.1, 1.7 Hz, 1H), 7.69 (dd, *J* = 8.7, 0.9 Hz, 1H), 7.67 – 7.45 (m, 7H), 7.16 – 7.04 (m, 2H), 5.09 (s, 2H).

^{13}C NMR (75 MHz, DMSO-d_6) δ 173.8, 163.8, 155.6, 155.0, 139.8, 139.7, 134.4, 132.5, 132.3, 131.7, 129.6, 129.5, 127.6, 127.2, 126.8, 125.4, 125.1, 123.9, 118.5, 72.9.

M.p.: 157.3 °C; **HPLC**: R_t=11.30 min, purity ≥ 99 %, **MS** (+APCI): 422 $[M+H]^+$.

2.4.5 Synthesis of 4-(((2-(2-bromophenyl)-4-oxo-4*H*-chromen-3-yl)oxy)methyl)-*N*-hydroxybenzamide (3e)

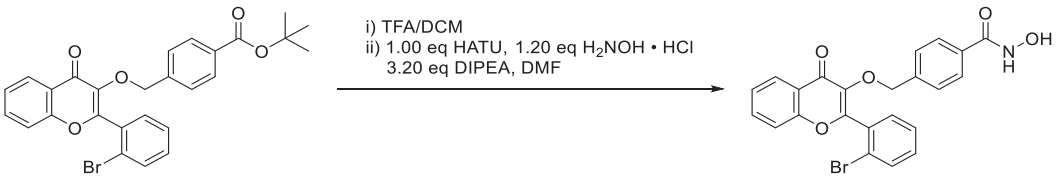

3e was synthesised according to general procedure 2.14 on a 1.0 mmol scale and the product was obtained as a white solid with a yield of 67 % (0.667 mmol, 311 mg).

^{1}H NMR (300 MHz, DMSO-d_6) δ 11.17 (d, *J* = 1.9 Hz, 1H), 9.01 (d, *J* = 1.9 Hz, 1H), 8.20 (ddd, *J* = 8.0, 1.7, 0.5 Hz, 1H), 7.91 – 7.77 (m, 2H), 7.71 (ddd, *J* = 8.5, 1.1, 0.5 Hz, 1H), 7.64 – 7.48 (m, 6H), 7.17 – 7.05 (m, 2H), 5.09 (s, 2H).

^{13}C NMR (75 MHz, DMSO-d_6) δ 173.9, 163.9, 156.9, 155.0, 139.8, 139.7, 134.5, 132.8, 132.4, 132.3, 131.8, 131.6, 127.7, 127.7, 126.8, 125.5, 125.2, 123.9, 122.3, 118.5, 73.0.

M.p.: 142.9 °C; **HPLC**: R_t= 12.06 min, purity ≥ 99 %, **MS** (+APCI): 466 $[M+H]^+$.

2.4.6 Synthesis of 4-(((2-(2,6-difluorophenyl)-4-oxo-4*H*-chromen-3-yl)oxy)methyl)-*N*-hydroxybenzamide (**3f**)

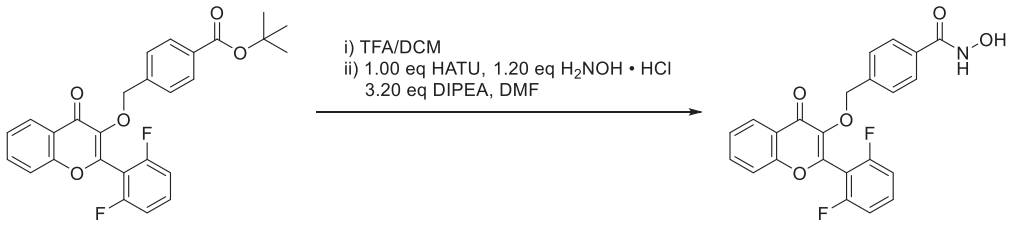

3f was synthesised according to general procedure 2.14 on a 1.0 mmol scale and the product was obtained as a white solid with a yield of 42 % (0.418 mmol, 177 mg).

^{1}H NMR (300 MHz, DMSO-d_6) δ 11.18 (s, 1H), 9.02 (s, 1H), 8.20 (dd, *J* = 8.0, 1.6 Hz, 1H), 7.86 (ddd, *J* = 8.7, 7.1, 1.7 Hz, 1H), 7.78 – 7.65 (m, 2H), 7.64 – 7.53 (m, 3H), 7.31 – 7.20 (m, 2H), 7.17 – 7.08 (m, 2H), 5.14 (s, 2H).

^{13}C NMR (75 MHz, DMSO-d_6) δ 173.3, 163.7, 159.5 (dd, *J* = 252.1, 6.2 Hz), 155.2, 147.5, 141.0, 139.3, 134.6, 134.0 (t, *J* = 10.5 Hz), 132.3, 127.7, 126.7, 125.6, 125.2, 123.7, 118.4, 112.0 (d, *J* = 24.2 Hz), 108.3 – 107.4 (m), 72.8.

M.p.: 183.6 °C; **HPLC**: R_t= 11.46 min, purity ≥ 99 %, **MS** (+APCI): 424 $[M+H]^+$.

2.4.7 Synthesis of 4-(((2-(2,6-dimethylphenyl)-4-oxo-4*H*-chromen-3-yl)oxy)methyl)-*N*-hydroxybenzamide (**3g**)

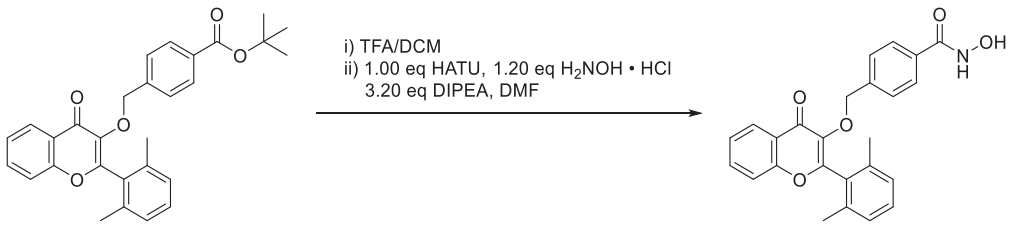

3g was synthesised according to general procedure 2.14 on a 1.0 mmol scale and the product was obtained as a white solid with a yield of 47 % (0.474 mmol, 197 mg).

^{1}H NMR (300 MHz, DMSO-d_6) δ 11.16 (s, 1H), 9.06 – 8.94 (m, 1H), 8.20 (dd, *J* = 8.0, 1.6 Hz, 1H), 7.83 (ddd, *J* = 8.6, 7.1, 1.7 Hz, 1H), 7.68 (dd, *J* = 8.6, 0.9 Hz, 1H), 7.61 – 7.49 (m, 3H), 7.37 (dd, *J* = 8.1, 7.1 Hz, 1H), 7.26 – 7.14 (m, 2H), 7.08 – 6.93 (m, 2H), 5.03 (s, 2H), 2.10 (s, 6H).

^{13}C NMR (75 MHz, DMSO-d_6) δ 173.7, 163.8, 157.3, 155.3, 140.0, 139.8, 137.0, 134.2, 132.2, 130.1, 129.9, 127.4, 126.7, 125.3, 125.1, 123.9, 118.5, 72.7, 19.2.

M.p.: 183.6 °C; **HPLC**: R_t= 12.45 min, purity ≥ 99 %, **MS** (+APCI): 416 $[M+H]^+$.

2.4.8 Synthesis of 4-(((2-(3,5-dimethylphenyl)-4-oxo-4*H*-chromen-3-yl)oxy)methyl)-*N*-hydroxybenzamide (**3h**)

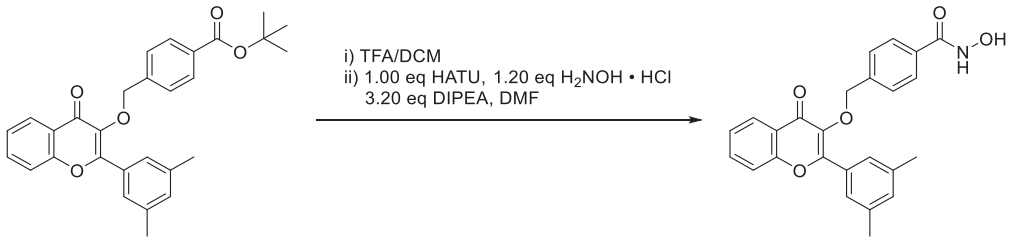

3h was synthesised according to general procedure 2.14 on a 1.00 mmol scale and the product was obtained as a white solid with a yield of 60 % (0.602 mmol, 250 mg).

^{1}H NMR (300 MHz, DMSO-d_6) δ 11.23 (d, *J* = 2.0 Hz, 1H), 9.04 (d, *J* = 1.9 Hz, 1H), 8.13 (dd, *J* = 8.0, 1.6 Hz, 1H), 7.83 (ddd, *J* = 8.5, 6.9, 1.7 Hz, 1H), 7.78 – 7.67 (m, 3H), 7.57 (d, *J* = 1.6 Hz, 2H), 7.51 (ddd, *J* = 8.1, 6.9, 1.3 Hz, 1H), 7.45 – 7.36 (m, 2H), 7.17 (s, 1H), 5.13 (s, 2H), 2.29 (s, 6H).

^{13}C NMR (75 MHz, DMSO-d_6) δ 174.0, 163.8, 156.1, 154.8, 139.8, 139.3, 137.6, 134.1, 132.3, 130.2, 128.0, 126.8, 126.2, 125.2, 125.0, 123.5, 118.5, 72.9, 20.9.

M.p.: 194.3 °C; **HPLC**: R_t= 13.31 min, purity = 96.4 %, **MS** (+APCI): 416 $[M+H]^+$

2.4.9 Synthesis of *N*-hydroxy-4-(((4-oxo-2-(pyridine-3-yl)-4*H*-chromen-3-yl)oxy)methyl)benzamide (**3i**)

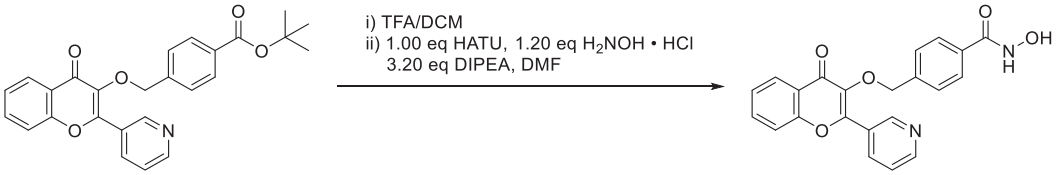

3i was synthesised according to general procedure 2.14 on a 0.467 mmol scale and the product was obtained as a white solid with a yield of 64 % (0.53 mmol, 206 mg).

^{1}H NMR (300 MHz, DMSO-d_6) δ 11.20 (s, 1H), 9.13 (dd, *J* = 2.3, 0.9 Hz, 1H), 9.04 (s, 1H), 8.70 (dd, *J* = 4.9, 1.6 Hz, 1H), 8.31 (dt, *J* = 8.1, 2.0 Hz, 1H), 8.15 (dd, *J* = 8.0, 1.6 Hz, 1H), 7.86 (ddd, *J* = 8.6, 7.0, 1.7 Hz, 1H), 7.77 (dd, *J* = 8.6, 1.1 Hz, 1H), 7.70 – 7.62 (m, 2H), 7.61 – 7.49 (m, 2H), 7.43 – 7.31 (m, 2H), 5.19 (s, 2H).

^{13}C NMR (75 MHz, DMSO-d_6) δ 173.8, 163.8, 154.9, 153.7, 151.2, 149.0, 139.6, 139.5, 135.9, 134.3, 132.4, 128.1, 126.8, 126.7, 125.3, 125.0, 123.5, 123.5, 118.6, 72.8.m.p.: °C; HPLC: Rt=6.60 min, purity = 95.1 %, ESI-MS:

M.p.: 175.0 °C; **HPLC**: R_t= 6.59 min, purity ≥ 99 %, **MS** (+APCI): 389 $[M+H]^+$.

2.5 Synthesis of 4-oxo-2-phenyl-4*H*-chromen-3-yl trifluoromethanesulfonate (**4**)

1.00 eq (3.65 mmol, 870 mg) of **1b** was dissolved in 50 mL of dry DCM and cooled on ice and 2.10 eq (7.76 mmol, 996 mg, 1.34 mL) of DIPEA were added. Afterwards, 2.00 eq of Tf_2O was added dropwise and stirred for 3 h to RT. The solvent was removed under reduced pressure, the residue resuspended in 50 mL of EtOAc, washed with dH_2O (x3) and brine (x1) and dried over Na_2SO_4. The product was purified by column chromatography (*n*-hexane/EtOAc) and the combined product fractions recrystallised from *n*-hexane /EtOAc. 1.30 g (3.51 mmol, 96 %) of **4** was obtained as colourless crystals.

^{1}H NMR (300 MHz, DMSO-d_6) δ 8.18 (dd, *J* = 8.0, 1.6 Hz, 1H), 8.02 – 7.88 (m, 3H), 7.90 – 7.80 (m, 1H), 7.78 – 7.58 (m, 4H).

^{13}C NMR (151 MHz, DMSO-d_6) δ 170.9, 159.3, 155.5, 136.1, 134.0, 133.0, 129.4 (d, *J* = 3.4 Hz), 128.4, 127.0, 125.7, 123.2, 119.5, 118.1 (q, *J* = 320.6 Hz).

M.p.: 110.9 °C; **HPLC**: R_t=16.50 min, purity ≥ 99 %, **MS** (+APCI): 371 $[M+H]^+$.

2.6 Synthesis of tert-butyl 4-((1,3-dioxoisoindolin-2-yl)methyl)benzoate (**5**)

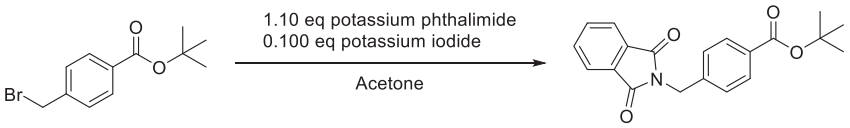

1.00 eq (14.5 mmol, 4.00 g) of *tert*-butyl 4-(bromomethyl)benzoate was combined with 1.10 eq (15.9 mmol, 2.95 g) of potassium phthalimide and 0.100 eq (1.45 mmol, 0.217 g) of KI in 50 mL oh acetone. After 16 h at reflux, the solution was cooled to ambient temperature and filtered through celite. The solvent was removed under reduced pressure and the residue washed with sat. aq. $NaHCO_3$ solution (x3) and dH_2O (x3). After recrystallisation in EtOH, 4.4 g (13 mmol, 90 %) of **5** was obtained as a colourless solid.

^{1}H NMR (600 MHz, DMSO-d_6) δ 7.96 – 7.89 (m, 2H), 7.89 – 7.83 (m, 4H), 7.52 – 7.36 (m, 2H), 4.84 (s, 2H), 1.52 (s, 9H).

^{13}C NMR (151 MHz, DMSO-d_6) δ 168.1, 165.1, 142.0, 135.1, 132.0, 130.9, 129.8, 127.9, 123.7, 81.1, 41.1, 28.2.**M.p.**: 149.2 °C; **HPLC**: R_t=16.37 min, purity ≥ 99 %, **MS** (+APCI): 282 $[M-^t Bu+2H]^+$.

2.7 Synthesis of tert-butyl 4-(aminomethyl)benzoate hydrochloride (**6**)

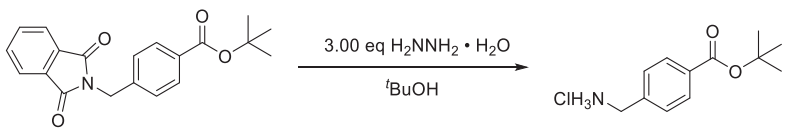

1.00 eq (11.9 mmol, 4.00 g) of **5** was combined with 3.00 eq (35.6 mmol, 38.8 g, 1.76 mmol) of hydrazine monohydrate in 50 mL of ^{t}BuOH and stirred for 16 h at 60 °C. The resulting precipitate was removed by filtration, thoroughly washed with DCM and the filtrate purified by flash column chromatography ((DCM/MeOH) +0.1% TEA). The obtained product was mixed with DCM, cooled on ice and precipitated with 3.00 eq (35.6 mmol, 8.89 mL) of a 4M HCl solution in dioxane. 2.72 g (11.2 mmol, 94 %) of **6** was obtained as a colourless solid.

^{1}H NMR (600 MHz, DMSO-d_6) δ 8.71 (s, 3H), 7.95 – 7.86 (m, 2H), 7.68 – 7.60 (m, 2H), 4.09 (s, 2H), 1.55 (s, 9H).

^{13}C NMR (75 MHz, DMSO-d_6) δ 164.5, 138.9, 131.1, 129.0 (d, J = 4.2 Hz), 80.9, 41.7, 27.7.

M.p.: 256 °C; **HPLC**: R_t=7.82 min, purity ≥ 99 %, **MS** (+APCI): 208 $[M+H]^+$.

2.8 Synthesis of *tert*-butyl 4-((4-oxo-2-phenyl-4*H*-chromen-3-yl)amino)benzoate (**7a**)

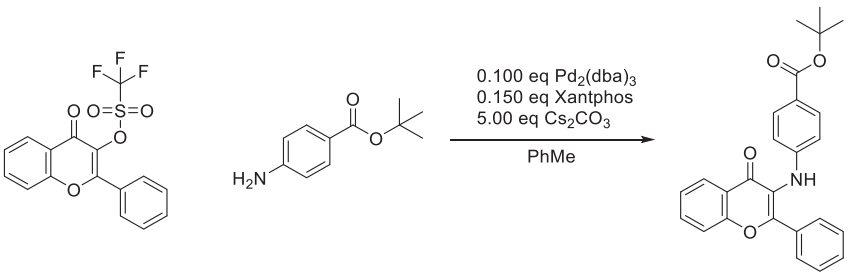

0.100 eq (0.162 mmol, 141 mg) of $Pd_2(dba)_3$, 0.150 eq (0.243, 141 mg) of Xantphos and 5.00 eq (8.1 mmol, 2.6 g) of Cs_2CO_3 were suspended in 10 mL of dry, degassed toluene and stirred for 10 minutes at ambient temperature. Subsequently, 1.00 eq (1.62 mmol, 600 mg) of **4** as well as 0.900 eq (1.46 mmol, 282 mg) of *tert*-Butyl 4-Aminobenzoate were added to the reaction mixture and stirred for 16 h at 100°C. The solution was filtered over celite, the solvent of the filtrate removed under reduced pressure and the product purified by flash column chromatography (Hex/EtOAc). 553 mg (1.34 mmol, 92 %) of **7a** was obtained as a yellow solid.

^{1}H NMR (600 MHz, DMSO-d_6) δ 8.10 (dd, J = 8.0, 1.7 Hz, 1H), 8.05 (s, 1H), 7.90 – 7.85 (m, 3H), 7.78 (dd, J = 8.5, 1.0 Hz, 1H), 7.59 (d, J = 8.8 Hz, 2H), 7.53 (ddd, J = 8.1, 7.1, 1.1 Hz, 1H), 7.50 – 7.46 (m, 3H), 6.63 (d, J = 8.7 Hz, 2H), 1.48 (s, 9H).

^{13}C NMR (151 MHz, DMSO- d_6) δ 175.7, 165.6, 161.2, 155.8, 151.1, 134.8, 132.1, 131.4, 131.0, 129.0, 128.6, 125.9, 125.7, 123.3, 121.8, 120.3, 119.0, 113.1, 28.4.

M.p.: 100.2°C; HPLC: R_t=17.60 min, purity ≥ 99 %, **MS** (+APCI): 414 $[M+H]^+$.

2.9 Synthesis of *tert*-butyl 4-((4-oxo-2-(155yridine-3-yl)-4*H*-chromen-3-yl)amino)benzoate (**7b**)

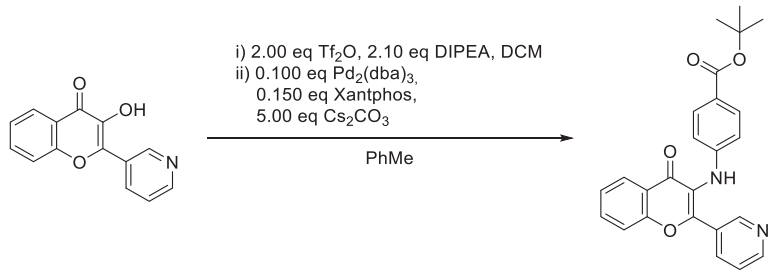

1.00 eq (2.10 mmol, 870 mg) of **1i** was dissolved in 50 mL of dry DCM and cooled on ice and 2.10 eq (4.18 mmol, 543 mg, 0.732 mL) of DIPEA were added. Afterwards, 2.00 eq (4.18 mmol, 1.18 g, 0.703 mL) of Tf_2O was added dropwise and stirred for 3 h to RT. The solvent was removed under reduced pressure, the residue resuspended in 50 mL of EtOAc, washed with dH_2O (x3) and brine (x1), dried over Na_2SO_4 and the solvent remove *in vacuo*. 0.100 eq (0.200 mmol, 183 mg) of $Pd_2(dba)_3$, 0.150 eq (0.300, 174 mg) of Xantphos and 5.00 eq (10.0 mmol, 3.3 g) of Cs_2CO_3 were suspended in 20 mL of dry, degassed toluene and stirred for 10 minutes at ambient temperature. Subsequently, 1.00 eq (2.00 mmol, 743 mg) of the triflated chromenone as well as 1.00 eq (2.00 mmol, 394 mg) of *tert*-Butyl 4-Aminobenzoate were added to the reaction mixture and stirred for 16 h at 100°C. The solution was filtered over celite, the solvent of the filtrate removed under reduced pressure and the product purified by flash column chromatography (Hex/EtOAc). 175 mg (0.422 mmol, 21 %) of **7b** was obtained as a yellow solid.

^{1}H NMR (600 MHz, DMSO-d_6) δ 9.04 (dd, *J* = 2.3, 0.9 Hz, 1H), 8.66 (dd, *J* = 4.9, 1.7 Hz, 1H), 8.30 – 8.19 (m, 1H), 8.15 – 8.08 (m, 2H), 7.89 (ddd, *J* = 8.7, 7.1, 1.7 Hz, 1H), 7.84 – 7.79 (m, 1H), 7.63 – 7.58 (m, 2H), 7.57 – 7.51 (m, 2H), 6.72 – 6.62 (m, 2H), 1.48 (s, 9H).

^{13}C NMR (126 MHz, DMSO-d_6) δ 175.0, 164.9, 158.4, 155.3, 151.1, 150.2, 148.6, 135.5, 134.3, 130.4, 127.8, 125.4, 125.2, 123.4, 122.8, 122.1, 120.2, 118.5, 112.8, 79.2, 27.8.

M.p.: 100.2°C; **HPLC**: R_t=12.17 min, purity ≥ 99 %, **MS** (+APCI): 415 $[M+H]^+$.

2.10 Synthesis of *tert*-butyl 4-(((4-oxo-2-phenyl-4*H*-chromen-3-yl)amino)methyl)benzoate (**7c**)

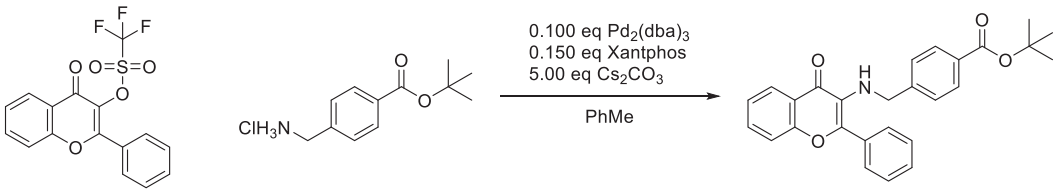

0.100 eq (0.150 mmol, 137 mg) of $Pd_2(dba)_3$, 0.150 eq (0.225, 130 mg) of Xantphos and 5.00 eq (7.50 mmol, 2.4 g) of Cs_2CO_3 were suspended in 10 mL of dry, degassed toluene and stirred for 10 minutes at ambient temperature. Subsequently, 1.10 eq (1.65 mmol, 611 mg) of **6** as well as 1.00 eq (1.50 mmol, 366 mg) of **4** were added to the reaction mixture and stirred for 16 h at 100°C. The solution was filtered over celite, the solvent of the filtrate removed under reduced pressure and the product purified by flash column chromatography (Hex/EtOAc). 600 mg (1.40 mmol, 94 %) of **7c** was obtained as a yellow solid.

^{1}H NMR (300 MHz, DMSO-d_6) δ 8.10 (ddd, *J* = 8.0, 1.7, 0.5 Hz, 1H), 7.93 – 7.82 (m, 2H), 7.75 (ddd, *J* = 8.7, 7.0, 1.7 Hz, 1H), 7.72 – 7.65 (m, 2H), 7.65 – 7.52 (m, 4H), 7.44 (ddd, *J* = 8.1, 7.0, 1.1 Hz, 1H), 7.10 – 6.99 (m, 2H), 5.37 (t, *J* = 7.5 Hz, 1H), 3.92 (d, *J* = 7.5 Hz, 2H), 1.49 (s, 10H).

^{13}C NMR (75 MHz, DMSO-d_6) δ 174.2, 164.6, 154.9, 147.7, 144.9, 133.6, 132.7, 130.1, 129.9, 129.5, 128.9, 128.6, 128.1, 127.4, 125.0, 124.6, 120.2, 118.3, 80.5, 48.8, 27.7.

M.p.: 136.6 °C; **HPLC**: R_t=20.08 min, purity ≥ 98.5 %, **MS** (+APCI): 428 $[M+H]^+$.

2.11 Synthesis of *N*-hydroxy-4-((4-oxo-2-phenyl-4*H*-chromen-3-yl)amino)benzamide (**8a**)

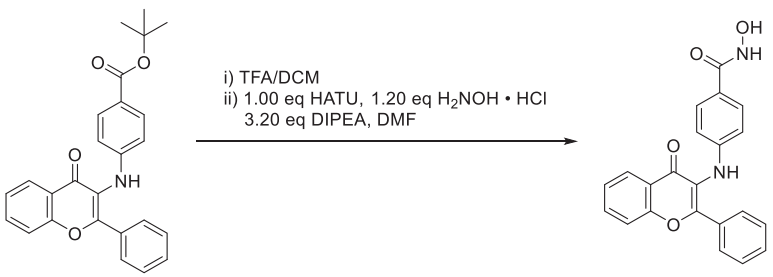

8a was synthesised according to general procedure 2.4 on a 0.630 mmol scale and the product was obtained as a yellow solid with a yield of 90 % (0.567 mmol, 211 mg).

^{1}H NMR (600 MHz, DMSO-d_6) δ 10.82 (s, 1H), 8.73 (s, 1H), 8.09 (dd, *J* = 8.0, 1.7 Hz, 1H), 7.93 – 7.88 (m, 2H), 7.86 (ddd, *J* = 8.7, 7.1, 1.7 Hz, 1H), 7.82 (s, 1H), 7.78 (dd, *J* = 8.5, 1.0 Hz, 1H), 7.53 (ddd, *J* = 8.1, 7.1, 1.1 Hz, 1H), 7.50 – 7.40 (m, 5H), 6.68 – 6.55 (m, 2H).

^{13}C NMR (126 MHz, DMSO-d_6) δ 175.3, 164.7, 160.4, 155.2, 149.1, 134.1, 131.6, 130.7, 128.3, 128.1, 127.9, 125.2, 125.1, 122.7, 121.6, 121.4, 118.4, 112.7.

M.p.: 190.1°C; **HPLC**: R_t= 10.30 min, purity ≥ 99 %, **MS** (+APCI): 373 $[M+H]^+$.

2.12 Synthesis of *N*-hydroxy-4-((4-oxo-2-(pyridine-3-yl)-4*H*-chromen-3-yl)amino)benzamide (**8b**)

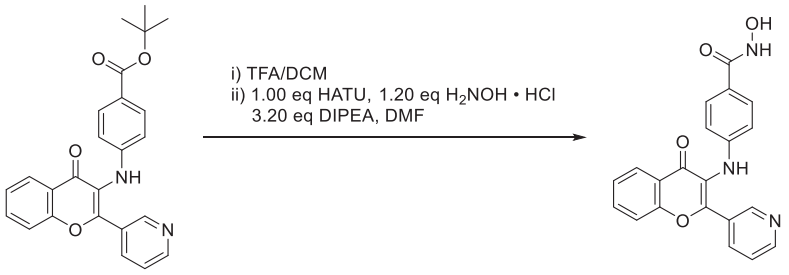

8b was synthesised according to general procedure 2.4 on a 0.63 mmol scale and the product was obtained as a yellow solid with a yield of 39 % (0.112 mmol, 41.7 mg).

^{1}H NMR (600 MHz, DMSO-d_6) δ 10.84 (s, 1H), 9.06 (d, *J* = 2.2 Hz, 1H), 8.65 (dd, *J* = 4.8, 1.6 Hz, 1H), 8.26 (dt, *J* = 8.0, 2.0 Hz, 1H), 8.10 (dd, *J* = 8.0, 1.6 Hz, 1H), 7.89 (d, *J* = 1.8 Hz, 1H), 7.89 – 7.86 (m, 1H), 7.80 (d, *J* = 8.4 Hz, 1H), 7.53 (tdd, *J* = 9.9, 5.8, 2.5 Hz, 2H), 7.51 – 7.47 (m, 2H), 6.70 – 6.59 (m, 2H).

^{13}C NMR (151 MHz, DMSO-d_6) δ 175.8, 165.1, 158.9, 155.9, 151.7, 149.4, 149.2, 136.1, 134.9, 128.6, 128.5, 126.0, 125.7, 124.0, 123.3, 122.9, 122.2, 119.1, 113.4.

M.p.: 135.9°C; **HPLC**: Rt= 5.90 min, purity ≥ 99 %, **MS** (+APCI): 374 $[M+H]^+$.

2.13 Synthesis of *N*-hydroxy-4-(((4-oxo-2-phenyl-4*H*-chromen-3-yl)amino)methyl)benzamide (**8c**)

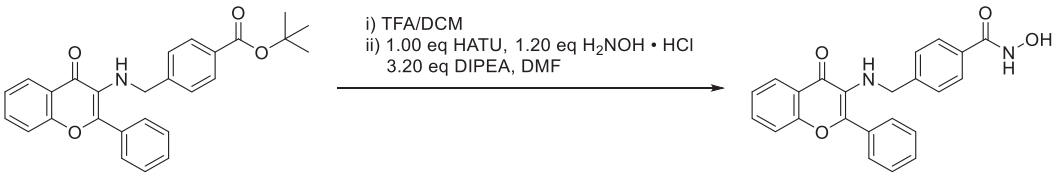

8c was synthesised according to general procedure 2.4 on a 0.700 mmol scale and the product was obtained as a yellow solid with a yield of 77 % (0.536 mmol, 207 mg).

^{1}H NMR (600 MHz, DMSO-d_6) δ 11.08 (s, 1H), 8.95 (s, 1H), 8.09 (dd, J = 8.0, 1.7 Hz, 1H), 7.92 – 7.81 (m, 2H), 7.74 (ddd, J = 8.7, 7.0, 1.7 Hz, 1H), 7.64 – 7.49 (m, 6H), 7.43 (ddd, J = 8.0, 7.0, 1.0 Hz, 1H), 7.07 – 6.95 (m, 2H), 5.26 (t, J = 7.4 Hz, 1H), 3.89 (d, J = 6.7 Hz, 2H).

^{13}C NMR (75 MHz, DMSO- d_6) δ 174.2, 164.0, 154.9, 147.7, 143.0, 133.7, 132.8, 131.4, 130.1, 129.7, 128.6, 128.2, 127.2, 126.8, 125.1, 124.6, 120.3, 118.3, 49.0.

M.p.: 178.9 °C; **HPLC**: R_t= 11.69 min, purity ≥ 99 %, **MS** (+APCI): 383 $[M+H]^+$.

2.14 Synthesis of 2-acetylphenyl 2-nitrobenzoate (**9**)

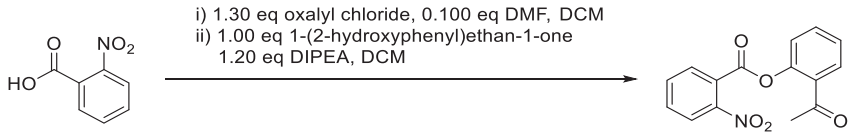

1.10 eq (44.0 mmol, 7.35 g) of 2-nitrobenzoic acid was suspended in 40 mL of dry DCM and 1.30 eq (52.0 mmol, 6.6 g, 4.4 mL) of oxalyl chloride as well as 0.10 eq (4.00 mmol, 0.292 g, 0.31 mL) of dry DMF were added to the reaction solution. After 3 h at reflux temperature, the solvent was removed under reduced pressure. Subsequently, 1.00 eq (40.0 mmol, 5.50 g, 4.86 mL) of 2′-hydroxyacetophenone was dissolved in 30 mL of dry DCM and 1.20 eq (48.0 mmol, 6.20 g, 8.36 mL) of DIPEA added. The obtained acid chloride was dissolved in 10 mL of dry DCM, added dropwise to the 2′-hydroxyacetophenone solution at 0 °C and the resulting reaction mixture stirred for 16 h to ambient temperature. DCM was removed under reduced pressure, the resulting residue resuspended in EtOAc and washed with dH_2O (x3) and brine (x1). The organic phase was dried over Na_2SO_4 and the solvent removed *in vacuo*. Finally, the residue was recrystallised from *n*-hexane/EtOAc. 10.93 g (38.4 mmol, 87 %) of **8** was obtained as organe crystals.

^{1}H NMR (300 MHz, DMSO-d_6) δ 8.17 (td, *J* = 7.6, 1.6 Hz, 2H), 8.08 – 7.86 (m, 3H), 7.75 (td, *J* = 7.8, 1.7 Hz, 1H), 7.52 (td, *J* = 7.6, 1.2 Hz, 1H), 7.34 (dd, *J* = 8.1, 1.2 Hz, 1H), 2.56 (s, 3H).

^{13}C NMR (75 MHz, DMSO-d_6) δ 197.4, 162.9, 147.8, 147.5, 133.8, 133.8, 133.4, 130.7, 130.3, 130.1, 126.9, 125.2, 124.2, 123.1, 29.1.**M.p.**: 125.2°C; **HPLC**: R_t=12.80 min, purity ≥ 99 %, **MS** (+APCI): 286 $[M+H]^+$.

2.15 Synthesis of 2-(2-nitrophenyl)-4*H*-chromen-4-one (**10**)

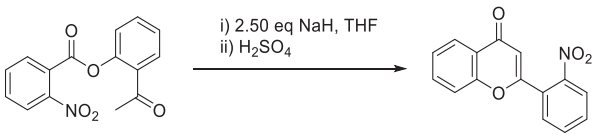

1.00 eq (8.76 mmol, 2.5 g) of **9** was dissolved in 75 mL of dry THF, 2.5 eq (21.9 mmol, 0.526 g) of NaH (60 % oil dispersion) were added and the resulting solution refluxed for 3 h. After the solution was cooled to ambient temperature, the solvent was removed under reduced pressure, the resulting residue resuspended in 100 mL of 1 M aq. HCl and the product extracted with EtOAc. The combined organic layers were dried over Na_2SO_4, the solvent removed, and the residue resuspended in 50 mL of conc. H_2SO_4. The solution was stirred for 30 minutes at 100°C, cooled to RT and poured on 500 mL of ice water. Precipitated product was collected by filtration, resuspended in EtOAc and filtered over a silica plug which was thoroughly washed with EtOAc. The solvent of the resulting filtrate was removed *in vacuo* and the residue recrystallised from EtOH. 452 mg (1.69 mmol, 19 %) of **10** was obtained as an orange solid over two steps.

^{1}H NMR (300 MHz, DMSO-d_6) δ 8.25 – 8.19 (m, 1H), 8.16 – 8.07 (m, 1H), 8.03 – 7.80 (m, 5H), 7.55 (dtd, J = 8.1, 3.4, 1.1 Hz, 2H), 6.81 (s, 1H).

^{13}C NMR (75 MHz, DMSO- d_6) δ 176.8, 161.8, 155.8, 147.5, 134.8, 134.1, 132.6, 131.6, 126.5, 126.0, 125.0 (d, J = 2.8 Hz), 123.2, 118.2, 111.0, 110.9.

M.p.: 180.8 °C; **HPLC**: R_t=9.77 min, purity = 96.5 %, **MS** (+APCI): 268 $[M+H]^+$.

2.16 Synthesis of 2-(2-nitrophenyl)-4*H*-chromen-4-one (**11**)

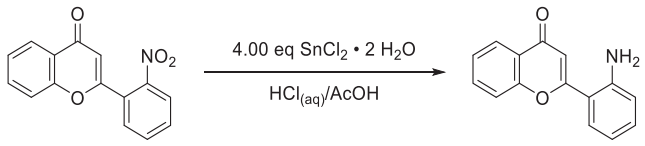

1.00 eq (2.28 mmol, 610 mg) of **10** was dissolved in 25 mL of glacial acetic acid. 4.00 eq of tin(II) chloride dihydrate was dissolved in 10 mL of concentrated HCl and added to the acetic acid solution. After 4 h at 90 °C, the reaction was cooled to ambient temperature and the solution basified (pH = 9) with an aqueous 25 % (w/w) NaOH solution. The product was extracted with chloroform, dried over Na_2SO_4 and the solvent removed under reduced pressure. After flash column chromatography (*n*-hexane/EtOAc), 390 mg (1.65 mmol, 72 %) of **11** was obtained as a yellowish solid.

^{1}H NMR (300 MHz, DMSO-d_6) δ 8.05 (ddd, *J* = 8.0, 1.7, 0.5 Hz, 1H), 7.80 (ddd, *J* = 8.7, 7.0, 1.7 Hz, 1H), 7.70 (ddd, *J* = 8.5, 1.2, 0.5 Hz, 1H), 7.49 (ddd, *J* = 8.1, 7.0, 1.2 Hz, 1H), 7.42 (dd, *J* = 7.9, 1.6 Hz, 1H), 7.22 (ddd, *J* = 8.6, 7.1, 1.6 Hz, 1H), 6.87 – 6.78 (m, 1H), 6.66 (ddd, *J* = 7.8, 7.1, 1.2 Hz, 1H), 6.55 (s, 1H), 5.68 (s, 2H).

^{13}C NMR (75 MHz, DMSO-d_6) δ 177.1, 165.1, 156.1, 147.2, 134.0, 132.0, 129.6, 125.4, 124.7, 123.4, 118.7, 116.7, 116.2, 115.3, 109.6.

M.p.: 150.9 °C; **HPLC**: R_t=11.94 min, purity ≥ 99 %, **MS** (+APCI): 238 $[M+H]^+$.

2.17 Synthesis of chromeno[3,2-*b*]indol-11(10*H*)-one (**12**)

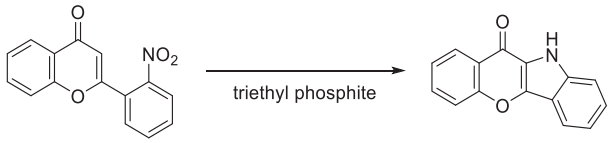

1.00 eq (2.00 mmol, 534 mg) of **10** was resuspended in 20 mL of triethyl phosphite under argon atmosphere. The solution was stirred for 16 h at 160°C. After the solution was cooled to 0°C, the precipitate was collected by filtration. The precipitate was recrystallised from EtOH. 178 mg (0.757 mmol, 38 %) of **12** was obtained as a brownish solid.

^{1}H NMR (300 MHz, DMSO-d_6) δ 12.17 (s, 1H), 8.40 – 8.27 (m, 1H), 8.01 (dq, J = 8.1, 0.9 Hz, 1H), 7.91 – 7.80 (m, 2H), 7.63 – 7.46 (m, 3H), 7.26 (ddd, J = 8.0, 6.4, 1.5 Hz, 1H).

^{13}C NMR (75 MHz, DMSO- d_6) δ 168.4, 155.3, 143.9, 137.0, 133.3, 128.1, 125.5, 124.2, 123.3, 120.9, 120.4, 119.4, 118.4, 114.7, 113.2.

M.p.: 192.7°C; **HPLC**: R_t=14.14 min, purity ≥ 99 %, **MS** (+APCI): 236 $[M+H]^+$.

2.18 Synthesis of tert-butyl 4-((11-oxochromeno[3,2-*b*]indol-10(11*H*)-yl)methyl)benzoate (**13**)

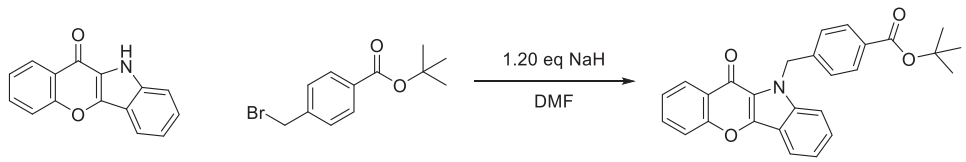

1.00 eq (0.638, 150 mg) of **12** was dissolved in 10 mL of dry DMF and cooled on ice. 1.20 eq (0.765 mmol, 30.6 mg) of NaH (60 % oil dispersion) were added, stirred for 30 minutes on ice and another 30 minutes at ambient temperature. 1.10 eq (0.701 mmol, 190 mg) of *tert*-butyl 4-(bromomethyl)benzoate were added to the reaction mixture and stirred at RT. After 16 h, the solvent was removed under reduced pressure, the residue resuspended in 5 mL of EtOH and poured on 100 mL of ice water. The resulting precipitate was collected by filtration, washed with dH_2O (x3) and recrystallised from EtOH. 220 mg (0.517 mmol, 81 %) of **13** was obtained as a colourless solid.

^{1}H NMR (300 MHz, Chloroform-*d*) δ 8.42 (ddd, *J* = 8.0, 1.6, 0.7 Hz, 1H), 8.04 (dt, *J* = 8.1, 1.0 Hz, 1H), 7.93 – 7.83 (m, 2H), 7.79 – 7.60 (m, 2H), 7.54 – 7.35 (m, 3H), 7.33 – 7.20 (m, 3H), 6.07 (s, 2H), 1.53 (s, 9H).

^{13}C NMR (75 MHz, Chloroform-*d*) δ 170.4, 165.5, 155.6, 145.4, 142.7, 138.1, 133.0, 131.3, 130.0, 128.6, 126.8, 126.3, 124.4, 124.0, 120.8, 120.4, 120.2, 118.2, 115.6, 110.8, 81.0, 48.0, 28.3.

M.p.: 194.7 °C; **HPLC**: R_t=21.61 min, purity ≥ 99 %, **MS** (+APCI): 426 $[M+H]^+$.

2.19 Synthesis of *N*-hydroxy-4-((11-oxochromeno[3,2-*b*]indol-10(11*H*)-yl)methyl)benzamide (**14**)

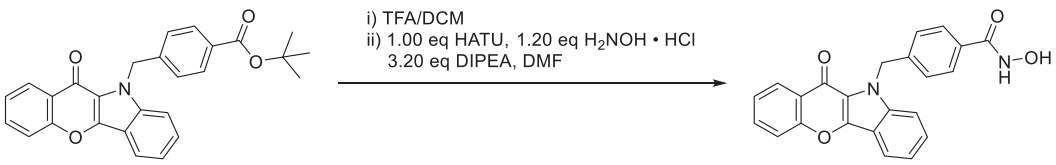

14 was synthesised according to general procedure 2.4 on a 0.470 mmol (**13**) scale and the product was obtained as a yellow solid with a grey of 50 % (0.234 mmol, 90 mg).

^{1}H NMR (600 MHz, DMSO-d_6) δ 11.11 (s, 1H), 8.99 (s, 1H), 8.28 (d, *J* = 7.9 Hz, 1H), 8.04 (d, *J* = 8.0 Hz, 1H), 7.85 (d, *J* = 6.4 Hz, 2H), 7.73 (d, *J* = 8.5 Hz, 1H), 7.67 – 7.60 (m, 2H), 7.54 (dt, *J* = 11.8, 6.7 Hz, 2H), 7.30 (t, *J* = 7.5 Hz, 1H), 7.26 (d, *J* = 8.0 Hz, 2H), 6.06 (s, 2H).

^{13}C NMR (75 MHz, DMSO-d_6) δ 169.2, 164.0, 154.9, 144.3, 141.3, 137.5, 133.6, 131.9, 128.6, 127.2, 126.7, 125.5, 124.4, 123.6, 121.0, 119.8, 119.4, 118.3, 114.5, 111.5, 46.9.

M.p.: 221.2°C; **HPLC**: R_t= 12.78 min, purity = 98.3 %, **MS** (+APCI): 385 $[M+H]^+$.

3 Biological evaluation

Cisplatin was purchased from Sigma (Germany) and dissolved in 0.9% sodium chloride solution, propidium iodide (PI) was purchased from PromoKine (Germany). Vorinostat was synthesized according to known procedures.[1] Stock solutions (10 mM) of the respective compounds were prepared with DMSO and diluted to the desired concentrations with the appropriate medium. All other reagents were supplied by PAN Biotech (Germany) unless otherwise stated.

3.1 Cell lines and cell culture.

The human ovarian carcinoma cell line A2780 was obtained from European Collection of Cell Cultures (ECACC, Salisbury, UK). The human tongue cell line Cal27 was obtained from the German Collection of Microorganisms and Cell Cultures (DSMZ, Germany). The corresponding cisplatin resistant CisR cell line Cal27CisR was generated by exposing the parental cell line to weekly cycles of cisplatin in an IC_{50} concentration over a period of 24 – 30 weeks as described in Gosepath *et al.* and Eckstein *et al.*. [2, 3] All cell lines were grown at 37°C under humidified air supplemented with 5% CO_2 in RPMI 1640 (A2780) or DMEM (Cal27) containing 10% fetal calf serum, 120 IU/mL penicillin, and 120 µg/mL streptomycin. The cells were grown to 80% confluency before being used in further assays.

3.2 MTT cell viability assay

The rate of cell-survival under the action of test substances was evaluated by an improved MTT assay as previously described.[4] In brief, A2780 and Cal27 cell lines were seeded at a density of 5,000 and 2,500 cells/well in 96 well plates (Corning, Germany). After 24 h, cells were exposed to increased concentrations of the test compounds. Incubation was ended after 72 h and cell survival was determined by addition of MTT solution (Serva, Germany, 5 mg/mL in phosphate buffered saline). The formazan precipitate was dissolved in DMSO (VWR, Germany). Absorbance was measured at 544 nm and 690 nm in a FLUOstar microplate-reader (BMG LabTech, Offenburg, Germany).

To investigate the effect of **6e** and **7j** on cisplatin-induced cytotoxicity, compounds were added 48 h before cisplatin administration. After 72 h, the cytotoxic effect was determined with a MTT cell viability assay and shift factors were calculated by dividing the IC_{50} value of cisplatin alone by the IC_{50} value of the drug combinations.

3.3 Enzyme assay

All human recombinant enzymes were purchased from Reaction Biology Corp. (Malvern, PA, USA). The HDAC activity assay of HDAC2 (catalog nr. KDA-21-277), 4 (catalog nr. KDA-21-279), 6 (catalog nr. KDA-21-213) and 8 (catalog nr. KDA-21-481) was performed in 96-well plates (Corning, Germany). Briefly 20ng of HDAC2 and HDAC8, 17.5ng of HDAC6 and 2ng of HDAC4 per reaction were used. Recombinant enzymes were diluted in assay buffer (50 mM Tris-HCL, pH 8.0, 137 mM NaCl, 2.7 mM KCl, 1 mM $MgCl_2$, and 1 mg/ml BSA). 80 µl of this dilution was incubated with 10 µl of different concentrations of inhibitors in assay buffer. After a 5 min incubation step the reaction was started with 10 µl of 300 µM (HDAC2), 150 µM (HDAC6) Boc-Lys(Ac)-AMC (Bachem, Germany) or 100 µM (HDAC4), 60 µM (HDAC8) Boc-Lys(Tfa)-AMC (Bachem, Germany). The reaction was stopped after 90 min by adding 100 µl stop solution (16mg/ml trypsin, 2 µM Panobinostat for HDAC2, HDAC6 and HDAC8, 2 µM CHDI0039 (kindly provided by the CHDI Foundation Inc., New York, USA) for HDAC4 in 50 mM Tris-HCL, pH 8.0, and 100 mM NaCl. 15 min after the addition of the stop solution the fluorescence intensity was measured at excitation of 355 nm and emission of 460 nm in a NOVOstar microplate reader (BMG LabTech, Offenburg, Germany).

3.4 Data Analysis

Concentration-effect curves were constructed with Prism 7.0 (GraphPad, San Diego, CA) by fitting the pooled data of at least three experiments performed in triplicates to the four parameter logistic equation. Statistical analysis was performed using t test or one-way ANOVA.

4 References

1. Spadafora, M. *et al.* Efficient Synthesis of Ratiometric Fluorescent Nucleosides Featuring 3-Hydroxychromone Nucleobases. *Tetrahedron* **65**, 7809–7816 (2009).

2. Irgashev, R. A., Sosnovskikh, V. Y., Sokovnina, A. A. & Röschenthaler, G. V. The first synthesis of 3-hydroxy-2-(polyfluoroalkyl)chromones and their ammonium salts. 3-Hydroxychromone in the Mannich reaction. *J. Heterocycl. Chem.* **47**, 944–948 (2010).

7 Summary and Outlook

Despite improving therapeutic options, the treatment of cancer remains a major health challenge. Target specific therapies and epigenetic strategies are urgently needed as the manifestation of resistances against first line drugs are common. Addressing epigenetic processes in cells that underwent malignant transformation becomes increasingly important in cancer treatment. Such epigenetic regulators are histone deacetylases (HDACs). Human zinc dependent HDACs are divided into three classes: class I (HDACs 1-3, 8), class II (IIa: HDACs 4, 5, 7, 9; IIb: HDACs 6, 10) and class IV (HDAC 11). Histone deacetylase inhibitors (HDACi) are clinically validated anticancer agents and particularly used in the treatment of haematological malignancies, that present dysregulated epigenetic processes. However, currently approved pan-HDACi suffer from severe side effects such as neutropenia, anaemia or cardio-vascular side effects, the occurrence of resistances is common and they show only limited efficacies in solid tumours. One approach to overcome the drawbacks of pan-HDACi is the design of HDACi that show a refined HDAC isozyme inhibition profile or are isozyme selective. However, the efficacy of HDACi with a refined isozyme inhibition profile or selective inhibitors remains to be established. The objective of this work was the design, synthesis and biological evaluation of novel HDAC class I/IIb and HDAC6 selective inhibitors

Development of HDAC class I/HDAC6 dual inhibitors.

Novel α,β-unsaturated hydroxamic acid derivatives overcome cisplatin resistance

Panobinostat, a potent pan-HDACi, served as a lead structure and was modified at the connecting unit (CU) with a hydroxylamine subunit to obtain HDAC class I/HDAC6 selectivity. The hydroxylamine was either converted with an isocyanate or with a carboxylic acid to the corresponding alkoxyurea or alkoxyamide and subsequently transformed into their corresponding hydroxamic acid (Scheme 38).

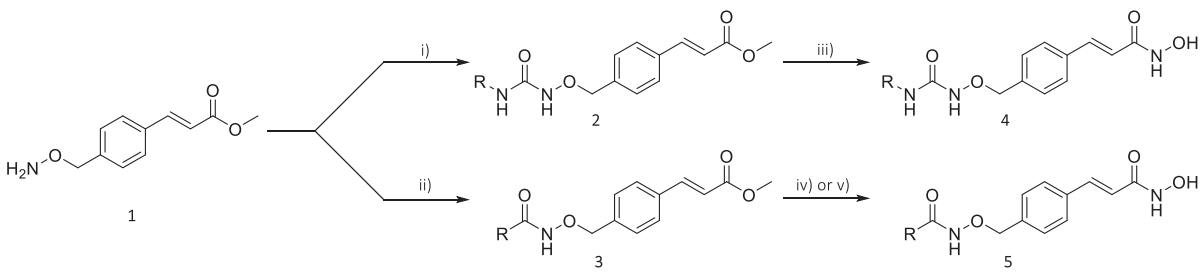

Scheme 38. Synthesis of the hydroxamic acids 6 a-g and 7 a-j 3. I) 1.00 eq Isocyanate, DCM, 16 h RT, 53 – 95 %; ii) 1.00 eq carboxylic acid, 2.00 eq DIPEA, 1.00 eq HATU, DMF, 16 h RT, 40 % - 95 %; iii) 30.0 eq $HONH_2$ (aq), 10.0 eq NaOH, DCM/MeOH, RT 16 h, 72 -92 %; iv) a) 5.00 eq LiOH/H2O, 16 h RT, b) 1.20 eq IBCF, 7.20 eq DIPEA, 5.0 eq $HONH_3Cl$, 16 h RT, 13-37 %; v) 10.0 eq hydroxylamine hydrochloride, 15.0 eq NaOMe, MeOH, MW 150 W, 70 °C, 30 mins, 34 % -37 %.

The obtained hydroxamic acids were subjected to HDAC isozyme profiling, HDAC whole cell inhibition assays and assessed for their antiproliferative activity in the human tongue squamous carcinoma cell line Cal27 and the human ovarian cancer cell line A2780. **MPK409**, exhibiting an alkoxyamide CU, was identified as the most potent HDACi in this series and demonstrated a HDAC class I and HDAC6 selectivity. In combination with cisplatin, **MPK409** caused a chemosensitisation of Cal27R towards cisplatin with a shift factor of 6.86 (Figure 25).

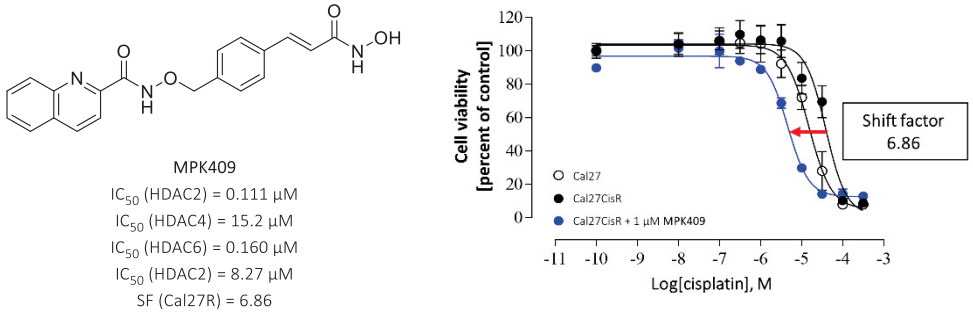

*Figure 25. **MPK409** restores cisplatin sensitivity of Cal27CisR. Treatment of Cal27CisR (●) with 1.00 µM of **MPK409** 48 h prior to cisplatin administration (blue dot) was able to reduce the IC_{50} value of cisplatin even below the IC_{50} of the parental cell line Cal27 (○).IC_{50} values were determined by MTT assay. The shift factor is defined as the ratio of the IC_{50} of cisplatin alone and the IC_{50} of the combination of **7j** with cisplatin (Table 4).*

The carba-analogue of KSK64

The second project dealt with the establishment of a synthetic procedure for the carba-analogue of the alkoxyurea based HDACi KSK64 and was realised according to Scheme 39. Cycloheptanone was subjected to a *Beckmann rearrangement* ring expansion reaction (**6**), followed by an *N*-Boc protection of the resulting lactam **7**. The *N*-Boc protected lactam **7** was, subsequently, hydrolysed under basis conditions (**8**) and coupled with *O*-benzyl hydroxylamine (**9**). After Boc deproction (**10**), the resulting amine was converted with triphosgene and 2,6-dimethoxy-4-methylquinolin-8-amine to the corresponding urea **11**. **MPK544** (**12**) was obtained after benzyl deprotection.

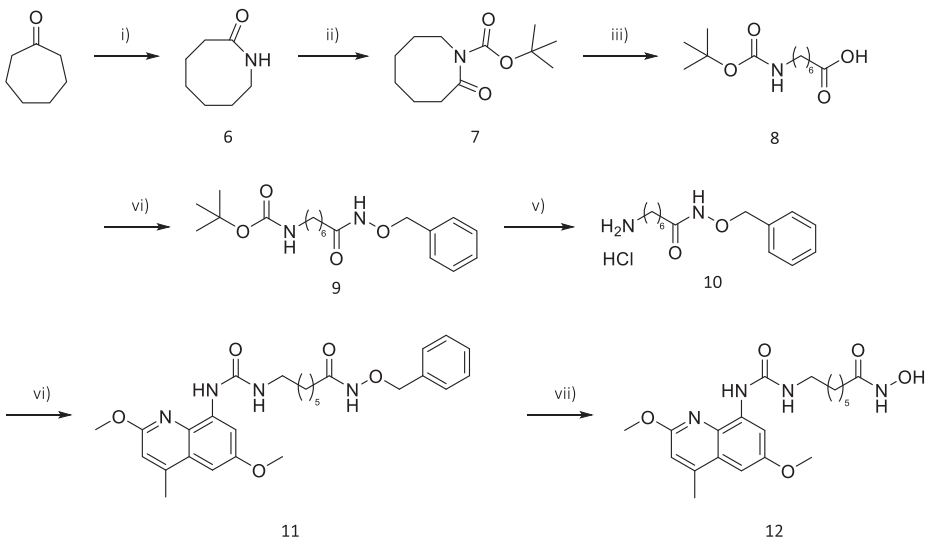

*Scheme 39. Synthesis of **MPK544** the carba analogue of **KSK64**. I) 1.50 eq hydroxylamine-O-sulfonic acid, HCO_2H; ii) 1.00 eq nBuLi, 1.00 eq Boc_2O, THF; iii) 10.0 eq LiOH, THF/H_2O; iv) 1.00 eq HATU, 2.00 eq DIPEA, 1.00 eq O-benzylhydroxylamine, DMF; v) 20.0 eq $HCl_{(dioxane)}$, DCM; vi) 0.330 eq triphosgene, 1.00 eq DIPEA, DCM; vii) H_2, Pd/C, MeOH.*

The carba-analogue of KSK64 (MPK544) was subsequently subjected to HDAC2 and HDAC6 isozyme profiling and their antiproliferative properties asses in the human tongue squamous carcinoma cell line Cal27 and the human ovarian cancer cell line A2780 (Scheme 40).

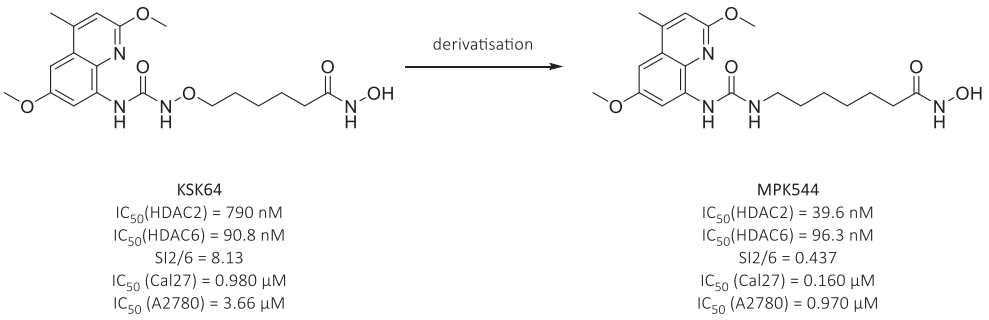

*Scheme 40. **MPK544**, the carba-analogue of **KSK64**. The selectivity index SI2/6 was calculated with the pIC_{50} values.*

Whilst KSK64 and MPK544 showed HDAC6 inhibitory activities in the same order of magnitude, they demonstrated significantly different HDAC2 inhibition values. In HDAC2, KSK64 and MPK544 exhibited an IC_{50} of 790 nM(SI2/6 = 8.13) and 39.6 nM (SI2/6 = 0.437), respectively. These data further emphasised the significance of the CU and indicate, that a derivatisation of HDACi with an alkoxyurea CU can result in a refined isozyme profile with HDAC6 preference.

Development of HDAC6 selective inhibitors

The Next generation of histone deacetylase 6 inhibitors.

HDAC6, an epigenetic eraser, is a metalloprotease that catalyses the deacetylation of non-histone proteins, such as α-Tubulin, Cortactin, HSP90 and Peroxiredoxin and play a key role in the regulation of microtubular processes, cell migration and cell-cell interactions As pharmaceutical target, it is of interest for the pharmacological intervention of cancer as well as in immunological and neurological diseases. However, whilst pan-HDACi have been proven to be effective anticancer agents, the efficacy of HDAC6 selective inhibitor remains controversial. The aim of this chapter focused on the design of novel HDAC6 selective inhibitors and their evaluation as anticancer agents. HDAC6 selective inhibitors usually show sterically demanding or branched surface CAP groups (sCAP), an aromatic linker and a hydroxamic acid zinc binding group.

The first approach to design HDAC6 selective inhibitors focussed on the innovation of nexturastat A, by the modification of the connecting unit with a hydroxylamine. The synthesis of the branched alkoxyurea based hydroxamic acids **15** was performed by the conversion of the hydroxylamine **13** with isocyanates (Scheme 41). Afterwards, **14** was converted into their corresponding hydroxamic acids **15**.

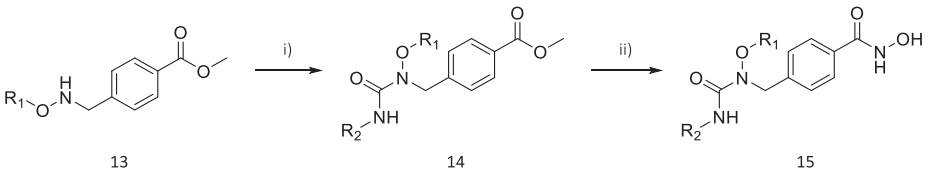

*Scheme 41. Synthesis of branched alkoxyurea based hydroxamic acids **15**. i) 1.00 eq RCNO, 1.00 eq DIPEA, DCM, ii) 30.0 eq $H_2NOH_{(aq)}$, 10.0 eq NaOH, DCM/MeOH.*

The branched alkoxyurea based hydroxamic acids **15** (**MPK265**) showed an up to 1.5-fold higher SI1/6 compared to nexturastat A, whilst maintaining its inhibitory activity (IC_{50} = 0.020 ± 0.003 µM) of HDAC6. To further increase HDAC6 selectivity, *N*-alkoxycarbamate based hydroxamic acids, with variable *O*-substituents, were synthesised according to Scheme 42.

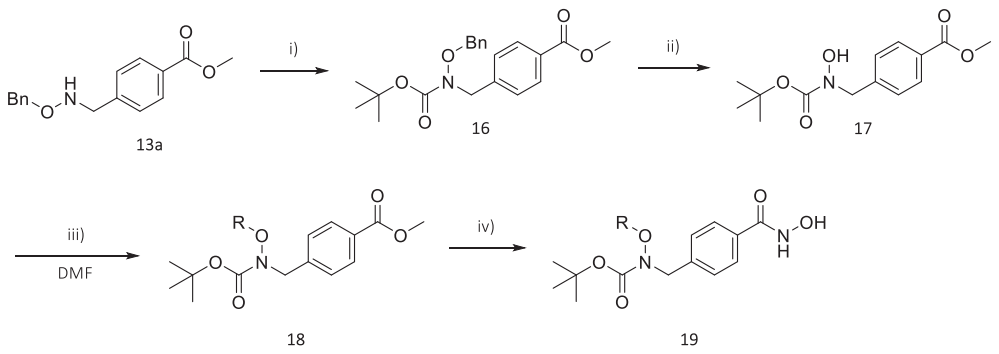

*Scheme 42. Synthesis of branched alkoxycarbamate based hydroxamic acids **19**. i) 1.20 eq Boc_2O, 3.00 eq TEA, DCM; ii) H_2, Pd/C, MeOH; iii) 1.20 eq NaH (60 %, mineral oil), 2.00 eq RX, DMF; iv) a) 10.0 eq LiOH, THF/MeOH; b) 1.00 eq HATU, 1.20 eq H_2NOH • HCl, 3.20 eq DIPEA, DMF.*

The branched ^{t}butyl-(alkoxycarbamate) based hydroxamic acids **19** (**MPK169**, R=Me) showed an up to 4.4-fold higher SI1/6 than nexturastat A (Scheme 43).

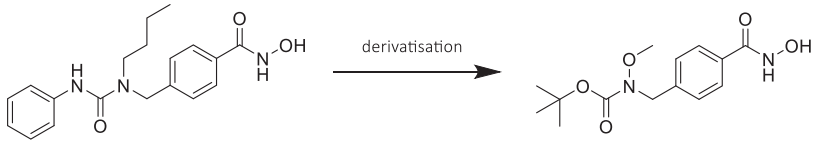

nexturastat A
IC_{50} (HDAC1) = 0.504 µM
IC_{50} (HDAC2) = 0.861 µM
IC_{50} (HDAC3) = 0.730 µM
IC_{50} (HDAC6) = 0.021 µM
SI1/6 = 24.0

MPK169
IC_{50} (HDAC1) = 1.59 µM
IC_{50} (HDAC2) = 2.53 µM
IC_{50} (HDAC3) = 1.79 µM
IC_{50} (HDAC6) = 0.015 µM
SI1/6 = 106

*Scheme 43. **MPK169**, a novel HDAC6 selective inhibitor.*

With the discovery of **MPK169** as potent and selective HDAC6 inhibitor, a transition from an occupational driven inhibition to an event driven proteolysis targeting chimera (PROTAC) mediated protein degradation was envisioned. Based on **19**, a PROTAC with pomalidomide as E3 recruiting element was designed and synthesised according to Scheme 44. The HDAC6 inhibitor **21** and the E3 recruiting element **20** was clicked by an azide-alkyne 1,3-dipolar cycloaddition to obtain the PROTAC **MPK779** (**22**).

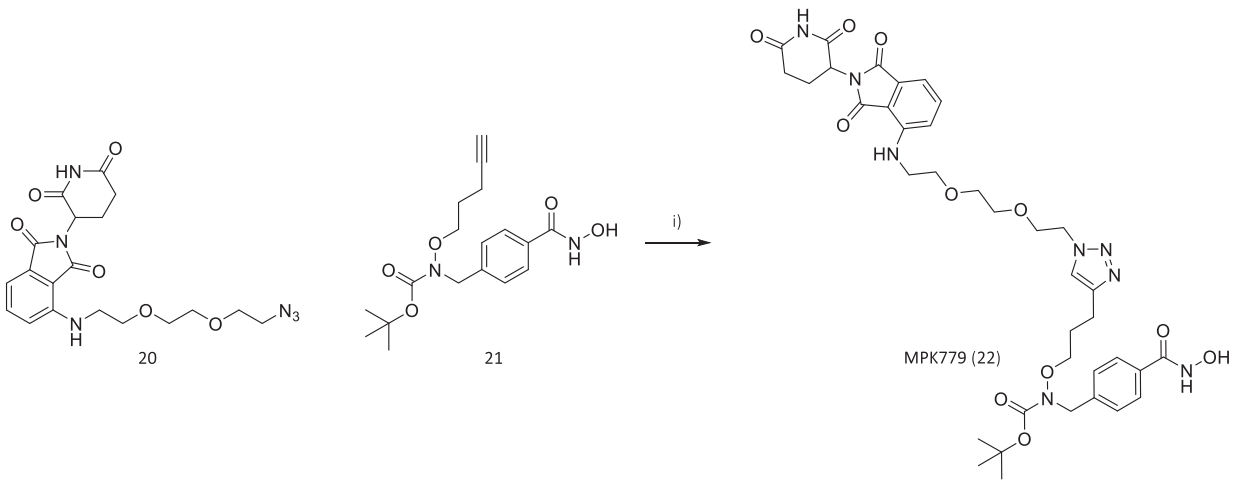

*Scheme 44. Synthesis of PROTAC **11** by a 1,3-dipolar cycloaddition. i) 1.10 eq. $CuSO_4$, 6.00 eq sodium L-ascorbate, H_2O/t-BuOH.*

Despite the increased alkoxy chain length in the cap region, **MPK779** demonstrated selectivity indices of up to 74.4 with an up to 3.10 higher SI1/6 then nexturastat A (Scheme 45).

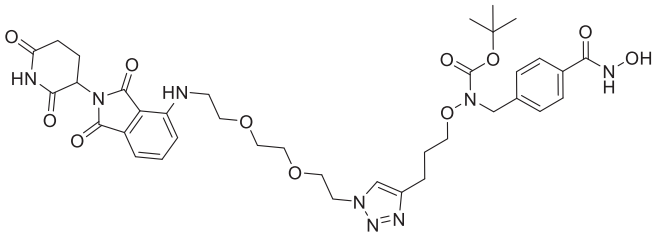

MPK779
IC_{50} (HDAC1) = 3.20 µM
IC_{50} (HDAC2) = 3.18 µM
IC_{50} (HDAC3) = 2.32 µM
IC_{50} (HDAC6) = 0.043 µM
SI1/6 = 74.4

Scheme 45. MPK779, a novel HDAC6 selective PROTAC.

Chromenones: A suitable CAP group to govern HDAC6 selectivity?

The final approach to design HDAC6 selective inhibitors focused on chromenones as sterically demanding CAP groups. Initially, the 2-substituted 3-hydroxy -4*H*-chromen-4-one derivatives **23** were obtained by an *Algar-Flynn-Oyamada* reaction and either alkylated with the benzyl linker **24** or converted with *tert*-butyl 4-(aminomethyl)benzoate **25** in a palladium catalysed manner (Scheme 46). The *tert*-butyl esters **26** and **27** were deprotected under acidic conditions and converted into their corresponding hydroxamic acids **26** and **27**.

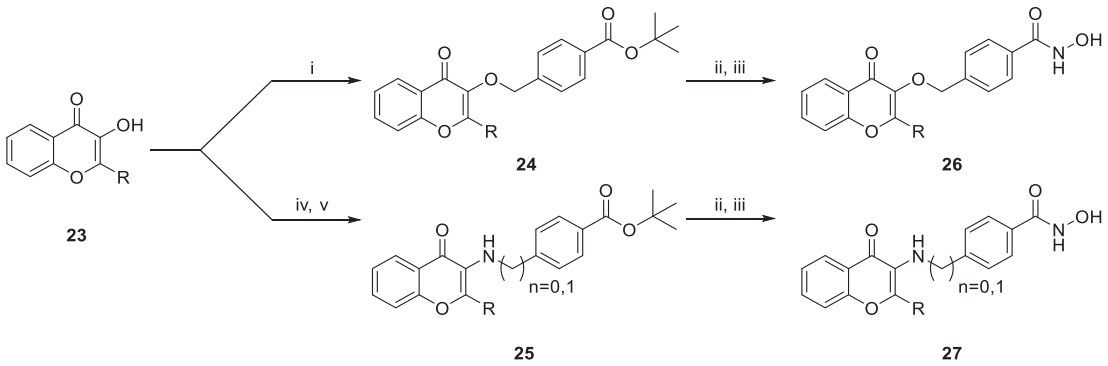

Scheme 46. Synthesis of chromenone based hydroxamic acids. I) 1.10 eq tert-butyl 4-(bromomethyl)benzoate, 5.00 eq K_2CO_3, DMF; ii) TFA/DCM; iii) 1.00 eq HATU, 3.20 eq DIPEA, 1.20 eq $HONH_3Cl$, DMF; iv) 2.00 eq Tf_2O, 2.00 eq DIPEA, DCM; v) 1.10 eq tert-butyl 4-(aminomethyl)benzoate, 5.00 eq $CsCO_3$, 0.100 eq $Pd_2(dba)_3$, 0.300 eq Xantphos, PhMe.

In order to obtain the annulated derivative of **27**, 2-(2-nitrophenyl)-4*H*-chromen-4-one (**28**) was subjected to a *Cadogan-Sundberg* reaction (Scheme 47), resulting in chromeno[3,2-*b*]indol-11(10*H*)-one (**29**). Finally, the heterocycle **29** was alkylated with the benzyl linker and converted into its corresponding hydroxamic acid **31**.

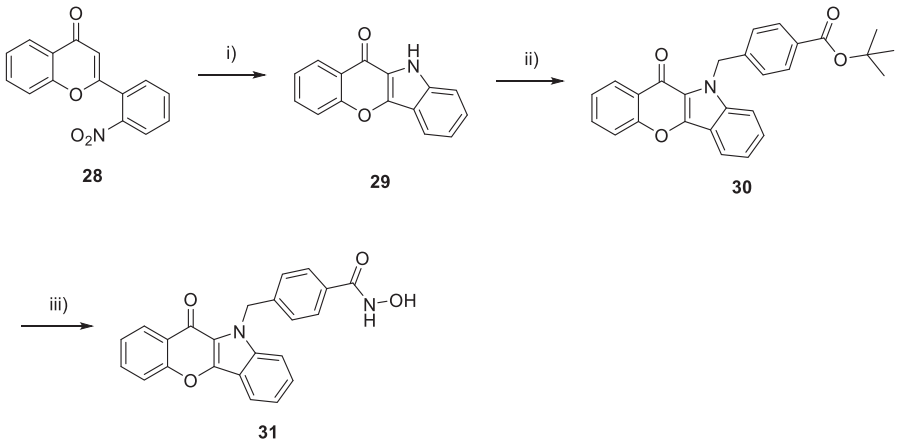

*Scheme 47. Synthesis of the annulated derivative **31**. i) $P(OMe)_3$, ii) 1.20 eq NaH (60 %, mineral oil), 1.10 eq tert-butyl 4-(bromomethyl)benzoate, DMF; ii) a) TFA/DCM b)1.00 eq HATU, 1.20 eq H_2NOH • HCl, 3.20 eq DIPEA, DMF.*

The sterically demanding chromenone based hydroxamic acids **26**, **27** and **31** were evaluated in HDAC2 and HDAC6 inhibition assays. Among the tested Compounds, **26** showed the highest SI2/6 (Scheme 48). The 2,5-dimethyl phenyl (**MPK781**) and the 3-pyridyl (**MPK509**) derivative of **26** exhibited an approximately 1.3-fold higher SI2/6 than the HDAC6 selective inhibitor nexturastat A (SI2/6 = 40.7). **MPK805** the 3,5-dimethyl derivative of **26** was the most selective compound with a HDAC2/6 selectivity

index (SI) of 269, which correlates to an approximately 1.6-fold higher SI2/6 with a 19-fold lower IC_{50}, compared to tubastatin A (IC_{50}(HDAC6) = 0.017 µM, SI2/6 = 166).

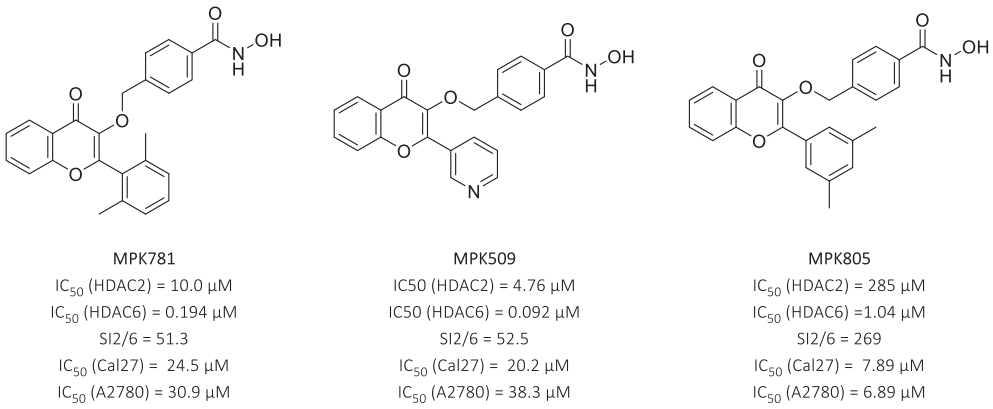

Scheme 48. Chromenones are suitable scaffolds for the design of HDAC6 selective inhibitors.

However, the nitrogen based CU of **27** and **31** exhibited only moderate HDAC6 selectivities and inhibitory activities. **26**, **27**, and **31** showed limited antiproliferative activities in the human tongue squamous carcinoma cell line Cal27 and the human ovarian cancer cell line A2780.

In summary, the employment of hydroxylamine as subunit in the CU of HDACi, resulted in the a refined HDAC isozyme profile with promising chemosensitising properties towards cisplatin. Furthermore, their utilisation in the modification of nexturastat A resulted in a significantly increased HDAC6 selectivity. Chromenones are suitable HDAC6 directing cap groups. Due the limited antiproliferative properties of the here reported HDAC6 selective inhibitors, they are suitable tools to explore their pharmaceutical potential in neurology, immunology or to might suppress metastasis and will be the focus of future biological evaluations.

8 References

1. Hartmann, T. Diversity and variability of plant secondary metabolism: A mechanistic view. *Entomol. Exp. Appl.* **80**, 177–188 (1996).

2. Gershenzon, J. & Dudareva, N. The function of terpene natural products in the natural world. *Nat. Chem. Biol.* **3**, 408–414 (2007).

3. Coqueiro, A. & Verpoorte, R. Alkaloids. in *Encyclopedia of Analytical Science* 77–84 (Elsevier, 2019). doi:10.1016/B978-0-12-409547-2.11675-0.

4. Vattekkatte, A., Garms, S., Brandt, W. & Boland, W. Enhanced structural diversity in terpenoid biosynthesis: Enzymes, substrates and cofactors. *Org. Biomol. Chem.* **16**, 348–362 (2018).

5. Hertweck, C. The biosynthetic logic of polyketide diversity. *Angew. Chemie - Int. Ed.* **48**, 4688–4716 (2009).

6. Valdez, B. C. *et al.* Romidepsin targets multiple survival signaling pathways in malignant T cells. *Blood Cancer J.* **5**, e357–e357 (2015).

7. Han, J. W. *et al.* Apicidin, a histone deacetylase inhibitor, inhibits proliferation of tumor cells via induction of p21WAF1/Cip1 and gelsolin. *Cancer Res.* **60**, 6068–74 (2000).

8. Wani, M. C., Taylor, H. L., Wall, M. E., Coggon, P. & McPhail, A. T. Plant antitumor agents. VI. Isolation and structure of taxol, a novel antileukemic and antitumor agent from Taxus brevifolia. *J. Am. Chem. Soc.* **93**, 2325–2327 (1971).

9. Tsuji, N., Kobayashi, M., Nagashima, K., Wakisaka, Y. & Koizumi, K. A new antifungal antibiotic, trichostatin. *J. Antibiot. (Tokyo).* **29**, 1–6 (1976).

10. Böhler, P. *et al.* The mycotoxin phomoxanthone A disturbs the form and function of the inner mitochondrial membrane. *Cell Death Dis.* **9**, 286 (2018).

11. Sun, W., Kalen, A. L., Smith, B. J., Cullen, J. J. & Oberley, L. W. Enhancing the Antitumor Activity of Adriamycin and Ionizing Radiation. *Cancer Res.* **69**, 4294–4300 (2009).

12. War, A. R. *et al.* Mechanisms of plant defense against insect herbivores. *Plant Signal. Behav.* **7**, 1306–20 (2012).

13. Smith, K. E., Halpin, C. G. & Rowe, C. The benefits of being toxic to deter predators depends on prey body size. *Behav. Ecol.* arw086 (2016) doi:10.1093/beheco/arw086.

14. Brown, B. A. *et al.* A UV-B-specific signaling component orchestrates plant UV protection. *Proc. Natl. Acad. Sci. U. S. A.* **102**, 18225–18230 (2005).

15. Mewis, I. *et al.* UV-B irradiation changes specifically the secondary metabolite profile in broccoli sprouts: Induced signaling overlaps with defense response to biotic stressors. *Plant Cell Physiol.* **53**, 1546–1560 (2012).

16. Tossi, V., Lombardo, C., Cassia, R. & Lamattina, L. Nitric oxide and flavonoids are systemically induced by UV-B in maize leaves. *Plant Sci.* **193**–**194**, 103–109 (2012).

17. Li, K., Buchinger, T. J. & Li, W. Discovery and characterization of natural products that act as pheromones in fish. *Nat. Prod. Rep.* **35**, 501–513 (2018).

18. Kudo, K., Ozaki, T., Shin-Ya, K., Nishiyama, M. & Kuzuyama, T. Biosynthetic Origin of the Hydroxamic Acid Moiety of Trichostatin A: Identification of Unprecedented Enzymatic Machinery Involved in Hydroxylamine Transfer. *J. Am. Chem. Soc.* **139**, 6799–6802 (2017).

19. Felsenfeld, G., Boyes, J., Chung, J., Clark, D. & Studitsky, V. Chromatin structure and gene expression. *Proc. Natl. Acad. Sci. U. S. A.* **93**, 9384–9388 (1996).

20. Waddington, C. H. The epigenotype. 1942. *Int. J. Epidemiol.* **41**, 10–13 (2012).

21. Allis, C. D. & Jenuwein, T. The molecular hallmarks of epigenetic control. *Nat. Rev. Genet.* **17**, 487–500 (2016).

22. Felsenfeld, G., Boyes, J., Chung, J., Clark, D. & Studitsky, V. Chromatin structure and gene expression. *Proc. Natl. Acad. Sci. U. S. A.* **93**, 9384–9388 (1996).

23. Kanherkar, R. R., Bhatia-Dey, N. & Csoka, A. B. Epigenetics across the human lifespan. *Frontiers in Cell and Developmental Biology* vol. 2 49 (2014).

24. Monk, D., Mackay, D. J. G., Eggermann, T., Maher, E. R. & Riccio, A. Genomic imprinting disorders: lessons on how genome, epigenome and environment interact. *Nat. Rev. Genet.* **20**, 235–248 (2019).

25. Donohoe, M. E. Epigenetic Regulation of X-Chromosome Inactivation. *Chromatin Regul. Dyn.* 353–371 (2017) doi:10.1016/B978-0-12-803395-1.00014-9.

26. Atlasi, Y. & Stunnenberg, H. G. The interplay of epigenetic marks during stem cell differentiation and development. *Nat. Rev. Genet.* **18**, 643–658 (2017).

27. Putiri, E. L. & Robertson, K. D. Epigenetic mechanisms and genome stability. *Clin. Epigenetics* **2**,

299–314 (2011).

28. Nicholson, T. B., Veland, N. & Chen, T. Writers, Readers, and Erasers of Epigenetic Marks. *Epigenetic Cancer Ther.* 31–66 (2015) doi:10.1016/B978-0-12-800206-3.00003-3.

29. Greenberg, M. V. C. & Bourc'his, D. The diverse roles of DNA methylation in mammalian development and disease. *Nature Reviews Molecular Cell Biology* vol. 20 590–607 (2019).

30. Zhang, T., Cooper, S. & Brockdorff, N. The interplay of histone modifications – writers that read. *EMBO Rep.* **16**, 1467–1481 (2015).

31. Yuan, R. *et al.* Natural products to prevent drug resistance in cancer chemotherapy: a review. *Ann. N. Y. Acad. Sci.* **1401**, 19–27 (2017).

32. Mohammad, H. P., Barbash, O. & Creasy, C. L. Targeting epigenetic modifications in cancer therapy: erasing the roadmap to cancer. *Nat. Med.* **25**, 403–418 (2019).

33. Suraweera, A., O'Byrne, K. J. & Richard, D. J. Combination therapy with histone deacetylase inhibitors (HDACi) for the treatment of cancer: Achieving the full therapeutic potential of HDACi. *Front. Oncol.* **8**, 1–15 (2018).

34. Haberland, M., Montgomery, R. L. & Olson, E. N. The many roles of histone deacetylases in development and physiology: Implications for disease and therapy. *Nat. Rev. Genet.* **10**, 32–42 (2009).

35. Asfaha, Y. *et al.* Recent advances in class IIa histone deacetylases research. *Bioorganic and Medicinal Chemistry* vol. 27 115087 (2019).

36. Hai, Y. & Christianson, D. W. Histone deacetylase 6 structure and molecular basis of catalysis and inhibition. *Nat. Chem. Biol.* **12**, 741–747 (2016).

37. Fuller, N. O. *et al.* CoREST Complex-Selective Histone Deacetylase Inhibitors Show Prosynaptic Effects and an Improved Safety Profile to Enable Treatment of Synaptopathies. *ACS Chem. Neurosci.* **10**, 1729–1743 (2019).

38. Basta, J. & Rauchman, M. The nucleosome remodeling and deacetylase complex in development and disease. *Transl. Res.* **165**, 36–47 (2015).

39. Grzenda, A., Lomberk, G., Zhang, J. S. & Urrutia, R. Sin3: Master scaffold and transcriptional corepressor. *Biochim. Biophys. Acta - Gene Regul. Mech.* **1789**, 443–450 (2009).

40. Cunliffe, V. T. Eloquent silence: developmental functions of Class I histone deacetylases. *Curr.*

Opin. Genet. Dev. **18**, 404–410 (2008).

41. Kurdistani, S. K., Tavazoie, S. & Grunstein, M. Mapping global histone acetylation patterns to gene expression. *Cell* **117**, 721–733 (2004).

42. Cutter, A. R. & Hayes, J. J. A brief review of nucleosome structure. *FEBS Lett.* **589**, 2914–2922 (2015).

43. Ramakrishnan, V., Finch, J. T., Graziano, V., Lee, P. L. & Sweet, R. M. Crystal structure of globular domain of histone H5 and its implications for nucleosome binding. *Nature* **362**, 219–223 (1993).

44. Imhof, A. & Becker, P. B. Modifications of the histone N-terminal domains: Evidence for an 'epigenetic code'? *Appl. Biochem. Biotechnol. - Part B Mol. Biotechnol.* **17**, 1–13 (2001).

45. Grunstein, M. Histone acetylation in chromatin structure and transcription. *Nature* **389**, 349–352 (1997).

46. Jambhekar, A., Dhall, A. & Shi, Y. Roles and regulation of histone methylation in animal development. *Nat. Rev. Mol. Cell Biol.* **20**, 625–641 (2019).

47. Rossetto, D., Avvakumov, N. & Côté, J. Histone phosphorylation: A chromatin modification involved in diverse nuclear events. *Epigenetics* **7**, 1098–1108 (2012).

48. Roth, S. Y., Denu, J. M. & Allis, C. D. Histone Acetyltransferases. *Annu. Rev. Biochem.* **70**, 81–120 (2001).

49. Bertrand, P. Inside HDAC with HDAC inhibitors. *European Journal of Medicinal Chemistry* vol. 45 2095–2116 (2010).

50. Yang, H. *et al.* Overexpression of histone deacetylases in cancer cells is controlled by interplay of transcription factors and epigenetic modulators. *FASEB J.* **28**, 4265–4279 (2014).

51. Diyabalanage, H. V. K., Granda, M. L. & Hooker, J. M. Combination therapy: Histone deacetylase inhibitors and platinum-based chemotherapeutics for cancer. *Cancer Lett.* **329**, 1–8 (2013).

52. Francois, J. *Basic principles of genetics. International Ophthalmology Clinics* vol. 8 (1968).

53. Seidel, C., Schnekenburger, M., Dicato, M. & Diederich, M. Histone deacetylase 6 in health and disease. *Epigenomics* **7**, 103–118 (2015).

54. Verdel, A. *et al.* Active maintenance of mHDA2/mHDAC6 histone-deacetylase in the cytoplasm. *Curr. Biol.* **10**, 747–749 (2000).

55. Chen, P. B. *et al.* Hdac6 regulates Tip60-p400 function in stem cells. *Elife* **2013**, 1–25 (2013).

56. Chen, P. B. *et al.* Hdac6 regulates Tip60-p400 function in stem cells. *Elife* **2013**, (2013).

57. Hai, Y. & Christianson, D. W. Histone deacetylase 6 structure and molecular basis of catalysis and inhibition. *Nat. Chem. Biol.* **12**, 741–747 (2016).

58. Miyake, Y. *et al.* Structural insights into HDAC6 tubulin deacetylation and its selective inhibition. *Nat. Chem. Biol.* **12**, 748–754 (2016).

59. Zhang, X. *et al.* HDAC6 Modulates Cell Motility by Altering the Acetylation Level of Cortactin. *Mol. Cell* **27**, 197–213 (2007).

60. Kovacs, J. J. *et al.* HDAC6 regulates Hsp90 acetylation and chaperone-dependent activation of glucocorticoid receptor. *Mol. Cell* **18**, 601–607 (2005).

61. Parmigiani, R. B. *et al.* HDAC6 is a specific deacetylase of peroxiredoxins and is involved in redox regulation. *Proc. Natl. Acad. Sci. U. S. A.* **105**, 9633–9638 (2008).

62. Hubbert, C. *et al.* HDAC6 is a microtubule-associated deacetylase. *Nature* **417**, 455–458 (2002).

63. Kawaguchi, Y. *et al.* The deacetylase HDAC6 regulates aggresome formation and cell viability in response to misfolded protein stress. *Cell* **115**, 727–738 (2003).

64. Pandey, U. B. *et al.* HDAC6 rescues neurodegeneration and provides an essential link between autophagy and the UPS. *Nature* **447**, 859–863 (2007).

65. Lee, J. Y. *et al.* HDAC6 controls autophagosome maturation essential for ubiquitin-selective quality-control autophagy. *EMBO J.* **29**, 969–980 (2010).

66. Sharif, T. *et al.* HDAC6 differentially regulates autophagy in stem-like versus differentiated cancer cells. *Autophagy* **15**, 686–706 (2019).

67. Beier, U. H. *et al.* Histone deacetylases 6 and 9 and sirtuin-1 control Foxp3+ regulatory T cell function through shared and isoform-specific mechanisms. *Sci. Signal.* **5**, ra45–ra45 (2012).

68. Sakamoto, K. M. & Aldana-Masangkay, G. I. The role of HDAC6 in cancer. *J. Biomed. Biotechnol.* **2011**, (2011).

69. Simões-Pires, C. *et al.* HDAC6 as a target for neurodegenerative diseases: What makes it different from the other HDACs? *Mol. Neurodegener.* **8**, 7 (2013).

70. Fukada, M. *et al.* Loss of deacetylation activity of Hdac6 affects emotional behavior in mice. *PLoS One* **7**, e30924 (2012).

71. Espallergues, J. *et al.* HDAC6 regulates glucocorticoid receptor signaling in serotonin pathways

with critical impact on stress resilience. *J. Neurosci.* **32**, 4400–4416 (2012).

72. Singh, H., Wray, N., Schappi, J. M. & Rasenick, M. M. Disruption of lipid-raft localized Gαs/tubulin complexes by antidepressants: A unique feature of HDAC6 inhibitors, SSRI and tricyclic compounds. *Neuropsychopharmacology* **43**, 1481–1491 (2018).

73. Hull, E. E., Montgomery, M. R. & Leyva, K. J. HDAC Inhibitors as Epigenetic Regulators of the Immune System: Impacts on Cancer Therapy and Inflammatory Diseases. *Biomed Res. Int.* **2016**, 1–15 (2016).

74. Licciardi, P. V. & Karagiannis, T. C. Regulation of Immune Responses by Histone Deacetylase Inhibitors. *ISRN Hematol.* **2012**, 1–10 (2012).

75. Moreno-Gonzalo, O. *et al. HDAC6 controls innate immune and autophagy responses to TLR-mediated signalling by the intracellular bacteria Listeria monocytogenes*. *PLoS Pathogens* vol. 13 (2017).

76. Knox, T. *et al.* Selective HDAC6 inhibitors improve anti-PD-1 immune checkpoint blockade therapy by decreasing the anti-inflammatory phenotype of macrophages and down-regulation of immunosuppressive proteins in tumor cells. *Sci. Rep.* **9**, 6136 (2019).

77. Li, D. *et al.* Microtubule-associated deacetylase HDAC6 promotes angiogenesis by regulating cell migration in an EB1-dependent manner. *Protein Cell* **2**, 150–160 (2011).

78. Turtoi, A., Peixoto, P., Castronovo, V. & Bellahcène, A. Histone deacetylases and cancer-associated angiogenesis: Current understanding of the biology and clinical perspectives. *Crit. Rev. Oncog.* **20**, 119–137 (2015).

79. Kaluza, D. *et al.* Class IIb HDAC6 regulates endothelial cell migration and angiogenesis by deacetylation of cortactin. *EMBO J.* **30**, 4142–4156 (2011).

80. Liu, J. *et al.* Both HDAC5 and HDAC6 are required for the proliferation and metastasis of melanoma cells. *J. Transl. Med.* **14**, 7 (2016).

81. Wang, X. C. *et al.* MiR-433 inhibits oral squamous cell carcinoma (OSCC) cell growth and metastasis by targeting HDAC6. *Oral Oncol.* **51**, 674–682 (2015).

82. Yang, C. J. *et al.* Nuclear HDAC6 inhibits invasion by suppressing NF-kB/MMP2 and is inversely correlated with metastasis of non-small cell lung cancer. *Oncotarget* **6**, 30263–30276 (2015).

83. Matthias, P., Yoshida, M. & Khochbin, S. HDAC6 a new cellular stress surveillance factor. *Cell Cycle* **7**, 7–10 (2008).

84. Kwon, S., Zhang, Y. & Matthias, P. The deacetylase HDAC6 is a novel critical component of stress granules involved in the stress response. *Genes Dev.* **21**, 3381–3394 (2007).

85. Boyault, C. *et al.* HDAC6 controls major cell response pathways to cytotoxic accumulation of protein aggregates. *Genes Dev.* **21**, 2172–2181 (2007).

86. Li, A., Chen, P., Leng, Y. & Kang, J. Histone deacetylase 6 regulates the immunosuppressive properties of cancer-associated fibroblasts in breast cancer through the STAT3–COX2-dependent pathway. *Oncogene* **37**, 5952–5966 (2018).

87. Fukada, M., Nakayama, A., Mamiya, T., Yao, T. P. & Kawaguchi, Y. Dopaminergic abnormalities in Hdac6-deficient mice. *Neuropharmacology* **110**, 470–479 (2016).

88. Jochems, J. *et al.* Antidepressant-like properties of novel HDAC6-selective inhibitors with improved brain bioavailability. *Neuropsychopharmacology* **39**, 389–400 (2014).

89. Govindarajan, N. *et al.* Reducing HDAC6 ameliorates cognitive deficits in a mouse model for Alzheimer's disease. *EMBO Mol. Med.* **5**, 52–63 (2013).

90. Millard, C. J., Watson, P. J., Fairall, L. & Schwabe, J. W. R. Targeting Class I Histone Deacetylases in a "Complex" Environment. *Trends Pharmacol. Sci.* **38**, 363–377 (2017).

91. Kalin, J. H. *et al.* Targeting the CoREST complex with dual histone deacetylase and demethylase inhibitors. *Nat. Commun.* **9**, 53 (2018).

92. Jung, M. *et al.* Amide analogues of trichostatin A as inhibitors of histone deacetylase and inducers of terminal cell differentiation. *J. Med. Chem.* **42**, 4669–4679 (1999).

93. Finnin, M. S. *et al.* Structures of a histone deacetylase homologue bound to the TSA and SAHA inhibitors. *Nature* **401**, 188–193 (1999).

94. Jung, M. Inhibitors of Histone Deacetylase as New Anticancer Agents. *Curr. Med. Chem.* **8**, 1505–1511 (2012).

95. McClure, J. J., Li, X. & Chou, C. J. Advances and Challenges of HDAC Inhibitors in Cancer Therapeutics. in *Advances in Cancer Research* vol. 138 183–211 (Academic Press, 2018).

96. Tzogani, K. *et al.* EMA Review of Panobinostat (Farydak) for the Treatment of Adult Patients with Relapsed and/or Refractory Multiple Myeloma. *Oncologist* **23**, 631–636 (2018).

97. Shen, S. & Kozikowski, A. P. Why Hydroxamates May Not Be the Best Histone Deacetylase Inhibitors - What Some May Have Forgotten or Would Rather Forget? *ChemMedChem* vol. 11

15–21 (2016).

98. Shi, Y. K. *et al.* Results from a multicenter, open-label, pivotal phase II study of chidamide in relapsed or refractory peripheral T-cell lymphoma. *Ann. Oncol.* **26**, 1766–1771 (2015).

99. Vandermolen, K. M., McCulloch, W., Pearce, C. J. & Oberlies, N. H. Romidepsin (Istodax, NSC 630176, FR901228, FK228, depsipeptide): A natural product recently approved for cutaneous T-cell lymphoma. *J. Antibiot. (Tokyo).* **64**, 525–531 (2011).

100. Iyer, S. P. & Foss, F. F. Romidepsin for the Treatment of Peripheral T-Cell Lymphoma. *Oncologist* **20**, 1084–1091 (2015).

101. Watson, P. J. *et al.* Insights into the activation mechanism of class i HDAC complexes by inositol phosphates. *Nat. Commun.* **7**, 11262 (2016).

102. Melesina, J., Praetorius, L., Simoben, C. V., Robaa, D. & Sippl, W. Design of selective histone deacetylase inhibitors: Rethinking classical pharmacophore. *Future Med. Chem.* **10**, 1537–1540 (2018).

103. Qiao, Z. *et al.* Chidamide, a novel histone deacetylase inhibitor, synergistically enhances gemcitabine cytotoxicity in pancreatic cancer cells. *Biochem. Biophys. Res. Commun.* **434**, 95–101 (2013).

104. Saito, A. *et al.* A synthetic inhibitor of histone deacetylase, MS-27-275, with marked in vivo antitumor activity against human tumors. *Proc. Natl. Acad. Sci.* **96**, 4592–4597 (1999).

105. Moradei, O. M. *et al.* Novel Aminophenyl Benzamide-Type Histone Deacetylase Inhibitors with Enhanced Potency and Selectivity. *J. Med. Chem.* **50**, 5543–5546 (2007).

106. Wagner, F. F. *et al.* An Isochemogenic Set of Inhibitors to Define the Therapeutic Potential of Histone Deacetylases in β-Cell Protection. *ACS Chem. Biol.* **11**, 363–374 (2016).

107. Haggarty, S. J., Koeller, K. M., Wong, J. C., Grozinger, C. M. & Schreiber, S. L. Domain-selective small-molecule inhibitor of histone deacetylase 6 (HDAC6)-mediated tubulin deacetylation. *Proc. Natl. Acad. Sci. U. S. A.* **100**, 4389–4394 (2003).

108. Butler, K. V. *et al.* Rational design and simple chemistry yield a superior, neuroprotective HDAC6 inhibitor, tubastatin A. *J. Am. Chem. Soc.* **132**, 10842–10846 (2010).

109. Bergman, J. A. *et al.* Selective histone deacetylase 6 inhibitors bearing substituted urea linkers inhibit melanoma cell growth. *J. Med. Chem.* **55**, 9891–9899 (2012).

110. Tavares, M. T. *et al.* Synthesis and Pharmacological Evaluation of Selective Histone Deacetylase 6 Inhibitors in Melanoma Models. *ACS Med. Chem. Lett.* **8**, 1031–1036 (2017).

111. Haggarty, S. J., Koeller, K. M., Wong, J. C., Grozinger, C. M. & Schreiber, S. L. Domain-selective small-molecule inhibitor of histone deacetylase 6 (HDAC6)-mediated tubulin deacetylation. *Proc. Natl. Acad. Sci. U. S. A.* **100**, 4389–4394 (2003).